UNIVERSITY OF BIRMINGHAM

ENHANCEMENT OF PANEL RADIATOR BASED HYDRONIC CENTRAL HEATING SYSTEM USING FLOW PULSATION

By

Mebrahtu Embaye

A thesis submitted to the
University of Birmingham for the

Degree of Doctor of Philosophy

School of Mechanical Engineering
College of Engineering and Physical Sciences
The University of Birmingham
April - 2016

ABSTRACT

Enhancing the heat output of the hydronic central heating system in buildings can play a major role in reducing energy consumption and CO_2 emission. Current hydronic panel radiators of the central heating systems are operating at constant flow strategy with On/Off thermostat control device resulting in significant energy consumption. The main aim of this PhD research is to investigate the effect of pulsed flow input on the energy consumption of panel radiators in hydronic central heating systems taking into account the user thermal comfort defined by ASHRAE standard 55 and EN ISO 7730.

The research work covers thermal performance of the hydronic panel radiator and the indoor comfort. The work was performed using dynamic control modelling using MatLab/Simulink software, Computational Fluid Dynamics (CFD) using COMSOL Multi-Physics and experimental testing to validate the modelling and prove the concept. The energy consumption performance and indoor comfort standards were investigated under constant flow rate and pulsed flow rate scenarios.

Results from the mathematical and numerical (CFD) modelling of the hydronic radiator with pulsed flow using frequency ranging from 0.0083Hz to 0.033Hz and amplitude ranging from 0.0326kg/s to 0.0412kg/s showed that 20% to 27% of energy saving can be achieved compared to the constant flow while maintaining the same radiator target surface temperature of 50^{o}C as recommended by the BS EN442 radiator test standards. The indoor comfort results were also achieved as

recommended by international standards including CO_2 concentration at 1000PPM±50PPM, relative humidity at 50±9%, comfort temperature at 20±1.6^{o}C, air velocity of below 0.15m/s and draught risk parameters of less than 15%. In addition to the hydronic heating panel radiator, the pulsed flow ventilation system was investigated analytically in MatLab/Simulink and results showed that about 34.5% of energy saving is possible from the fan energy consumption compared to the constant flow. Also using the pulsed flow applied in this work the pump power can be reduced by about 12% compared to the pump operating at constant flow.

The radiator was also tested at various inlet temperature ranges from 60^{o}C to 75^{o}C at interval of 5^{o}C and energy saving of 23.4% at 60^{o}C to 24.9% at 75^{o}C was achieved. The numerical results agreed well with experimental results with maximum deviation of radiator temperature output of ±4.1%, indoor temperature ±2.83% and energy saving of ±1.7%. The energy saved due to the pulsed flow is attributed to the enhancement of the radiator heat transfer performance that leads to higher heat output at lower average mass flow rate of the hot water. The above described results highlight the potential of pulsed flow in reducing energy consumption and CO_2 emission of hydronic heating systems without compromising thermal comfort.

ACKNOWLEDGEMENTS

I would like to express the deepest appreciation to my Ph.D supervisor Dr. Raya Al-Dadah, for her continuous support of my Ph.D research, her patience, her kindness, her motivation and her immense knowledge. Her guidance helped me in the entire time of my Ph.D research including writing scientific papers, discussion on new ideas of the research, financial support and writing my thesis. My research would not have been possible without her invaluable support of all matters during the entire period of research study time.

I would like to express my deep gratitude to Dr. Saad Mahmoud for his various invaluable suggestions and guidance, through the entire period of my PhD study. His tireless scientific guidance his immense knowledge and his support in all of the research work are invaluable for the completion of this research thesis.

I would like to express my deep and special appreciation to the University of Birmingham, EPSRC and the Fusion Innovation Ltd for supporting me financially for my PhD study.

I would like to thank Mr Simon Rowan for helping me to construct my test rig and for his continuous assessment and commissioning of the test facilities.

I wish to thank Dr. Ahmed Elsayed for his recommendation and discussion of modelling software used for this research work.

I would like to thank all my family and friends for their moral support during my PhD study.

I would like also to express my appreciation to all staff members of the School of Mechanical Engineering, University of Birmingham who have supported me during my study time.

CONTENTS

LIST OF FIGURES

LIST OF TABLES

ABBREVIATIONS

ANN	Artificial Neural Network
ASHP	Air source Heat Pump
ASHRAE	American Society of Heating, Refrigerating, and Air-Conditioning Engineers
BBOE	Bottom-Bottom Opposite End
BREDEM	Building Research Establishment of Domestic Energy Model
CALEBRE	Consumer-Appealing Low Energy technologies for Building Retrofitting
CFD	Computational Fluid Dynamics
CHP	Combined Heat and Power
CIBSE	Chartered Institution of Building Services Engineers
DCV	Demand based Controlled Ventilation
DR	Draught Risk
HVAC	Heating Ventilation Air Conditioning
IAQ	Indoor Air Quality
LHRES	Latent Heat of Thermal Energy Storage
MIMO	Multi Input Multi-Output
MPC	Model Predictive Control
PCM	Phase Change Material
PD	Percentage of Dissatisfied
PED	Percentage Experience Draught

TBOE	Top Bottom Opposite End
TBSE	Top Bottom Same End
TES	Thermal Energy Storage

NOMENCLATURE

Symbols	*Description*	*Unit*
A	area	(m^2)
ACH	air change	(1/hr)
Amp	amplitudes	(kg/s)
C	concentration	(mol/m^3)
CF	constant flow	(-)
C_p	specific heat capacity	(J/(kg.K))
D	diffusion coefficient	(m^2/s)
d_h	hydraulic diameter	(m)
ES	percentage of energy saved	(%)
F	total force acting per volume	(N/m^3)
f	flow frequencies	(Hz)
G	sum of irradiation	(W/m^2)
Gh	CO_2 generation rate	(l/s)
G_m	mutual irradiation	(W/m^2)
Gr	Grashof number,	(-)
G_{sur}	irradiation from surface	(W/m^2)
g	gravitational acceleration	(m/s^2)

H	characteristics height	(m)
h	local heat transfer coefficient	(W/(m^2.K))
h_{fg}	specific latent heat of vaporisation	(kJ/kg)
h_g	heating value of gas	(kJ/kg)
I	identity matrix	(-)
I_{so}	solar heat flux	(W/m^2)
J	total local radiosity	(W/m^2)
k	thermal conductivity	(W/(m.K))
K_p	proportional gain	(-)
K_i	integral gain	(-)
K_D	deferential gain	(-)
L	thickness	(m)
LMTD	Log Mean Temperature Difference	(K)
M	mass	(kg)
$\dot{m}$	mass flow rate	(kg/s)
m_g	mass flow rate of gas	(kg/s)
N	inward mass flux in	(mol/(m^2.s))
P_{atm}	atmospheric pressure	(Pa)
Per	perimeter	(m)
PF	pulsed flow	(-)
Pr	Prandtl number	(-)
P_s	saturation pressure	(Pa)
P_T	turbulent kinetic pressure	(Pa)
$\dot{Q}$	rate of heat output	(W)
q	heat flux	(W/m^2)

$\dot{Q}_s$	rate of nominal heat output supply	(W)
R	thermal resistance	($(m^2K)/W$)
Ra	Rayleigh number	(-)
Re	Reynolds number	(-)
RH	relative humidity	(%)
RP	rising period	(-)
RXN	reaction rate	($mol/(m^2s)$)
SHGC	solar heat gain coefficient	(W/m^2)
Sp.Q	specific heat output	(kJ/kg)
SS	steady state	(-)
St	Strouhal number	(-)
T	Temperature	(^oC)
t	time	(s)
T_b	bulk temperature	(^oC)
TI	turbulence intensity	(%)
T_{sur}	surface temperature	(^oC)
T_{mean}	mean temperature of the radiator	(K)
U	average velocity	(m/s)
U_a	overall heat transfer	($W/(m^2.K)$)
u	vector velocity	(m/s)
u_s	control signal	(-)
U'	uncertainty	(-)
V	volume of room	(m^3)
Vel	flow velocity	(m/s)
VF	view factor	(-)

$\dot{V}$	volume flow rate	(m^3/s)
V'	root mean square velocity	(m/s)
wv	sine wave function	(-)

Greek symbols	***Description***	***Unit***
ø	phases angle	(-)
β	expansion coefficient	(1/K)
ε_s	constant surface emissivity	(-)
σ_s	Stefan-Boltzmann constant	($kg/(s^3 K^4)$)
ε_T	rate turbulence dissipation	(J/(kg.s))
μ	dynamic viscosity	($N.s/m^2$)
k_T	turbulence kinetic energy	(J/kg)
ω	specific humidity	(kg/kg)
η	efficiency	(%)
α	absorbance radiation	(-)
Δ	difference	(-)
ρ	density	(kg/m^3)

Subscripts	***Description***
amb	ambient

cons	consumption
env	envelope
gen	moisture generation
hex	heat exchanger
ind	indoor
in	inlet
int.gain	internal heat gain
lat.vent	latent heat of ventilation
out	outlet
rad	radiator
rad/air	space between radiator metal skin and air
rad/w	space between hot water and radiator skin
rm	room
sen.vent	sensible heat of ventilation
thermo	thermocouple
w	water
win	window

LIST OF PUBLICATIONS

Journal papers:

1. M. Embaye, R. K. AL-Dadah, S. Mahmoud. Numerical evaluation of indoor thermal comfort and energy saving by operating the heating panel radiator at different flow strategies. Energy and Buildings (2016), http://dx.doi.org/10.1016/j.enbuild.2015.12.042 (accepted for publication)
2. M. Embaye, R. K. AL-Dadah, S. Mahmoud. Thermal performance of hydronic radiator with flow pulsation – Numerical investigation. Applied Thermal Engineering 2015; 80:109-117.
3. M. Embaye, R. K. AL-Dadah, S. Mahmoud**.** Effect of Pulsed flow modulation on energy consumption of a radiator in a centrally heated building. International Journal of Low-Carbon Technologies 2014; 0: 1-11.
4. M. Embaye, R. K. AL - Dadah, S. Mahmoud. Experimental investigation of flow pulsation on hydronic central heating system. International Journal of Energy (accepted).
5. M. Embaye, R. K. AL - Dadah, S. Mahmoud. Modelling of heating and ventilation system using flow pulsation for energy saving and indoor air quality. International journal of Energy Conversion and Management (to be submitted).
6. A. Elsayed, M. Embaye, R. K. AL-Dadah, S. Mahmoud, A.Rezk. Thermodynamic performance of Kalina cycle system 11 (KCS11): feasibility of using alternative zoetrope mixtures International Journal of Low-Carbon Technologies 2013; 0:1–10.

Conference papers:

1. M. Embaye, R. K. AL-Dadah, S. Mahmoud. Heating and ventilation flow pulsation for energy saving and indoor air quality, 14th International conference on Sustainable energy technology Nottingham, UK 2015.
2. M. Embaye, R. K. AL-Dadah, S. Mahmoud. Effect of flow pulsation on heating performance of panel radiators in central heating systems-CFD analysis, 13th International Conference on Simulation and Experiments in Heat Transfer and its Applications A Coruna Spain 2014.
3. M. Embaye, R. K. AL-Dadah, S. Mahmoud, A. Elsayed. Effect of flow pulsation on energy consumption of a radiator in a centrally heated building, International Conference on Applied Energy (ICAE 2013) Pretoria South Africa 2013.
4. M. Embaye, R. AL-Dadah, S. Mahmoud. A. Rezk. Theoretical investigation of ammonia – water kalina cycle system. Heat Powered Cycles Conference 2012, ECN The Netherlands.

CHAPTER 1

INTRODUCTION

1.1 Background

Buildings in Europe account for 40% of primary energy use and 50% of the extracted natural resources according to Energy Performance Buildings Directive 2010/31/EU. Buildings energy demand will increase further as the world population increases. High energy efficiency is required for all the buildings including the new ones in order to achieve the target of nearly zero energy buildings after 2020. From the 40% of energy consumed in buildings 60%-66% is used for heating and ventilation system, this can reach 80% if the hot water services are added [1].

In the UK, the statistical data of building energy consumption varies from 40% to 46%; from this space heating accounts for 66% of energy consumption and 25% CO_2 emission. 90% of the UK dwellings use central heating system to heat their homes; however 70% of the existing central heating system does not fulfil the minimum UK building energy regulations [2].

The European Union is demanding for a reduction in energy consumption of 20% by 2020. In order to satisfy such requirements, the UK has targeted the largest single source of energy consumption namely residential buildings to achieve 52% reduction

in its total energy consumption [3]. Enhancing the energy efficiency of heating, ventilation and air conditioning system including the domestic central heating system can play a key factor in achieving this target [4].

The heating, ventilation and air conditioning (HVAC) systems consists of primary and secondary components. The primary components include the chiller or boiler used to generate cooling or heating energy. For heating application the heat sources include boilers (condensing and non-condensing), combined heat and power (CHP), heat pumps and electric heating. The secondary component include the heat emitting devices and the auxiliary components for operating the HVAC system including the circulation pump, valves, fans and control equipment [5, 6].

There are various types of heating systems that can be classified on the basis of the heat emitter including: radiators, natural convectors, fan convectors, radiant panels, electrical heaters, warm air heaters, base board skirts and under floor heating. Most of the currently existing central heating systems in the market use either water (hydronic) or air as working fluid. The hydronic system itself can be categorised into various systems including, hot water, condenser and steam systems [6].

The comfort of indoor environment depends on the performance of the HVAC system. The indoor environmental comfort can be classified into four main categories; indoor air quality; thermal comfort, acoustic comfort and visual. According to ASHRAE standards 55, maintaining indoor comfort is key objective when one attempts to reduce the energy consumption of buildings integrated with central heating system [7, 8]. The current hydronic heating system in most of UK houses is operating at constant

flow with On/Off thermostat control system which is inefficient with high energy consumption and CO_2 emission. Finding alternative operating condition for the heating and ventilation system that leads to improved energy efficiency for the building appliance is important.

Various works have been carried out to reduce energy consumption of buildings including: building automation, building insulation, advanced control system for central heating system and application of renewable energy sources (solar thermal and heat pumps) [7, 8]. Though various attempts have been used to reduce energy consumption from central heating system, no published work on flow pulsation for central heating system was found in literature. In consideration of all the HVAC system standards this work proposes to enhance the panel radiator of hydronic heating system by changing the constant flow (convectional) to pulsed flow strategy.

1.2 Mechanism of heat transfer enhancement by pulsed flow

The heat transfer enhancement achieved due to pulsed flow is caused by the changes in the velocity distribution inside the flow channels of the radiators. Figure 1.1 shows the flow nature in a channel for both constant (a) and pulsed flow cases. The flow nature of the puled flow mechanism figure 1.1(b) shows clearly the improvement in the flow mixing and the disturbance to the boundary layers by creating vortices. The nature of flow mechanism in the channels due to the pulsed flow leads to higher Reynolds number that creates higher flow mixing leading to flow turbulence and breakup of the boundary layer along the fluid side wall of the flow channels. The high mixing behaviour of flow highlights the advantage of the pulsed flow strategy in enhancing the convection heat transfer at the solid/fluid interfaces. Improving the

flow mixing along the flow channels of the panel radiator also maximise heat flux distribution uniformity along the surface of the radiator [84 and 101]. Further using flow pulsation can help in reducing fouling inside the flow channels. Fouling has negative impact for any heat exchanger particularly radiators with channels that cannot be cleaned easily.

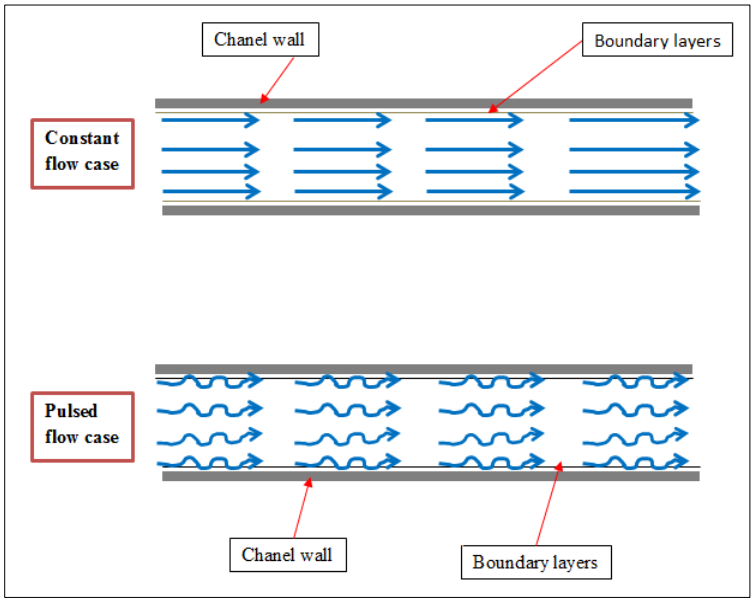

Figure 1.1 the flow nature of pulsed flow and constant flow cases

1.2 Project aim and objectives

- The main of aim of this work is to enhance the thermal performance of hydronic panel radiator heating system by changing the radiator inlet flow strategy from constant flow to a pulsed flow strategy without changing the installed radiator or compromising the user comfort. The work will involve (i) investigating the effect of pulsed flow on heat transfer enhancement of the panel radiator leading to energy saving compared to constant flow strategy and (ii) investigating the effect of pulsed flow to the radiator on heating the space to achieve thermal comfort as

recommended by international comfort standards. To achieve the aim of the project, the following objectives are set.

- Carry out comprehensive literature review regarding (i) energy consumption of buildings and space heating system, (ii) various types of central heating system in UK and Europe, (iii) various methods of enhancing heat transfer, (iv) various methods of enhancing hydronic heating systems including advancement in control systems and (vi) indoor thermal comfort criterion.
- Develop a thermodynamic control model of the central heating system integrated with heated space (room) using MatLab/Simulink to assess the dynamic behaviour of the system, indoor comfort, and energy saving due to the pulsed flow.
- Develop a CFD model using COMSOL for the radiator operating at constant and pulsed flow. This is to investigate the thermal performance of the radiator and optimise the system numerically in terms of energy saving due to the pulsed flow compared to constant flow.
- Develop a CFD model using COMSOL for the heated space integrated with spatial transient surface temperature of the radiator at constant and pulsed flow scenario to investigate numerically the indoor thermal comfort and indoor air quality of the heated space.
- Design and develop experimental test facility to validate the numerical results of the central heating system against the experimental results and prove the hypothesis of this thesis.

1.3 Thesis outline

The work carried in this project is presented in eight chapters as follows:

Chapter One presents the introduction of the thesis including the background, aim and objectives of the research as well as thesis outline.

Chapter Two presents the extensive literature review to identify recent development in research related to the proposed work. This chapter presents literature review on: energy consumption of buildings, central heating system, methods of heat transfer enhancements, enhancement of hydronic central heating system, indoor comfort development, and effect of control system on energy saving as well as indoor comfort.

Chapter Three presents the development of thermodynamical control model of the central heating system integrated with heated space using MatLab/Simulink. The chapter describes the dynamic behaviour of central heating at constant flow (conventional flow) and at pulsed flow (this work) using On/Off control feedback system as well as using PID control feedback system. Also it describes work to investigate the potential of energy saving due the pulsed flow compared to constant flow while maintaining the indoor thermal comfort and indoor air quality at an acceptable level as recommended by international standards.

Chapter Four CFD of hydronic panel radiator at constant and pulsed flow in COMSOL. The chapter describes radiator CAD design (type10 and Type11 radiators), investigation of radiator at various inlet temperatures, investigation of radiator at various pulsed flow amplitudes and various pulsed flow frequencies. The effect of flow pulsation in terms of energy savings compared to constant flow and the reasons

of the heat transfer enhancement due to the proposed pulsed flow strategies were also described.

Chapter Five describes the finite element modelling (CFD) developed in COMSOL for the heated room integrated with the spatial temperature distribution of the radiator at constant flow and at pulsed flow scenarios. The chapter also describes work carried out to investigate the effect of pulsed flow on the indoor thermal comfort, indoor draught parameters and indoor air quality.

Chapter Six presents the experimental facilities. This chapter describes the design and selection of required components, selection and calibration of measuring, instrumentation, commissioning of test rig and experimental test procedures. This chapter also describes the setup of the control system used to produce the pulsating flow.

Chapter Seven presents experimental results and validation of the numerical results against experimental results. This chapter presents the experimental results of radiator operating at constant and pulsed flow and experimental results of the heated room at constant and pulsed flow scenarios. The chapter also compares the numerical results to the experimental results for the hydronic panel radiator and the heated room at constant and pulsed flow scenarios to validate the modelling.

Chapter eight presents the conclusions and recommendation for future work. This chapter describes the major findings from the research carried out in this project and

suggests future work regarding enhancing the central heating system using flow pulsation.

CHAPTER 2

LITERATURE REVIEW

2.1. Introduction

Heating and ventilation are the main energy consumption contributors in the building sector. Thus extensive research has been carried out to enhance the efficiency of heating appliances without compromising the occupants' wellbeing and indoor air quality. This chapter presents an extensive review of the research carried out on various types of central heating systems to reduce energy consumption and improve indoor air quality without compromising human comfort.

The heating system can be enhanced using various techniques including:-

- Using passive or active heat transfer enhancement techniques to increase heat transfer like improving geometrical design configurations of the heating appliances, surface coating and improving the bulk fluid flow pattern.
- Select appropriate position for the emitter (heating appliance) in the space to be heated to interact with ventilation air.
- Design appropriate control system to improve the building heating automation system.

All of the above mentioned points and other related techniques that help improving the performance of the heating system have been reviewed to identify the state of the

art of domestic heating appliances in terms of thermal performance, carbon emission and user comfort.

2.2. Building energy consumption

The energy statistical data indicates that buildings consume around 50% of the energy consumed in developed countries [9]. Energy consumption of building accounts for 40% of the UK total energy consumed per year; from this space heating accounts for 66% of energy consumption and 25% CO_2 emission. 90% of the UK dwellings use central heating system to heat their homes; however, 70% of the existing central heating system does not fulfil the minimum UK building energy regulations [2]. According to report from the UK Department of Energy and Climate Change; the overall energy consumption by sector from 1970 to 2014 is shown in figure 2.1 [10] where the domestic sector consumes about 60Mtoes of energy in 2014.

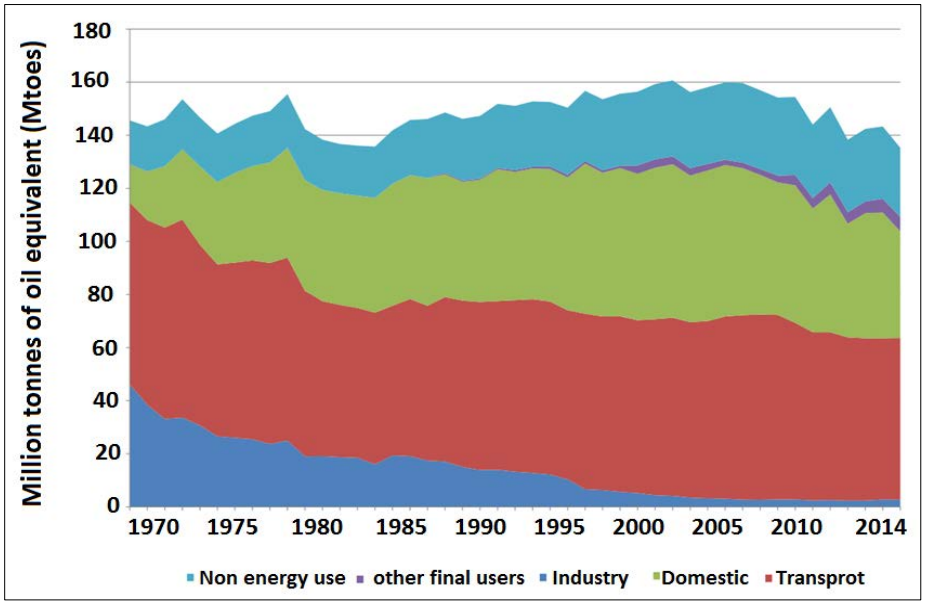

Figure 2.1 final energy consumption by sector, UK (1970 to 2014) [10]

Figure 2.2 shows the energy and emission sharing of the domestic buildings in UK [11] where space heating and hot water service contribute up to 84% of energy consumption and 71% of CO_2 emission.

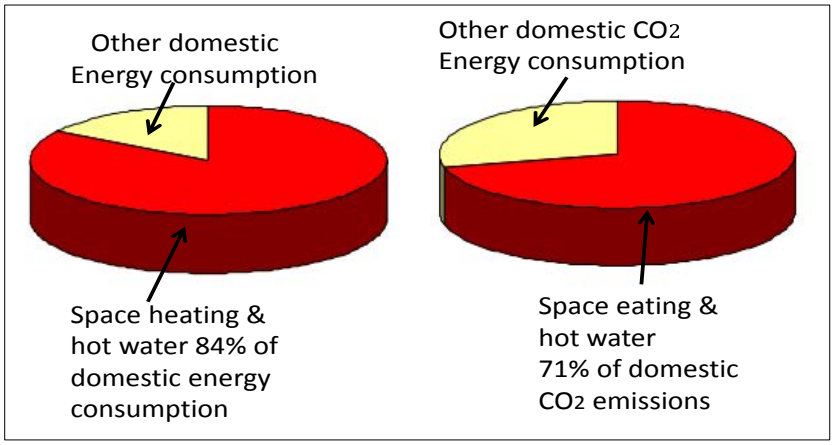

Figure 2.2 domestic energy consumption and CO_2 emissions in the UK [11]

To reduce the energy consumption of the residential building sector; improving the energy performance of buildings is vital for achieving EU climate goal in reducing CO_2 emission by 20% in 2020. The UK government is also committed to Kyoto protocol (1997) to reduce the greenhouse gas emission by 80% in 2050. The UK government has planned for new domestic buildings to have zero carbon by 2016 and for non-domestic buildings to have zero carbon foot print by 2019 [11-14].

The UK reliance on primary energy (gas) for heating system is the main concern to UK policy makers in order to achieve the 2050 target of buildings de-carbonisation. According to the UK policy makers; heat pumps are considered as an alternative option for future heating sectors; but full reliance on heat pump could result in higher electricity use. To balance the higher energy consumption of heating system

exploiting waste heat and other renewable energy sources such as biomass need to be considered [15]. Figure 2.3 shows the domestic heating and hot water sector- 2020 vision in UK [11].

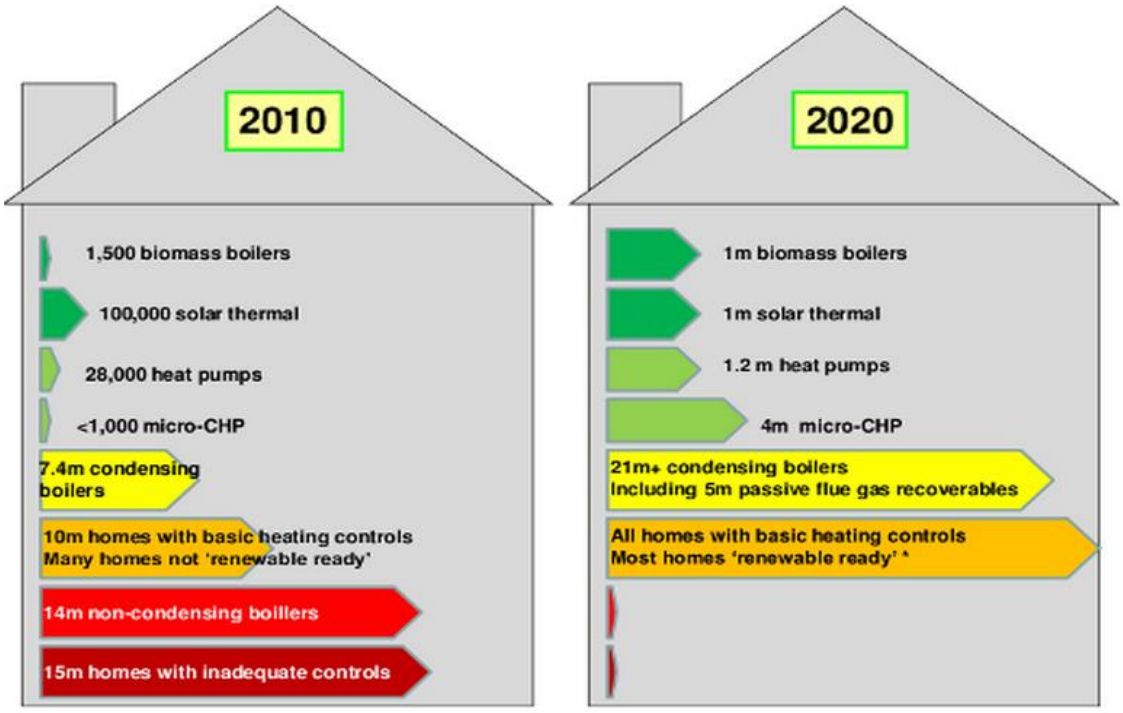

Figure 2.3 the domestic heating and hot water sector UK- 2020 vision [11]

To implement the future plan of the central heating system in UK comprehensive assessment of building energy consumption and the main contributors are required to be reviewed.

Danny et al [16] investigated the impact of weather fluctuation including summer and winter on building energy consumption concluding that there is peak energy consumption in hot summer for cooling and cold winter for heating. Although energy saving in buildings is of paramount research interest; improving energy efficiency in

buildings must not be implemented at the cost of indoor air quality (IAQ) and indoor comfort environments.

Hall et al [17] carried out CALEBRE project (2008-2013) to investigate the technology suitable for retrofit in UK domestic buildings that can reduce energy consumption and CO_2 emission without compromising comfort of the occupants. The main approach of the retrofit plan was to improve air tightness, decrease the U-value of external material of building envelope including walls, doors, glazing, floors and ceilings in addition to upgrading and enhancing the efficiency of heating appliances. They concluded that significant amount of energy can be saved from the buildings retrofit plan and their work was adopted by E.ON energy company.

Parkinson et al [18] studied the impact of improving energy efficiency in real estate asset concluding that improving the performance of energy appliances helps reducing the marginal cost of energy consumption thus increasing the asset value. Obyn et al [19] studied the budget allocated to buildings on the basis of appropriate heating system to match the economic margin of house owners. Based on that various detached dwellings were modelled using TRNSYS software and evaluated on the basis of investment cost; operating cost; primary energy consumption and CO_2 emission impact. They concluded that; on the basis of environmental and economical point of view; for highly insulated house, the performance of heating installation is not important when selecting the heating system. However it was identified that installing a heat recovery unit on the existing condensing gas boiler gives better performance on the basis of environmental and user economy. The use of efficient HVAC system and exploiting the availability of renewable energy sources that can be

integrated to the building of energy supply system is important for sustainable energy saving from buildings [20].

Mikk et al [21] carried out a study to estimate heat loss in buildings showing about 50% of unnecessary heat loss can be avoided using low temperature heating appliances (supply temperature of 45^{o}C to 35^{o}C) controlled by PI thermostat . This approach can keep the loss below 1% for detached houses in northern and central Europe climates. Wittchen et al [23] assessed the energy requirement for heating of a building using EPIQR software that fulfils the European standard EN 832:1998. The aim of the developed model was to calculate the heat required to heat a room which is helpful for HVAC engineers to estimate the energy consumption of the buildings. Thus the model can help to design appropriate heat emitters, predict retrofit for existing appliances and to predict actual heat loss.

Thermal energy storage (TES) can be used to reduce buildings energy consumption. The main contribution of thermal energy storage to the reduction of energy consumption is to match the demand and supply of heat when they do not coincide. The main drawback of this approach is the high space demand of the storage system. Hence alternative way of efficient energy storage for buildings is needed to overcome the drawback of TES. Phase change material (PCM) incorporated in buildings envelope construction including walls, ceilings, floors, and windows is a good option for energy storage. PCM for storing the latent heat is more effective in reducing energy consumption in buildings than storing the sensible heat approach. The passive construction solution with PCM potentially reduces energy consumption by reducing heat load in the building envelope. In addition to that it improves the comfort of the

occupants by minimising the temperature fluctuation of the indoor environments [23-24].

2.3 Central heating system

Generally the environmental impact of buildings including CO_2 emission depends on the energy consumption of heating, ventilation and air conditioning system (HVAC). The HVAC system consists of primary and secondary systems. The primary system consists of the chiller or boiler which generates the cooling or heating fluid while the secondary system consists of auxiliary components for operating the system including the circulation pump, valves, fans and control equipment [25]. Figure 2.4 shows the typical central heating system in UK dwellings.

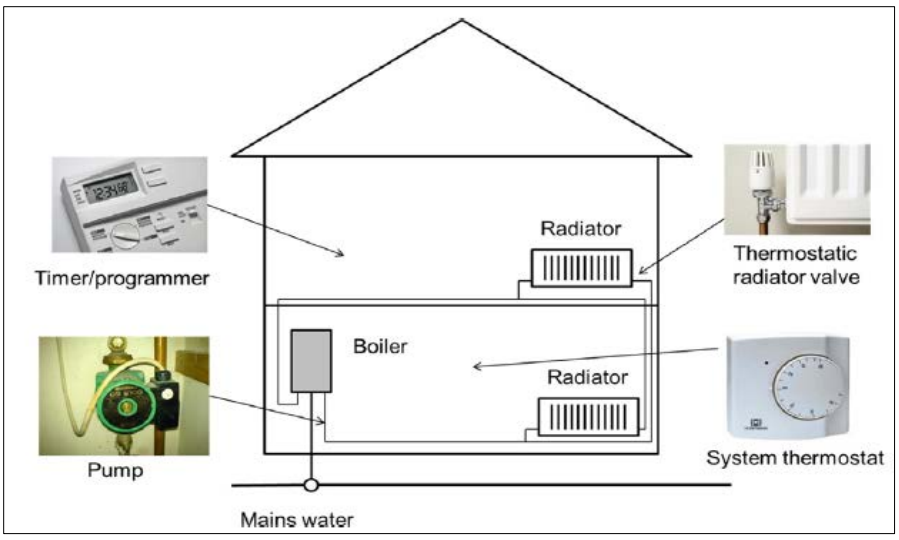

Figure 2.4 schematic of a typical UK central heating system [25]

According to CIBSE guide F; there are various types of heating systems that can be categorised based on the heat emitter including: radiators, natural convectors, fan convectors, radiant panels, electrical heaters, warm air heaters, base board skirts, and

underfloor heating. Based on working fluid (energy carrier materials) heating system can also be categorised as air heating or water (hydronic) heating. Based on the heat source it can be categorised as boilers, combined heat and power (CHP), heat pump and electric heating [6]. Some of the examples of common heat sources are shown in table 2.1. Also tables 2.2 and 2.3 summarise the advantage and disadvantage of the distribution fluid and heat emitter appliance currently existing in the market [6, 26-27].

Table 2.1 examples of common heat sources, distribution networks and emitters form CIBSE guide F 2006

Heat source	Heat emitters	Distribution network
Gas, LPG, oil, coal, electricity, CHP, solar, biomass, wind, heat pump (ground and air sources)	radiators, panel heaters, ceiling panels, natural convector, underfloor heating, storage heater, fan convector and high temperature radiant panels	Water (low, medium, and high temperatures); air, steam, and electricity

Table 2.2 characteristics and comparisons of different heat distribution media

Flow type	Characteristics	advantage	disadvantage
Water	High density, high heat capacity , potential of large temperature between supply and return; smaller volume required than air	Require less space, compact design, small volume ducts required, easy installation, cheap maintenance cost	It require heat emitter to transfer heat to the space
Air	Low heat capacity, small temperature differences between supply leads to large volume design requirement	No heat emitter needed, direct heat, no other heat transfer medium needed	Large volume of air required, leads to large air duct design, the fan can have high energy usage and high CO_2 emission

Steam	Use of latent heat of condensation leads to high heat transfer capacity, operate at high pressure	Exploited latent heat of condensation and permitted large transfer of heat	Required water treatment and higher maintenance cost, extra safety

Table 2.3 comparison between different heat emitters

Emitter type	advantage	disadvantage
Radiator	Good balance of radiant and convective heat transfer, good thermal comfort, cheap; low maintenance cost and good temperature control	Fairly slow thermal response
Natural convectors	Fast control response, unobtrusive	Occupy more space and floor space, high temperature stratification in space
Fan convector	Fast thermal response	It is noisy, high maintenance, occupy more floor space
Under floor heating	Unobtrusive, acceptable indoor temperature distribution low stratification	Lower heat output, slow response, high maintenance and installation cost
Warm air heaters	Faster thermal responses	Noisy and higher indoor temperature stratification
High temperature radiant panels	Faster thermal response, use for space with high air change rate and high ceilings	mounted at high level to avoid higher intensity of radiation and indoor discomfort
Low temperature radiant panels	Low maintenance cost and unobtrusive	Very slow response to control

According to the information found in CIBSE guide F designers of the heating system should consider the following important design recommendation to deliver an appropriate heating system [6, 26-27].

- Minimise the running cost and select the right fuel with lower tariff
- Improve load matching and consider de-centralised heating to minimise standing losses in large sites
- Select appropriate position of the heating appliance in the space to be heated
- Select the right size of the distribution systems such as pumps and consider maintenance cost, installation, insulation of distribution network including pipes, valves and other potential of heat loss components.
- Where feasible; consider utilization of heat recovery technology and condensing boiler as it gives better efficiency at part load.

Based on the studies published in [6, 26-28] the HVAC designers should not only depend on the optimization of energy consumption; there are other important factors that need to be considered. The indoor environmental factors that affect the occupant comfort and productivity of individuals are:

- Indoor air temperature
- Radiant indoor temperature
- Indoor relative humidity
- Indoor air velocity
- Indoor air qualities (IAQ) determined by CO_2 concertation

Thus any new heating system design which target saving energy consumption in buildings should ensure the required comfort factors of the occupants [29-31].

Ibrahim et al [32] assessed the advantage and disadvantages of six types of domestic water heating systems. The six water heating systems were wood, oil/gas, electric,

heat pumps, solar and instantaneous systems (Combi boilers). They concluded that the instantaneous supply approach is more appropriate provided continuous supply of energy/fuel is available. However to meet 2050 target of CO_2 emission reduction by 80% as committed by the UK government, Ibrahim et al concluded that alternative way of heat supply for central heating system is required such as heat pumps.

Maivel et al [33] and Kilkis et al [34] investigated the effect of return temperature on condensing boiler temperature and seasonal heat pump performance. They concluded that lower return temperature of the heating radiator can help to increase the seasonal performance of heat pump by 9%. Ucar et al [35] carried out a study to exploit the renewable solar energy using solar collector, heat pump and energy storage tank to supply energy for heating the building using radiator emitter as shown in figure 2.5. Three types of seasonal storage systems including storage tank without insulation on ground, storage tank with insulation on ground and underground storage tank without insulation were investigated using numerical simulation ANSYS. Their simulation results showed that the highest saving and solar fraction were achieved from the storage tank buried under the ground and the second highest saving and solar fraction was achieved from the storage tank on ground with insulation.

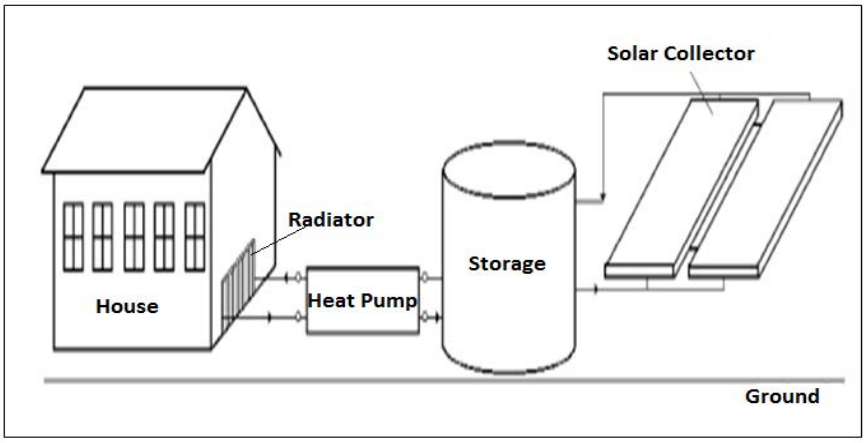

Figure 2.5 schematic diagram of solar heating system with storage tank on the ground [35]

Kelly et al [36] studied air source heat pump (ASHP) coupled with PCM enhanced buffer tank for space heating and domestic hot water of UK detached houses as shown in figure 2.6. Their work showed that the electrical energy consumption of the heat pump increased during the load shift of the buffer tank to higher CO_2 emission. Therefore further research is required to establish the advantage of the PCM material at the load shifting scenario.

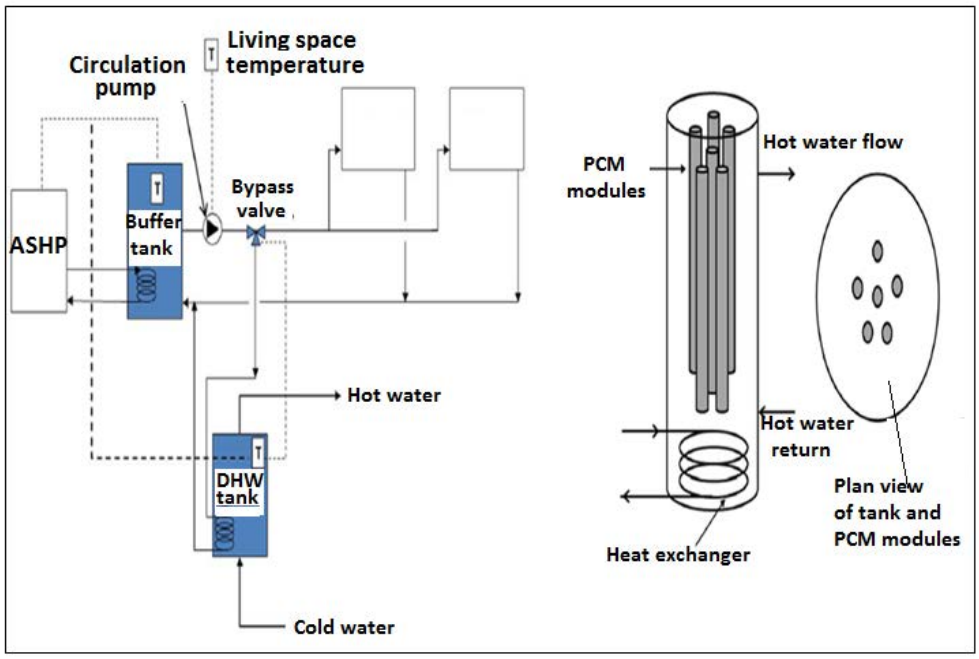

Figure 2.6 the modelled heating system supplied by the ASHP (with PCM-enhanced buffer tank) and detail of buffer tank with integrated phase change modules [36]

Gupta et al [37] studied the ground source heat pump contribution to reduction of CO_2 emission from heating systems including space heating and hot water services. They developed building regression model based on the heat pump coefficient of performance (COP) and model results were validated using UK building energy establishment domestic energy model (BREDEM). It was concluded that the results are in a good agreement with existing model where correct response to the ambient temperature variation and accurate prediction of energy consumption while

maintaining performance of the heat pump were achieved. In addition to that significant CO_2 reduction was achieved.

Nuytten et al [38] investigated the advantage of CHP integrated with thermal heat storage (TES) for district heating system and concluded that the CHP coupled with TES offer better service flexibility in district heating system compared to the traditional district heating system and to increase the degree of service flexibility, a powerful CHP and larger TES buffer are required. Lauenburg et al [39] investigated experimentally and numerically the optimum district heating system return temperature to the radiator by incorporating a heat exchanger to control the return temperature. They concluded that the optimum return temperature can be achieved by selecting the optimum radiator supply temperature and flow rate coupled with appropriate adaptive control strategy.

Cao et al [40] investigated the effectiveness of ventilation system in conditioned rooms using eight various flow strategies and concluded that; the ventilation system efficiency should be determined on the basis of the heat removal, elimination of pollutant, sufficient supply of fresh air to the zone to be conditioned. William et al [41] developed hybrid ventilation system to reduce the energy consumption and achieve indoor environmental condition that fulfils the occupants' comfort level. The reported hybrid ventilation system was designed to manipulate the natural and mechanical ventilation depending on the indoor environmental conditions.

Chmutina et al [42] studied restructuring the energy system by de-centralising energy (DE). According to the projects attempted in various countries to restructure the

energy distribution from centralised sector to de centralised sector; it was concluded that although money is a crucial barrier but to convince the government and policy makers is the main challenge for implementing the de-centralization as fast as it should be.

2.4 Methods of heat transfer enhancements

Heat transfer can be enhanced using various methods which can be grouped as passive or active techniques. The passive methods of heat transfer enhancement do not require direct application of external power. Examples of passive enhancement methods are; rough and extended surface, vertex generator, nanofluids. Active enhancement techniques require continuous supply of power and include surface vibration; electro-magnetic fields; and mechanical mixing device [43-45].

2.4.1 Passive heat transfer enhancement methods

Castellões et al [45] investigated heat transfer enhancement using corrugated wave channel design for low Reynolds number laminar flow. They concluded that corrugated channel improved the local heat transfer coefficient by about 50%. Kareem et al [46] studied numerically spiral corrugated tube heat exchanger to enhance heat transfer of water flowing at low Reynolds number ranging from 100 to 700. They concluded that heat transfer enhancement ranges from 21.7% to 60.5% while the friction factor was increased by 19.2 - 36.4%.

Liu et al [47] studied numerically the heat transfer augmentations of turbulent flow using novel rectangular round grooves (see figure 2.7a). Five cases were numerically analysed including conventional groove arrangement and results showed that high heat transfer augmentation can be achieved using the rectangular round grooves compared to the conventional groove arrangement. Gutierrez et al [48] studied numerically and experimentally the heat transfer performance of grooved channel with curved flow deflectors. The results showed increasing the Nusselt number by about 31% in addition to decreasing the pressure drop by 74% compared to the grooved channel without deflectors.

Awasarmol et al [49] carried out a study to enhance heat transfer using perforated rectangular fin arrays at different inclinations experimentally. The aim of the experimental tests was to quantify the enhancement of natural convection heat transfer coefficient for perforated rectangular fin arrays compared to solid rectangular fins array. The experiment was conducted at various perforation diameters (6mm - 12mm) and various inclination angles (0-90). They concluded that about 32% increase in heat transfer was achieved by the perforated fins at 12mm perforated diameter compared to the solid fins. Korichi et al [50] studied numerically the heat transfer enhancement by mounting obstacles periodically and in alternating arrangement on the upper and lower wall of the channel at low flow Reynolds number of ($50 \leq Re \leq 1000$). Results showed that high heat transfer enhancement can be achieved by interrupting the thermal boundary layer using obstacles. Heat transfer enhancement of Nusselt number was about 123.1%, for Reynolds number ranging from 50 to 500 and 48.5 % for Reynolds number ranging from 500 to 1000.

Gunes et al [51] studied the potential of heat transfer enhancement experimentally by inserting a coiled wire in a tube. They investigated the effect of coiled wire pitch to diameter ratio (P/D) ranging from 1 to 3; and Reynolds number of 3500 to 27000, with uniform heat flux applied on the external surface of the tube using air as a working fluid. Results were compared to the plain tube and significant heat transfer enhancement (up to 36.5%) was achieved using the inserted coiled wire. Sahin et al [52] studied numerically and experimentally the use of coiled wire turbulators with different pitches to enhance the heat transfer of flow in concentric tube heat exchangers at Reynolds number ranging from 3000 to 17000. They concluded that the heat transfer enhancement using the turbulators coil compared to plain heat exchanger was maximum of 2.28 at pitch distance of 15mm. Zheng et al [53] investigated the potential of heat transfer enhancement using porous inserts and concluded that there is high potential of heat transfer enhancement using the porous inserts.

Soti et al [54] studied heat transfer enhancement using flexible thin structure for inducing flow deformation. They showed that the high development of wake vortices along the plate promoted the mixing of the flow along the channels thus reducing the thickness of the thermal boundary layers and enhancing the heat transfer of the channel. Abdollahi et al [55] numerically studied the winglet vertex generator to enhanced heat transfer in the rectangular heat sinks and concluded that this approach enhanced the heat transfer but it also increased the pressure drop.

Zhang et al [56] studied experimentally the heat transfer enhancement for circular tube fitted with left-right helical blade rotors. Results showed that the left-right helical blade rotor increased the Nusselt number by 182.2% compared to plain tube.

Promvonge et al [57] studied the use of conical nozzles with different pitch ratios as a flow generator for enhancing heat transfer. Also they studied the use of snails for generating swirling flow at the inlet of the test tube. They conclude that; the application of conical nozzles and snails can increase the heat transfer rate by about 278% and 206% respectively compared to the plain tube and up to 315% enhancement was possible by integrating the snail and the conical nozzles simultaneously. Bhadouriy et al [58] studied experimentally and numerically the heat transfer of flow in an annulus formed by an inner twisted square duct and outer circular pipe at various flow parameters including laminar and turbulent flow. They concluded that there is high potential of heat transfer enhancement using the twisted inner duct particularly when the flow is laminar but the enhancement was limited when Reynolds number exceeded 10000.

Yousefi et al [59] studied the effect of Al_2O_3-H_2O nanofluids concentration by weight on heat transfer enhancement at various flow Reynolds number. It was concluded that heat transfer coefficient was increased by 57.1% at concentration 0.06% by weight of nanofluids particles in water at Reynolds number of 2080. Mohamad [60] theoretically studied the effect of nanofluids on heat transfer enhancement. According to the published work a controversial conclusion was reached compared to the previous work regarding the effect of nanofluids for heat transfer enhancement. Hence heat transfer rate by convection decreased because of the reduction in buoyancy force of the material mixed with nanofluids.

Table 2.4 summary of passive flow heat transfer enhancement techniques

Authors	Concept	Test methodology	Application	% Maximum heat transfer enhancement
Castellões et al [45], Kareem et al [46]	Passive flow turbulators generated using corrugated wave channel design	Numerical	Industrial heat exchangers	60.5%
Liu et al [47], Gutierrez et al [48]	Passive flow turbulators generated using round or rectangular grooves design	Numerically	Industrial heat exchangers	74%
Awasarmol et al [49]	Passive flow turbulators generated using perforated rectangular fins design	Experimental	Industrial heat exchangers	32%
Korichi et al [50]	Passive flow turbulators generated using obstacles periodically in the flow channels	Numerical	Industrial heat exchangers	123.1%,
Gunes et al [51], Sahin et al [52], Zheng et al [53]	Passive flow turbulators generated using inserting a coiled or porous wire in the flow channels	Experimental	Industrial heat exchangers	36.5%
Soti et al [54], Bhadouriy et al [58]	Passive flow turbulators generated using flexible thin structure design in the flow channels	Numerical	Industrial energy harvesting	59%
Abdollahi et al [55], Zhang et al [56]	Passive flow turbulators generated using winglet vertex generator or helical blade rotors	Numerical	Industrial heat sink in chemical industries	182.2%
Promvonge et al [57]	Passive flow turbulators generated using conical nozzles design mechanism	Experimental	Industrial heat exchangers	278%
Yousefi et al [59], Mohamad [60]	Passive flow turbulators generated using nanofluids technology	Experimental	Industrial heat exchangers	57.1%

It can be concluded from Table 2.4 that; heat transfer using passive flow mechanisms have achieved significant enhancement of heat exchanger in the process industries. However this achievement is applied at the cost of significant changes to the design geometry of the heat exchangers. Therefore they cannot be easily applied to the existing heat exchangers such as hydronic radiators.

Some of the main passive heat transfer enhancement design configurations found in literature are shown in figure 2.7.

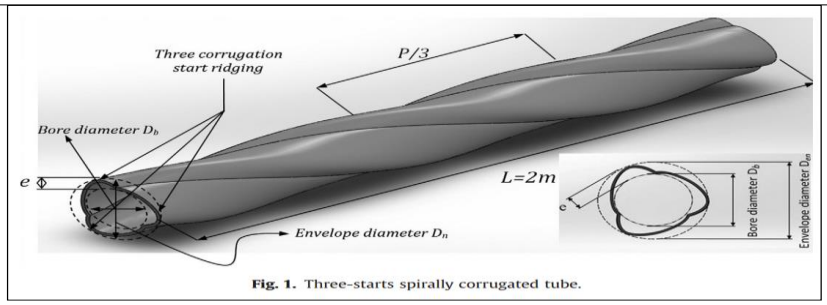

(a)Three-starts spirally corrugated tube [46]

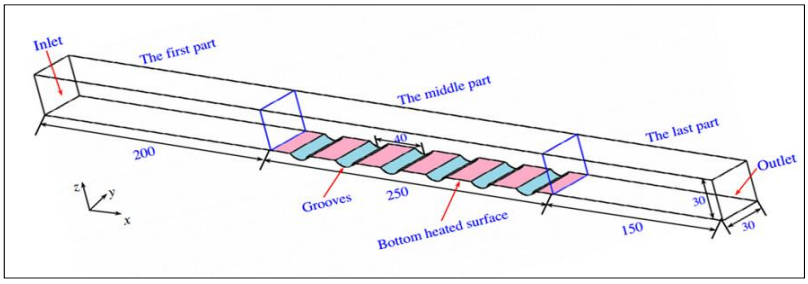

(b) Rectangular flow channel with attached grooves [47]

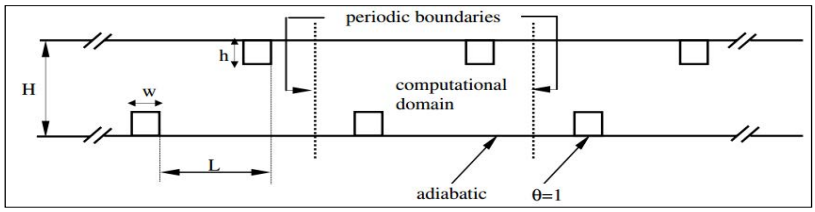

(c) Rectangular flow channel with attached obstacle fin [50]

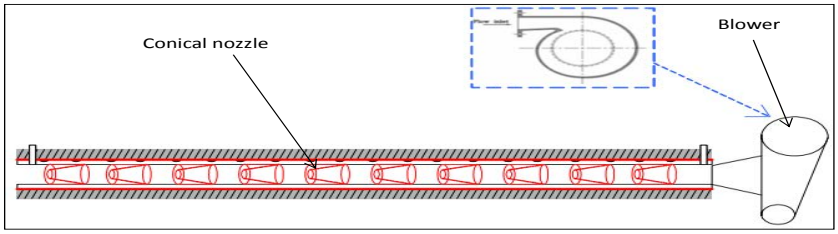

(d) Tested tube fitted with conical nozzle and snails [57]

Figure 2.7 examples of techniques for passive heat transfer enhancement

Chung et al [61] studied numerically heat transfer enhancement of electronic components at laminar flow. The numerical results showed that grooves are able to produce high heat transfer enhancement of up to factor of five to the Nusselt number.

2.4.2. Active heat transfer enhancement

Active heat transfer enhancement techniques require active supply of external power for operating the system. Active heat transfer enhancement methods include surface vibration; electro-magnetic fields; mechanical mixing devices and flow pulsation [43-45].

Lakeh et al [62] studied experimentally and numerically the effect of electrical field on heat transfer enhancement of fully developed internal flow. The electrical field induced secondary flow which created strong swirls along the channel leading to significant heat transfer enhancement of 173%. Kaneda et al [63] numerically investigated the effect of the external magnetic field on heat transfer performance of laminar flow in pipes. A single coil magnetic field surface and constant heat flux supply were used to heat the pipe. They concluded that the heat transfer and fluid flow strongly depends on the position of the magnetic coil leading to heat transfer enhancement of up to 10%. Peng et al [64] numerically investigated the heat transfer performance of rectangular channel using electro hydro dynamic (EHD) effect. The system was optimized based on the electrode arrangement in the channel and they examined single electrode and multiple electrode arrangement in the channel. They concluded that the increasing the number of electrodes in the channel beyond 7 does not contribute to the heat transfer enhancement of the system.

Tajik et al [65] and Orandrou et al [66] studied the potential of heat transfer enhancement by acoustic streaming in closed cylindrical enclosure filled with water experimentally. The acoustic streaming wave was generated by inducing vibrating plate on the lower side of the plate by means of ultrasonic bolted langevin transducers. In this work the upper side of the plate was heated by constant heat flux and the side walls were applied with constant temperature. Result showed that heat transfer enhancement of 390% was achieved by using the acoustic streaming wave generated using ultrasonic vibrations.

Li et al [67] experimentally investigated the effect of ultrasonic vibration on heat transfer performance in copper tubes with various surface characteristics including smooth, screwed and finned tubes. The test was applied at various vibration frequencies ranging from 21kHz to 45kHz and ultrasonic power ranging from 30W to 90W. They concluded that the higher heat transfer performance can be achieved at 21kHz of vibration frequency and 90W of ultrasonic power. They also showed that changing the channel surface from smooth to finned and screwed surface increase the heat transfer enhancement.

Various researches have been carried out to enhance the heat transfer performance of heating appliance using active heat transfer enhancement methods. However this work will concentrate on active heat transfer enhancement using the concept of flow pulsation and this is reviewed in detail in section 2.4.3.

2.4.3. Heat transfer enhancement using flow pulsation

Sailor et al [68] carried out a series of experiments to investigate the heat transfer enhancement due to flow pulsation. The experiment was conducted by operating air jet at constant and pulsed flow. Results showed that maximum heat transfer enhancement of 50% was achieved by pulsed flow compared to the steady flow and it was recommended that further research is required to optimise the duty cycle of the pulsed flow. Mohammadpour et al [69] studied numerically flow pulsation based on square and sinusoidal waveform on concave surface. They concluded that the heat transfer enhancement is higher at pulsed flow jet compared to the constant jet with highest heat transfer enhancement achieved for the square wave compared to the sine wave. Figure 2.8 shows the proposed inlet flow and the corresponding Nusselt number by Mohammadpour et al.

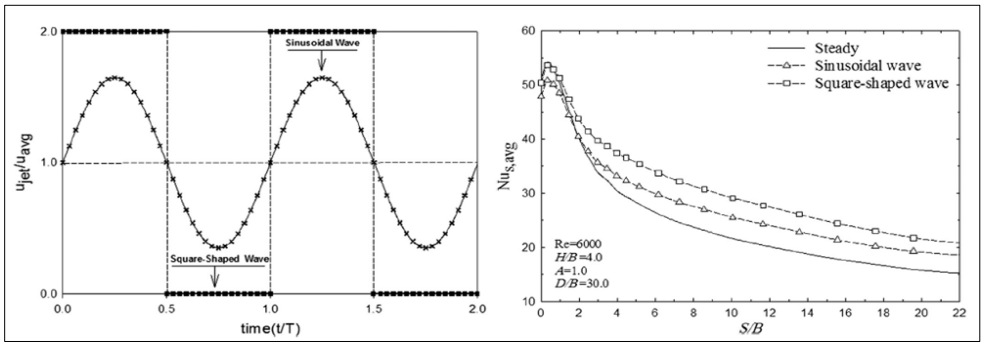

Figure 2.8 velocity profiles at inlet jet (left) and local time-averaged Nusselt numbers (right) [69]

Wang et al [70] studied flow pulsation combined with winglet design to enhance heat transfer of industrial heat exchangers and concluded that up to 24% heat transfer enhancement was possible. Saitoh [71] investigated experimentally the effect of flow pulsation on augmentation of heat transfer in a rectangular duct. They concluded that

heat transfer can be enhanced by flow pulsation due to creating vortices, and breaking the thermal boundary layers. Dec et al [72] experimentally investigated heat transfer enhancement by flow pulsation using tail pipe of combustor. The test was performed to assess the effect of flow amplitudes, flow frequency, and mean flow rate. Results showed that the Nusselt number increased up to 2.5 times that of the constant flow at the same mean Reynolds number.

Zohir [73] experimentally studied the effect of flow pulsation flow pulsation on the heat transfer of flow in the annulus of concentric double pipe heat exchanger at various flow frequencies, and velocity (Reynolds number). Ball valve was used to generate the flow pulsation in the annulus where cold water is flowing and constant flow of hot water was applied via the inner pipe. Results showed that transfer enhancement of 90% and 20% for counter and parallel flow arrangement respectively. Habib et al [74] investigated experimentally effect of flow pulsation on heat transfer of turbulent flow. The test was carried out at Reynolds number ranging from 5000 to 29000, flow frequencies ranging from 1 to 8Hz and constant heat flux applied at the walls of the channels. Results showed that the effect of flow pulsation on heat transfer (Nusselt number) decreased with increasing Reynolds number and flow frequency.

Jafari et al [75] studied numerically the effect of flow pulsation on heat transfer of flow in a corrugated channel. The simulation was performed at low Reynolds number including 50,100,150 and also pulsating velocity in the form of Strouhal number (Strouhal number is a dimensionless value used for analysing oscillating unsteady fluid flow dynamics and is expressed as ((frequency*length)/(velocity))) ranging from 0.05 to 1 and the selected amplitude was between 0 and 0.25. They concluded that

heat transfer due to pulsation depends on the pulsating velocity and 20% enhancement was achieved at Reynolds number of 150 and Strouhal number of 0.25.

Olayiwola et al [76] studied the effect of flow pulsation on heat transfer enhancement in a finned rectangular channel experimentally. The tested flow parameters include flow frequency, flow amplitudes and flow Reynolds number of 16 to 54Hz; 0.28 to 0.53mm and 50 to 1140 respectively. Results showed that maximum heat transfer enhancement of 2.5 times compared to that of constant flow case was achieved. Guoneng et al [77] experimentally investigated the augmentation of heat transfer in a rectangular flat plate using impinging jet of cross flow (On/Off). The tests were performed at different jet to cross flow ratio and investigated the effect of jet diameter at Reynolds number ranging from 1434 to 1525. Results showed that the heat transfer coefficient increased with the increase of the jet to cross flow ratio; however it decreased with increasing the diameter of jet while keeping other parameters constant.

Pourgholam et al [78] investigated numerically the effect of using oscillating blade, rotating blade, and stationary blade on heat transfer from a cylindrical channel at Reynolds number ranging from 50 and 100. They concluded that 32% higher heat transfer performance was achieved at flow Reynolds number of 50 and about 64% enhancement was achieved for the Reynolds number of 100. Shi et al [79] studied numerically the heat transfer enhancement of a channel fitted with oscillating plate. The simulation results showed the potential of the oscillating plate of heat transfer enhancement by disrupting the thermal boundary layer at the walls leading to higher Nusselt number.

Baffigi et al [80] studied convection heat transfer enhancement using active pulsating jet for flow in vertical heating channel at various inclinations. It was concluded that convection heat transfer can be improved using vertical and inclined channels by pulsating flow strategies by up to 17%. Gomaa et al [81] experimentally investigated the effect of oscillating flow on heat transfer from a vertical surface. They concluded that heat transfer enhancement of 45% was achieved due to the oscillation of the flow depending on the pulsed flow amplitude.

Mahapatra et al [82] studied heat transfer enhancement using bi-heater alternating switch over time period placed at the bottom of the enclosure. They investigated the potential of natural convection heat transfer enhancement at Rayleigh number (Ra) ranging from 10^3 to 10^6 and constant Prandtl number of 0.71. The arrangement of bi-heater (two heaters) is such that heat is pulsed at different time periods. Results showed that heat transfer is enhanced by 37.7% and 29% for Ra = 10^3; and Ra= 10^6 respectively at time period of 0.01 seconds. The enhancement decreased as the time period increases to 0.2 for Ra = 10^3 and Ra= 10^6 to 8.4% and 12.5% respectively. Generally the enhancement is significantly affected by the time period (frequency) of the heater On/Off alternating operation.

It is clear from table 2.5 that all the previous work performed to enhance the heat transfer of heat exchangers using flow pulsation were applied for industrial purpose. Table 2.5 also shows that the effect of heat transfer enhancement using flow pulsation is more effective for fluid flow with low Reynolds number. Therefore and due to the low Reynolds number of the flow in domestic hydronic radiator based central heating,

flow pulsation can have potential for heat transfer enhancement that leads to low energy consumption.

Table 2.5 summary of pulsed flow active heat transfer enhancement techniques

Authors	Concept	Test methodology	Application	Range of Reynolds number	% Maximum heat transfer enhancement
Sailor et al [68], Habib et al [74]	Pulsating flow generated using air jet or air blower	Experimental	Industrial heat exchangers	4500-29000	50%
Mohammadpour et al [69]	Pulsating flow generated using square and sinusoidal waveform	Numerical	Industrial heat exchangers	6000	15%
Wang et al [70]	Pulsating flow generated using winglet design	Numerical	Industrial heat exchangers	1200	24%
Saitoh [71]	Pulsating flow generated using valve and eccentric cam connected to pulley	Experimental	Industrial heat exchangers	930	60%
Dec et al [72]	Pulsating flow generated using tail pipe of combustor	Experimental	Industrial heat exchangers	3100 to 4750	2.5 %
Zohir [73]	Pulsating flow generated using ball valve	Experimental	Industrial heat exchanger	10200	20%
Jafari et al [75], Olayiwola et al [76]	Pulsating flow generated oscillating flow mechanism	Numerical and Experimental	Industrial heat exchangers	50-1140	250%
Guoneng et al [77]	Pulsating flow generated using impinging jet (on/off)	Experimental	Industrial heat exchangers	1434 - 1525	230%
Pourgholam et al [78], Shi et al [79], Gomaa et al [81]	Pulsed flow generated using plate blade,	Numerical and Experimental	Industrial heat exchangers	50 - 1000	90.1%
Mahapatra et al [82]	Pulsed flow generated using bi-heater alternating switch	Numerical	Industrial heat exchangers	10000	12.5%

Some of the configurations used for heat transfer enhancement techniques using flow pulsation are shown in figure 2.9.

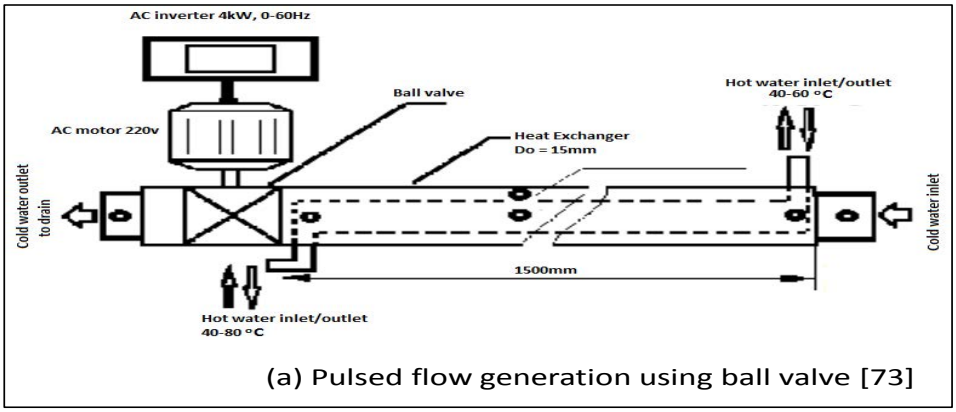

(a) Pulsed flow generation using ball valve [73]

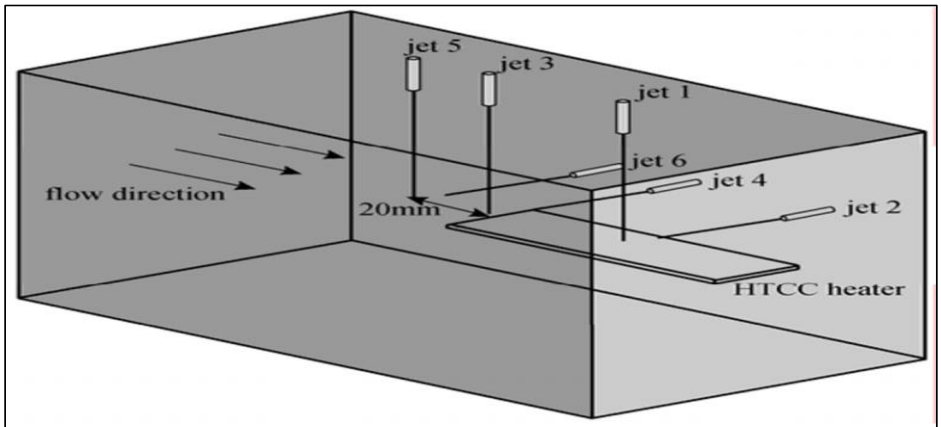

(b) Sketch map of impinging jet [77]

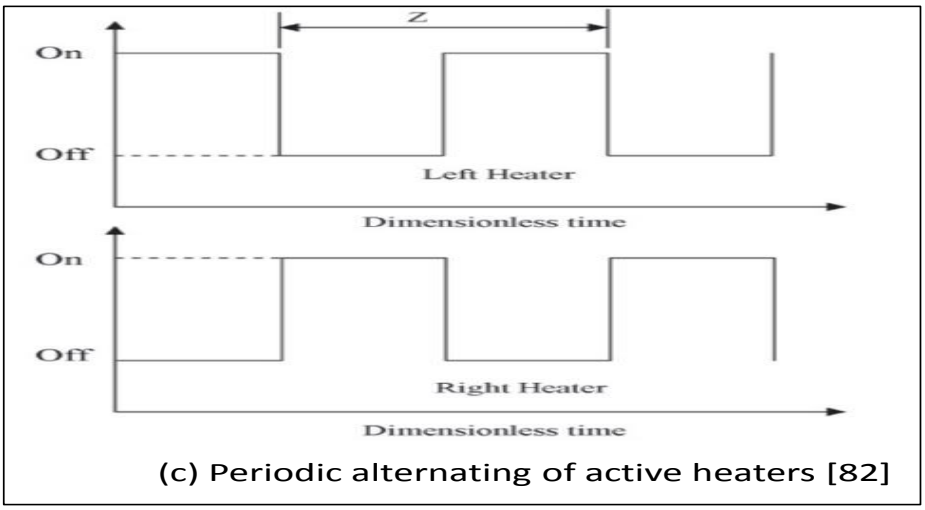

(c) Periodic alternating of active heaters [82]

Figure 2. 9 example of heat transfer enhancement techniques using pulsation

Klein et al [83] conducted experimental tests to investigate the heat transfer enhancement of cooling electronic chips using arrays of flow jets by the principle of flow pulsation. The cooling enhancement of the pulsed flow was investigated at a range of Reynolds number, Strouhal number and actuation amplitudes 756 to 1260, 0 to 0.052 and 0.45mm to 0.75mm respectively. It was concluded that about 34% heat transfer enhancement was achieved.

2.5. Hydronic heating systems and enhancement methods

Considerable research has been carried out to improve the hydronic hot water domestic central heating systems. The studies can be categorised in two groups one related to the heating source and the second is related to the heating appliance. Heating sources include heat pumps, district heating, boiler (Combi boiler, Condensing boiler), and CHP (Combined Heat and Power). The main hydronic heating appliances in the market include panel radiators with and without convective fins, floor heating (Low temperature radiation heating), fan and coils and skirting's (baseboard). Hydronic (water based) heating devices are predominantly used for internal heat emission within the residential sector in Europe. Panel radiators are the most dominant heat emitter appliance in the UK due to their compact design, less space requirement in the rooms and ease of installation to new buildings or retrofitting [84] in existing buildings. The review in this section is focused on the work carried out to enhance the hydronic panel radiator of central heating systems.

Myhren et al [85] studied numerically enhancing the energy efficiency in exhaust-ventilated buildings with a hot water heating system using a ventilation radiator combined with heat emission devices (adding forced air flow on the surface of the radiator (see figure 2.10a)). A CFD model of the proposed system was developed and results showed that; the heat output can be increased by 20% compared to traditional radiators. Myhren et al [7] conducted an optimization work of the heat output of ventilation radiator by varying the distribution of the vertical longitudinal convection fins. The CFD results showed that heat transfer can be enhanced by slightly changing the geometrical design of the fins, decreasing the fin to fin distance and cutting the middle section of the fin array. Myhren et al [4] studied the interaction of the heat emitted from the panel radiator and the ventilation system. They found that convection heat transfer output from panel radiator can be improved by increasing air flow on its heat transferring surface.

Tsioliaridou et al [86] studied numerically and experimentally a new design of the convective radiator combined with ventilation chamber for heating in the winter and cooling in the summer as alternative replacement for the conventional radiator. Different tests were performed to assess the energy consumption of the air conditioning system. They concluded that about 30% of energy consumption can be saved using the newly proposed design compared to the conventional radiator.

Ploski et al [87] investigated enhancing hydronic heating system using baseboard device integrated with air supply. The aim of the work was to minimize the supply temperature by pre-heating the incoming ventilation airflow. They concluded that the

heat output of their proposed system can produce about 21% more heat compared to the traditional hydronic baseboard heating.

Shati et al [88] studied the possibility of enhancing heat output from the panel radiator by coating the wall behind the radiator in different colours. The study concluded that, the wall coated with higher emissivity (smooth black surface) material can improve the heat output of the heating panel radiator. Beck et al [89] investigated the possibility of heat transfer enhancement by placing one or two high emissivity metal sheets between the interior surfaces of double panel radiators. Results revealed that placing two high emissivity metals on the interior side of the double panel radiator can produce about 88% of that of finned double panel radiator.

Kerrigan et al [90] used heat pipes to improve the heat output of domestic heating at supply temperature as low as 55^{o}C. They concluded that the heat pipe based naturally aspirated convector is a possible alternative for replacing of traditional panel radiators subsequent to using low temperature water heating systems such as heat pumps.

Kerrigan et al [91] investigated numerically and experimentally the performance of geothermal heat pump (GHP) using heat pipe based radiators. The GHP is a renewable energy that produces low temperature hot water. Since the supply temperature of conventional radiators is higher than that of GHP alternative design of efficient emitter is required. Heat pipe based radiator was developed to utilise the low grade geothermal heat for domestic heating. They conclude that the power density of the heat-pipe radiator is more than twice that of conventional radiator. Kilkis [92] designed a ground source heat pump (GSHP) combined with energy conversion

system (energy recovery system) to exploit the waste heat supplied to the heating radiator to heat the space numerically at various inlet and outlet flow conditions. GSHP is renewable energy source system and the assessment achieved significant amount of CO_2 reduction compared to radiator operating using condensing boiler as heat source.

Diaz et al [93] studied numerically and experimentally the effect of using stoneware covered aluminium radiator on the heat output of the heating radiators. They concluded that the effect of the stoneware material helps to delay the heating of aluminium radiator due to the difference in specific heat capacity of the materials. This approach helps the aluminium radiator to maintain heating for longer time compared to traditional radiator. Roy et al [94] carried out a study to optimize the heat output from the hydronic panel radiator using phase change material for energy storage. They concluded that 20-25% of energy can be saved compared to the traditional radiators.

Aydar et al [95] studied numerically the effect of different radiator connection at top-bottom same end (TBSE) and top-bottom opposite end (TBOE) on their heating performance. The numerical results showed that TBOE is the optimum radiator connection with higher heat output and the results were validated with experimental work with 3.6% deviation. Embaye et al [96] studied numerically the use of pulsed flow in a radiator. They investigated the pulsed flow at frequencies ranging from 0.0083Hz to 0.033Hz and amplitude ranges from 0.0326kg/s to 0.0422kg/s and results were compared to the constant flow. They concluded that about 20% of energy can be saved due to the pulsed flow compared to the constant flow.

Some of the recent design configurations used to improve the hydronic panel radiator heat output in central heating system are shown in figure 2.11.

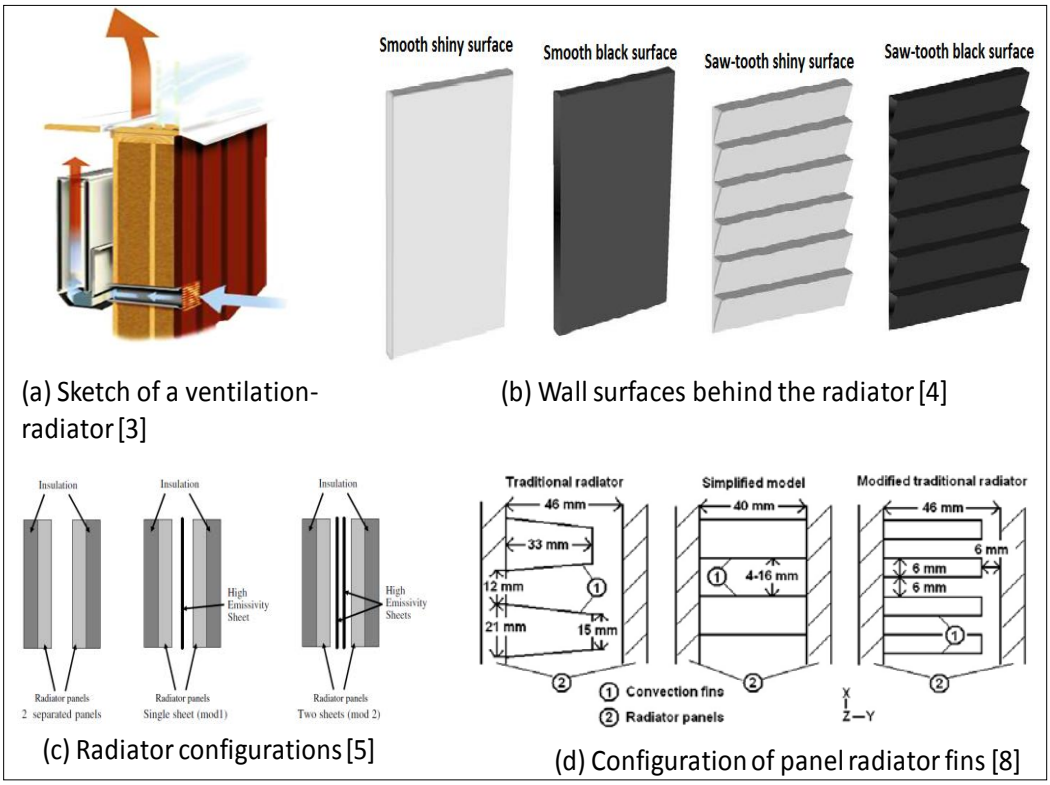

Figure 2.10 examples of techniques used to enhance the performance for hydronic panel radiators

2.6 Indoor comfort

According to ASHRAE standards 55 maintaining indoor comfort is a key objective when one attempts to reduce the energy consumption of buildings integrated with central heating systems. Various research works have been published regarding enhancing the performance of heating systems and the user indoor comfort condition. The indoor environmental comfort can be classified into four main categories; indoor air quality; thermal comfort, acoustic comfort and visual comfort. Investigating the

indoor environmental condition of occupants' satisfaction is the most common practice for the thermal indoor comfort and the indoor air qualities perceptions [97-98]. This review will concentrate on the indoor thermal comfort (indoor comfort temperature and indoor humidity, indoor velocity, indoor radiant temperature) and indoor air quality (IAQ) including indoor CO_2 concentration.

2.6.1 Thermal comfort and Indoor air qualities (IAQ)

According to ISO7730, 2005 indoor thermal comfort is defined as state of mind in terms of satisfaction with thermal environment which depends on the individual psychology and physiology; it can also be defined as the interaction of the air ventilation supply and the heating source of the space to be heated. Indoor air quality is the overall results of the interaction between building volume (envelope) incoming outdoor air, air ventilation system, indoor occupants and contaminant sources [99-100]. Thus any attempt to improve the heating or cooling systems should consider the indoor comfort of the occupants.

Myhren et al [4] studied numerically the indoor comfort using ventilated hydronic radiator as a heat source with ventilating air flow of 7l/s per person as recommended by the Swedish standards. They concluded that ventilated radiators are able to create more stable thermal comfort climate than the traditional radiators. Myhren et al [101] numerically studied the indoor comfort of on office room at high, medium and low radiator surface temperature and floor heating. They concluded that the room installed with low temperature radiators can offer lower indoor temperature fluctuations which

lead to lower energy consumption and better occupants comfort as shown in figure 2.12.

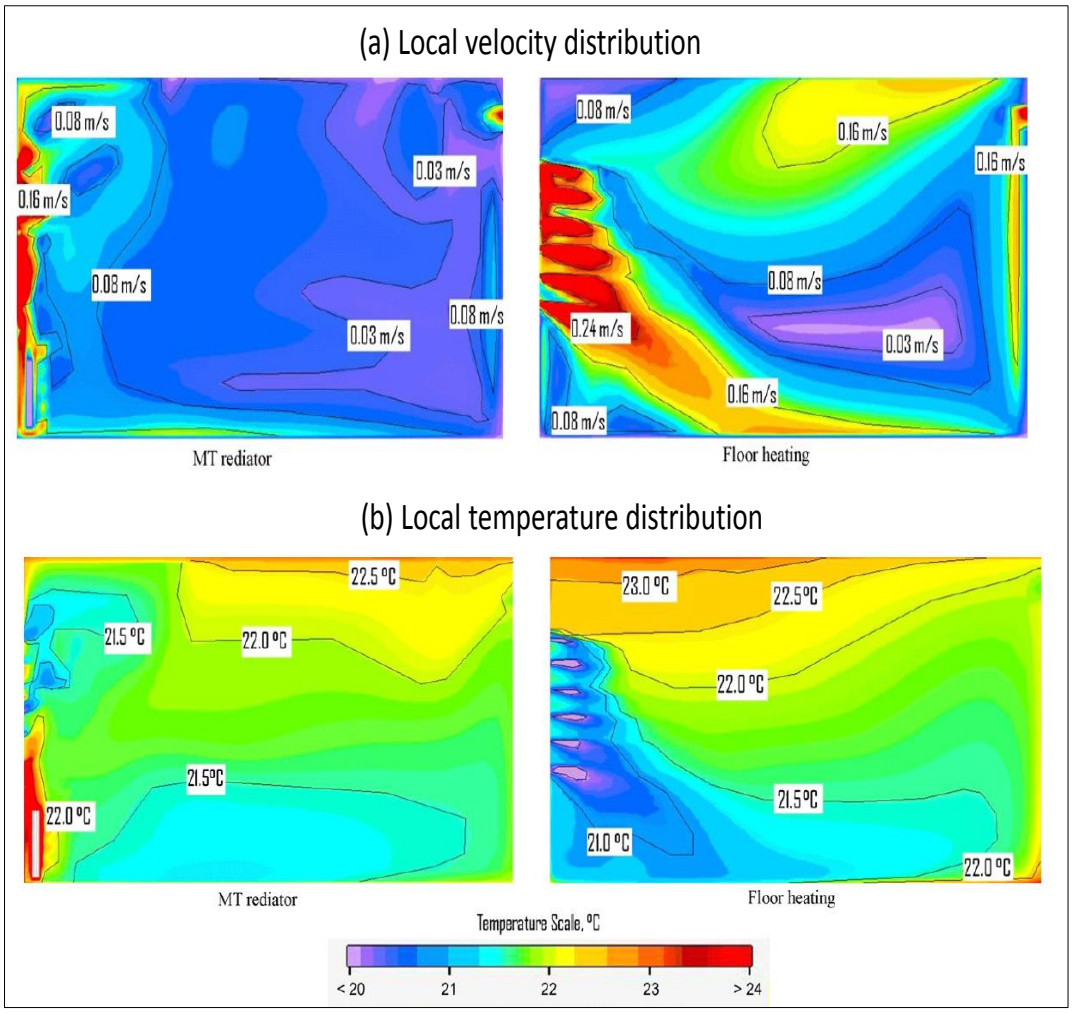

Figure 2.11 CFD predicted contour of (a) Local velocity distribution (b) Local temperature distribution [101]

Sun et al [102] numerically studied indoor environment and space ventilation. The concept of virtual temperature measurement sensor was developed to overcome the temperature stratification of the indoor environment. They concluded that the use of virtual sensor can compensate for the effect of non-uniform temperature distribution in the room. Wang et al [103] coupled Building Simulation (BS) with CFD to predict the thermal comfort in a heated room. They concluded that accurate prediction can be

achieved for naturally ventilated buildings by assuming the outside wind velocity as inlet velocity to the building openings in the external wall.

Horikiri et al [104] investigated the effect of wall thickness on energy consumption and indoor comfort. They concluded that thermal loss of thin wall with thickness of 20cm is 53% higher compared to wall thickness of 40cm while having the same convection heat transfer coefficient. Arslan et al [105] and Ge et al [106] studied the cold draught problem in buildings. They concluded that extreme cold outdoor temperature combined with poor glazing transmittance can cause cold indoor draught. Sevilgen et al [107] developed 3D CFD model of heated space using two radiators as heat source and with virtual sitting of manikin in the room to investigate thermal comfort. They concluded that indoor comfort can be improved using better insulation of outside wall and better window glazing. Properly insulated walls and windows created stable indoor comfort and low energy consumption.

Tian et al [108] investigated experimentally the indoor temperature, air speed, and CO_2 concentration in a ventilated office. The thermal comfort and thermal efficiency was studied using well defined thermal indices including Predictive Mean Vote (PMV), calculated from measured data targeting to satisfy the requirement of ISO 7730 and ASHRAE 55-2010. They concluded that stratum ventilation with supply air of 21^{o}C produce good comfort of occupants including lower temperature difference following PMV (-4 to 1.1), lower CO_2 concentration, comfortable air velocity and acceptable ventilation effectiveness of 1.5. Liua et al [109] investigated numerically the thermal comfort of a conditioned room using stratum ventilation system. They described the indoor temperature, indoor velocity and Predicted Mean Vote (PMV)

values and concluded that all results were in agreement with recommendation of ISO7730 regulations.

Moriske et al [110] experimentally investigated indoor air pollution using three types of heating systems including coal burning, open fire burning and central heating system. The concentrations of CO and CO_2 were measured in 16 homes comparing 7 coal burning homes, 1 open fire burning home and 8 central heating systems. They concluded that coal burning and open fire burning produce higher CO and CO_2 concentration that can cause indoor discomfort.

McGill et al [111] studied the indoor air quality (IAQ) in UK homes with natural and mechanical ventilation. According to the case study, it was found that there is high CO_2 concentration in most of the tested homes due to lack of appropriate ventilation systems. Ncube et al [112] carried out a preliminary study to develop a new technique for rapid assessment of Indoor Environment Quality (IEQ) in the UK air conditioned offices. They concluded that the main factors that require rapid measurement are thermal comfort, Indoor Air Quality (IAQ), acoustic comfort and lighting. Based on their results an empirical formula was developed for assessing the indoor air quality and used in a computer program called Indoor Environment Quality Assessment Tool (IEQAT).

Seoa et al [113] and Yang et al [114] developed a model to optimize the heating and cooling (HVAC) the energy consumption in buildings using genetic algorithm in the TRNSYS software. The proposed multi-island genetic algorithm optimization model was capable of reducing energy consumption of buildings significantly with

acceptable comfort criterion. Buli et al [115] investigated numerically and experimentally the effect of CO_2 sensor position on the control response of the ventilating system. Based on the results obtained it was concluded that positioning the CO_2 sensor at the centre of the room gives accurate measurement of concentration regardless of the room height. Warren et al [116] studied the potential of CO_2 based control system on the energy consumption of buildings. They concluded that about 50% of energy consumption can be saved using ventilation system controlled by carbon dioxide (CO_2) concentration response sensor.

Chan et al [117] studied the effect of airborne bacterial profile in indoor environment and recommended that airborne bacteria should be included in the indoor air quality (AIQ) standards. Wolkoff [118] investigated the indoor concentration of volatile organic compounds (VOC) on the health and comfort of the indoor occupants. He concluded that threshold measuring of odour and irritation are recommended in the indoor air quality to assess the effect of deteriorated performance for cardiovascular as well as pulmonary. Wan et al [119] introduced a new method of indoor temperature and indoor relative humidity set up to save energy from buildings. They recommended that the cooling load can be reduced by setting the indoor temperature and indoor humidity (combination indoor temperature and indoor humidity control system).

Makhoul et al [120] numerically studied the thermal comfort of occupants using the integrated ceiling diffuser and personalised ventilator coaxial nozzle system. By placing the coaxial nozzle between air stream and the room air it allows effective delivery of clean air. Various simulations were carried out to assess the effect of

nozzle supply temperature and flow rate on the performance of the cooling system and on occupant comfort and they concluded that using this method better thermal comfort of the occupants can be maintained while energy savings of 34% is possible compared to the conventional systems

Chengmin et al [121] assessed the domestic heating system on the basis of heat source including heat pump, coal based boiler and gas based boiler to investigate the environmental and economic impacts. Based on the assessment for one year operating scenario of the three mentioned sources; the heat pump can offer better indoor comfort and good economic impact if the COP is above 3. While if the COP value is below 3, it offered better indoor comfort but high economic cost.

2.7. Effect of control system on energy consumption of central heating system

Smart control management of central heating system can play important role to reduce energy consumption and improve the comfort of the occupants. Heating, Ventilation and Air Conditioning (HVAC) systems are designed for extreme condition demands of the space to be heated or cooled. The load of the buildings envelope is changing throughout the day depending on the occupants' activities, ambient temperature, solar load, lighting and equipment loads. For the case of heating and ventilation appliances the design capacity is always larger than the actual load demand of the space to be heated. Therefore the deviation from the design load leads to high energy consumption of the buildings and affects the occupants comfort if the system is

running without appropriate control system [122]. In this section the work done related to buildings control system is reviewed.

Peeters et al [123] studied the energy consumption of heating appliances in Belgium. The research found that the operating efficiency of heating appliances in operation is as low as 30%. To overcome the excess energy consumption it was recommended to design appropriate control system that better matches supply to demand.

Tahersima et al [124] developed a control system to eliminate the drawback of thermostatic radiator valve (TRV) as shown in figure 2.12. They concluded that the contribution of the TRV to energy saving and comfort was significant; but with the drawback of high oscillation and instability during the low heating demand of heating conditions. Thus they developed a control system called linear parameter varying model (LPV) which was able to eliminate the oscillation due to TRV. LPV advanced controls system helped to minimise the operating process system fluctuation.

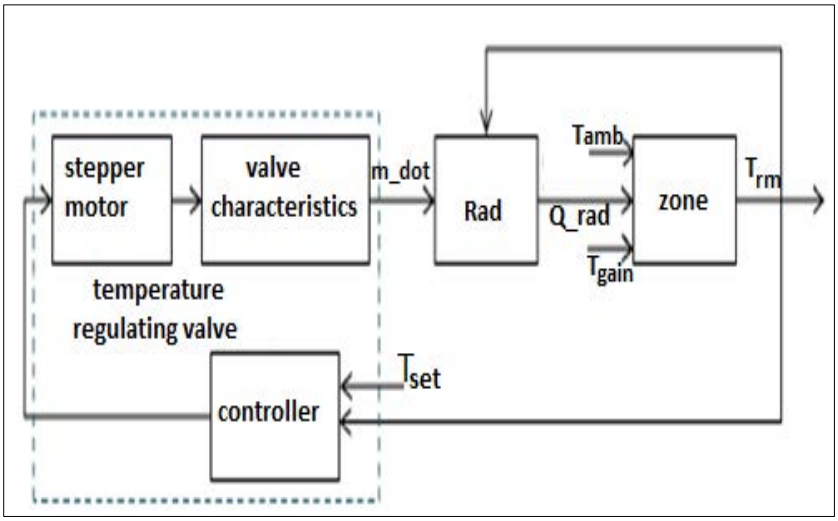

Figure 2.12 closed loop control system of room and radiator [124]

Embaye et al [125] investigated the fluctuation of indoor temperature using PID control system compared to the On/Off control system. Results showed that using PID control system can create better indoor stability with lower indoor temperature fluctuations of $\pm 1^{o}C$. They also concluded that the PID control system can reduce the energy consumption and improve indoor comfort. Gamberi et al [126] developed a mathematical model to control the central heating system using Newton–Raphson Method (NRM) in Matlab/Simulink to investigate the capability of the software on buildings thermodynamic modelling. They conclude that Simulink is a potential design software for buildings thermodynamical modelling. Kulkarni et al [127] investigated the optimal control in residential space-conditioning system by replacing the two position control system (On/Off) with proportional control strategy. They concluded that the proposed control system was advantageous for stability and comfort of the occupants.

Qi et al [128] developed a multi input multi-output (MIMO) control strategy that can control indoor air temperature and humidity simultaneously by varying the speeds of both compressor and supply fan of the HVAC system. They concluded that the MIMO control strategy created better indoor temperature and humidity conditions compared with single input and single output (SISO) and On/Off control systems. Homod et al [129] studied integrated control system by controlling both the available natural ventilation and HVAC system in buildings. They improved the conventional control system using Model Guide For Comparison (MGFC) and applied physical empirical hybrid modelling to predict the rate of indoor environment change for the thermal comfort. They concluded that the integrated control system maintained the thermal comfort of indoor occupants at lower energy consumption.

Nassif [130] developed Demand based Controlled Ventilation (DCV) to control the level of indoor CO_2 concentration and to reduce energy consummation. He concluded that about 23% of energy can be saved compared to the traditional control system. West et al [131] developed Model Predictive Control (MPC) system to optimize the thermal comfort, indoor air quality (IAQ) including CO_2 and associated energy consumption of the heating and ventilation system. They concluded that the building model operating for 51 days and 10 days showed that about 19% and 32% reduction in energy consumption can be achieved respectively.

Moon et al [132] studied Artificial Neural Network (ANN) using predictive and adaptive control logic for indoor comfort control. They concluded that using this approach, the standard deviation of indoor temperature percentage of overshoots and undershoots of the desired indoor comfort ranges can be decreased which results in a user comfort. Bakos et al [133] developed Artificial Neural Network (ANN) to control a small scale central heating system. Various tests were carried out using neural networks control system and concluded that the neural networks can be used for dynamic control modelling application of complex non-linear energy system.

Gustafsson et al [134] developed a control system to improve the district heating system substation. The new control was designed to increase the ΔT of the radiator (heat emitter) to enable lower return temperature (boiler) to the district heating source. They concluded that this approach leads to higher primary fuel efficiency of the district heating system as shown in figure 2.13.

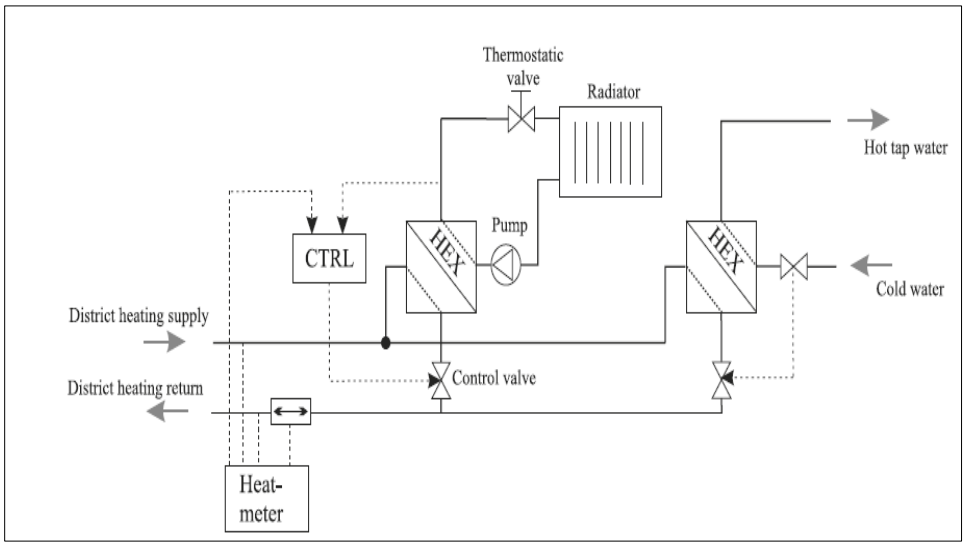

Figure 2.13 district heating substation using energy meter information for space-heating control [134]

Liu et al [135] studied adaptive control system to reduce energy demand of building on the basis of user comfort profile and concluded that about 11% of energy saving can be achieved compared to the traditional control system. Lehmann et al [136] studied a wireless control technique for the thermostat (On/Off valve) and concluded that about 30% of energy can be saved compared to the traditional control strategy currently employed in central heating.

Schmelas et al [137] developed a control system for heating and cooling system of buildings using adaptive and predictive computation method based on multiple linear regressions. The control algorithm was compared to conventional control strategies of building thermal energy services. They concluded that the adaptive and predictive computation control system achieved the pump running time saving of 81% while the indoor thermal comfort was improved compared to the conventional system. Liao et al [138] investigated experimentally and numerically the use of boiler control to reduce

energy consumption of heating systems. They controlled the boiler based on the demand and the outdoor temperature as shown in figure 2.14. Results showed that appropriate control of the boiler can reduce energy consumption by 20% because most domestic boilers are oversized to accommodate energy margin capacity. Thus operating the boiler with optimum control system is necessary to better match the heat load of heating systems to the demand.

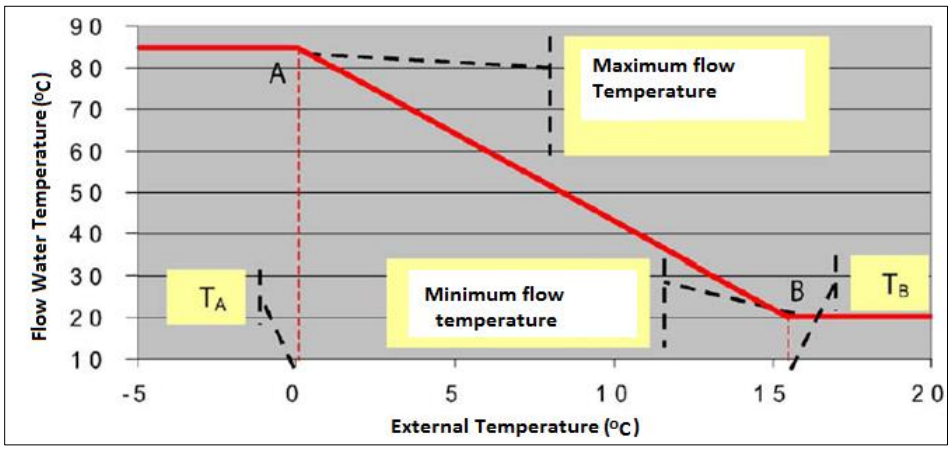

Figure 2.14 external temperature compensated boiler control algorithm [138]

2.8 Summary

In this chapter a comprehensive literature review was carried out regarding research work for improving the performance of hydronic central heating systems in terms of energy consumption and thermal comfort of occupants. The review also included means of enhancing the heat transfer performance of fluids in various applications such as using corrugated tubes, attaching grooves or obstacles to the channel surfaces, fitting nozzles/snails within the fluid channel to generate vertices and enhance turbulence and mixing thus increasing heat transfer rate. The use of flow pulsation for enhancing heat transfer was also reviewed and have shown promising results in

applications like process heat exchangers, electronic cooling and various industrial applications. It also included research on the various control systems used in the HVAC systems and the comfort criterion used to assess human comfort.

There are many techniques for enhancing convective heat transfer, most of these techniques require significant changing on the geometry of the radiators; thus they cannot be applied for existing heating systems. However pulsating the flow in channels has shown significant heat transfer enhancement and can be applied by changing the operation of the radiator valve. Thus it can be applied to existing as well as new heating systems.

Although, various studies have been carried out to enhance heat transfer of heating or cooling devices using flow pulsation for various industrial applications; little attention has been given to using these methods in panel radiator based hydronic heating systems. To the best of the author's knowledge hydronic central heating system operating using flow pulsation has not been reported except in a patent filed by the company supporting this project and the publication by the author of this thesis.

Therefore, this work aims to investigate the effects of different flow pulsation schemes on the performance of the hydronic radiators of domestic central heating system to achieve energy saving without compromising the user comfort. This work involves dynamic control modelling, numerical modelling (CFD), finally experimental testing to validated the modelling and prove the concept.

CHAPTER 3

DYNAMIC MODELLING OF HYDRONIC RADIATOR HEATING SYSTEM

3.1 Introduction

The control strategy used in any domestic central heating system can play a major role in improving its energy consumption and carbon emissions. Current control technologies commonly used in residential homes and offices in the UK are based on switching the radiators On/Off at certain intervals using radiator valves, thermostats and timing programmers. The interest of using advanced control systems such as adaptive control, wireless thermostat control, model predictive control (MPC) for central heating is growing gradually. These control techniques are shown to improve the indoor environments of the occupants and reduce energy consumption by 30% [135-147]. Although, various studies have been carried out to enhance industrial heating and cooling devices using flow variation as well as advanced control systems little attention has been given to the residential hydronic heating systems.

Therefore, this chapter investigates the effects of different flow schemes on the performance of the hydronic radiators of domestic central heating system and develops a control strategy that can achieve energy saving from heating and ventilation without compromising the user comfort. The work involves mathematical modelling of radiator central heating system comprising of boiler (heat source), room

(heat load) and ventilation (fresh air source). The research work also evaluated the indoor environment in terms of the indoor thermal comfort (temperature, humidity) and the indoor air quality (CO_2 concentration) using MatLab/Simulink software. Part of the work presented in this chapter has been published in [125].

3.2 Modelling central heating system in MatLab/Simulink

Simulink is industrial software developed for graphical programming by Math works for dynamic modelling, simulation, and analysis of multi domain systems. It consists of graphical interface block diagram tools, customizable block libraries and extensive integration tools with the MATLAB work space and M-files. Simulink is widely used for automatic control, digital signal processing and Model Based Design (MBD) in aerospace and automation industries [125-126]. Figure 3.1 shows the flow diagram of the overall model of the central heating system comprising of sub models for boiler, hydronic radiator, heated space and the control system. The developed control model was designed for constant and pulsed flow operating scenarios of the radiator in MatLab/Simulink software.

Figure 3.2 shows a schematic diagram of hydronic central heating system including heat source (boiler), circulation pump (pump), bypass valve (B.valve), return valve (R. valve), inlet valve, outlet valve (O. valve), panel radiator heat emitter (P. radiator) and heated room (heated space). The main heat losses from the proposed room are; heat loss by ventilation, heat loss through the window and heat loss through building structure. Each of the components is evaluated analytically and simulated dynamically using MatLab/Simulink as a single component and then integrated to form a complete

central heating system. The indoor comfort temperature is used to drive the control algorithm for the proposed central heating system used in this work. This indoor temperature is calculated dynamically using the transient mass and energy conservation equations.

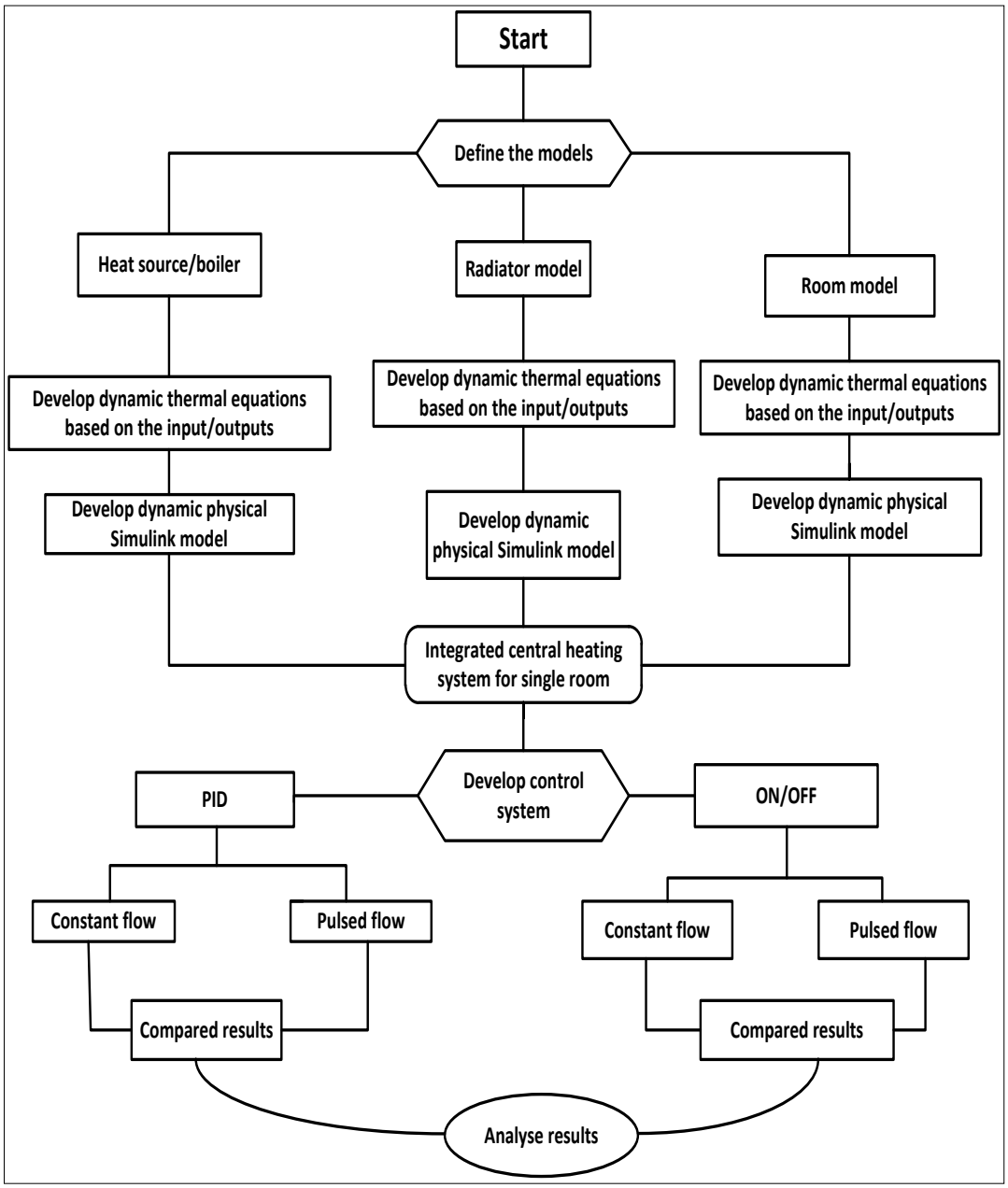

Figure 3.1 flow diagram of developed dynamic model of the central heating system

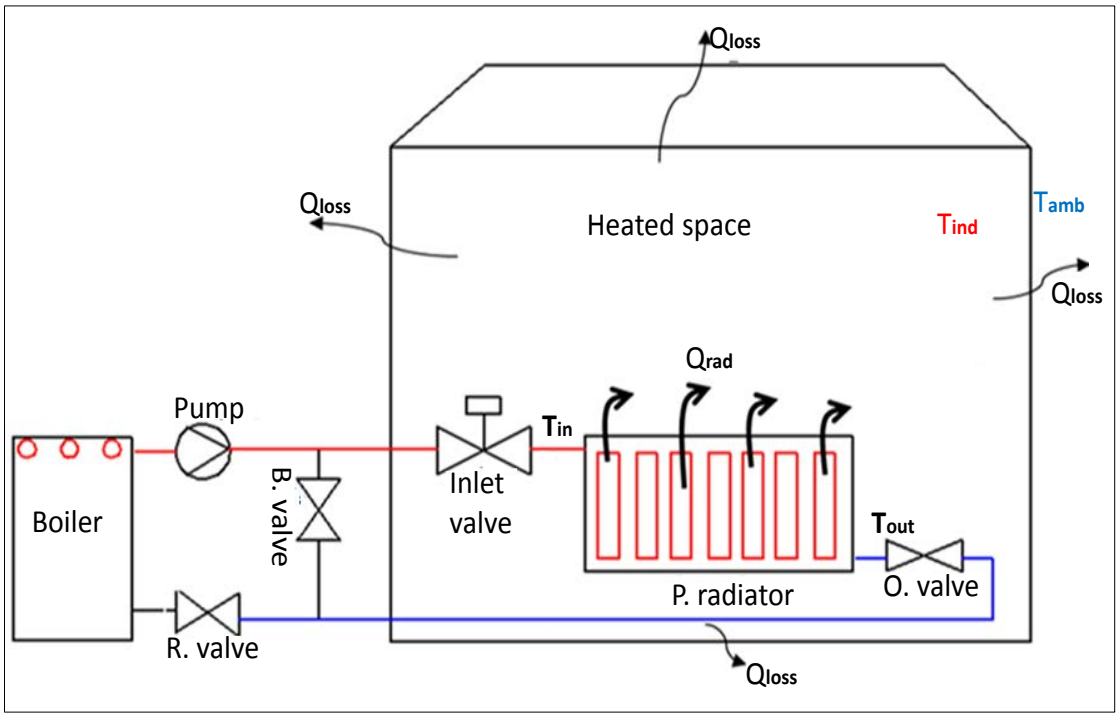

Figure 3.2 schematic description of the central heating system for proposed work

3.2.1 Dynamic modelling of boiler (heat source)

Figure 3.3 shows a schematic diagram of the energy flow in a gas fired boiler commonly used in domestic central heating systems. The energy balance of gas fired boiler consists of energy input from the combustion of fuel ($\dot{Q}_{input}$), heat loss to the surrounding room ($\dot{Q}_{rm}$), heat loss in the flue gas ($\dot{Q}_{flue}$) and the useful heat energy for production of hot water ($\dot{Q}_{w}$) [27, 145]. The modelled boiler for this work is assumed to be gas fired Combi-boiler with 90% efficiency and stainless steel heat exchanger according to the manufacturer (Worcester Bosch Group).

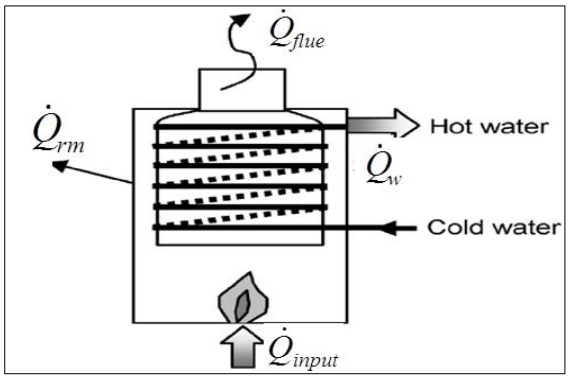

Figure 3.3 schematic diagram of boiler (heat source)

The transient energy balance equation for the boiler is given as eq. (3.1).

$$((MCp)_{hex} + (MCp)_{w}).\frac{d}{dt}\left(\frac{T_{in} + T_{out}}{2}\right) = \eta * \dot{Q}_{input} - \dot{Q}_{w} \tag{3.1}$$

Where;

$$\dot{Q}_{input} = mg.h_g = \dot{Q}_{rm} + \dot{Q}_{w} + \dot{Q}_{flue} \tag{3.2}$$

$$\dot{Q}_{w} = \dot{m}.C_p.(T_{out} - T_{in}) \tag{3.3}$$

$$\eta = \frac{\dot{Q}_{w}}{\dot{Q}_{input}} \tag{3.4}$$

Equation 3.1 can be rearranged to determine the hot water outlet temperature as eq. (3.5).

$$T_{out} = 2\int\left(\frac{\eta.\dot{Q}_{input}}{(MCp)_{hex} + (MCp)_{w}} - \frac{\dot{Q}_{w}}{(MCp)_{hex} + (MCp)_{w}}\right)dt \tag{3.5}$$

Where symbols are defined as; $\dot{Q}$, η, M, T, C_p, mg, t and h_g are heat transfer rate (W), efficiency (%), mass (kg), temperature (^oC), specific heat capacity (kJ/(kg.K), mass flow rate of natural gas (kg/s), time (s) and heating value of gas (kJ/kg) respectively. The subscripts are defined as: input, hex, out, in, w, rm, and g are input, heat exchanger, outlet, inlet, water, room, and natural gas respectively.

Equation 3.5 was used to develop the dynamic model of the boiler using Simulink software and figure 3.4 shows the model block diagram including the input, output and control parameters. The input parameters include heat input from the natural gas (Qi_dot), temperature of the inlet water (T_in), and inlet mass flow rate of the water to be heated (m_dot). The output parameter is the boiler outlet temperature which is inlet to the radiator. The control system is driven by the outlet temperature of the boiler and controls the flow rate of natural gas using the feedback controller, temperature sensor and set point.

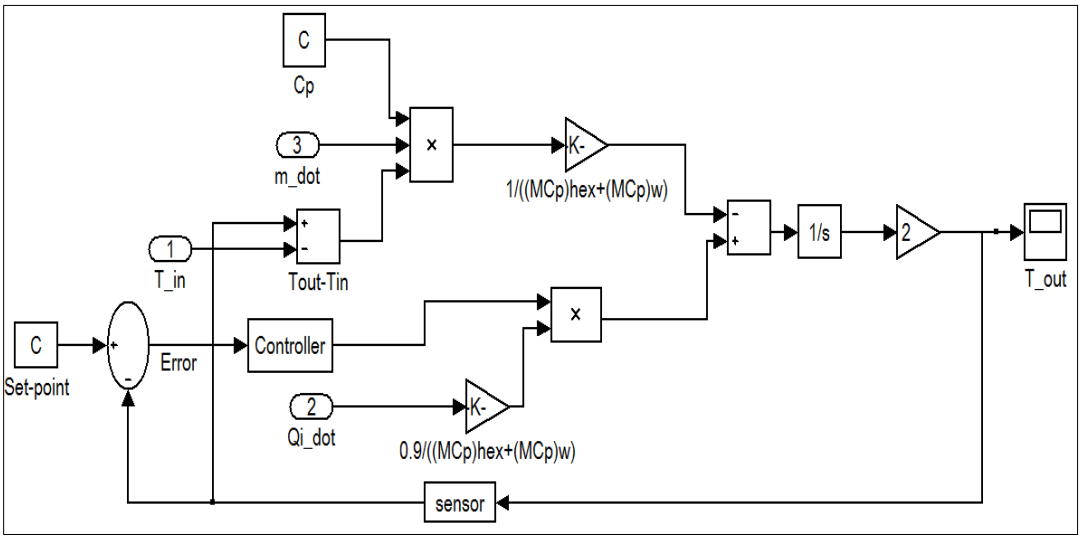

Figure 3.4 the Simulink block diagram of the boiler dynamic model

3.2.2 Dynamic modelling of hydronic panel radiator (heat emitter)

Hydronic panel radiator is a heat emitter that uses hot water as energy carrier and emits heat from its metallic surface. Hydronic panel radiators are the most common heat emitters used in UK and EU due to its compact design. In central heating system the radiator is operating under closed loop condition commonly controlled using thermostatic valve (TRV) [146]. There are two types of hydronic panel radiators namely non fined and fined hydronic panels with the same duct configuration design. The radiator used in this work is assumed to be single fin panel radiator known as type11. Figure 3.5 shows a schematic diagram highlighting the energy and mass flow into and out of the radiator.

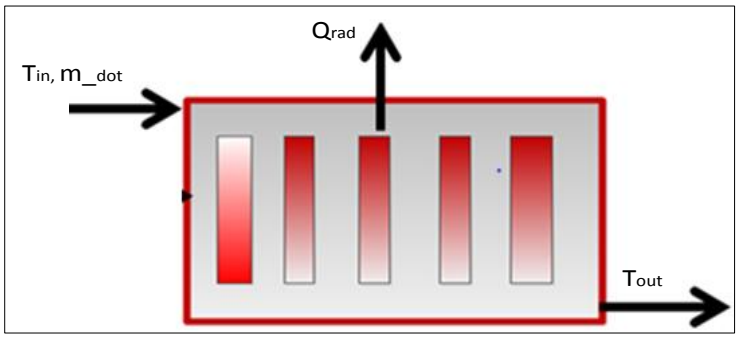

Figure 3.5 schematic diagram of the hydronic panel radiator

The transient energy equation of the radiator is expressed by eq. (3.6) where $\dot{Q}_s$ is the radiator heat output (nominal heat output) calculated using eq. (3.7) and $\dot{Q}_{rad}$ is the actual radiator heat output determined by eq. (3.8).

$$((MCp)_{rad} + (MCp)_w)\frac{d}{dt}\left(\frac{(T_{out} + T_{in})_{rad}}{2}\right) = \dot{Q}_s - \dot{Q}_{rad} \tag{3.6}$$

$$\dot{Q}_S = \dot{m}_W . Cp_W . \left(T_{rad,in} - T_{rad,out} \right) \tag{3.7}$$

$$\dot{Q}_{rad} = (Ua)_{rad} . A_{rad} (LMTD) \tag{3.8}$$

Ua is the overall heat transfer coefficient of the radiator calculated by eq. 3.9 as:

$$\frac{1}{(Ua)} = \frac{1}{h_{rad/w}} + \frac{L_{rad}}{k_{rad}} + \frac{1}{h_{rad/air}} \tag{3.9}$$

Where;

$$h_{rad/air} = h_{convection} + h_{radiative}$$

Where: $h_{rad/air}$ is a radiation and convection heat transfer coefficient between the radiator and air in the room; $h_{rad/w}$ is the convective heat transfer coefficient between hot water and the radiator metal skin; k_{rad} is the radiator skins conductivity and L_{rad} is the thickness of the radiator skin.

LMTD is the Log Mean Temperature Difference of the radiator calculated using eq. (3.10).

$$LMTD = \frac{T_{rad.in} - T_{rad.out}}{\ln\left(\frac{T_{rad.in} - T_{ind}}{T_{rad.out} - T_{ind}} \right)} \tag{3.10}$$

Equations (3.6) to (3.10) were rearranged to determine the radiator outlet temperature as:

$$T_{rad.out} = 2\int\left(\frac{(\dot{m}Cp)_w}{(MCp)_{rad}+(MCp)_w}(T_{in}-T_{out})_{rad} - \frac{((Ua).A)_{rad}}{(MCp)_{rad}+(MCp)_w)}(LMTD)\right)dt \qquad (3.11)$$

Where the symbols defined as: A, $\dot{Q}$, LMTD, M, Ua, T, C_p, $\dot{m}$ and t are; area (m^2) heat transfer rate (W), Log Mean Temperature Difference (^oC), mass (kg), overall heat transfer coefficient ($W/m^2.K$), temperature (K), specific heat capacity (J/kg.K), mass flow rate (kg/s) and time (s) respectively. The subscripts rad, out, in, w and ind are radiator, outlet, inlet, water and indoor respectively.

Figure 3.6 shows the Simulink block diagram of the hydronic radiator modelled using equation 3.11, it consists of the radiator input parameters, output parameters and controller system.

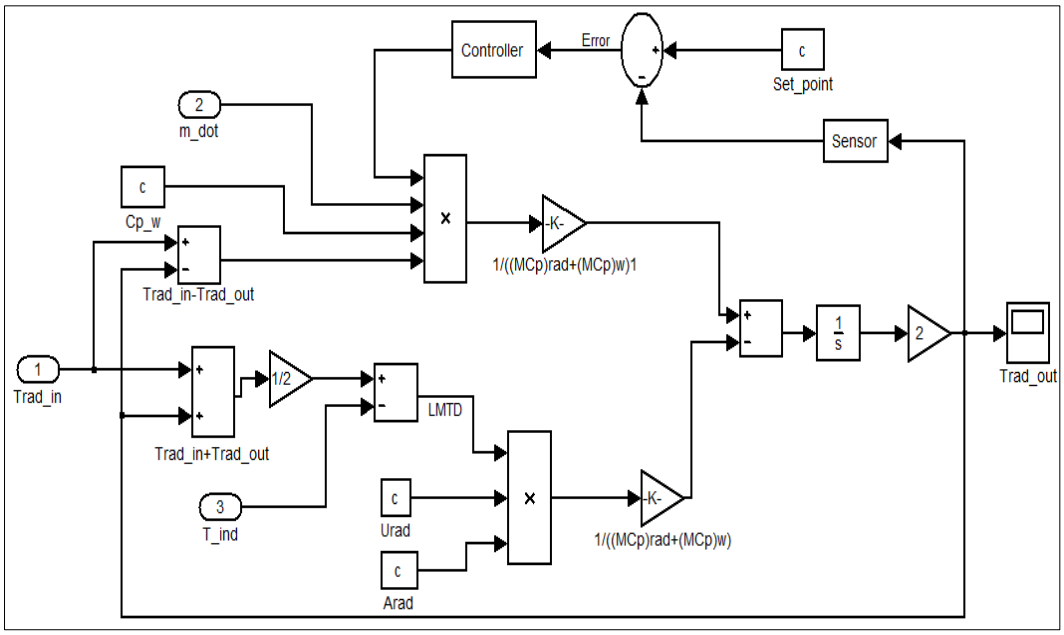

Figure 3.6 the dynamic Simulink diagram of the radiator

The input parameters are the radiator inlet temperature ($T_{rad,in}$) and mass flow rate of hot water (m_dot), while the output parameters are the heat output of the radiator and

water outlet temperature. The control scheme is driven by the temperature output of the radiator which is used to control the hot water mass flow rate to the radiator. The control box consists of the temperature sensor, set point and the main feedback control.

3.2.3 Dynamic modelling of the room (space to be heated)

Figure 3.7 shows a schematic diagram of the heated space with hydronic radiator illustrating all heat transfer processes including; heat loss through the walls, ceiling, floor, windows, heat input to the room from the Sun and the radiator (heat emitter), mechanical ventilation and infiltration due to the temperature and pressure difference between the heated space and the ambient.

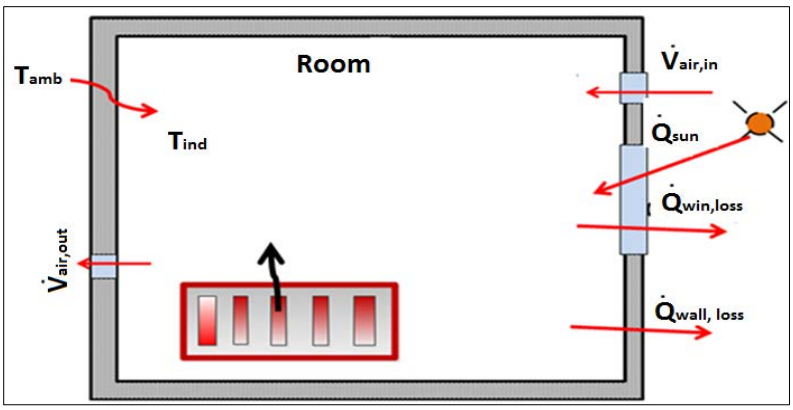

Figure 3.7 schematic diagram of the room space to be heated

Eq. (3.12) gives the transient energy transfer of the room including; input heat by source ($\dot{Q}_{rad}$), internal heat gain ($\dot{Q}_{gain}$), ventilation heat loss ($\dot{Q}_{sen.vent}$), building structure heat loss ($\dot{Q}_{env}$) and heat loss via window ($\dot{Q}_{win}$).

$$V_{rm} \cdot \rho_{air} C_{p,air} d\frac{T_{ind}}{dt} = \dot{Q}_{rad} + \dot{Q}_{gain} - \dot{Q}_{sen.vent} - \dot{Q}_{env} - \dot{Q}_{win} \quad (3.12)$$

The heat transfer via the window includes the heat transfer by conduction and convection of the glazing and the solar heat gain coefficient (SHGC). The heat loss via window and the solar heat gain to the room are calculated mathematically using eq. (3.13) and eq. (3.14).

$$\dot{Q}_{win} = A_{win} (Ua)_{win} (T_{so} - T_{ind}) + I_{so} . SHGC . A_{win} \quad (3.13)$$

$$T_{so} = T_{amb} + \frac{\alpha . I_{so}}{h_{amb}} \quad (3.14)$$

Where: $\dot{Q}_{win}$, A , Ua, T_{so} , T_{ind}, T_{amb}, I_{so}, SHGC, α and h_{amb} are rate of heat transfer through window (W), surface area (m^2), overall heat transfer coefficient (W/(m^2.K)) solar temperature (^oC), indoor comfort temperature (^oC), outdoor temperature (^oC), solar heat flux (W/m^2), solar heat gain coefficient (W/m^2), radiation absorptivity (-) and outdoor convection heat transfer coefficient (W/(m^2.K)) respectively.

The heat transfer through the building structure ($\dot{Q}_{env}$) includes the heat transfer via the roof, floor and walls as given by eq. (3.15). Figure 3.8 shows a schematic diagram for the heat transfer process between the indoor temperature (T_{ind}) and ambient temperature (T_{amb}) through a wall consisting of several layers. The overall thermal resistance to heat transfer through the composite wall can be calculated as the sum of individual resistances of the layers according to Kirchhoff current law using eq. (3.16) to eq. (3.18) [147].

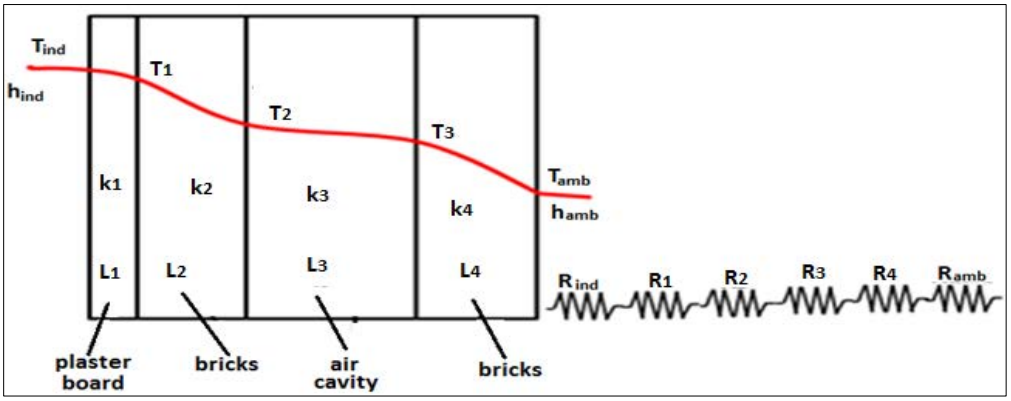

Figure 3.8 heat transfer through the wall layers of building and its thermal resistance

$$\dot{Q}_{env} = (Ua.A)_{wall}(T_{ind} - T_{amb}) + (Ua.A)_{roof}(T_{ind} - T_{amb}) + (Ua.A)_{floor}(T_{ind} - T_{soil}) \quad (3.15)$$

$$(Ua) = \frac{1}{R_{total}} \quad (3.16)$$

$$R_{total} = R_{ind} + R_1 + R_2 + R_3 + R_4 + R_{amb} = \frac{1}{h_{ind}} + \frac{L_1}{k_1} + \frac{L_2}{k_2} + \frac{L_3}{k_3} + \frac{L_4}{k_4} + \frac{1}{h_{amb}} \quad (3.17)$$

$$R_{total} = \frac{1}{h_{ind}} + \sum_{0}^{j} \frac{l_j}{k_j} + \frac{1}{h_{amb}} \quad (3.18)$$

Where: $\dot{Q}_{env}$, A, Ua, T_{ind} ,T_{amb} , h_{amb}, h_{ind}, R, k_j and l_j, are heat transfer through room envelope (W), surface area (m^2), overall heat transfer coefficient ($W/m^{2.}K$), indoor temperature (^oC), outdoor temperature (^oC), outdoor heat transfer coefficient ($W/m^{2.}K$), indoor heat transfer coefficient ($W/m^{2.}K$), wall layer thermal resistance ($m^{2.}K/W$), thermal conductivities of j^{th} wall layer (W/m.K) and j^{th} wall layer thickness (m) respectively.

Buildings always need fresh air supply to dilute the indoor contamination; as a result ventilation is required to supply enough fresh air to the indoor occupant. The energy consumption due to ventilation depends on the number of air changes (ACH) and volume of the room. The sensible heat loss due to ventilation is calculated using eq. (3.19) to (3.20).

$$\dot{Q}_{sen.vent} = \rho_{air} \cdot \dot{V}_{air} \cdot C_{p,air} \cdot (T_{ind} - T_{amb}) \tag{3.19}$$

$$\dot{V}_{air} = \frac{ACH \cdot V_{rm}}{3600} \tag{3.20}$$

Where: $\dot{Q}_{sen.vent}$, V_{rm}, $\dot{V}$, ρ, Cp, and ACH, are sensible heat ventilation (W), volume of room (m^3), volume flow rate (m^3/s), density (kg/m^3), specific heat capacity (kJ/kg), and air change of (1/hr) (the value of air change is 0.6(1/hr) and can be found in [101]) respectively .

The internal heat gain of the room ($\dot{Q}_{gain)}$ is the summation of heat generated from computers, people due to metabolic process and respiration as well as heat released from electrical lights as expressed by eq. (3.21).

$$\dot{Q}_{gain} = People + computer + electrical \tag{3.21}$$

Eq. (3.12) can be rearranged to determine the room temperature variation with time to give eq. (3.22).

$$T_{ind} = \int \left(\frac{1}{V_{rm} \cdot \rho_{air} C_{p,air}} (\dot{Q}_{rad} + \dot{Q}_{gain} - \dot{Q}_{vent} - \dot{Q}_{env} - \dot{Q}_{win}) \right) dt \quad (3.22)$$

Figure 3.9 shows the block diagram of the radiator heating Simulink model developed for the heated space based on equation 3.22. It consists of four sub-models representing window heat transfer (Q_win Subsys), ventilation heat transfer (Q_vent Subsys), internal heat gain (Q_int Subsys) and building envelope heat loss (Q_env Subsys). Also Simulink model includes the control system model consisting of control box, temperature sensor, set point, driver parameter (T_ind) and controlled parameter (Q_rad).

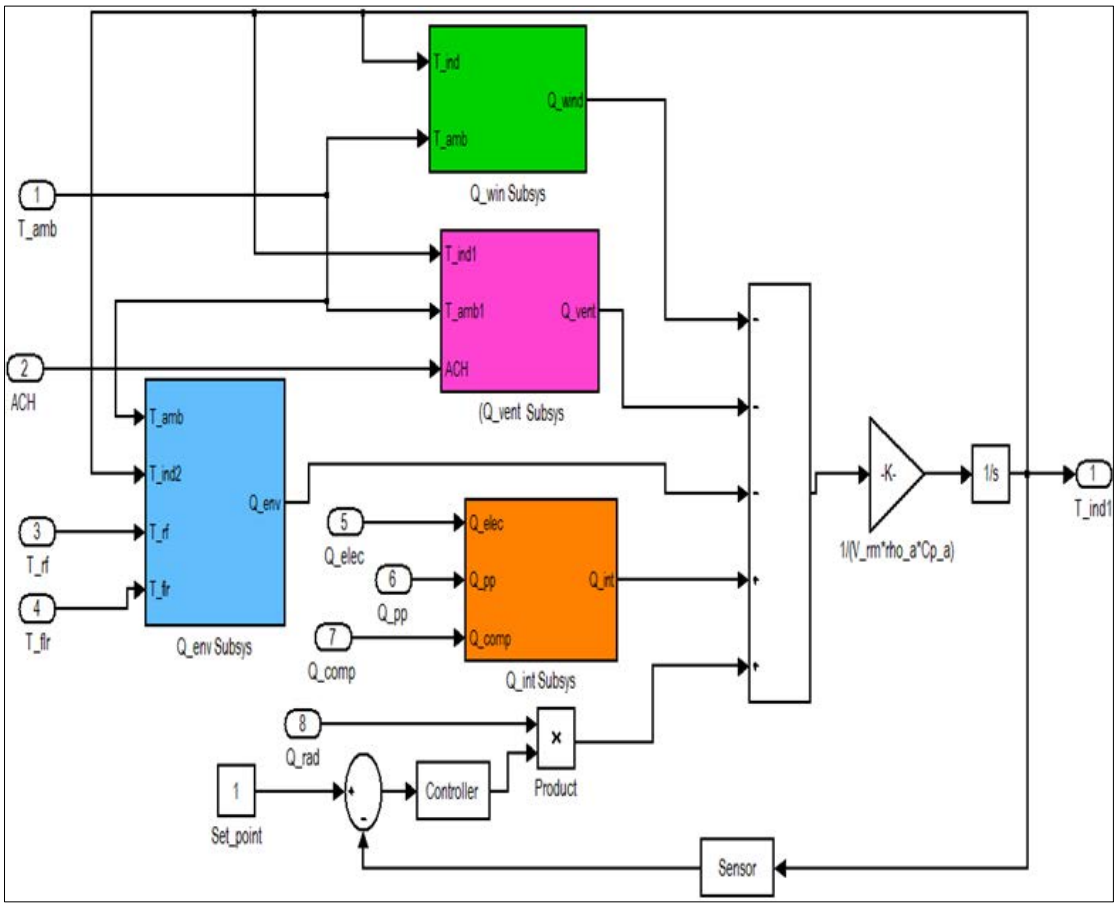

Figure 3.9 the dynamic Simulink diagram of the room space to be heated

3.3 Control system

The heating, ventilation and air conditioning (HVAC) system is designed to deliver higher capacity than the demand of space to overcome extreme conditions. The load of the buildings envelope is changing throughout the day and depends on the occupants, ambient temperature, solar load, lighting as well as equipment loads. Therefore the deviation from the design operating conditions leads to imbalance of the occupants comfort and high energy consumption of the buildings if the system is running without appropriate control system [148]. The radiator based hydronic central heating system operates in a closed loop scheme where On/Off (Relay) control system is used in conventional heating system while PID control system will be used in this work. Both control systems are available as a built-in control block diagram in the MatLab/Simulink software and can be used for modelling the central heating control system in this work.

3.3.1 TRV On/Off control relay

On/Off control system is commonly used in the UK for operating hydronic central heating systems [125]. Figure 3.10 shows the On/Off control system consisting of a relay, a set point and a sensor. The system is operating based on the feedback from the indoor temperature that controls the flow of hot water to the radiator depending on set point temperature for the space to be heated and mathematically presented using equations (3.23) to (3.25).

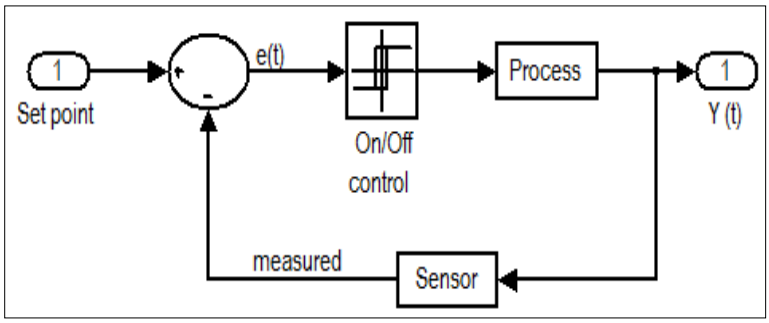

Figure 3.10 block diagram of the On/Off relay control system

The error is culculated :

$$e(t) = Set\ po\text{int} - measured \tag{3.23}$$

The relay is on for :

$$Set\ po\text{int} - measured \subset 0 \tag{3.24}$$

The relay is off for :

$$Set\ po\text{int} - measured \supseteq 0 \tag{3.25}$$

3.3.2 PID control system

PID is universally accepted control algorithm in automation industries, it is commonly used due to its robust performance in a wide range of applications and it is a user friendly control system [125]. PID consists of three parameters including Proportional, Integral, and Derivative coefficients. It operates by calculating the proportional, integral, and derivative of the response which is then used to compute the desired actuation output.

The proportional parameter determines the ratio of the response output to the system error (the difference between set point and measured process variable); its main function is to increase the speed of the response. The function of the integral term is to add the error with time, and hence helps to stabilise the system once it reaches steady state. The derivative term is directly proportional to the process variable change rate; this term is used to increase the control speed to respond for overall variable change rate. The PID control system is mathematically represented using eq. (3.26) and the Simulink block diagram is shown in figure 3.11.

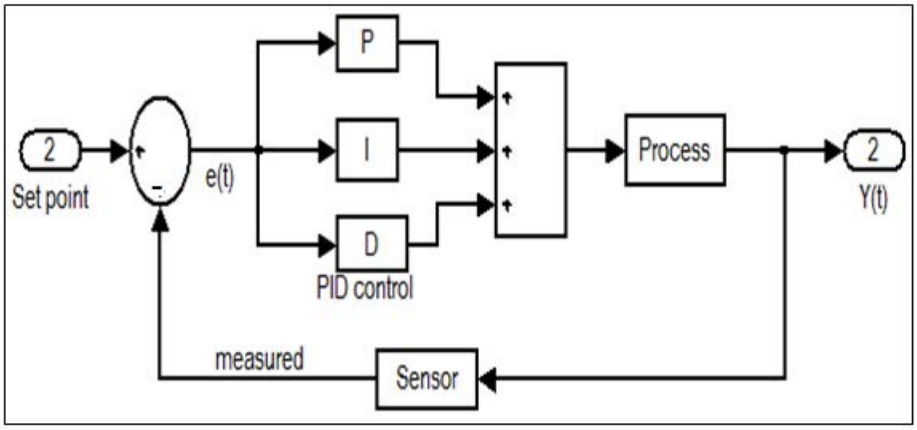

Figure 3.11 block diagram of the PID relay control system

$$u_s(t) = K_p e(t) + K_i \int e(t)dt + K_D \frac{de}{dt} \qquad (3.26)$$

Where: u_s is the control signal, K_p is proportional gain; K_i integral gain; K_D deferential gain; e is error signal, and t is time.

3.4 Dynamic modelling of radiator central heating system

Figure 3.12 shows the radiator central heating system dynamic model developed in Simulink software. The developed model includes room model, boiler model, radiator model and the control system model to predict the indoor temperature. The developed integrated dynamic model of radiator central heating system is used to investigate the performance of hydronic central heating system using constant and pulsed mass flow rates. For the control system, both On/Off and PID control models as described in section 3.3 are used for both flow conditions.

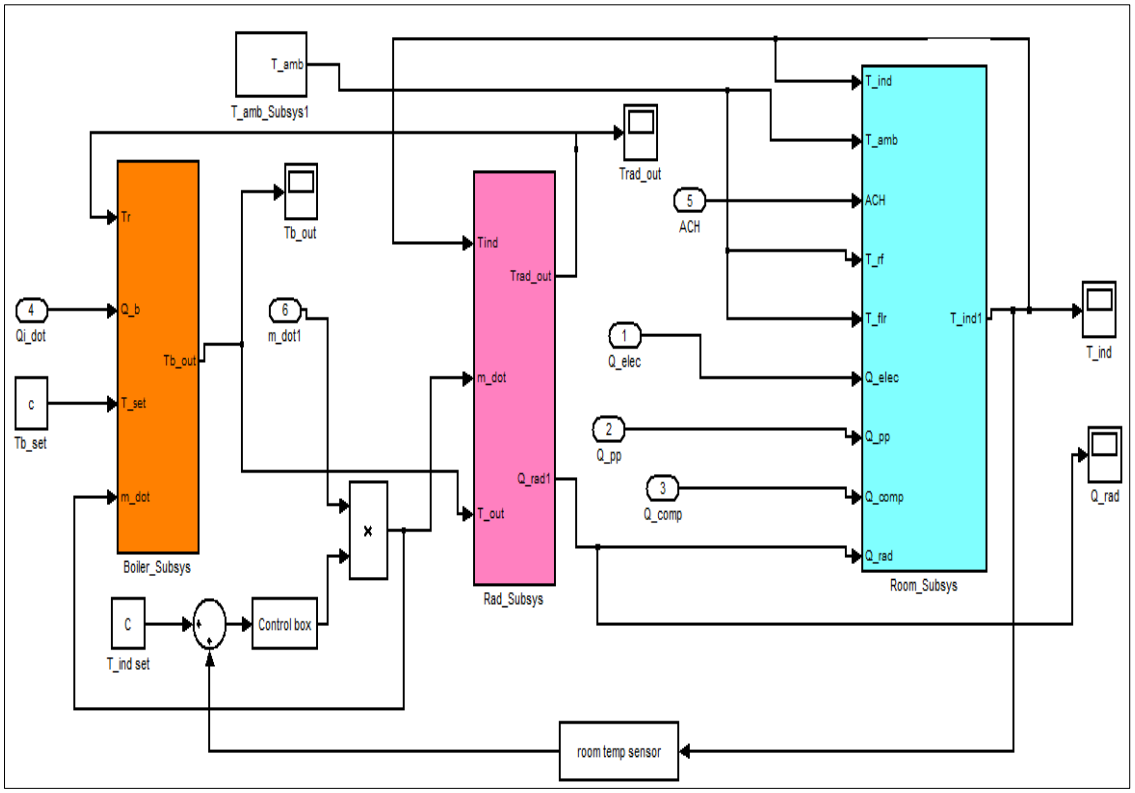

Figure 3.12 the dynamic Simulink diagram of the radiator central heating system

3.4.1 Modelling inputs and assumptions

The work presented in this section is concerned with modelling the dynamic thermal performance of a single room heated by hydronic panel radiator using Matlab/Simulink software. Initially the empty heated room (heated room with no occupants) was modelled using the following assumptions:

- The room temperature is assumed to be uniform.
- Initially the only heat source is the radiator; all other heat gains from the Sun, people, light bulbs and other appliances are neglected.
- The simulation is carried out using UK winter ambient temperature conditions shown in figure 3. 13 as recommended by ASHRAE standard 55.
- The room is assumed to be empty and the only heat loss is due to the thermal properties of the building (envelope) and the air ventilation.

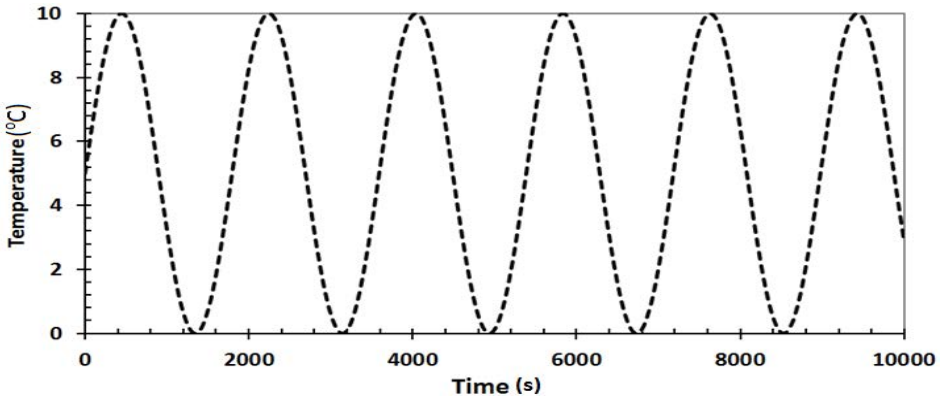

Figure 3.13 UK winter ambient temperature fluctuations (UK Met)

The input values of the thermal properties of the building structure and the hydronic panel radiator are shown in Tables 3.1. The dimensions of the room are 3.5m width, 5.5m length, 2.7m high and 2*1.5m^2 of window. The radiator operating temperatures were taken from the British Standard BS EN 442-2 radiators and convectors Part 2 [91] where the hot water inlet, outlet and indoor temperatures of 75^{o}C, 65^{o}C and 20^{o}C respectively were recommended. The mass flow rate of the radiator was calculated using the standard value of the hot water inlet and outlet temperatures of the hydronic radiator and the nominal heat output reported by the manufacturer. Based on the maximum nominal heat output of 1000W, the hot water mass flow rate is calculated as 0.024kg/s using (eq. (3.7) from section 3.2.2).

Table 3.1 the thermal properties of buildings materials and hydronic panel radiator heater

Components	Materials	K (W/m.K)	c (J/kg.K)	U (W/m^2.K)	ρ(kg/m^3)	UA (W/K)
Internal wall	Plasterboard	0.16	840	0.35	950	13.23
External wall	Brick	0.77	800	0.86	1700	9.3
Window	Glass	0.96	750	3.1	2400	9
Floor	Screed	0.41	840	0.35	1200	7
Ceiling	Wood wool	0.10	1000	0.3	500	6
Radiator	Steel (AISI 316)	16.2	475	9	7850	18.7
Room envelope	Air	0.025	1005	-	1.2	-
Door	wood	0.14	1200	-	650	-
Working fluid	water	-	4180	-	1000	-

Figure 3.14 shows the input mass flow profiles for the constant and pulsed flow scenarios.

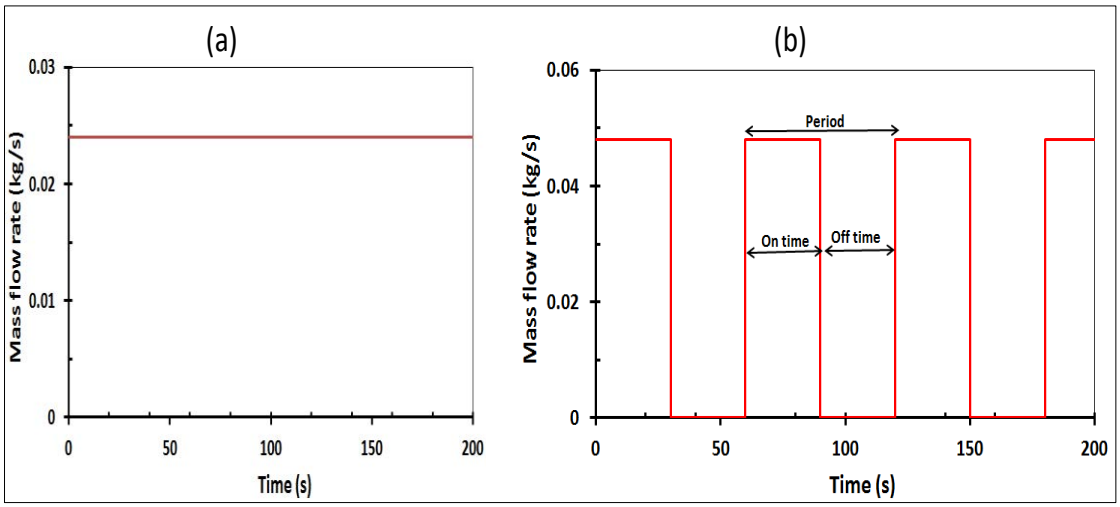

Figure 3.14 (a) the constant inlet mass flow profiles and (b) pulsed flow inlet mass flow rate profile of the proposed hydronic heating radiator

The central heating system was investigated for both the constant flow condition typically used in the UK hydronic heating systems (Figure 3.14 (a)) and the proposed pulsed flow strategy investigated in this work (Figures 3.14(b)). For the pulsed flow a range of pulse duty cycles (50% to 80%), amplitude (0.024kg/s to 0.048kg/s) and frequencies (0.017Hz to 0.033Hz) where investigated.

3.4.2 Modelling results at constant flow

The modelling was carried out using the dynamic Simulink block diagram shown in figure 3.12 that represents the room (space to be heated) coupled with hydronic heating system (radiator and boiler). Results were generated by applying the assumptions and all the input values described in section 3.4.1.

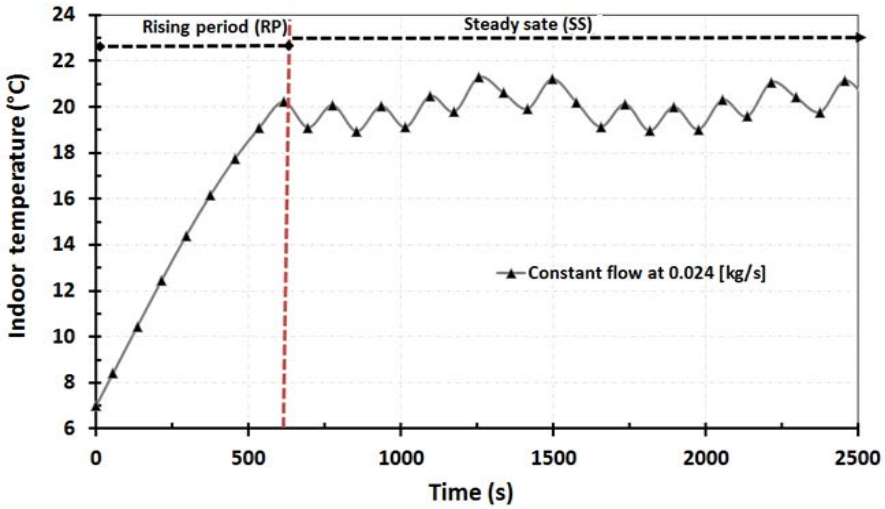

Figure 3.15 the indoor temperature at constant flow scenario

The radiator was operated in a closed loop scenario using the On/Off control system shown in figure 3.14(a) for constant flow case (typically used in the UK). Results were analysed on the basis of indoor temperature fluctuation and the energy consumption of the radiator. The radiator at constant flow was simulated using the calculated mass flow rate of 0.024kg/s. Figure 3.15 shows the results of indoor temperature when the radiator was operated at constant flow (conventional flow).

It is clear from figure 3.15 that the indoor temperature at constant flow fluctuated $20^{o}C\pm1.7^{o}C$ which is within the limit recommended temperature of $20^{o}C\pm2^{o}C$. Also the rising period to reach steady state temperature is about 600s. This was used as reference indoor temperature for the radiator operated at pulsed flow conditions in the following sections. The radiator at pulsed flow was operated using various flow duty cycles, amplitudes and frequencies. All the pulsed flow results were compared to the constant flow case to investigate the potential of energy saving due to the pulsed flow without compromising occupants comfort.

3.4.3 Simulink results of pulsed flow at various duty cycles

Figure 3.16 shows the pulsed flow rate with flow amplitude of 0.0384kg/s, frequency of 0.0027Hz and various duty cycles used in this investigation. The duty cycle is defined as the ratio of the on cycle duration to the total cycle period as shown in figure 3.14 (b) using eq. (3.27).

$$\text{Duty cycle} = \left(\frac{\text{on cycle period}}{\text{Total cycle period}} \right) \times 100 \tag{3.27}$$

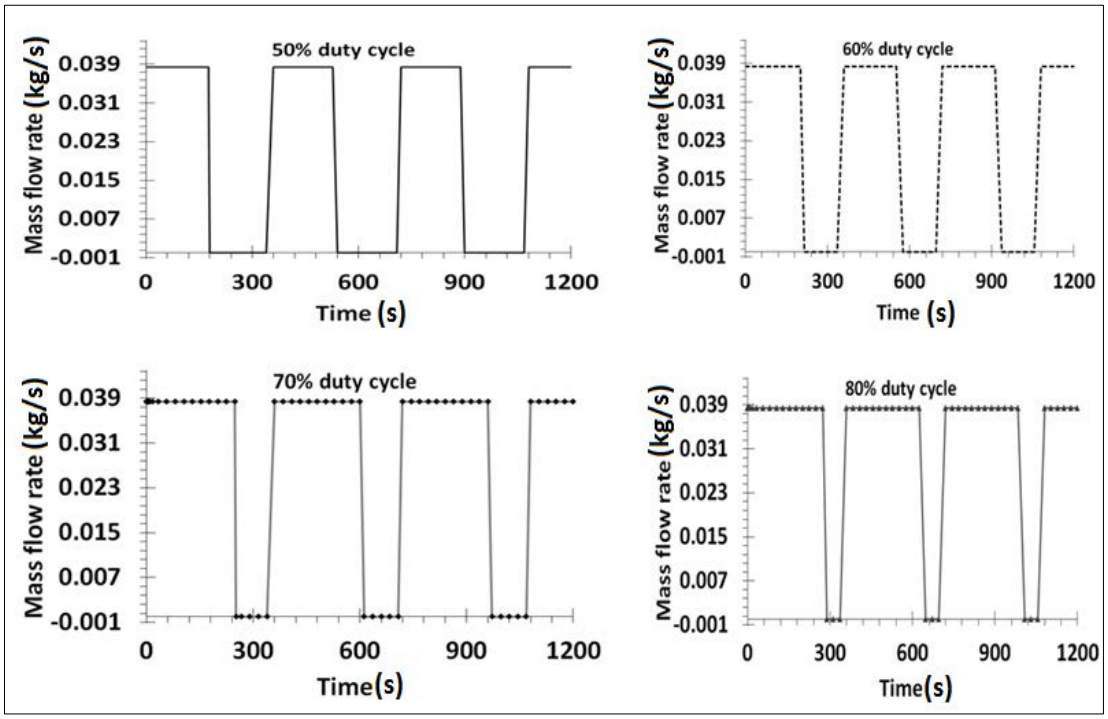

Figure 3.16 input radiator pulsed flow at various duty cycles and an amplitude of0.0384kg/s

Figure 3.17 shows the room temperature variation with time for the pulsed flow input strategies shown in figure 3.16 compared to that of the constant flow indoor temperature shown in figure 3.15. It can be seen that the room temperature increases

to the target temperature of 20°C within the first 700 seconds (the rising period) and then it fluctuates around 20°C during the steady state period by ±2°C. Also, figure 3.17 shows that; as the percentage of duty cycle increases the rising period (RP) is shortened from 450s at 50% to 360s at 80%.

The rate of energy consumption for the rising period and steady sate period at constant flow scenario (traditional central heating flow strategy) is calculated using eq. (3.28) and eq. (3.29) respectively. The rate of energy consumption for the rising period and steady sate period at pulsed flow scenario (proposed flow for this work) is calculated using equations (3.30) and (3.31) respectively.

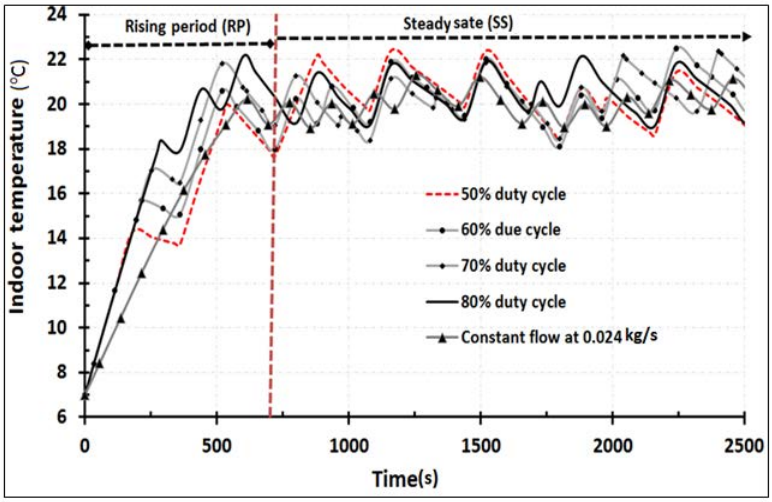

Figure 3. 17 indoor temperature output for radiator operating at constant flow and radiator operating at pulsed flow of various duty cycle

$$\dot{Q}_{cons,CF,RP} = \dot{m}_w Cp_w \Delta T \tag{3.28}$$

$$\dot{Q}_{cons,CF,SS} = (\text{TRV on ratio}) * (\dot{m}_w Cp_w \Delta T) \tag{3.29}$$

$$\dot{Q}_{cons.PF,RP} = (\text{Duty cycle}) * (\dot{m}_w Cp_w \Delta T) \tag{3.30}$$

$$\dot{Q}_{cons,PF,SS} = (\text{Duty cycle - TRV off ratio}).(\dot{m}_w Cp_w \Delta T) \quad (3.31)$$

$$\text{Where : TRV on ratio} = \frac{\text{On time of relay controler}}{\text{Total time}}$$

$$\text{TRV off ratio} = \frac{\text{Off time of relay controler}}{\text{Total time}}$$

The rate of energy savings for both rising and steady state periods due to the pulsed flow compared to the constant flow is calculated using eq. (3.32) and (3.33) respectively using the difference between the rate of energy consumed by the constant flow and the rate of energy consumed by pulsed flow. The indoor temperature fluctuation also is calculated using eq. (3.34).

$$ES_{RP} = \frac{(\dot{Q}_{cons,CF,RR} - \dot{Q}_{cons,PF,RP})}{\dot{Q}_{cons,CF,RP}} \times 100 \quad (3.32)$$

$$ES_{SS} = \frac{(\dot{Q}_{cons,CF,SS} - \dot{Q}_{cons,PF,SS})}{\dot{Q}_{cons,CF,SS}} \times 100 \quad (3.33)$$

$$T_{ind}\,(\text{flactution}) = T_{ind}\,(\max) - T_{set} \text{ or } T_{set} - T_{ind}(\min) \quad (3.34)$$

Where: ES is the percentage of energy saved (%), $\dot{Q}$ is the rate of energy consumed (W). Subscript CF is for constant flow, PF is for pulsed flow, RP is for rising period, SS is for steady state and cons is for consumption. Table 3.2 presents the energy saving calculated for radiator operating at various pulsed flow duty cycles. Results of radiator simulated at pulsed flow duty cycle is compared to the constant flow strategy

on the basis of energy saving and indoor temperature fluctuation. It is clear from table 3.2 that the highest energy saving and lowest temperature fluctuation is achieved at flow duty cycle of 50%. Therefore pulsed flow with 50% duty cycle was further investigated at various flow amplitudes and frequencies as discussed in the following sections.

Table 3.2 calculated results at various pulsed flow duty cycle compared to constant flow

Flow frequencies (Hz)	Flow amps (kg/s)	duty cycles (%)	Average mass flow rate (kg/s)	Rate energy cons rate at RP level (W)	Rate energy cons at SS (W)	ES (%) at RP	ES (%) at SS	Fluctuations of the indoor Temp (K)
0.0027	0.0384	50	0.0192	827	375	17.3	20.3	±2.2
		60	0.023	838	390	16.2	18.75	±2.8
		70	0.0269	880	400	12.0	16	±2.8
		80	0.0307	914	420	8.6	12.5	±3.0
CF	CF	CF	0.024	1000	480	----	----	

3.4.4 Simulink results of pulsed flow at various amplitudes

To investigate the effects of flow amplitude on energy saving, the best operating condition shown in table 3.2 was simulated at various flow amplitudes ranging from 0.024kg/s to a0.048kg/s. Table 3.3 shows the indoor temperature variation at various flow amplitudes but constant flow duty cycle of 50% and constant flow frequencies of 0.0027Hz. It is clear from table 3.3 that at flow amplitudes of 0.024kg/s and 0.0307kg/s the percentage of energy saving is negative indicating that pulsed flow consumes more energy compared to constant flow (see equations 3.32 to 3.33). However as the pulsed flow amplitude increased to 0.0384kg/s the energy saving is positive indicating that pulsed flow consumes less energy than the constant flow.

Increasing the pulsed flow amplitude from 0.0384kg/s to 0.048kg/s; results in reducing the energy consumption of the central heating systems. Therefore the pulsed flow with amplitudes of 0.0384kg/s produced the highest energy saving of 17.3 in the rising period and 20.3% in the steady state period. Also this pulsed flow showed best indoor temperature fluctuation of ±2.2K.

Table 3. 3 calculated results at various pulsed flow amplitudes compared to constant flow

Flow frequencies (Hz)	duty cycles (%)	Flow amps (kg/s)	Average mass flow rate (kg/s)	Rate energy cons rate at RP level (W)	Rate energy cons at SS (W)	ES at RP (%)	ES at SS (%)	Fluctuations of the indoor Temp (^{o}C)
0.0027	50	0.0480	0.024	835	400	16.42	16	±3
		0.0384	0.0192	827	375	17.3	20.3	±2.2
		0.0307	0.015	1086	450	-8.6	6.25	±2.2
		0.0240	0.012	1236	490	-23.6	-2.08	±3.0
CF	CF	CF	0.024	1000	480	----	----	

The calculated results in table 3.3 highlight the potential of flow pulsation in reducing energy consumption of the hydronic central heating system. The best select pulsed flow amplitude calculated in in table 3.3 was investigated at various flow frequencies in the following sections.

3.4.5 Simulink results of pulsed flow at various frequencies

In order to investigate the effects of cycle frequency on energy saving, the best operating condition shown in table 3.2 was simulated at various cycle frequencies ranging from 0.0017Hz to 0.033Hz. Figure 3.18 shows the indoor temperature

variation at various frequencies but with constant flow amplitude of 0.0384kg/s. It is clear from figure 3.18 that as the flow frequency decreases higher fluctuation of the indoor temperature occurs. For example as the frequency decreased from 0.033Hz to 0.0017Hz the indoor temperature fluctuation increased from $20^{o}C \pm 1.7$ to $20^{o}C \pm 3^{o}C$. Therefore the frequency value of 0.033Hz can keep the temperature fluctuation in the room within the required comfort level of ±2K.

Table 3.4 presents the energy saving at various pulsed flow frequency compared to the constant flow operating condition and the indoor temperature fluctuation. It is clear that the highest saving (21.9%) can be achieved at flow frequency of 0.033Hz, flow amplitude of 0.0384 kg/s and average mass flow rate of 0.0192kg/s compared to the constant flow rate of 0.024kg/s. The saving is achieved while keeping the indoor temperature within the limit of the standard fluctuation 2K, which fulfils the comfort temperature required by the user.

Table 3.4 energy saved based on the flow frequency at constant amplitudes and selected 50% duty cycles flow pulsation.

Flow frequencies (Hz)	Flow amps (kg/s)	Average mass flow rate (kg/s)	Energy cons rate at TS level (W)	Energy cons rate at SS (W)	E_saved at RP (%)	E_Saved at SS (%)	Fluctuation Indoor T (K)
0.033	0.0384	0.0192	800	375	20	21.9	20±1.7
0.016	0.0384	0.0192	815	382	18.5	20.3	20±2
0.0027	0.0384	0.0192	827	384	17.3	20	20±2.1
0.0017	0.0384	0.0192	845	403	15.5	16	20±3
CF	CF	0.024	1000	480			

Figure 3.19 highlights the effect of the best pulsed flow compared to the constant flow on the predicted indoor temperature response time. It can be seen that the pulsed flow results in shortening the system response (rising period) from 600seconds to

450seconds which is useful for the comfort of the occupants and reduces the energy consumption in buildings.

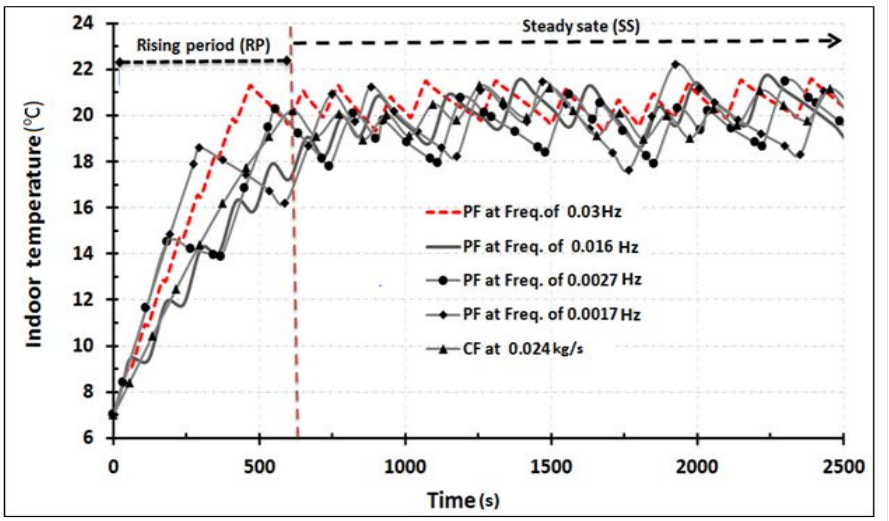

Figure 3.18 indoor temperature at various frequency, 50% on duty cycle; 0.0384 flow amplitudes and average mass flow rate of 0.0192(kg/s)

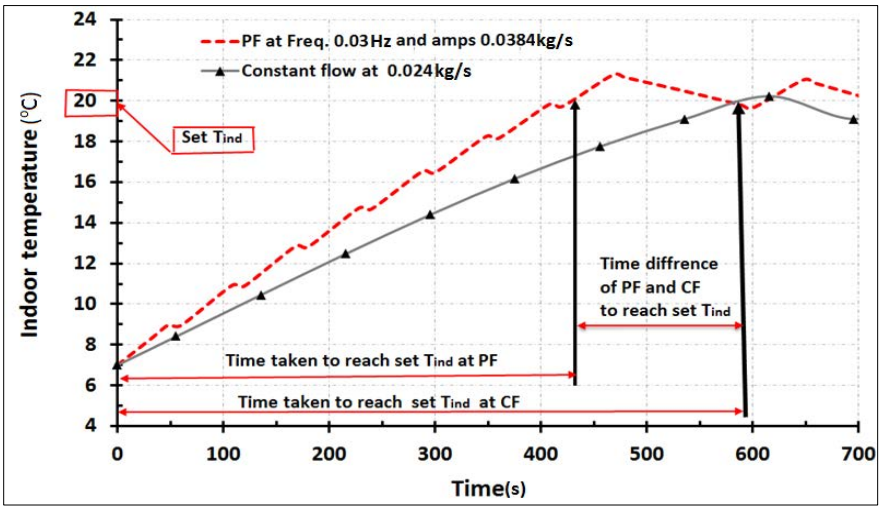

Figure 3.19 time response of indoor temperature for the best pulsed flow (PF) compared to the constant flow (CF)

Figures 3.20 show the average rate of energy consumption in the hydronic heating system for constant flow scenario compared to the best pulsed flow operated at 50% duty cycle, 0.0384kg/s amplitude and 0.033Hz. The energy saving in figure 3.20 was

achieved with the radiator operated using On/Off control system for both constant and pulsed flow scenarios.

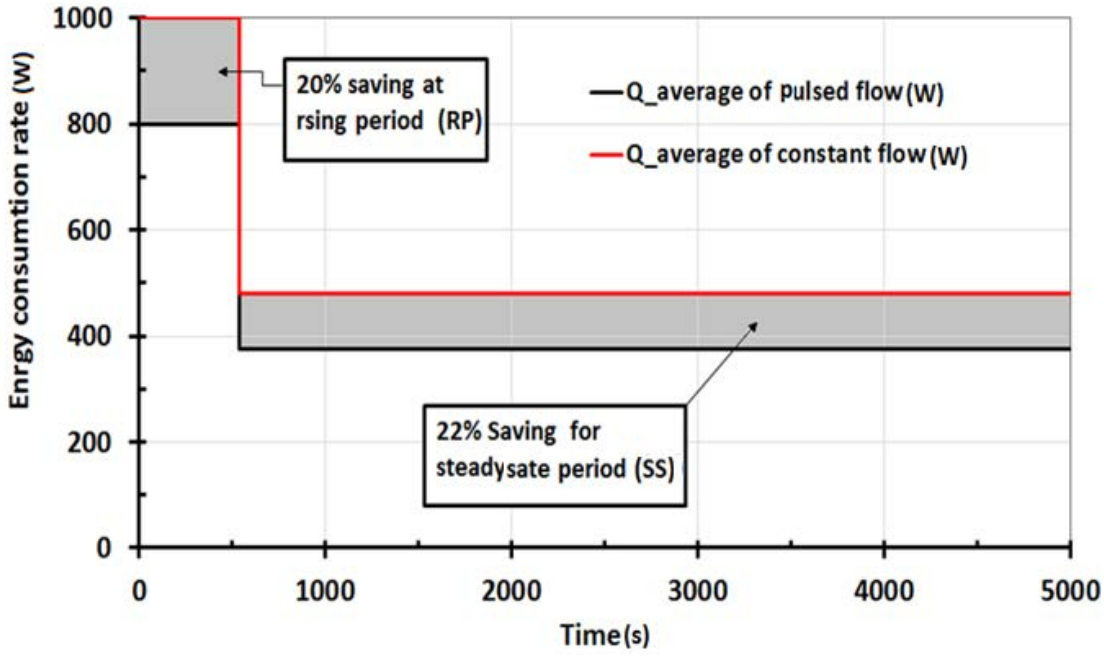

Figure 3.20 average percentage energy saving rate at the selected flow pulsation compared to the constant mass flow case radiator operating using On/Off (relay) control system.

3.4.6 Effect of PID control system

All the above results are obtained using On/Off (relay) control system and show that there is a potential for flow pulsation in central heating systems. To investigate the effect of PID control, the On/Off control system is replaced by the three terms PID feedback control strategy described by figure 3.11 and eq. (3.26). The PID control system used for this work is tuned using the built in program available in the MatLab/Simulink software. The hydronic central heating system operated using PID control system was analysed on the basis of energy saving and further improvements in the comfort condition of the occupants. Figure 3.21 shows the indoor temperature

fluctuation with radiator operating using PID control system for the best pulsed flow and the constant flow case. It is clear from figure 3.21 that the fluctuation of the indoor temperature is reduced from 20±1.7 to 20±1^{o}C for the heating system operating under PID control compared to the central heating system operating using On/Off control system. The indoor fluctuation is within the limit of the indoor temperature comfort level recommended by both ASHRAE standard 55 and EN ISO 7730.

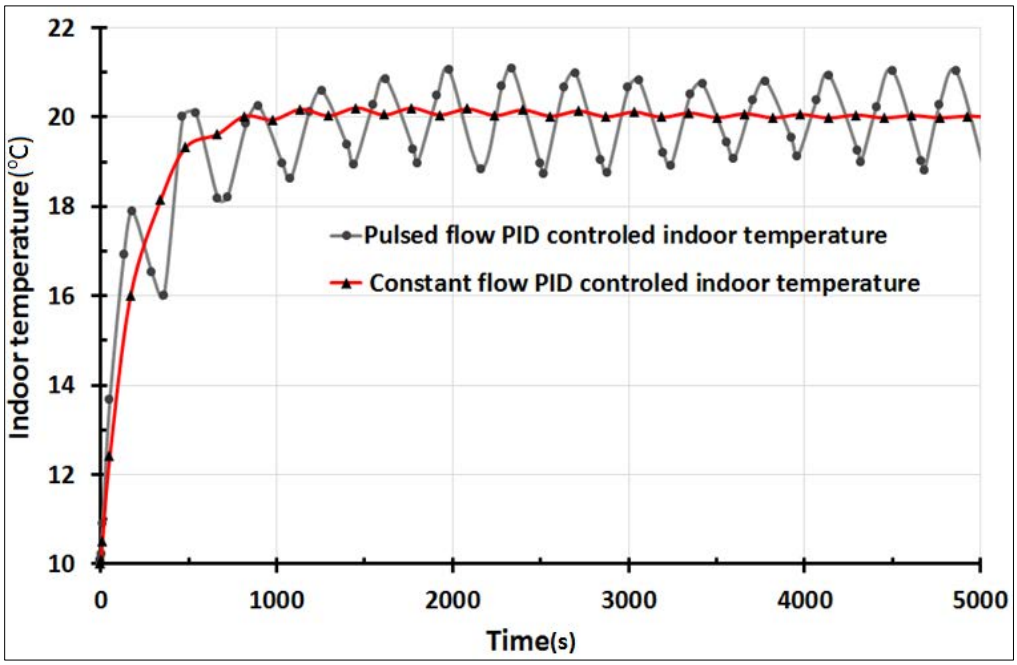

Figure 3.21 indoor comfort temperature after PID control system is applied to the hydronic central heating system

Figure 3.22 shows the energy saving with PID control strategy where around 27% of energy can be saved. Clearly this is higher saving than that of using only the pulsed flow strategy which gave 22% energy saving as shown in figure 3.20, thus highlighting the potential of using PID control with the pulsed flow strategy.

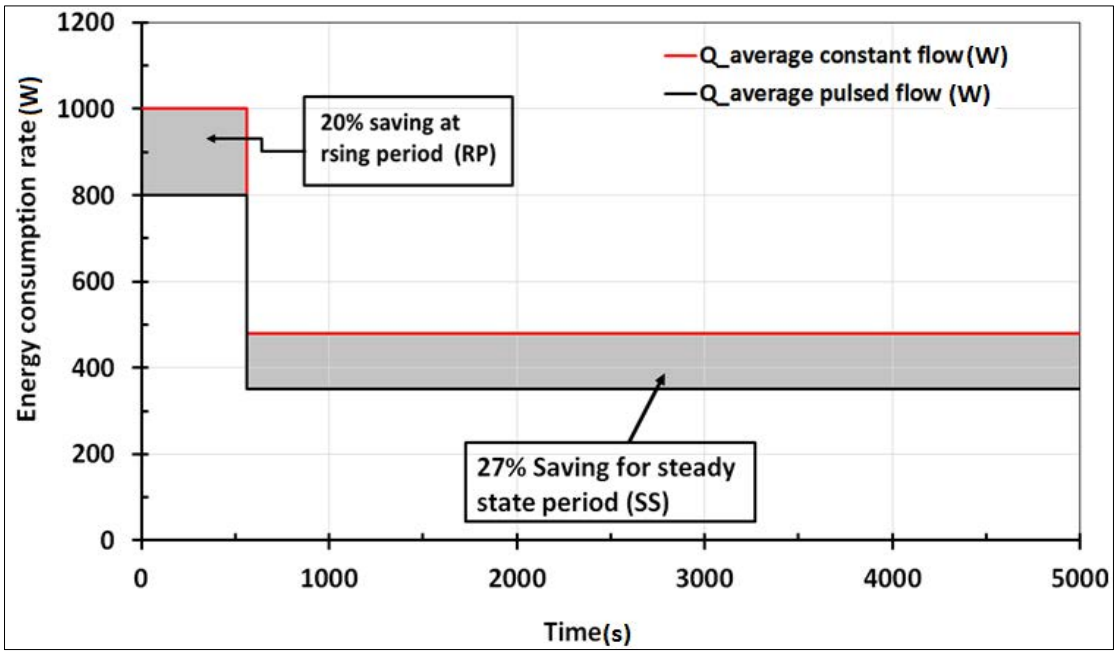

Figure 3.22 average percentage energy saving rate at the selected flow pulsation compared to the constant mass flow case radiator operating using PID based control system

3.5 Modelling indoor thermal comfort and indoor air quality

In section 3.4 of this chapter the radiator central heating system is modelled at constant and pulsed flow conditions with all heat sources other than the panel radiator neglected. The indoor temperature (air temperature and radiant temperature) was investigated and the potential of energy saving due to the pulsed flow was evaluated in comparison with the conventional constant flow. However other comfort parameters including humidity, indoor CO_2 concentration (indoor air quality (IAQ)) should be evaluated to assess the effect of pulsed flow on the user comfort.

The indoor environmental comfort can be classified into four main categories including indoor air quality (IAQ); thermal comfort (air temperature, radiant temperature, relative-humidity and indoor velocity), acoustic comfort and visual

comfort as shown in figure 3.23. Investigating the indoor environmental condition of occupants' satisfaction is the most common practice for the thermal indoor comfort and the indoor air qualities perceptions. According to ISO7730, 2005, indoor thermal comfort is defined as state of mind in terms of satisfaction with thermal environment which depends on the individual psychology and physiology. It can also be defined as the interaction of the air ventilation supply and the heating source of the space to be heated. Indoor air quality (IAQ) is the overall result of the interaction between building volume (envelope) incoming outdoor air; ventilation system, indoor occupants and contaminant sources [100-101 and 149]. The room was modelled by taking into account all internal heat sources including occupants, electrical appliances and considering the latent heat of the supplied air through ventilation as well as the solar heat gain.

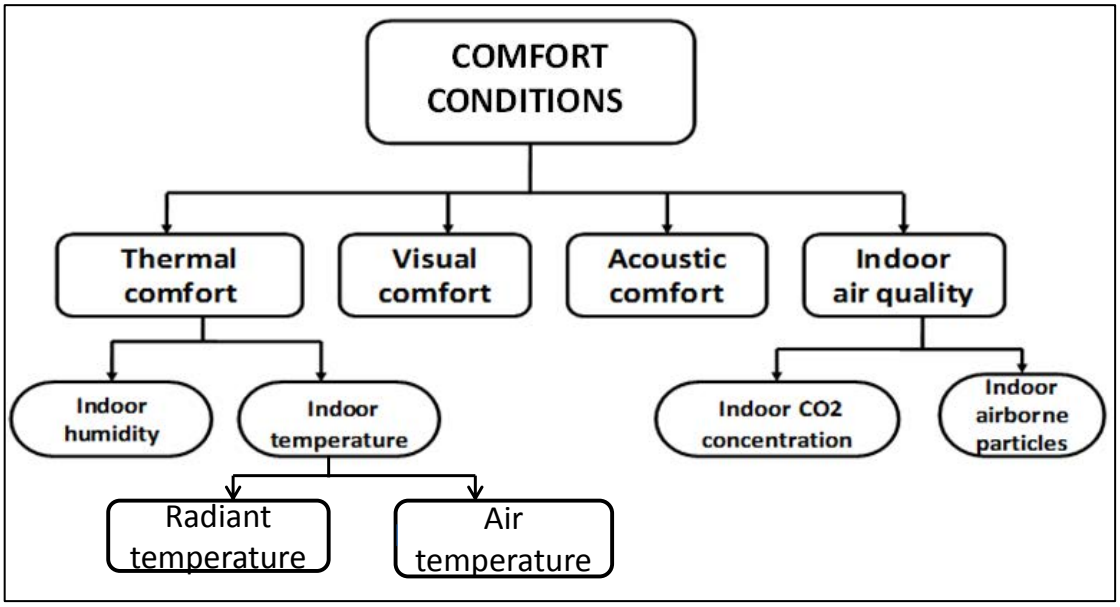

Figure 3.23 comfort conditions in indoor environment

Figure 3.24 shows a typical central heating system consisting of heat source (boiler), flow distribution components (circulation pump, valves, and pipes), heat emitter

(panel radiator) and heated space (room). Heat sources other than the radiator are; solar heat gain and internal gain (light, occupants and computers). The main heat losses from the room are; heat loss by ventilation and heat loss through building structure including the windows. All the indoor conditions including temperature, humidity level, and CO_2 concentration are calculated using the mass and energy balance equations.

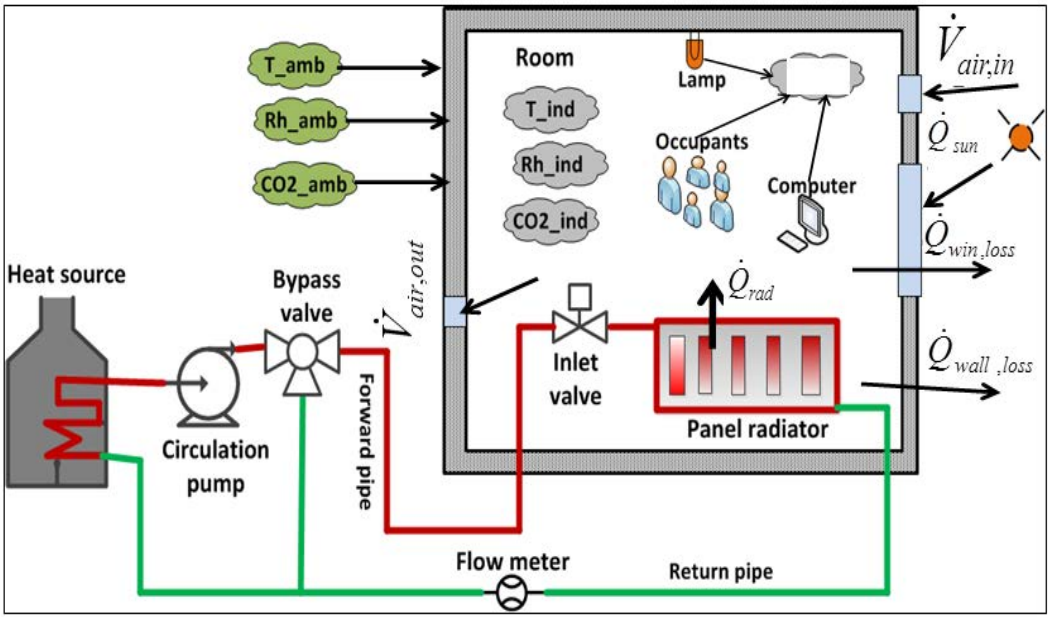

Figure 3.24 schematic illustration of indoor comfort parameters

To enable the investigation of multi input and multi output parameters for indoor thermal comfort as well as the indoor air quality (IAQ), advanced modelling of the central heating system is required. This is performed using; embedded user defined MatLab m-code which can be integrated to the Simulink graphical interface and is user friendly. Following sections described the models developed for indoor temperature, indoor humidity and indoor CO_2 concentration. These models were then integrated to develop a complete model of the whole central heating system. The

closed loop feedback control system was also integrated to the model to operate the system based on the indoor comfort parameters response.

3.5.1 Indoor temperature model

The indoor temperature was modelled using the transient heat transfer eq. (3.22) modified to include the latent heat of the ventilated air given by eq. (3.35).

$$\dot{Q}_{lat.vent} = \rho_a . h_{fg} . \dot{V} . (\omega_{ind} - \omega_{amb}) \tag{3.35}$$

The indoor room temperature is thus expressed using eq. (3.36).

$$T_{ind} = \int \left(\frac{1}{V_{rm} . \rho_{air} C_{p.air}} (\dot{Q}_{rad} + \dot{Q}_{gain} - \dot{Q}_{lat.vent} - \dot{Q}_{sen.vent} - \dot{Q}_{env} - \dot{Q}_{win}) \right) dt \tag{3.36}$$

Where: $\dot{Q}_{rad}$, $\dot{Q}_{win}$, $\dot{Q}_{env}$, $\dot{Q}_{sen.vent}$, $\dot{Q}_{gain}$, $\dot{Q}_{lat.vent}$, V_{rm}, ω_{amb}, $\omega_{ind,}$ $\dot{V}$ and h_{fg} are: heat gain from radiator (eq. (3.8)), heat transfer through the window (eq. (3.13)), heat loss through wall of envelope (eq. (3.15)), sensible heat of ventilation (eq. (3.19)), internal heat gain (eq. (3.21)), latent heat of ventilation (W), volume of the room, outdoor specific humidity, indoor specific humidity, ventilation volume flow rate and specific latent heat of vaporisation of water (kJ/kg) respectively. Figure 3.25 shows the block diagram of the dynamic indoor temperature model developed to solve eq. (3.36). The Matlab m-code programmed for the indoor temperature model is shown in Appendix A.

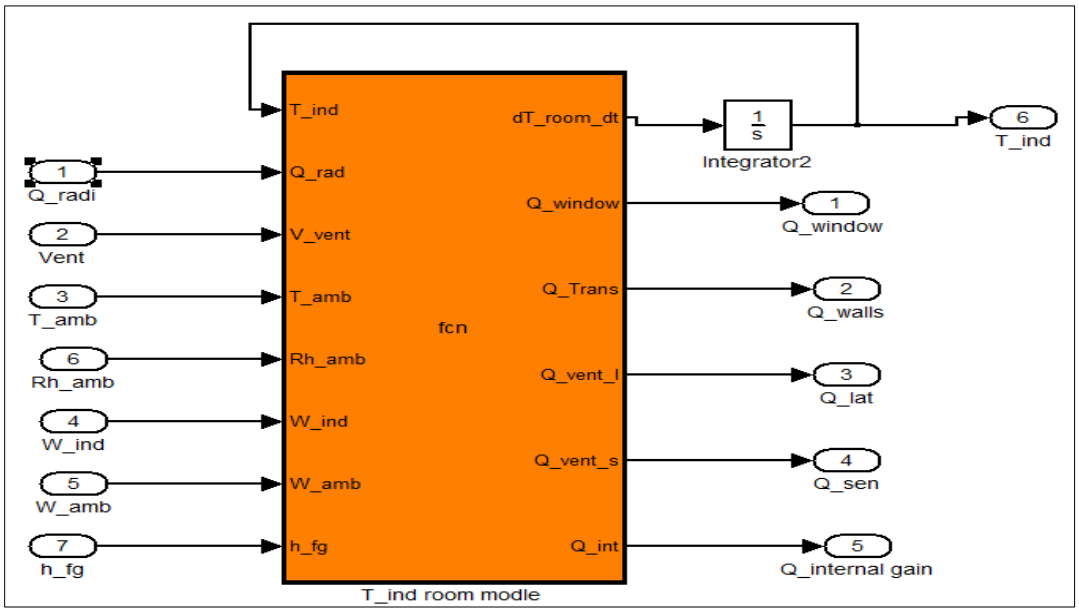

Figure 3.25 the embedded Simulink dynamic model of indoor temperature

3.5.2 Indoor humidity model

According to ASHRAE 55-1992, relative humidity (RH) is defined as the presence of water vapour in air that can cause thermal discomfort for the indoor occupants. To avoid the discomfort due to indoor humidity; it is recommended that humidification/dehumidification processes are required in order to keep indoor air relative humidity within the range of 25% - 60%. Indoor humidity can be calculated mathematically using transient mass balance eq. (3.37) [150].

$$\rho_{air} V_{rm} \frac{d\omega_{ind}}{dt} = (\dot{m}_{air})(\omega_{amb} - \omega_{ind}) + \dot{m}_{gen} + \dot{m}_{add/rev} \tag{3.37}$$

$$\omega_{amb} = \frac{0.622 . Rh_{amb} . P_{s.amb}}{P_{atm} - (Rh_{amb} . P_{s.amb})} \tag{3.38}$$

$$P_{s.amb} = \frac{\ln\left(77.345+0.0057T_{amb} - \frac{7235}{T_{amb}}\right)}{(T_{amb})^{8.2}} \tag{3.39}$$

$$P_{s.ind} = \frac{\ln\left(77.345+0.0057T_{ind} - \frac{7235}{T_{ind}}\right)}{(T_{ind})^{8.2}} \tag{3.40}$$

The indoor moisture content can then be expressed as eq. (3.41) while the indoor relative humidity is given as eq. (3.42)

$$\omega_{ind} = \int\left(\frac{(\dot{m}_{air})(\omega_{amb} - \omega_{ind}) + \dot{m}_{gen} + \dot{m}_{add/rev}}{\rho_{air} V_{rm}}\right)dt \tag{3.41}$$

$$RH_{ind} = \frac{\omega_{ind} . P_{atm}}{P_{s,ind} - (\omega_{ind} + 0.622)} \tag{3.42}$$

Where: RH, ω, $\dot{m}$, $P_{s.ind}$, V_{rm}, $P_{s\cdot amb}$, $\dot{m}_{gen}$, $\dot{m}_{add/rev}$, T and P_{atm} are; relative humidity (%), specific humidity (kg/kg), mass flow rate of air (kg/s), indoor saturation pressure (Pa), volume of the room (m^3), saturation pressure of the ambient air (Pa), moisture generation rate from occupants ($1.157*10^{-5}$ kg/s), moisture added or removed by air conditioning (kg/s), temperature (K) and atmospheric pressure (Pa) respectively. Figure 3.26 shows the block diagram of the developed dynamic indoor humidity model which includes the latent heat loss, moisture generation, indoor saturation pressure, and saturation pressure of the ambient air.

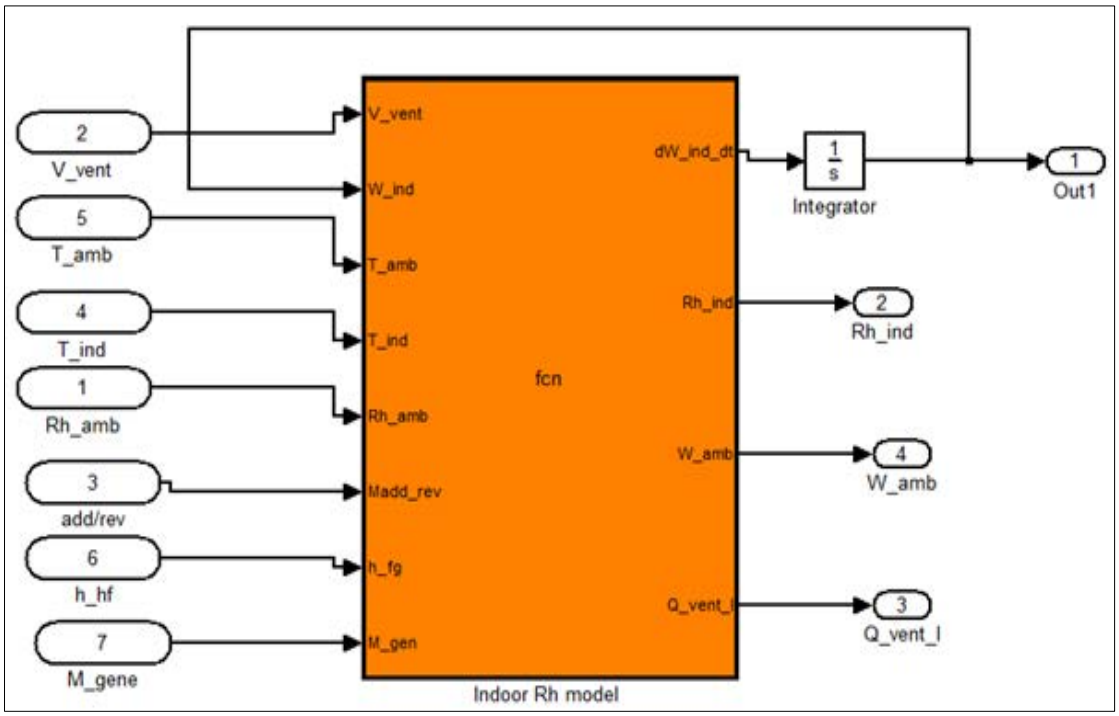

Figure 3.26 the embedded Simulink dynamic model of indoor humidity level

3.5.3 Indoor CO_2 concentration model

Indoor CO_2 concentration is an indicator of the indoor air quality which is recommended to be less than 1000ppm [150]. Also the difference in CO_2 concentration of the indoor air and outdoor air should be about 700ppm with outdoor concentration ranging from 350 to 400 PPM [150]. ASHRAE 62-1999 recommended an acceptable ventilation flow rate of 7.5 l/s per person and 0.6l/m^2 of floor area in the occupied zone. The recommended ventilation flow rate is able to dilute the CO_2 generated by respiration of the occupants and remove air born contaminants as well as supply adequate oxygen to the occupants of the room. ASHARAE also predicted higher ventilation than the recommended flow rate if the indoor heat gain is not compensated by cooling [151]. Indoor CO_2 concentration can be determined using mass balance as eq. (3.43) and eq. (3.44).

$$V_{rm}\frac{dC_{ind}}{dt} = Gh + \dot{V}C_{out} - \dot{V}C_{ind} \tag{3.43}$$

$$C_{ind} = \int \left(\frac{Gh + \dot{V}C_{out} - \dot{V}C_{ind}}{V_{rm}}\right) dt \tag{3.44}$$

Where; C_{ind} and C_{out} are; indoor and outdoor carbon dioxide concentration (PPM). Gh is the human CO_2 generation rate which depends on human activities (metabolic rate) and varies from 0.005l/s (1Met) to 0.01l/s (2Met) according to ASHRAE.

Figure 3.27 shows the block diagram of the dynamic indoor CO_2 concentration model developed using eq. (3.44) and it includes indoor CO_2 concentration model which takes into account CO_2 entering the room though ventilation, PID control model, CO_2 generation from occupants and conversion of PPM to standard unit.

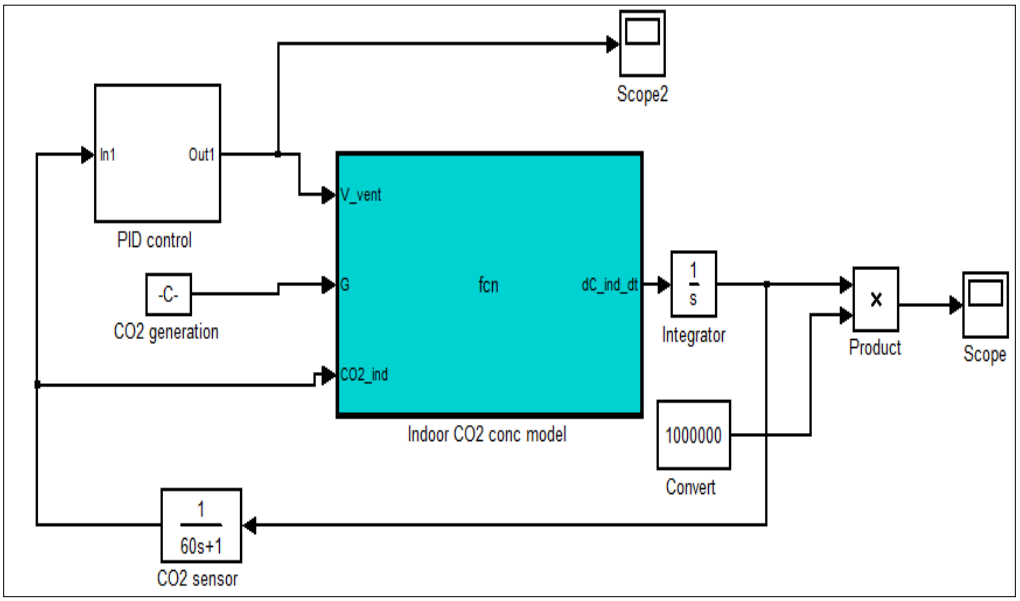

Figure 3.27 the embedded Simulink dynamic model of indoor CO_2 concentration

3.5.4 Integrated embedded dynamic indoor thermal comfort and Indoor Air Quality (IAQ)

Figure 3.28 shows the radiator central heating system integrated model of the embedded user defined models of indoor temperature model (figure 3.25), indoor humidity (figure 3.26), CO_2 concentration (figure 3.27) and the models of the boiler, radiator as well as the PID control system developed in sections 3.2.1 to 3.3.2. The integrated model will be used to investigate the indoor temperature, humidity and CO_2 level at constant and pulsed flow conditions. The three governing equations used to develop the embedded function shown in figure 3.28 are expressed in eq. (3.36), eq. (3.42) and eq. (3.44) and the detailed description of the embedded MatLab m-code is given in Appendix A.

In this work a living room with 5 people inside was considered with dimensions of 4m width, 5m length, 2.7m high and $2*1.5m^2$ of windows. A typical UK winter average ambient temperature, relative humidity, and CO_2 were applied at 5^oC (figure 3.11), 80% and 400PPM respectively. The model is for central heating system using radiator as heat emitter and controlled fan for ventilation fresh air supply. The work aims to investigate the indoor thermal comfort condition and indoor air quality (IAQ) including humidity, temperature and CO_2 concentration at constant and pulsed flow strategies of the radiator hot water and the ventilation fan fresh air. The indoor CO_2 was modelled dynamically based on the demand based control system.

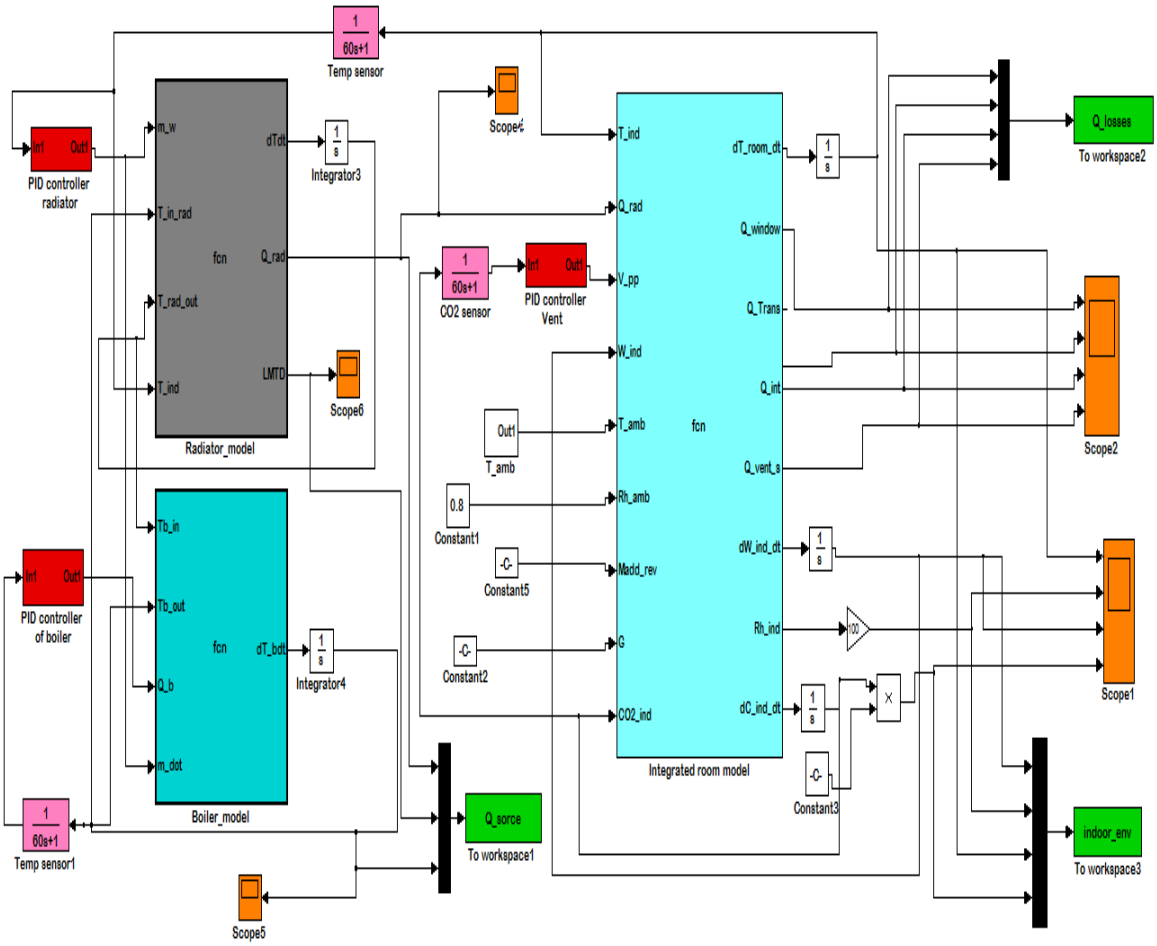

Figure 3.28 dynamic model central heating system integrated with indoor thermal comfort and Indoor Air Quality (IAQ)

The results are investigated in terms of the indoor comfort level and the energy saving due to the pulsed flow compared to the constant flow cases. The thermal properties of the simulated room are taken from section 3.4.1, table 3.1 of this chapter. The thermal input parameters of the boiler and radiator model are also defined in section 3.2 of this chapter. The constant flow profile and pulsed flow profile for both the hot water flow to the radiator and the ventilation fan are shown in figure 3.14. The hot water supply to the radiator was applied at 0.024kg/s for constant flow case. The pulsed flow to the radiator was applied using the best conditions selected based on results presented in section 3.4 of this chapter with average flow rate of 0.0192kg/s at flow amplitudes of

0.0384kg/s, 50% duty cycle and frequency of 0.033Hz. The ventilations fan fresh air supply was applied at 10 l/s per person for constant flow case and average flow rate of 6.6 l/s per person for pulsed flow at amplitudes of 13.2 l/s and flow frequency of 0.033Hz.

The moisture generation of occupants depends on the occupants' activities; this model assumed moisture generation level of seated persons. Table 3.5 shows the UK weather conditions where for the winter months of November to February the average outdoor temperature is 5^{o}C, outdoor relative humidity is 80% and solar heat gain of 37.8 W/m^2. The CO_2 generation of human being depends on the metabolic rate which in turn depends on the human activities. Figure 3.29 shows the CO_2 generation of seated person to be 0.00416 l/s per person [152].

Table 3.5 the UK average weather parameters [152]

Month	Temperature (°C)	Relative humidity (%)	Vapour pressure (Pa)	Solar gain (horizontal) (W/m²)
January	5.0	85	740	23.1
February	3.4	80	620	45.1
March	7.6	71	740	105.3
April	9.4	73	860	155.1
May	11.3	76	1010	163.2
June	16.2	75	1370	178.2
July	16.7	74	1400	165.5
August	16.6	81	1530	121.5
September	15.2	83	1420	106.5
October	13.7	87	1360	62.5
November	7.5	87	900	27.8
December	3.4	90	700	17.4

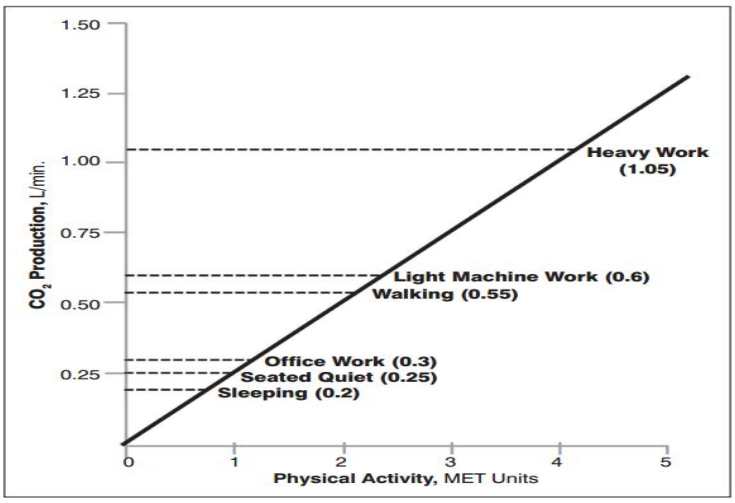

Figure 3.29 CO_2 generation of human based on physical activities (MET rate)

Figure 3.30 shows the internal heat gain variation with time from computer, occupants, electrical equipment, and also the heat loss due to building structure and heat loss through the window glazing. The internal heat gained was assumed as a constant supply of heat to the room according to ASHRAE; a seated person can release about 100W of heat to the room and the electrical equipment contribute about 200W thus a total of 700W of heat was used. The heat loss through the window and building structure depends on the outdoor temperature and were calculated based on material properties given in table 3.1, section 3.3.

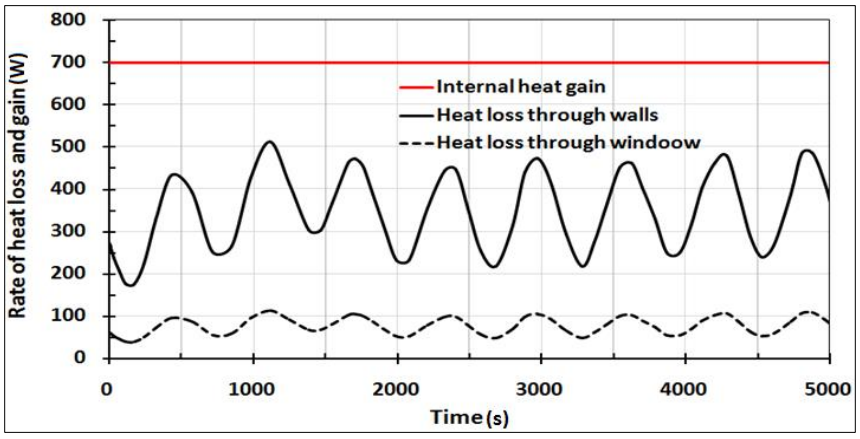

Figure 3.30 the internal heat gain, heat loss due to building structure and heat loss through windows

To simulate the room with occupants for prediction of indoor thermal comfort and IAQ the following assumption are used.

- The parameters $\dot{m}_{add/rev}$ in the eq. (3.41) was neglected, no added moisture by humidification and no removed moisture by dehumidification
- The indoor temperature, humidity, and CO_2 concentration are uniformly distributed in the room
- The heat transfer coefficient of air from the surface area of the radiator was applied as constant value of 8.5 W/ (m^2.K) [95].

3.5.5 Simulink modelling results at constant flow

Figure 3.31 shows the indoor temperature, humidity, and CO_2 concentration in the heated room with the heating system operating at constant flow scenario.

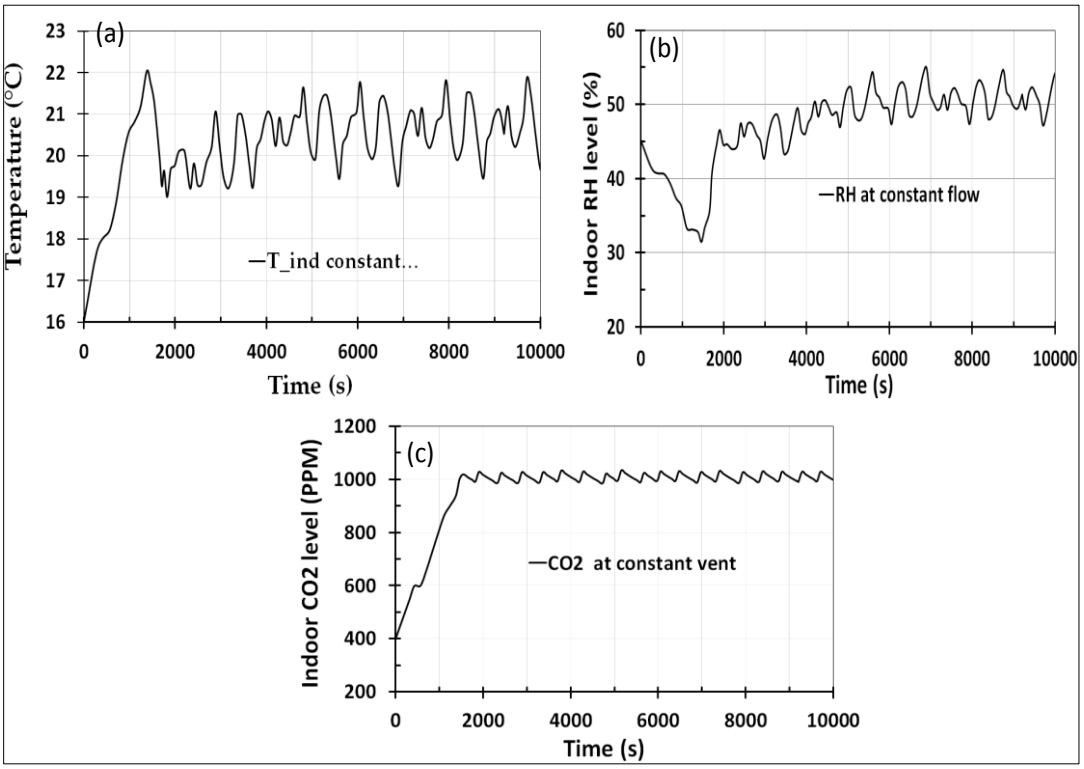

Figure 3.31 (a) indoor temperature, (b) indoor humidity and (c) indoor CO_2 concentration for the system operating at constant flow scenario

It can be seen from figure 3.31 that the indoor comfort parameters including temperature, humidity and CO_2 concentration for the central heating system operating at constant flow are 20°C±2°C, 50%±5% and 1000PPM±100PPM respectively. All the indoor comfort parameters at constant flow are achieved within the recommended values of ASHRAE. Thus the results of the constant indoor comfort parameters were used as a reference for comparison with pulsed flow indoor comfort results in the next section.

3.5.6 Modelling results of constant flow compared pulsed flow

Figure 3.32 shows the indoor environment of the room including the indoor temperature profile, relative humidity and CO_2 concentration of the pulsed flow to the radiator and by the ventilation fan compared to the constant flow.

Results show that indoor temperature of 20 °C ±1.8°C, indoor relative humidity of 50% +5% and the indoor CO_2 concentration of 1000PPM ±50PPM were achieved as recommended by the indoor comfort standard of ISO 7730-2005, ASHRAE 55-1992, and ASHRAE 62-1999 which are adopted by the international community of building services. Also results are in good agreement with constant flow results of the indoor environment. Therefore pulsating the flow does not affect the occupants comfort but results in significant energy saving of up to 27% as reported in section 3.4.6.

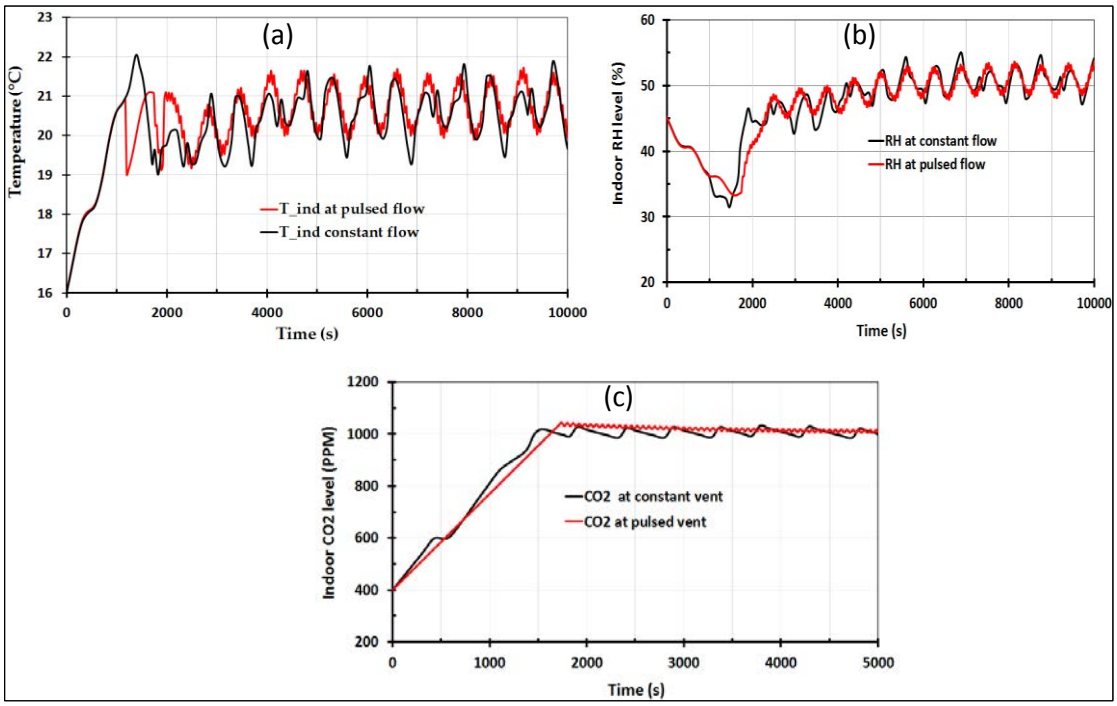

Figure 3. 32 (a) indoor temperature, (b) indoor humidity and (c) indoor CO2 concentration

Figure 3.33 shows the boiler outlet temperature (inlet to the radiator) and the log mean temperature difference (LMTD) of the radiator for both pulsed and constant flow cases. It can be seen that an average boiler exit temperature of 75^{o}C and an average radiator LMTD of 50^{o}C were achieved using the embedded control system.

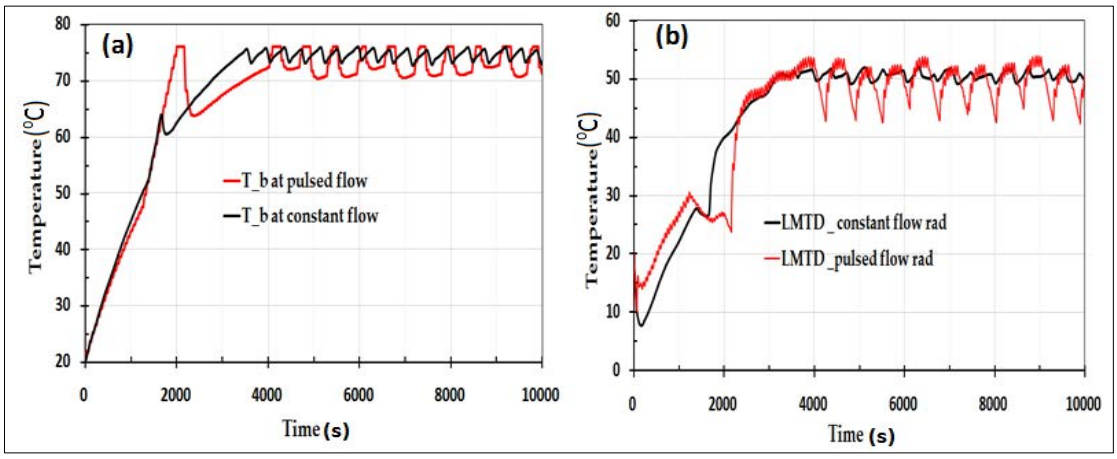

Figure 3.33 (a) boiler outlet temperature and (b) LMTD of the panel radiator for both constant and pulsed flow cases

Figure 3.34 shows the rate of heat output (eq. (3.8)) and the specific heat output (defined by (eq. (3.45)) of the radiator at constant as well as pulsed flow scenarios. As shown in figure 3.34 (b) the specific heat output of the radiator of pulsed flow is higher than that of constant flow. The higher the specific heat output; the lower the hot water mass flow rate supplied to the radiator leading to lower energy consumption for the heating system. This clearly highlights the potential of flow pulsation to enhance the panel radiators of central heating systems.

$$\text{Sp.Q} = \frac{\dot{\text{Q}}_{output}}{\dot{m}} \tag{3.45}$$

Where: Sp.Q is the specific heat output (kJ/kg); $\dot{Q}_{output}$ is the rate of heat output (kW), $\dot{m}$ is the inlet mass flow rate (kg/s).

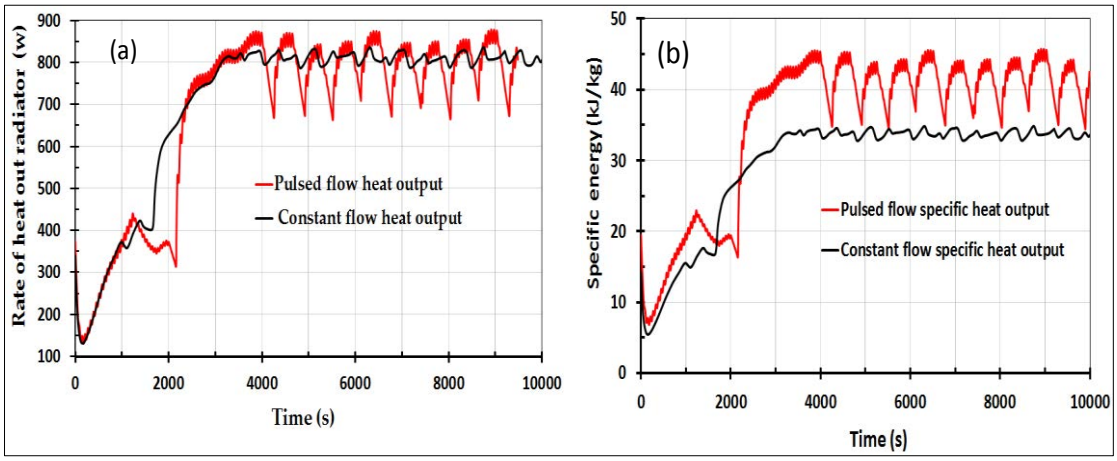

Figure 3.34 (a) rate of heat output of the radiator (b) specific heat output of radiator

Figure 3.35 shows the rate and specific energy consumption due to ventilation for both constant flow and pulsed flow where higher specific energy consumption was

found for the pulse flow than that of the constant flow condition. The energy consumption of the fan used for ventilating the heated space depends on the mass flow rate of fresh air and hence the higher is the specific energy of the ventilation (energy density), the lower the mass flow rate of fresh air which leads to lower energy consumption by ventilation fan. In this case the air flow rate by the fan is controlled by the indoor the level of CO_2 concentration (Demand based control system).

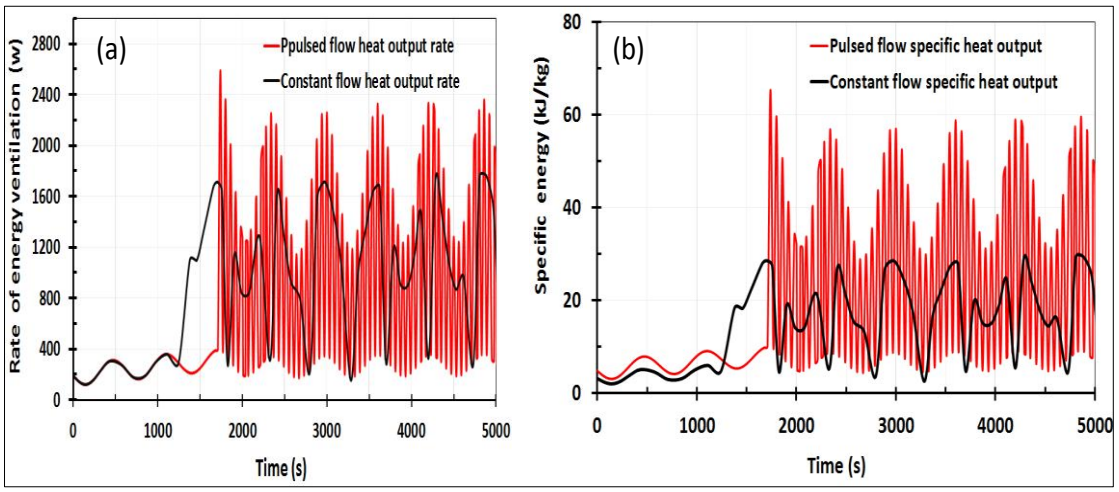

Figure 3.35 ventilation (a) rate of energy output and (b) specific energy rate

Figure 3.36 shows the average specific energy consumed by the heating radiator and the ventilation fan for both constant as well as pulsed flow conditions. The energy saved in percentage due to the applied pulsed flow compared to the constant flow is calculated using eq. (3.46).

$$ES(\%) = \left(\frac{\dot{m}_{CF} - \dot{m}_{PF}}{\dot{m}_{CF}}\right) \times 100 \qquad (3.46)$$

Where: $\dot{m}_{CF}$ the mass flow rate of air or hot water (kg/s) at constant flow cases, $\dot{m}_{PF}$ mass flow rate of air or hot water at pulsed flow cases (kg/s) and ES(%) is the energy saving. The ES(%) was expressed in terms of mass flow rate as the temperature difference and specific heat capacity of the air and water are constant for both constant as well as pulsed flow conditions. Figure 3.36 shows that about 20% of energy can be saved for the heating radiator and 34.5 % for the ventilation fan by applying pulsed flow. The presented results highlight the potential of using flow pulsation to enhance the specific heat output of the heating and ventilation systems and hence saving significant amount of energy without compromising occupants comfort.

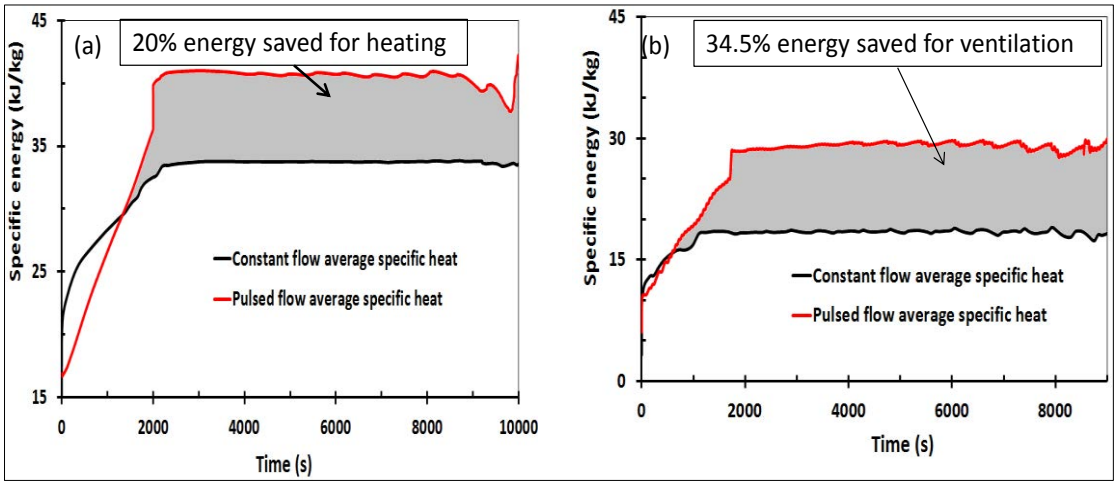

Figure 3.36 the saved energy due to pulsed flow compared to the constant flow case (a) saved energy for heating and (b) saved energy for ventilations

The power consumption of the central heating system consists of the thermal energy consumption associated with the boiler and the electrical energy consumption (mainly from the circulation pump). The 20% improvement in the specific heat output from the radiator is related to thermal energy consumption from the boiler.

As for the pump electrical energy consumption, it was not considered due to being small (around 6% of the total energy consumed [153]) compared to the thermal energy consumption. However, using the pulsed flow applied in this work the pump power consumption was calculated analytically using equations provided in [154] and showed that a reduction of about 12% compared to the pump operating at constant flow can be achieved. This is because the amplification of pump power at the peak of the pulse flow is compensated by the off time period of the pulsed flow as shown in figure 3.14(b).

3.6 Summary

First thermal simulation was used to investigate the feasibility of enhancing the performance of hot water heating system by changing the flow strategy from constant flow to pulsed flow. Mathematical modelling of a single empty room heated using hydronic heater radiator was developed, this modelling includes coupling of the thermal performance of the radiator, air in the heated space, heat transfer through walls and windows and boiler using Simulink / MatLab software.

Results of this initial simulation showed that 20-22% of the energy consumed using current constant flow heating method in centrally heated buildings can be saved by changing the constant flow to pulsed flow. Further improvement was achieved by changing the On/Off feedback control system to PID feedback control with the pulsed flow where results showed that energy saving can be increased up to 27% while the fluctuation in the desired indoor temperature decreased from $\pm 1.7^{o}K$ to $\pm 1^{o}K$. The results from this work highlighted the potential of applying flow pulsation together

with PID controllers in radiator hydronic central heating systems for energy saving in buildings.

Secondly a more realistic room was mathematically modelled to investigate the effect of flow pulsation for radiator hot water and fan air ventilation using a living room with 5 occupants. A control system was developed using MatLab/Simulink software to assess the indoor thermal comfort and indoor air quality (IAQ). The model was developed to control the indoor air quality and thermal indoor comfort of occupants, including temperature of $20^{o}C \pm 2^{o}C$, CO_2 level of 1000PPM ± 100PPM) and relative humidity of 50%± 10 %.

Results of the second model showed that using flow pulsation in hydronic panel central heating system can achieve an average of 20% energy saving compared to the constant flow currently used. Also, using pulsating air flow to the heated space (for ventilation purpose) controlled on the basis of indoor CO_2 concentration achieved energy saving of 34.5% from the fan power consumption. The proposed demand based control system on the basis of indoor CO_2 concentration is able to keep indoor air qualities (CO_2) and indoor relative humidity at an acceptable level of 1000PPM±50PPM and 50%±5% respectively. The significant saving achieved by flow pulsation indicates the potential of using this approach to reduce energy consumption while maintaining the indoor comfort requirement in buildings. Also using the pulsed flow applied in this work the pump power can be reduced by about 12% compared to the pump operating at constant flow.

CHAPTER 4

CFD SIMULATION OF HYDRONIC PANEL RADIATOR

4.1 Introduction

In chapter 3 the hydronic panel radiator was analysed mathematically at various flow strategies including the pulsed flow and constant flow conditions. The Simulink based investigation in chapter 3 showed that; there is a clear potential of energy saving when the radiator is operated at pulsed flow compared to the radiator operated at constant flow. However the Simulink modelling is based on the lumped heat transfer analysis assuming uniform heat transfer coefficient for the entire radiator surface. Thus further investigation of the radiator using computational fluid dynamics simulation (CFD) is performed to predict the effect of pulsating flow on heat transfer with the radiator and the temperature distribution on the radiator surface which affects the heat transfer to the room.

The finite element CFD simulation is a very powerful tool to investigate the heat transfer performance of various devices, including heat exchangers [63, 68,159], building central heating system [156, 157], hydronic radiators [84, 89, 95, 158], single phase and multiphase flows [155, 160]. The work presented in this chapter includes CFD simulation of the hydronic radiator at constant and pulsed flow conditions using COMSOL Multiphysics software [155, 160].

The aim of this research is to investigate the effect of pulsed flow rate on the energy consumption of panel radiators in hydronic central heating systems compared to the constant flow using CFD simulation. Two types of radiators (single finned radiator (type 11) and radiator without fins (type 10)) were simulated at constant and pulsed flow conditions. The pulsed flow conditions were used to investigate the effects of flow amplitudes, frequencies and effect of inlet temperature. Results of the pulsed flow were compared to those of constant flow on the basis of specific heat output to analyse the potential for energy saving due to the pulsed flow strategies while maintaining the LMTD of the radiator at 50K for the 75^{o}C inlet hot water temperatures as recommended by EN BS 442 radiator standards [95]. Part of the work presented in this chapter is published [96].

4.2 Governing equations of CFD modelling

A CFD package called COMSOL Multi-physics software was used to perform the numerical simulation. COMSOL is a finite element modelling and solver software for numerous engineering applications including coupled heat transfer and fluid flow analysis. COMSOL has extensive interface to other software, such as the MATLAB and CAD software (SOLID WORK) [163]. The CFD simulation of the radiators was carried out using conjugate heat transfer physics with the main governing equations including conservation of momentum, mass, and energy equations.

Conservation of momentum involves evaluating the forces acting on the flow elements and calculating the rate of momentum change as; eq.4.1.

$$\rho\frac{\partial u}{\partial t}+\rho(u.\nabla)u=\nabla.[-pI+(u+\mu_T)$$

$$(\nabla u+(\nabla u)^T)-\frac{2}{3}(u+\mu_T)(\nabla.u)I-\frac{2}{3}\rho\kappa_T I]+F \qquad (4.1)$$

Where :

$$\mu_T=\rho C_1\frac{\kappa_T{}^2}{\varepsilon_T}$$

Where:∇, ρ, u, p, I, F, ε_T, μ, μ_T, k_T,t and C_1 are vector differential operator, density, vector velocity, pressure, identity matrix of [3*3], total force acting per volume, the turbulence dissipation rate, dynamic viscosity, turbulence dynamic viscosity, the turbulence kinetic energy, time and model constants respectively.

The mass conservation equation is expressed as; eq. (4.2).

$$\frac{\partial\rho}{\partial t}+\nabla.(\rho V)=0 \qquad (4.2)$$

Where; the first term on the left side of eq. (4.2) is the density variation with time and the second term is the vector differential of density multiplied by velocity.

Conservation of energy equation is expressed as; eq. (4.3).

$$\rho C_p\frac{dT}{dt}+\rho C_p V.\nabla T=\nabla.(k\nabla T)+Q \qquad (4.3)$$

Where: C_P, T, Q, k, and V are specific heat capacity, temperature, heat source other than viscous, thermal conductivity and volume respectively. Also the term on the left side of eq. (4.3) is the rate of change of the total internal energy plus the internal energy transported by the flow while the term on the right side is heat transfer by conduction plus heat sources other than vicious.

According to published work the k-ε turbulence model predicts actual flow patterns more accurately than any other turbulent models [162]. Thus k- ε turbulence model with heat transport turbulence model of Kays-Crawford was selected for this work as it predicts the behaviour of laminar and turbulent flow accurately. The values for the turbulence model of k_T (turbulent kinetic energy), ε_T (turbulent dissipation rate), and the pressure are calculated using eq. (4.4), eq. (4.5) and eq. (4.6) respectively.

$$\rho\frac{\partial \kappa_T}{\partial t}+\rho(u.\nabla)\kappa_T=\nabla[(\mu_T+\frac{\mu_T}{\sigma_k})\nabla\kappa_T]+p_T-\rho.\varepsilon_T \tag{4.4}$$

$$\rho\frac{\partial \varepsilon_T}{\partial t}+\rho(u.\nabla)\varepsilon_T=\nabla[(\mu_T+\frac{\mu_T}{\sigma_\varepsilon})\nabla\varepsilon_T]+C_{\varepsilon 1}\frac{\varepsilon_T}{\kappa_T}p_T-C_{\varepsilon 1}.\rho\frac{\varepsilon_T^{\,2}}{\kappa_T} \tag{4.5}$$

$$p_T=\mu_T[\nabla u:(\nabla u+(\nabla u)^T)-\frac{2}{3}(\nabla.u)^2]-\frac{2}{3}\rho\kappa_T\nabla.u \tag{4.6}$$

Where: P_T is the pressure, σ_k, σ_ε and $C_{\varepsilon 1}$ are constants.

As part of the governing equations the following user defined boundary conditions were considered to perform the modelling of the proposed radiators at both pulsed and

constant flow conditions. The heat transfer coefficient on the surface of the radiator was considered as natural convection which is calculated using the commonly used empirical correlation presented in [4, 96]. The natural convection heat transfer coefficient of air on the surface of the radiator was calculated using eq. (4.7).

$$h = 0.59.(Ra)^{1/4}.\left(\frac{k}{L}\right) \tag{4.7}$$

Where; Ra is the Rayleigh number given as:

$$Ra = Gr.Pr \tag{4.8}$$

Grashof numbers (Gr) and Prandtl number (Pr) are expressed as:

$$Gr = \left(\frac{g.\beta(T_{sur} - T_{amb})L^3}{\nu^2}\right) \quad \text{and} \quad Pr = \frac{\mu C_p}{k} \tag{4.9}$$

Where β is thermal expansion coefficient determined as:

$$\beta = \frac{2}{T_{sur} + T_{amb}} \tag{4.10}$$

Where: h, L, T_{sur}, T_{amb}, g, k, ν, μ and C_p are local convection heat transfer coefficient, characteristics length, surface temperature, ambient temperature, gravitational acceleration, thermal conductivity, kinetic viscosity, dynamic viscosity and specific heat capacity respectively.

The surface-to-ambient radiation was also applied on the surface of the radiator to calculate the heat transfer by radiation as eq. (4.11).

$$Q_{rad} = A\,\varepsilon_s\,\sigma_s((T_{amb})^4 - (T_{sur})^4) \qquad (4.11)$$

Where: ε_s is radiator surface emissivity assumed constant as 0.9, σ_s is the Stefan-Boltzmann constant 5.67 x 10^{-8} ($WK^{-4}m^{-2}$), T_{amb} is the ambient temperature, T_{sur} surface temperature of the radiator and A is the surface area of the radiator.

On the water domain, gravity effect was applied to exploit the buoyancy force due to density difference of the hot water expressed as; eq. (4.12).

$$F = -g.(\Delta\rho) \qquad (4.12)$$

Where: F is the volume force (N/m^3), g is the gravitational constant of 9.81 m/s^2 and $\Delta\rho$ is the density difference of hot water domain due to the temperature variation in the flow channels.

4.2.1 Radiators modelling set up

The thermal performance of the 3D hydronic heating radiator was simulated using the pulsed and constant hot water flow. The geometry of two types of radiators including single panel hydronic radiator with attached fins (type11), and single panel radiator

without fins (Type10) were developed in COMSOL. The two types of radiators are made from the same material with dimension of 1000mm width and 600mm height. All the thermal properties of the two types of radiators are the same; the only difference is the addition of fins to the type11; to investigate the effect of fins on the heat output of the radiator. Figure 4.1 shows the dimensions of radiators modelled and their main components created in COMSOL. Figure 4.2 shows the CAD profile of the two types of radiators and the fin configuration of the type11 radiator.

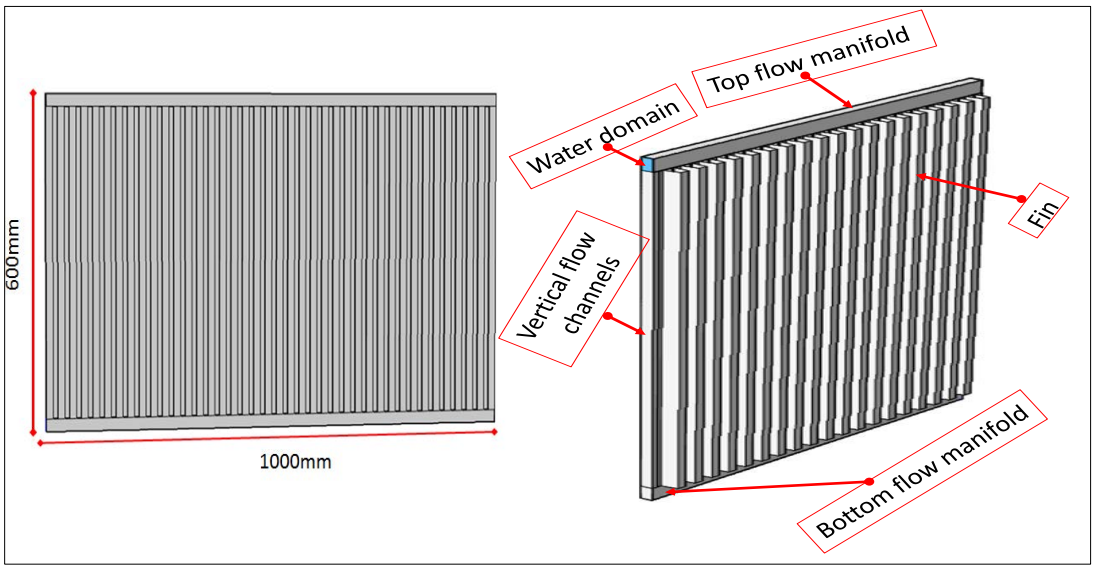

Figure 4.1 hydronic radiator dimension and the main parts

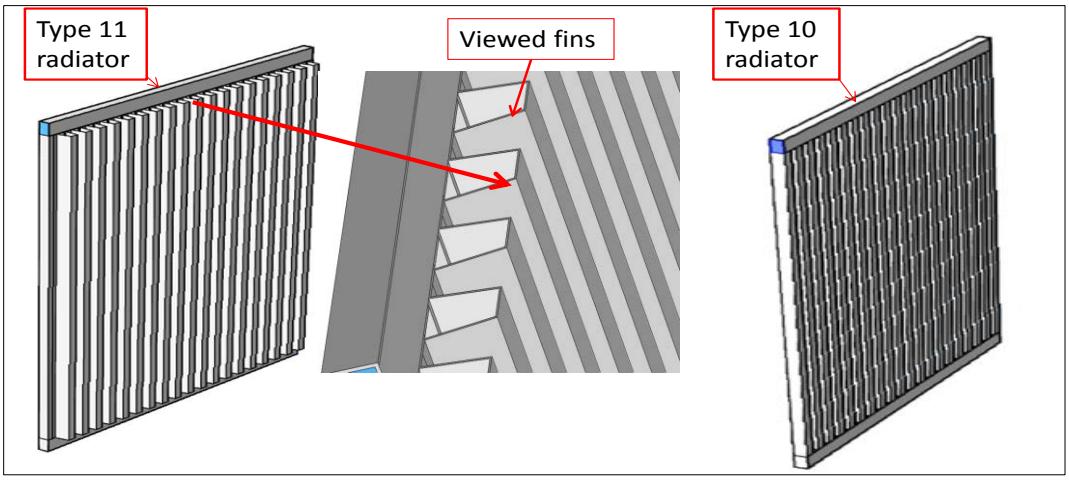

Figure 4.2 the CAD profile of the type 11 and type 10 radiators proposed for this work

The hydronic panel radiator models comprised of the rectangular vertical ducts (flow channels 12.5mm side with thickness of 1mm), rectangular horizontal collector duct (flow manifold 12.5 width and 22.5mm height), fins 540 mm high with thickness of 0.5mm and the water domain. The materials for the selected hydronic panel radiators are obtained from the manufactures catalogue, with thermal properties presented in table 4.1.

Table 4.1 thermal properties for the for radiator model

Domain type	Materials type	K (W/m.K)	Cp(J/(kg.K))	ρ (kg/m^3)
Fluid	Water	0.58	4180	1000
Channels	Steel	16.5	475	7850
Fins	Steel	16.5	475	7850

The inlet mass flow rate was calculated using the nominal heat output ($\dot{Q}_s$) given by the manufacturer of the hydronic radiator expressed as eq. (4.13) and eq. (4.14) [95, 183].

$$\dot{Q}_S = \dot{m} Cp \Delta T \tag{4.13}$$

$$\dot{m} = \frac{\dot{Q}_S}{Cp \Delta T} \tag{4.14}$$

Where; Cp is specific heat of water (kJ/(kg.K)), ΔT is the inlet (75^{o}C) and outlet (65^{o}C) temperature difference as recommended by EN 442 radiator standards [95-96 and 183]. The mass flow rate of the radiator was found to be 0.022kg/s for typ11 radiator and 0.0174kg/s for type10 radiator.

Flow arrangement of the hydronic radiator as described by the hot water inlet and outlet positions of the radiator is important for thermal analysis of the radiator. Figure 4.3 shows schematic diagram of the three common flow arrangements of hydronic panel radiator existing in the market [95, 183]. The three main flow arrangements are top-bottom opposite end (TBOE), top bottom same end (TBSE) and bottom-bottom opposite end (BBOE). TBOE produces the highest thermal performance of the radiator compared to the other two flow arrangements as reported by Aydar et al [95]. Thus the radiators modelled in this work were set to have top-bottom opposite end (TBOE) flow arrangement as shown in figure 4.3 (a).

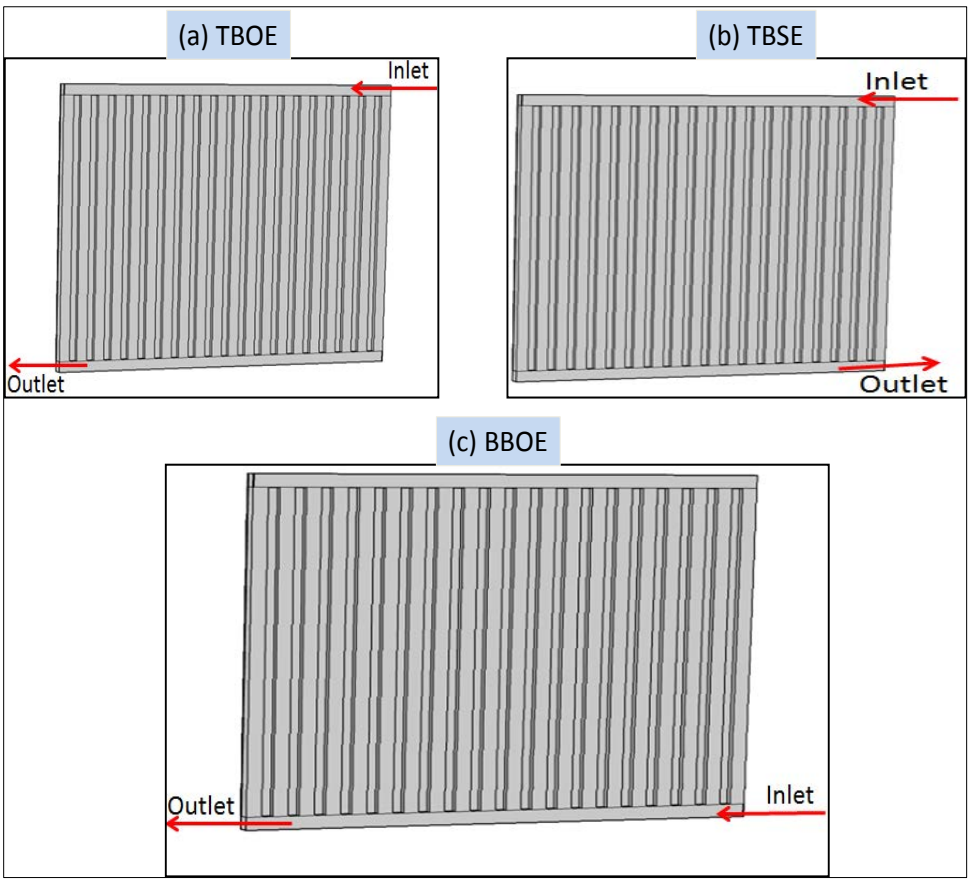

Figure 4.3 the various flow arrangements of the hydronic panel radiator

4.2.2 Mesh sensitivity of the radiator finite element modelling

Meshing plays important role in developing the finite element models. Meshing sensitivity was carried out to analyse the impact of mesh quality on the thermal performance output of the hydronic radiators modelled in this research. Panel radiator with attached fins (type11) was simulated at constant and pulsed flow rate using various mesh element numbers as shown in table 4.2. The radiator was meshed using tetrahedral mesh type, as it give better mesh quality for complicated design shapes. The radiator hot water outlet temperature of the two flow scenarios (constant and pulsed) were used to investigate the impact of meshing on the thermal output. Figure 4.4 and figure 4.5 shows the hot water outlet temperature of the radiators operating at constant flow rate and pulsed flow rate respectively.

Table 4.2 the element number of meshing procedure

Number of runs	Mesh element number
run 1	1513919
run 2	928335
run 3	551296
run4	100000

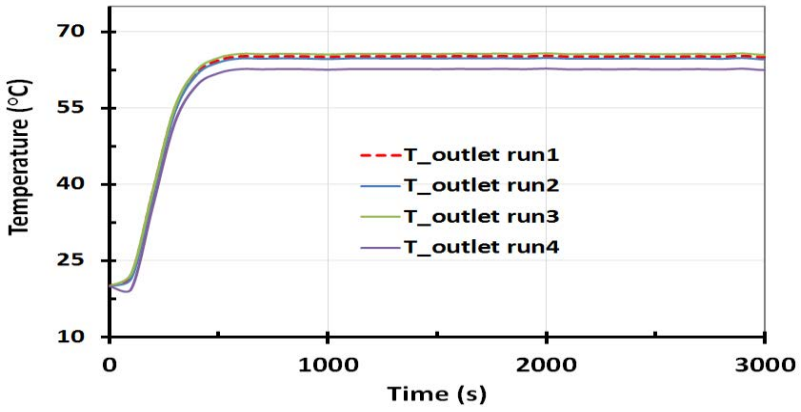

Figure 4.4 outlet temperature of the hot water at constant flow rate radiator type11

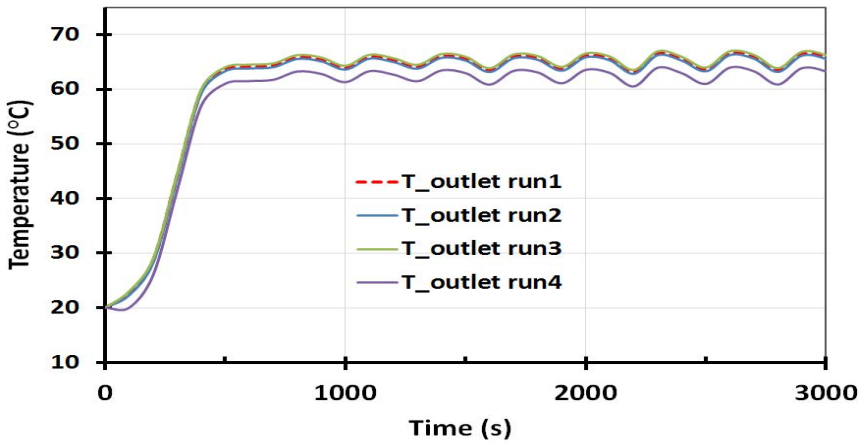

Figure 4.5 outlet temperature of the hot water at pulsed flow rate radiator type11

Figure 4.4 and figure 4.5 shows the average deviation of outlet temperature between the first three runs are 0.25% and 0.28% for radiator at constant and pulsed flow rate respectively. However for the fourth run considerable temperature difference was obtained as it is clearly shown in figures 4.4 and 4.5. Thus based on the results of mesh sensitivity gained the element number shown in run3 (with element number of 551296) was used to simulate the radiators.

4.3 Finite element modelling results and discussion

The finite element modelling of the radiator was mainly carried out at two main flow strategies; namely constant flow scenario (conventional flow) and pulsed flow scenario (proposed in this work). All radiators were simulated at constant inlet and ambient temperature of 75^{o}C and 20^{o}C respectively, but with different input conditions to achieve water outlet temperature of 65^{o}C and radiator LMTD of 50K. Sections 4.3.1 to 4.3.4 describe the results of modelling the hydronic radiator at

constant flow including modelling two types of radiators, validating the modelling techniques, and investigating the effect of inlet temperature. Sections 4.3.5 to 4.3.9 describe the results of modelling the radiators using pulsed flow including investigating the effect of pulse amplitude and frequency on the performance of the two radiators used. Results of the pulsed flow were compared to the results of constant flow to examine the potential of energy saving due to the proposed pulsed flow strategy. Simulation results were analysed using the specific heat output (eq. (3.45) chapter 3), the rate of heat output (eq. (3.8) chapter 3), LMTD (eq. (3.10) chapter 3), mean radiator temperature eq. (4.15) and hot water outlet temperature. Further investigation of the thermal performance of the radiator type11 was also carried out using various hot water inlet temperatures.

$$T_{mean} = \frac{T_{w,in} + T_{w,out}}{2} \tag{4.15}$$

4.3.1 Radiator thermal performance at constant flow

In this section all radiators were simulated at constant inlet water temperature and constant flow rate. The full size (1000mm*600mm), hydronic radiator with attached fin (type11) was simulated using inlet mass flow rate of 0.022kg/s at constant flow rate. Figure 4.6 (a) shows the temperature distribution on the surface of type11 radiator and figure 4.6 (b) shows the variation of specific heat output, LMTD, mean temperature and outlet temperature of the radiator.

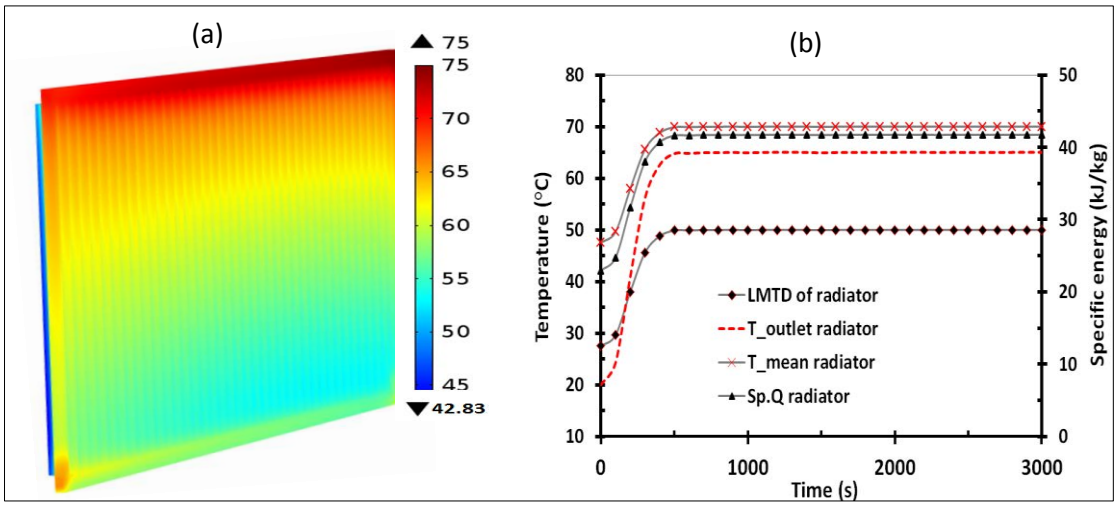

Figure 4.6 (a) contour of local surface temperature distribution (^{o}C); (b) LMTD, outlet temperature, mean temperature and rate of specific heat output for full size constant flow radiator

It is clear from figure 4.6 (b) that water outlet temperature of 65^{o}C (T_outlet radiator) and LMTD of 50^{o}C were achieved as recommended by EN 442 radiator standard test. Although the finite element model of the full size radiator gives a good prediction of the thermal output of the radiator; this is achieved at high cost of computer memory and longer computational run time. To complete this single run 13G of memory space and 32 hours of running time were required. To avoid the memory constraint and to save running time, the effect of reducing the size of the modelled radiator (scaling down) will be investigated on the water outlet and LMTD.

Based on the structure of radiator geometry; the simulated full size type11 hydronic panel radiator was cut vertically into half to give a dimension of 500mm width and 600mm height. This half size radiator was simulated with the inlet mass flow rate halved to 0.011kg/s. Figure 4.7 shows the modelling results of the half size type11 radiator at constant flow rate.

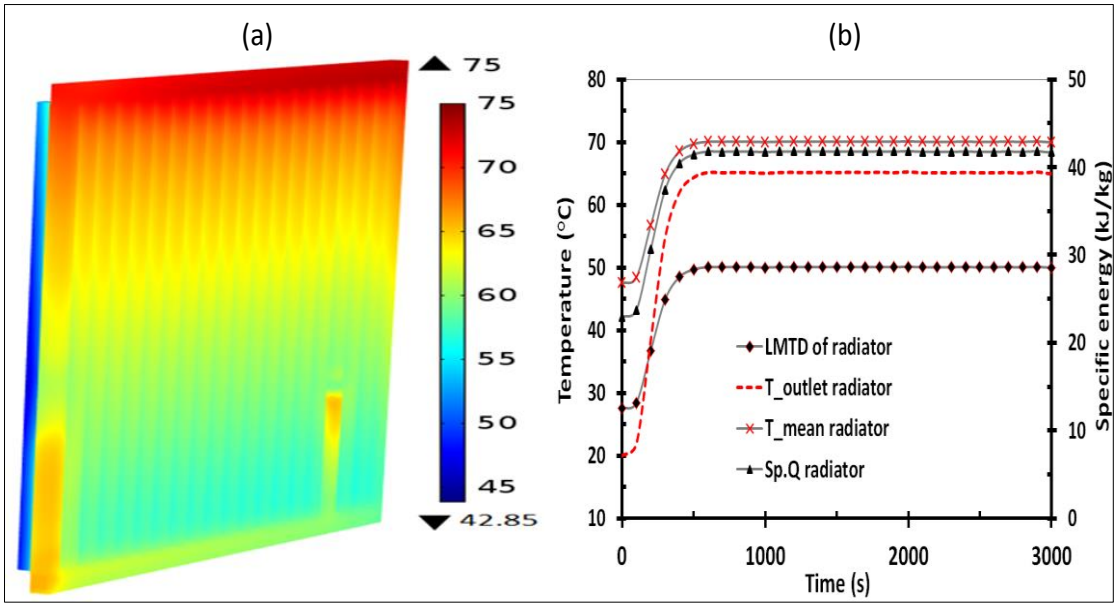

Figure 4.7 (a) contour of local surface temperature distribution (^{o}C); (b) LMTD, outlet temperature, mean temperature and rate of specific heat output for half size constant flow radiator

It is clear from the results of half size (figure 4.7) and full size (figure 4.6) radiators that the specific heat output, the mean temperature, outlet temperature of the water and LMTD of the radiators are similar. The maximum difference in the outlet water temperature between those achieved with full-size radiator and those of the half size is 0.18% highlighting the good agreement. However simulating half the radiator resulted in reducing the computational time and memory constraints where 6G memory space and 8hours running time are needed. Thus less than half memory space and four times less running time than that of the full size radiator were required for modelling the half size radiator. Therefore the half size radiator was used in the modelling work carried out in this project.

4.3.2 CFD results of type10 and type11 radiators at constant flow

The panel radiator without fins (type10) and that with fins (type11) were simulated at 0.0087kg/s and 0.011kg/s respectively, constant inlet temperature of 75°C and ambient temperature of 20°C. The two radiators have the same size of 500 mm width and 600mm height. Figure 4.8 shows the heat output from the radiator, the water outlet temperature, radiator mean surface temperature, and LMTD for both Type11 and Type10 panel radiators.

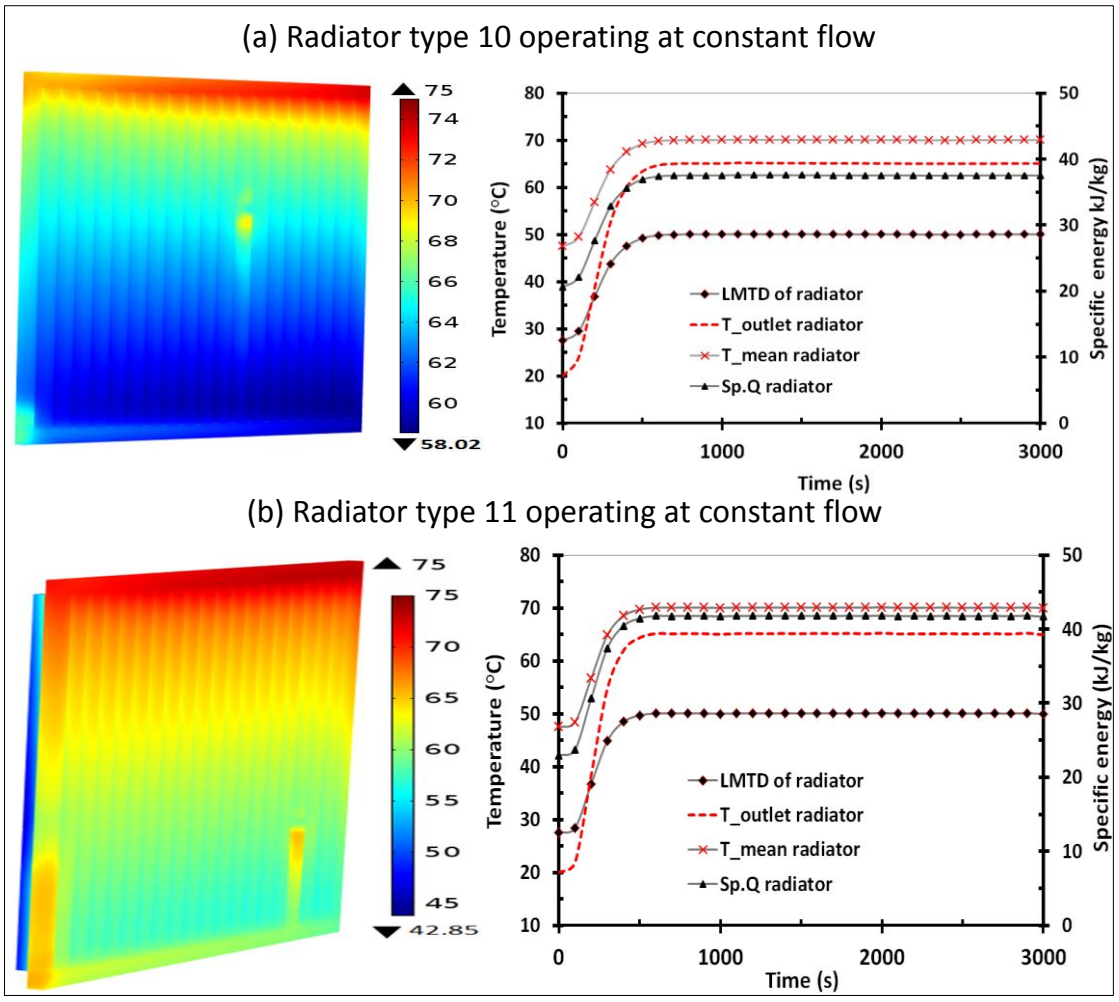

Figure 4.8 contour of local surface temperature LMTD, outlet temperature, mean temperature, rate of specific heat output for (a) type 10 radiators and (b) type11 radiator using constant flow rate

Figure 4.8 shows that the two types of radiators have same outlet temperature, mean surface temperature and LMTD of 65^{o}C, 70^{o}C and 50^{o}C respectively as recommended by EN BS 442 radiator standards. However it is clear that higher specific heat output is achieved by type11 radiator compared to that of type10 radiator; due to the higher heat transfer surface area associated with fins. As the type11 radiator has advantage on type10 radiator in terms of heat output is commonly used in residential homes; further modelling of type11 radiator was carried out at various inlet hot water temperatures while maintaining other parameters constant in section 4.3.4.

4.3.3 Validation of the radiator at constant flow

Before proceeding to investigating the radiator using pulsed flow rate it is important to validate the CFD results against experimental work. The CFD results of type11 radiator at 75^{o}C hot water inlet were validated against the experimental results reported by [95-96 and 156]. The validation was based on surface mean temperature, LMTD and hot water outlet temperature. The percentage of deviation for the numerical and experimental results is calculated using eq. (4.16).

$$\text{Diff }\% = \left| \frac{Exp - CFD}{\text{Exp}} \right| * 100 \qquad (4.16)$$

Where; Diff %, Exp and CFD are percentage of deviation, experimental results and computational results respectively.

Table 4.3 compares the predicted hot water outlet temperature, radiator surface mean temperature and LMTD to the experimental results reported in [95] at the same flow rate, hot water inlet temperature and ambient temperature.

Table 4. 3 CFD results and experimental results of the type11 panel radiator

Specifications	CFD	Exp	Diff %
Ambient temperature (^{o}C)	19.89	19.89	
Inlet temperature (^{o}C)	74.76	74.76	
Outlet temperature (^{o}C)	65.7	64.71	1.53
Mean temperature (^{o}C)	70.35	69.76	0.8
Log mean temperature difference (K)	50.35	49.76	1.2

As shown in table 4.3, the CFD results of type11 radiator are in good agreement with the experimental results where maximum deviation of 1.53%. Therefore the CFD simulation methodology developed using COMSOL can be used to investigate the performance of the hydronic heating radiator at various operating conditions including pulsed flow.

4.3.4 CFD of type11 radiator at various inlet temperature

The UK 2020 vision as described by [11] requires increasing the use of heat pumps for heating of buildings. These heat pumps tend to deliver hot water at lower temperature compared to those delivered by boilers. Therefore investigating the radiator heat transfer performance at various hot water inlet temperatures at constant

flow rate (this section) and pulsed flow rate (section 4.3.11) is important to identify the potential of using low temperature heat sources for hydronic heating systems.

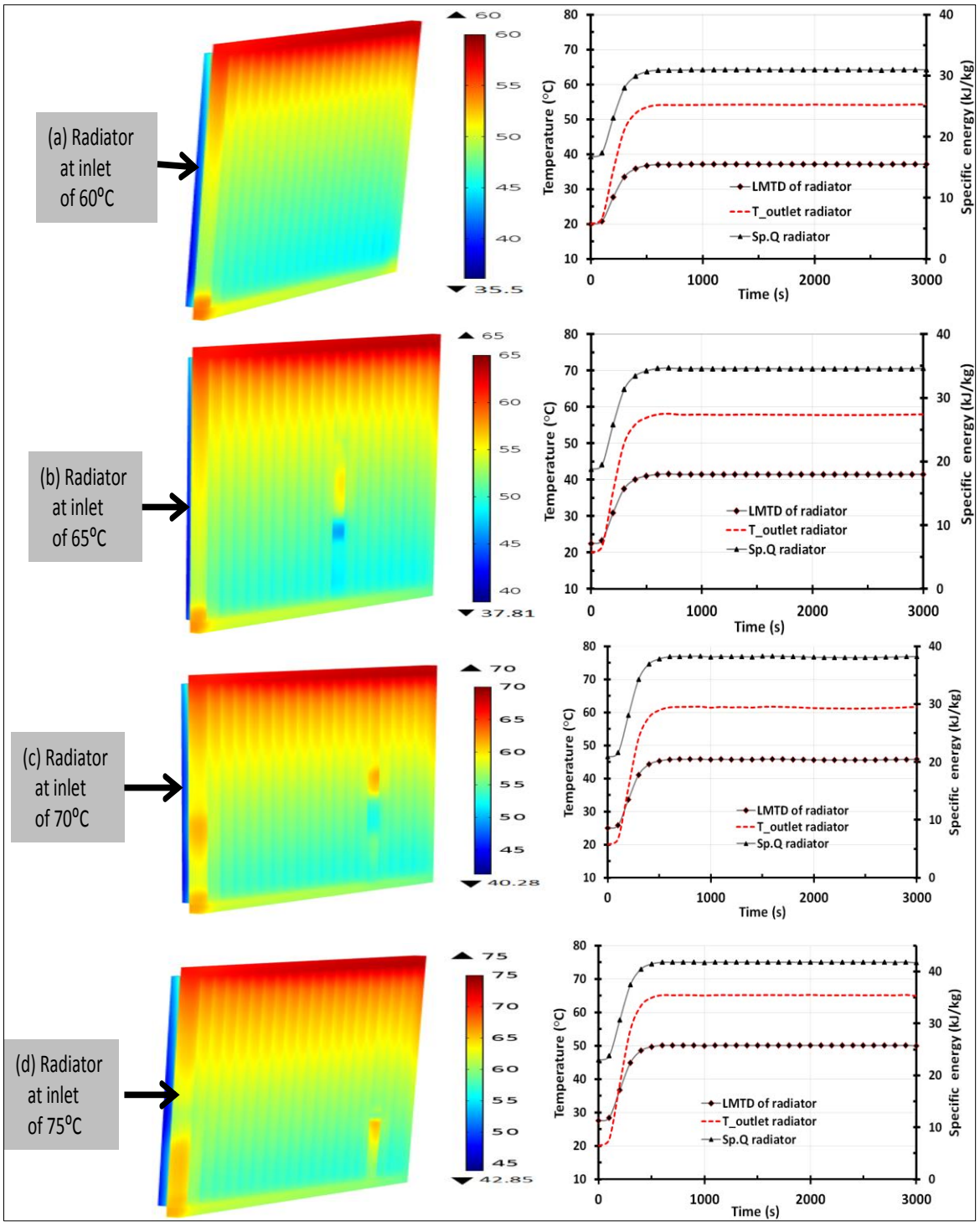

Figure 4.9 contours of local surface temperature LMTD, outlet temperature, mean temperature; rate of specific heat output for the radiator simulated using constant flow

The type11 radiator was simulated at constant flow rate of 0.011kg/s using various hot water inlet temperatures of 75^{o}C, 70^{o}C, 65^{o}C and 60^{o}C. Figure 4.9 shows the variation of hot water outlet temperature, LMTD and specific heat output of the radiator type11 at various hot water inlet temperatures. Results showed that the specific heat output, the LMTD and the outlet temperature decrease as the inlet temperature of the radiator decreases. Thus the heat output of the radiator is directly proportional to the inlet temperature of hydronic radiator.

4.3.5 Finite element modelling results at pulsed flow

Using pulsed flow the finite element modelling of radiators with dimension of 500mm*600mm were carried out to investigate the effect of flow amplitudes and frequency for both type10 and type 11 radiators. Flow pulsation through the radiator channels causes disturbance to the bulk fluid and at the walls of the channels leading to the creation of vortices and enhancing heat transfer from the fluid to the channel walls. This flow disturbance depends on the non-dimensional Strouhal number [71] and the Reynolds number expressed using eq. (4.17) and eq. (4.18) respectively.

$$\mathrm{St} = \frac{\mathrm{f}\,.\,\mathrm{L}}{\mathrm{Vel}} \tag{4.17}$$

$$\mathrm{Re} = \frac{Vel.d_h}{\nu} \tag{4.18}$$

The hydraulic diameter of the inlet channel is expressed using eq. (4.19).

$$d_h = \frac{4.A}{2\,Per} \qquad (4.19)$$

Where; St is Strouhal number (the effective values of Strouhal number for heat transfer enhancement ranging from 0.05 to 1 [71]), Re is Reynolds number, d_h hydraulic diameter, Per is perimeter of inlet channel, A is cross sectional area of the inlet channel, f is flow frequency, L characteristics length, Vel is flow velocity and ν is the kinematic viscosity.

The thermal boundary condition of the pulsed flow radiator model is the same as the constant flow case with the only difference being pulsating the hot water flow at inlet rather than using constant flow. The modelling of the hydronic radiators at pulsed flow condition was carried out using the same governing equations described in section 4.2 and the model set up described in section 4.2.1. Also all the thermal boundary conditions described in section 4.2.1 that were used to model the constant flow conditions were used for modelling the pulsed flow except for the radiator inlet boundary condition where the inlet flow velocity profile shown in figure 3.14a (chapter 3) was used.

4.3.6 Effect of flow amplitudes on type11 radiator

The effect of flow pulsation was investigated using various input flow velocity amplitudes at constant flow frequency of 0.033Hz and constant inlet temperature of 75^{o}C. The input values of the flow amplitude are shown in table 4.4 where the reduction in mass flow rate of pulsed flow compared to constant flow (%) was calculated using eq. (4.20)

$$\text{mass reduction}(\%) = \left(1 - \frac{\text{Average}\dot{m}_{CF}}{\text{Average}\dot{m}_{PF}}\right).100 \quad (4.20)$$

Where: $Average.\dot{m}_{CF}$ is the average constant mass flow rate and $Average.\dot{m}_{PF}$ is the average mass flow rate at pulsed flow.

Table 4.4 pulsed flow amplitudes at constant frequency of 0.033Hz type11 radiators

Amplitudes (kg/s)	Average mass flow rate (kg/s)	Mass reduction (%) (pulsed flow compared to constant flow)	Flow frequencies (Hz)	Inlet temp (^{o}C)
0.0206	0.0103	5	0.033	75
0.0196	0.0098	10	0.033	75
0.0184	0.0092	15	0.033	75
0.0174	0.00870	20	0.033	75
0.0163	0.00815	25	0.033	75

Figure 4.10 shows the predicted LMTD, hot water outlet and mean surface temperature of the radiator variation with time at various flow amplitudes while maintaining other parameters constant. It is clear from figure 4.10 that, the temperature of the radiator increases as the flow amplitude increases. Particularly the LMTD of the radiator increased from 48^{o}C at flow amplitude of 0.0163kg/s to 51^{o}C at flow amplitude of 0.0206kg/s.

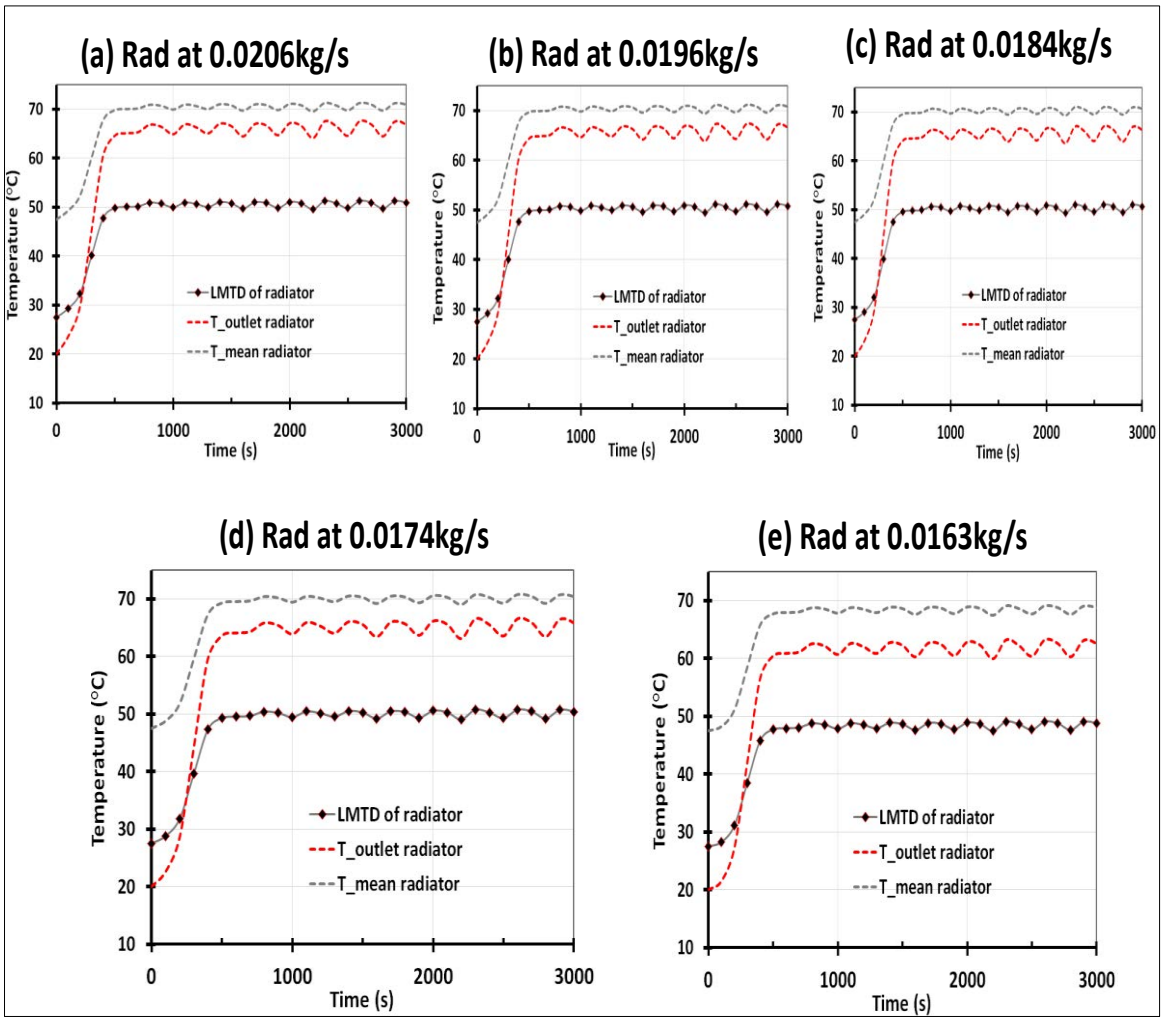

Figure 4.10 LMTD, outlet temperature, mean temperature of the type11 radiator operating at various velocity flow amplitudes while keeping other parameters constant

Figure 4.11 shows the specific heat output of the radiator at various flow amplitudes, and it is clear that the highest specific heat output was achieved at flow amplitude of 0.0174kg/s. At this flow amplitude, the radiator achieved LMTD of 50^{o}C (see figure 4.10(d)) which is consistent with EN442 radiator standards. The higher specific heat output of the radiator indicates that lower hot water flow rate can be used to produce the required heat load. Thus using pulsed flow, the load on the central heating boiler can be decreased leading to reduction in fossil fuel consumption and CO_2 emission.

Thus the selected best flow amplitude of 0.0174kg/s was used to investigate the effect of pulsed flow frequency.

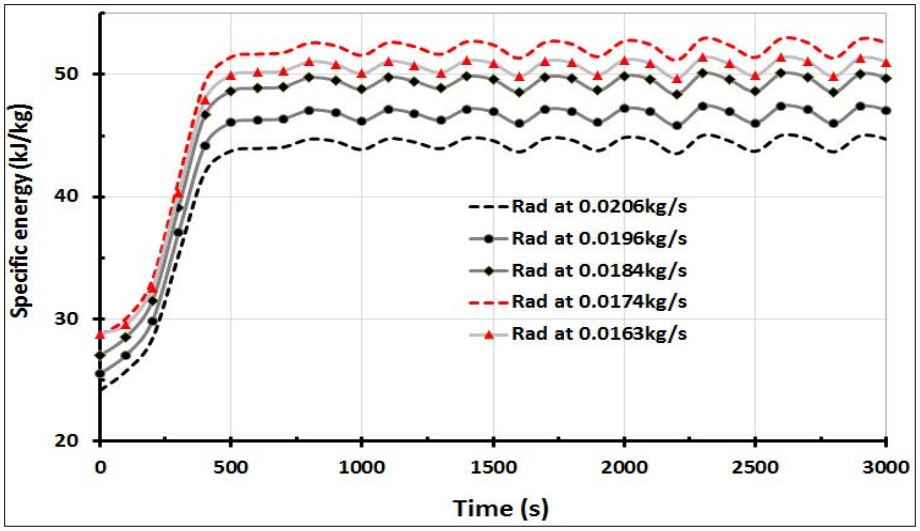

Figure 4.11 specific heat output of the type11 radiator operating at various flow amplitudes while maintaining other parameters constant

4.3.7 Effect of flow frequencies on type11 radiator

The effect of flow pulsation was studied using various input flow frequencies, constant flow amplitude of 0.0174kg/s and constant inlet temperature of 75^{o}C. The input values used for modelling the radiator at various flow frequencies are shown in table 4.5. The radiator was simulated at various flow frequencies and the flow frequency that produced the best specific heat output with lower temperature fluctuation was selected as the best operating pulsed flow for further investigation.

Figure 4.12 shows variation with time of the LMTD, water outlet and mean surface temperature of the radiator at various flow frequencies while maintaining other parameters constant. It is clear from figure 4.12 that the mean surface temperatures of

the radiator for all proposed flow frequencies are similar with a value of 70°C. However the radiator with lower flow frequency gained higher thermal inertia, this higher inertia is achieved at the cost of higher radiator surface temperature fluctuation that can cause discomfort to the occupants of the heated space. Based on the lowest temperature fluctuation, the frequency of 0.033Hz was selected as the best operating pulsed flow conditions.

Table 4.5 pulsed flow frequency at constant amplitudes of 0.0174kg/s for type11 radiators

Amplitudes (kg/s)	Average mass (kg/s)	Mass reduction (%) (pulsed flow compared to constant flow)	Flow frequencies (Hz)	Inlet temp (°C)
0.0174	0.0087	20	0.033	75
0.0174	0.0087	20	0.016	75
0.0174	0.0087	20	0.011	75
0.0174	0.0087	20	0.0083	75

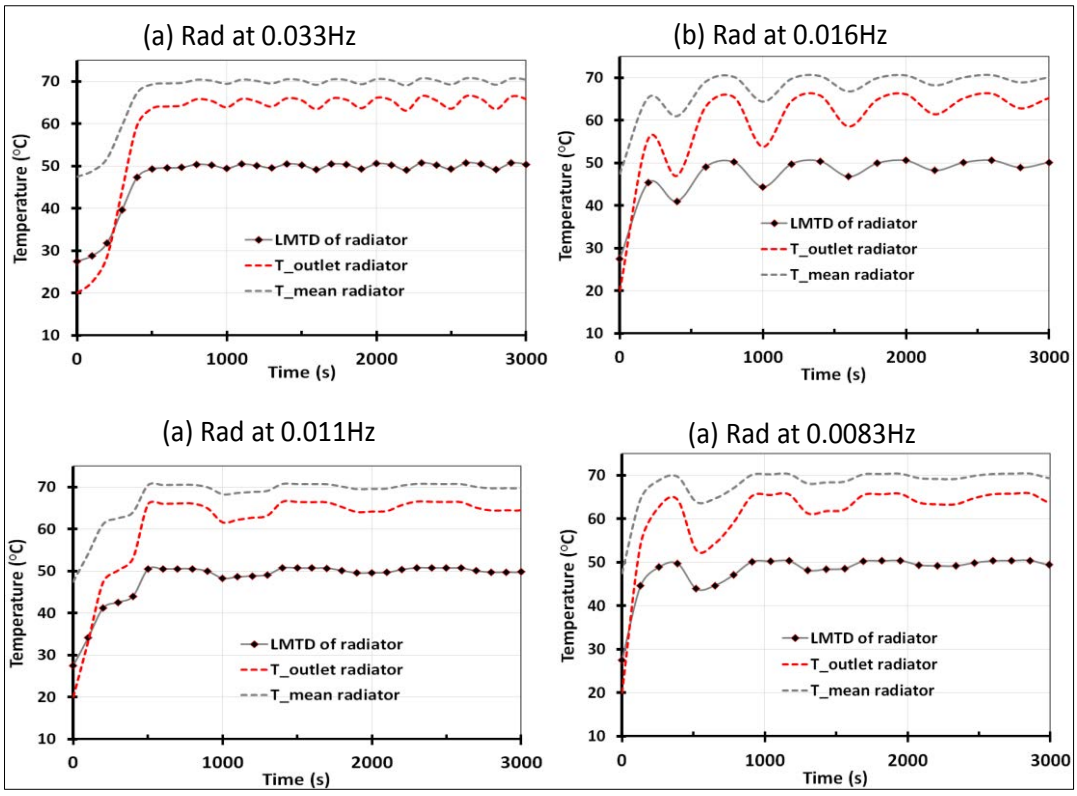

Figure 4.12 LMTD, outlet temperature, mean temperature of the type11 radiator operating at various flow frequencies while maintaining other parameters constant

Figure 4.13 shows the specific heat output variation of the simulated radiator at various flow frequencies. It is clear that there is no visible difference in the average specific heat output of the radiator. However figure 4.13 shows that higher fluctuation and fast thermal inertial were produced when the radiator was operating at flow frequencies ranging from 0.0083Hz to 0.016Hz while the radiator was operating at flow frequency of 0.033 lower fluctuations of 0.7% was achieved. Based on the fluctuation and specific heat output rate of the radiator the best operating flow frequency is 0.033Hz .

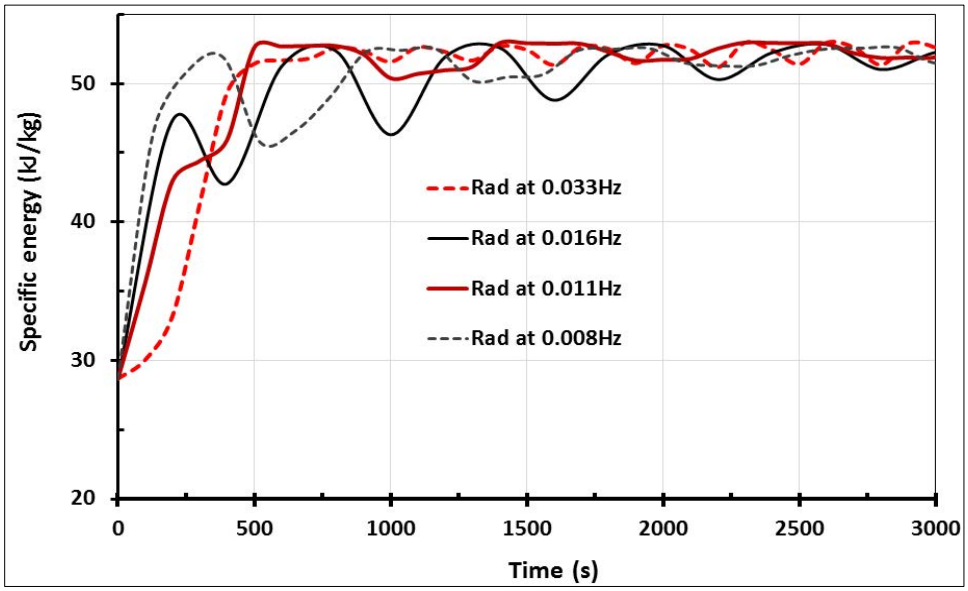

Figure 4.13 specific heat output of the type11 radiator operating at various flow frequencies

Based on the effect of flow amplitudes and flow frequencies the best operating pulsed flow was selected as 0.0174kg/s (20% less average mass flow rate than that of constant flow) and 0.033Hz respectively. Further investigation of the pulsed flow using radiator type10 (radiator without fins) is presented in the following section. The

aim of this modelling is to investigate the effect of pulsed flow on the type10 radiator compared to the type11one.

4.3.8 Effect of flow amplitudes on type10 radiator

The effect of flow pulsation on the heat transfer performance of radiator type10 was carried out using various input flow amplitudes at constant flow frequencies of 0.033Hz and constant inlet temperature of 75^{o}C. The input values of the flow amplitude are shown in table 4.6 where the reduction in mass flow rate of pulsed flow compared to constant flow (%) was calculated using eq. (4.20).

Table 4. 6 pulsed flow for type10 radiators at various flow amplitudes

Amplitudes (kg/s)	Average mass (kg/s)	Mass reduction (%) (pulsed flow compared to constant flow)	Flow frequencies (Hz)	Inlet temp (^{o}C)
0.0166	0.0083	5	0.033	75
0.0156	0.0078	10	0.033	75
0.0148	0.0074	15	0.033	75
0.0140	0.0070	20	0.033	75
0.0130	0.0065	25	0.033	75

Figure 4.14 shows the predicted variation of LMTD, hot water outlet and mean surface temperature of the radiator with time at various flow velocity amplitudes while maintaining other parameters constant. It is clear from figure 4.14 that the temperature of the radiator increases as the flow amplitude increases. Particularly the LMTD of the radiator increased from 48.5^{o}C at flow amplitude of 0.0130kg/s to 51.5^{o}C at flow amplitude of 0.0166kg/s.

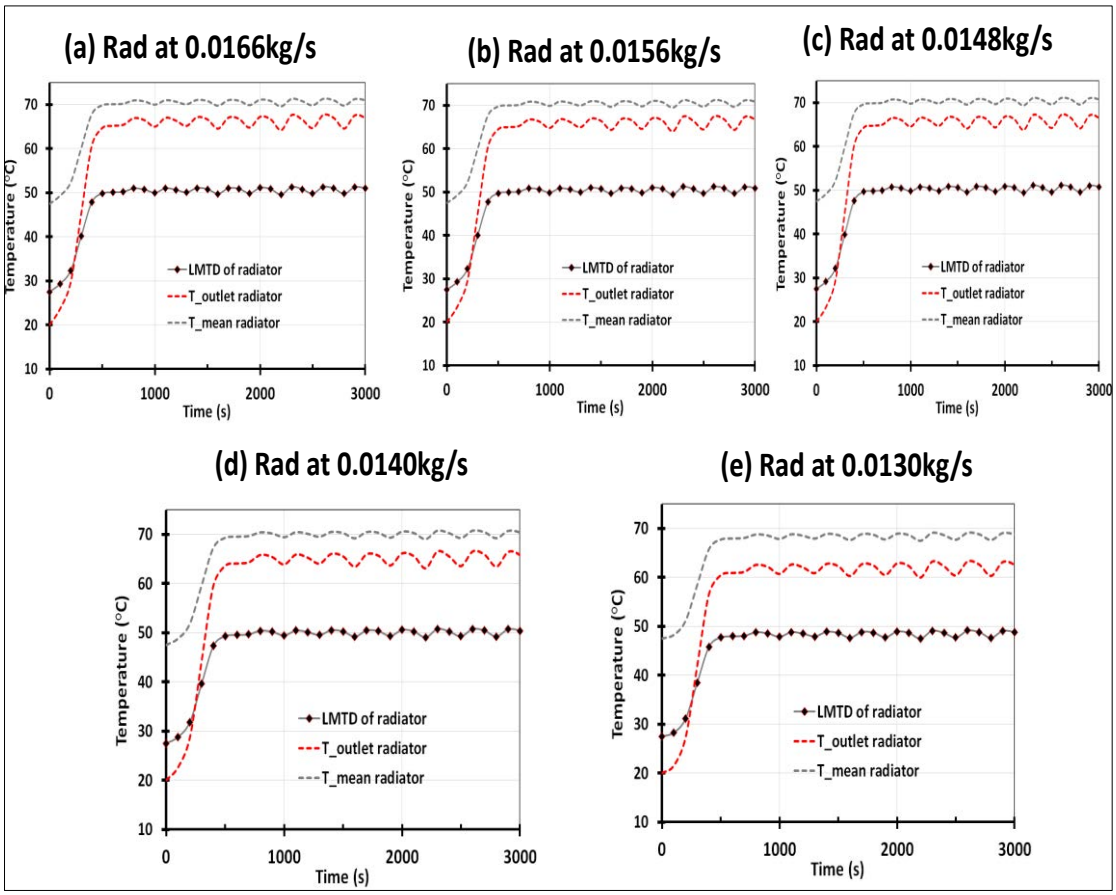

Figure 4.14 LMTD, outlet temperature, mean surface temperature of the type10 radiator operating at various flow amplitudes while keeping other parameters constant

Figure 4.15 shows the specific heat output of the radiator at various pulsed flow amplitudes. It is clear that the highest specific heat output was achieved at flow amplitude of 0.0140kg/s. At this flow amplitude, the radiator achieved LMTD of 50^{o}C±0.5 (see figure 4.14 (d)) which is consistent with EN442 radiator standards requirement. The higher specific heat output of the radiator indicates that lower hot water flow rate can be used to produce the same heat load. Thus the selected best flow amplitude of 0.0140kg/s was numerically simulated to investigate the effect of pulsed flow frequency.

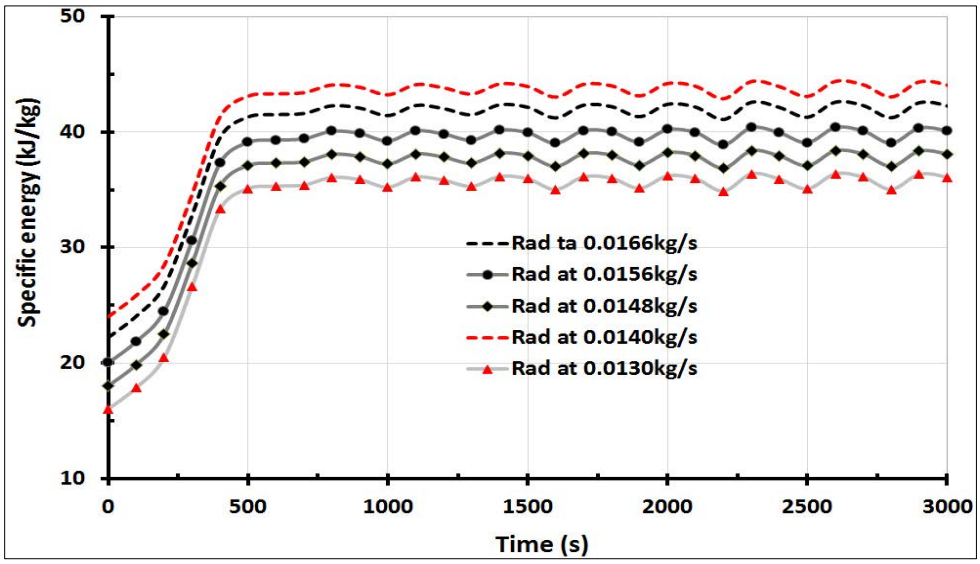

Figure 4.15 specific heat output of the type10 radiator operating at various flow amplitudes while maintaining other parameters constant

4.3.9 Effect of flow frequencies on type10 radiator

To investigate the effect of flow pulsation on the heat transfer performance of type10 radiator CFD simulation was carried out using various input flow frequencies at constant flow amplitude of 0.0140kg/s and constant inlet temperature of 75^{o}C as shown in table 4.7. The radiator was simulated at various flow frequencies ranging from 0.0083Hz to 0.033Hz and the flow frequency that produced the best specific heat output with low temperature fluctuation will be selected as the best pulsed flow operating conditions.

Table 4.7 various pulsed flow frequencies used with radiator type10

Amplitudes (kg/s)	Average mass (kg/s]	Mass reduction (%) (pulsed flow compared to constant flow)	Flow frequencies (Hz)	Inlet temp (^{o}C)
0.0140	0.0070	20	0.033	75
0.0140	0.0070	20	0.016	75
0.0140	0.0070	20	0.011	75
0.0140	0.0070	20	0.0083	75

Figure 4.16 shows the variation of radiator type10 LMTD, water outlet and mean surface temperature with time at various flow frequencies while maintaining other parameters constant.

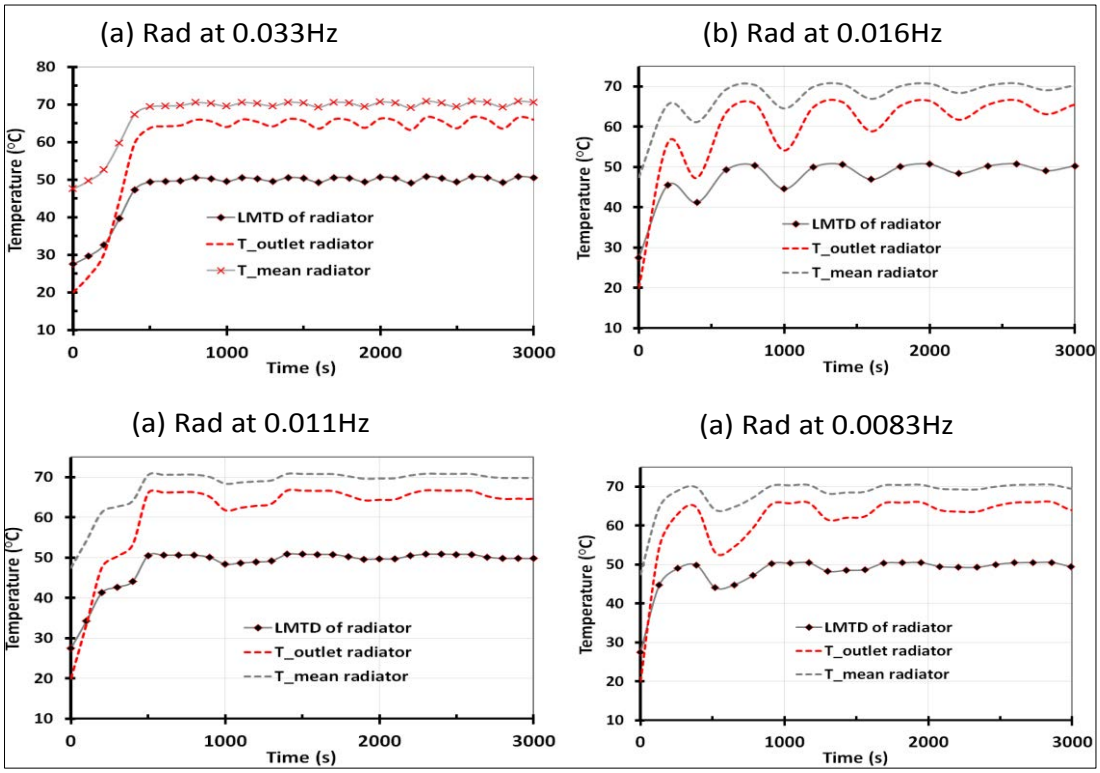

Figure 4.16 LMTD, outlet temperature, mean temperature of the type10 radiator operating at various flow frequencies while maintaining other parameters constant

It is clear from figure 4.16 that the radiator mean surface temperatures are similar at all flow frequencies. The radiator with lower flow frequencies gained higher thermal inertia, this higher inertia is achieved at the cost of higher radiator surface temperature fluctuation that may cause discomfort to the occupants of the heated space. Based on the lowest temperature fluctuation the frequency of 0.033Hz was selected as the best pulsed flow operating frequency.

Figure 4.17 shows the predicted specific heat output of radiator type10 at various flow frequencies. Figure 4.17 shows that high fluctuation and fast thermal inertial are produced when the radiator was operating at flow frequencies ranging from 0.0083Hz to 0.016Hz while when the radiator was operating at flow frequency of 0.033Hz lower temperature fluctuations of 0.5% was achieved. Based on the temperature fluctuation and specific heat output rate of the radiator, the best flow frequency is 0.033Hz.

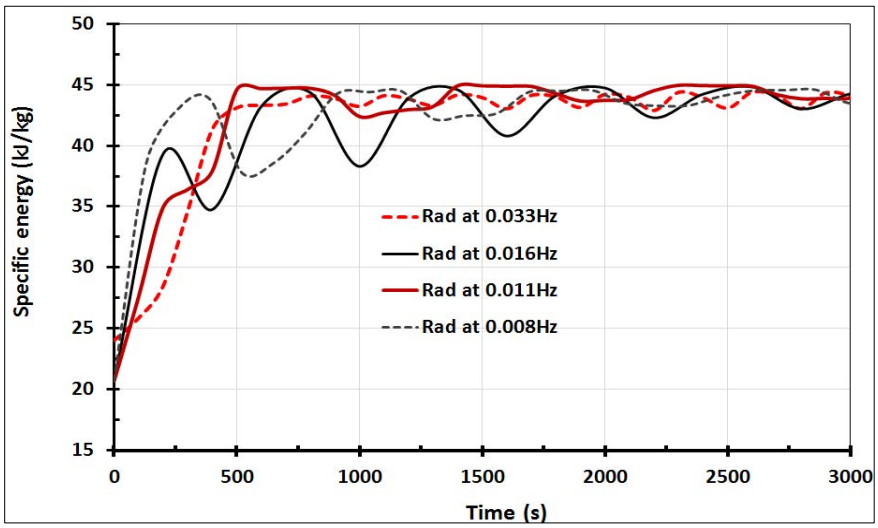

Figure 4.17 specific heat output of type10 radiator operating at various flow frequencies

Based on the effect of flow amplitudes and flow frequencies, the best pulsed flow operating condition was selected as 0.0140kg/s (20% less average mass flow rate than that of constant flow) and 0.033Hz respectively for type10 radiator.

4.3.10 Effect of pulsed flow on type10 compared to the type11

In sections 4.3.6 to 4.3.7 the best pulsed flow conditions for type11 radiator are shown to be 0.0174kg/s amplitude and 0.033Hz frequencies. In sections 4.3.8 to 4.3.9 the

best pulsed flow conditions for radiator type10 are shown to be 0.014kg/s amplitude and 0.033Hz frequency. In this section the performance of type10 radiator operating at best pulsed flow conditions compared to that of type11 radiator operating at its best pulsed flow conditions are investigated. Both radiators were simulated at inlet hot water temperature of 75^{o}C, ambient temperature of 20^{o}C and their best pulsed flow conditions. Figure 4.18(a) shows the predicted results of type10 radiator operating at the best pulsed flow condition and figure 4.18(b) shows the predicted results of type10 radiators operating at the best pulsed flow conditions.

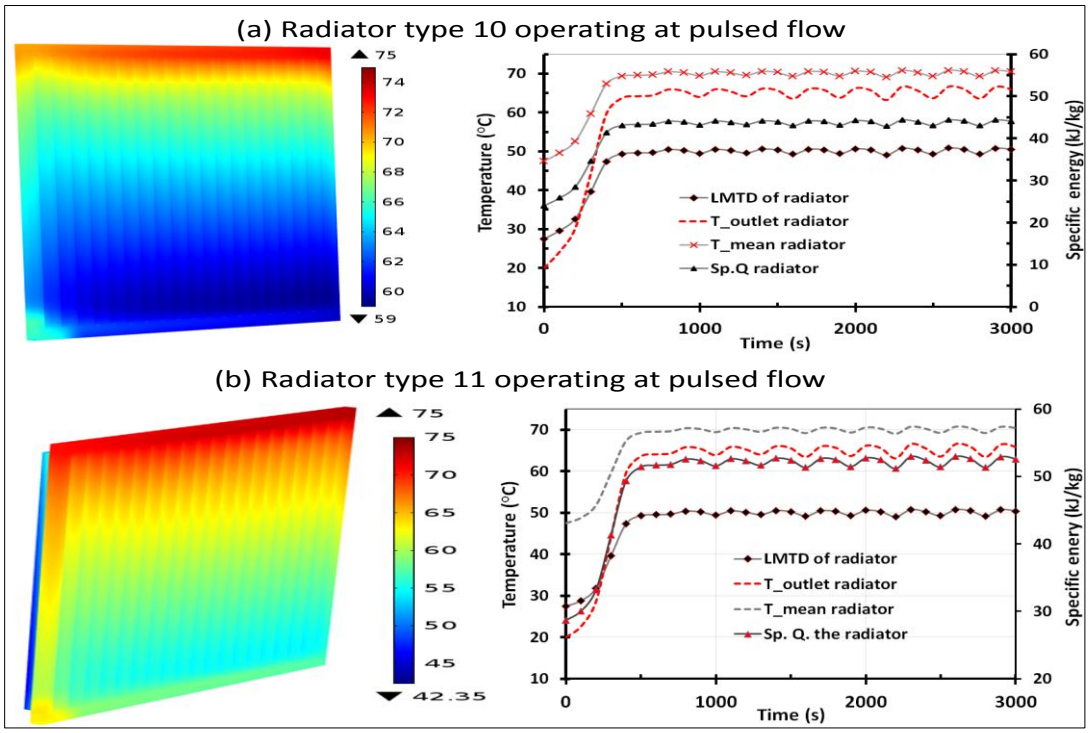

Figure 4.18 contour of local surface temperature LMTD, outlet temperature, mean temperature, rate of specific heat output for (a) type10 radiators and (b) type11 radiator at pulsed flow

It is clear from figure 4.18 that the LMTD, mean radiator surface temperature, water outlet temperatures are similar for both the type10 and type11 with values consistent with EN442 radiator standard. However the specific heat output of type11 radiator is

higher (52.5kJ/kg) than that of the type10 radiator (43kJ/kg) because of its higher surface area due to the attached fins. Type11 radiator gives higher specific heat output and it is the most commonly used in central heating systems. Thus Type11 radiator was selected for further investigation at various hot water inlet temperatures in the following section.

4.3.11 Effect of pulsed flow inlet temperatures on type11 radiator

The radiator type11 was modelled at various hot water inlet temperatures while maintaining other operating parameters constant using the best pulsed flow as shown in Table 4.8 and figure 4.19 show the results of simulation at various inlet temperatures.

Table 4.8 various inlet temperatures at constant flow frequency and amplitudes

Inlet temp (^{o}C)	Amplitudes (m/s)	Average mass (kg/s)	Mass of pulsed flow compared to constant flow (%)	Flow frequencies (Hz)
75	0.0174	0.0087	20	0.033
70	0.0174	0.0087	20	0.033
65	0.0174	0.0087	20	0.033
60	0.0174	0.0087	20	0.033

Figure 4.19 shows the radiator surface temperature distribution and variation of water outlet, radiator mean surface temperature, LMTD and specific heat output with time for best pulsed flow at hot water inlet temperature varying from 60^{o}C to 75^{o}C. Investigating the effect of flow pulsation at low hot water inlet temperature helps to exploit low grade heat source in hydronic heating system. For example the use of ground sources heat pumps for hydronic heating is growing rapidly due to their high

energy efficiency which increases as the heating temperature decreases with 65°C down to 40°C being typical heating temperature.

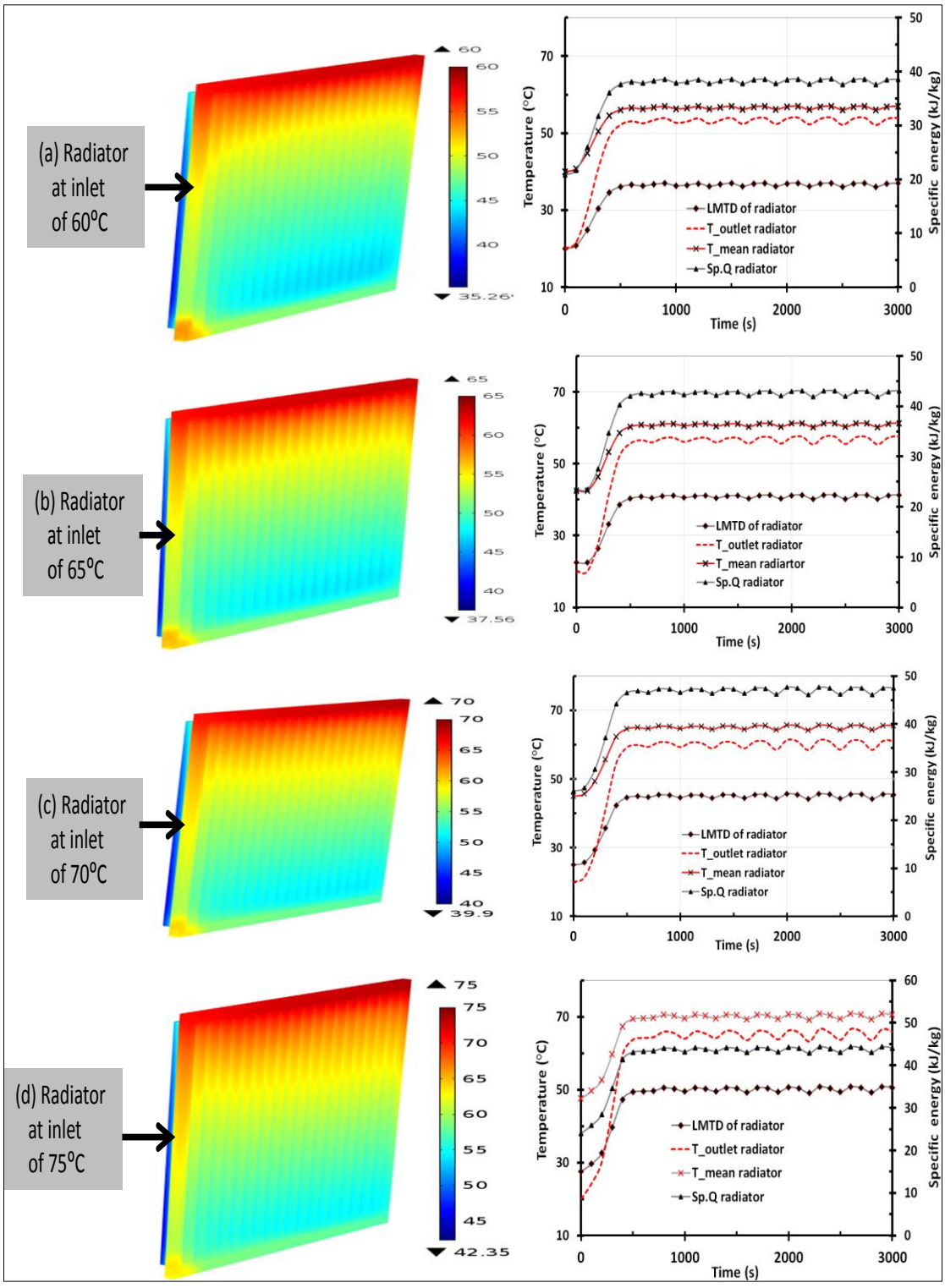

Figure 4.19 contours of local surface temperature LMTD, outlet temperature, mean temperature; rate of specific heat output for the radiator simulated using pulsed flow

It is clear from figure 4.19 that the mean radiator surface temperature, LMTD, outlet water temperature and specific heat output decrease with the decrease in the hot water inlet temperature. The pulsed flow specific heat output compared to the constant flow specific heat output for the two radiators operating at various flow conditions are described in the following section.

4.4 Energy saving analysis due to the pulsed flow

Energy saving due to the pulsed flow compared to the constant flow is determined using the specific heat output of the radiators as given by eq. (3.42) in chapter 3. Energy saving is related to the average supply mass flow rate required to achieve the target LMTD of 50^{o}C. The effect of pulsed flow in terms of specific heat output was investigated for the two types of radiators at various hot water inlet temperatures. Figure 4.20 shows the specific heat output of radiators type10 (a) and type11 (b) at pulsed flow compared to their corresponding constant flow at inlet temperature of 75^{o}C. The shaded area in figure 4.20 shows the saved specific heat output due to the pulsed flow for both radiator without fins (type10) and radiator with fins (type11) compared to operating at constant flow conditions.

The percentage of instantaneous and average energy savings for type10 and type11 radiators can be estimated using eq. (4.21).

$$ES\,(\%) = \left(\frac{Sp.Q \quad \text{Pulsed flow}}{Sp.Q \quad \text{Constant flow}} - 1 \right) \times 100 \qquad (4.21)$$

Where: ES (%) is percentage of specific energy saving.

Using eq. (4.21), 24.9 % of average heat output can be saved for type11 radiator and about 18.9 % for type10 radiator due to the pulsed flow compared to the constant flow radiator.

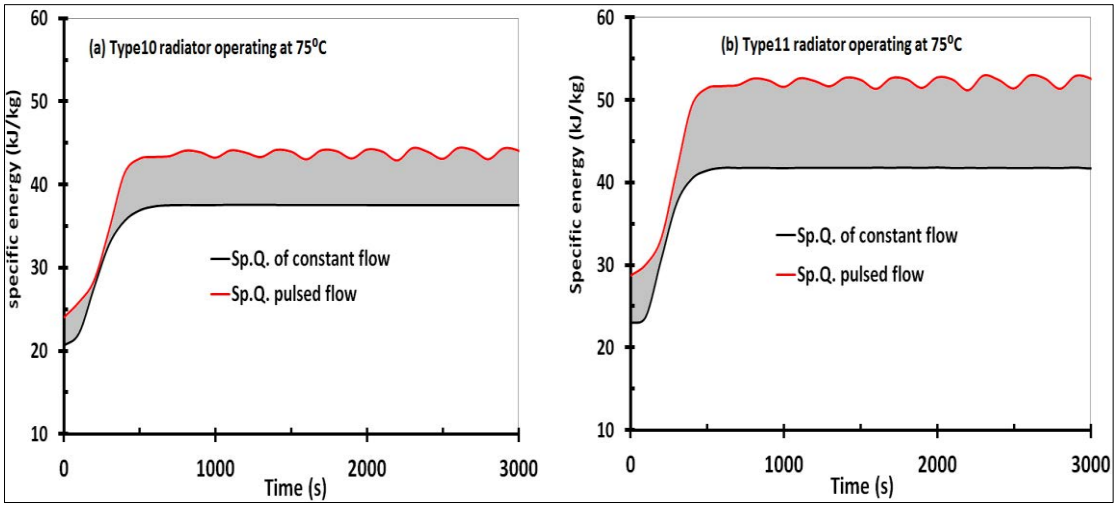

Figure 4.20 rate of specific heat output for (a) type10 radiator and (b) type11 radiator both operating at pulsed and constant flow scenarios

In type11 higher savings was gained due to the higher surface areas of the fins. This shows that the benefit of using pulsed flow is more significant for the radiator with fins compared to the radiator with no fins. In addition to the energy saving due to the pulsed flow, the thermal inertia of the panel radiators is improved leading to better control response of the system and comfort of the occupants. Figure 4.21 shows the specific heat output of type11 radiator at pulsed flow compared to constant flow cases at various inlet temperatures.

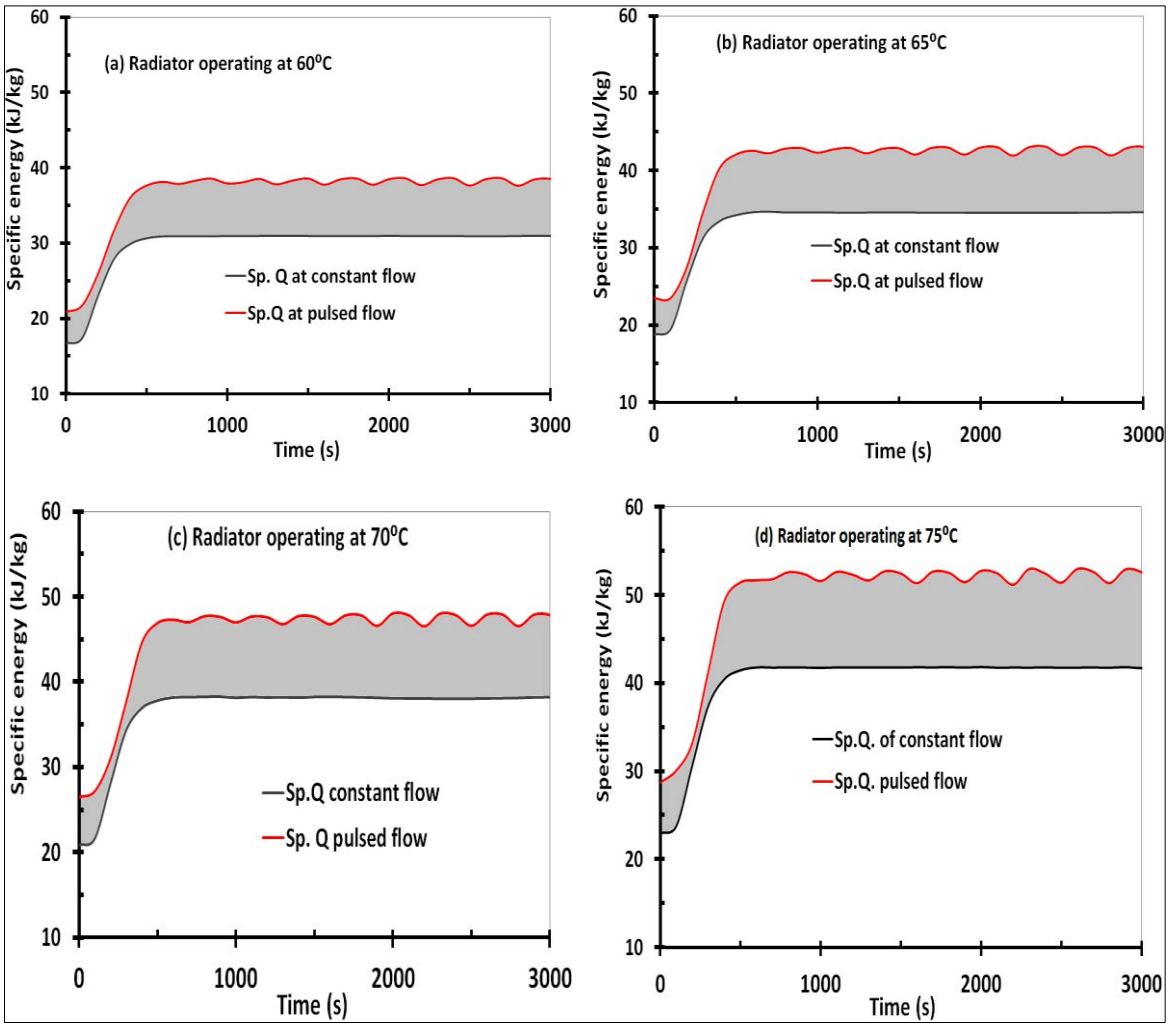

Figure 4.21 rate of specific heat output of type11 radiator at various inlet temperature pulsed flow compared to constant flow

It is clear from figure 4.21 that flow pulsation has almost the same degree of energy saving regardless of the inlet hot water temperature. The percentage of instantaneous and average energy savings for type11 radiator operating at various hot water inlet temperatures can be estimated using eq. (4.21). Figure 4.22 shows the instantaneous energy saving for type11 radiator while table 4.9 shows the average energy savings due to the pulsed flow compared to the constant flow at various inlet temperatures.

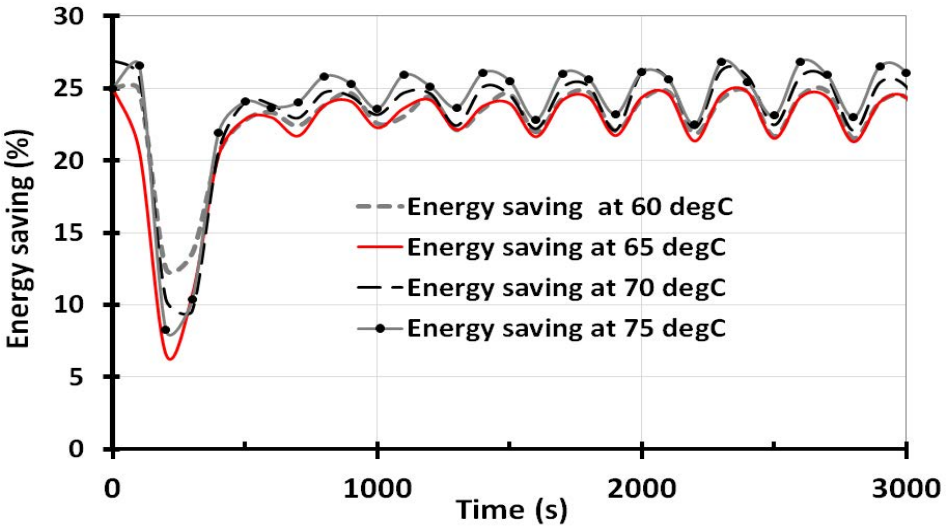

Figure 4. 22 the instantaneous heat transfer enhancement based on the specific energy saving

As shown in figure 4.22 and table 4.9 the percentage of energy saving for radiator type11 operating at various inlet temperatures are similar with average value ranging from 23.4% to 24.9%. The enhancement of the specific heat output of the radiator at pulsed flow is attributed to the lower average mass flow rate for radiator operating at pulsed flow compared to the radiator operating at constant (conventional) flow.

Table 4.9 saved energy due to pulsed flow at varying inlet temperature of type11 radiator

Inlet temperature	Energy saving due the pulsed flow compared to the constant flow
60^{o}C	23.40%
65^{o}C	23.36%
70^{o}C	24.1%
75^{o}C	24.90%

The finite element modelling of radiators showed that, there is high potential of energy saving due to the pulsed flow compared to constant flow to the hydronic heating system. This energy saving is due to the heat transfer enhancement of hydronic radiator which is analysed in the following section.

4.5 Pulsed flow enhancement mechanism

In this investigation, it is envisaged that the energy saving achieved in the pulsed flow is due to the heat transfer enhancement caused by the changes in the velocity distribution inside the flow channels of the radiators. Figure 4.23 shows the velocity variation in four channels at different positions from the flow inlet within radiator type11 (channel 1 at 90mm, channel 2 at 196mm, channel 3 at 302mm and channel 4 at 408mm) for pulsed and constant flow conditions. The shaded part of figure 4.23 (b) to 4.23 (e) shows the improvement in the average velocity of the pulsed flow compared to the constant flow. The higher flow velocity in the channels due the pulsed flow leads to higher Reynolds number that creates higher flow mixing leading to flow turbulence and breakup of the boundary layer along the water side wall of the radiator channels. The high mixing behaviour of flow highlights the advantage of the pulsed flow strategy in enhancing the convection heat transfer at the solid/fluid interfaces. Improving the flow mixing along the flow channels of the panel radiator also maximises heat flux distribution uniformity along the surface of the radiator [84 and 101]. Further using flow pulsation can help in reducing fouling inside the hydronic heating channels. Fouling has negative impact for any heat exchanger particularly radiators with channels which cannot be cleaned easily.

Figure 4.24 shows the variation of heat transfer coefficient with time for both pulsed flow using best conditions and constant flow conditions. The convective heat transfer coefficient is calculated using the eq. (4.22).

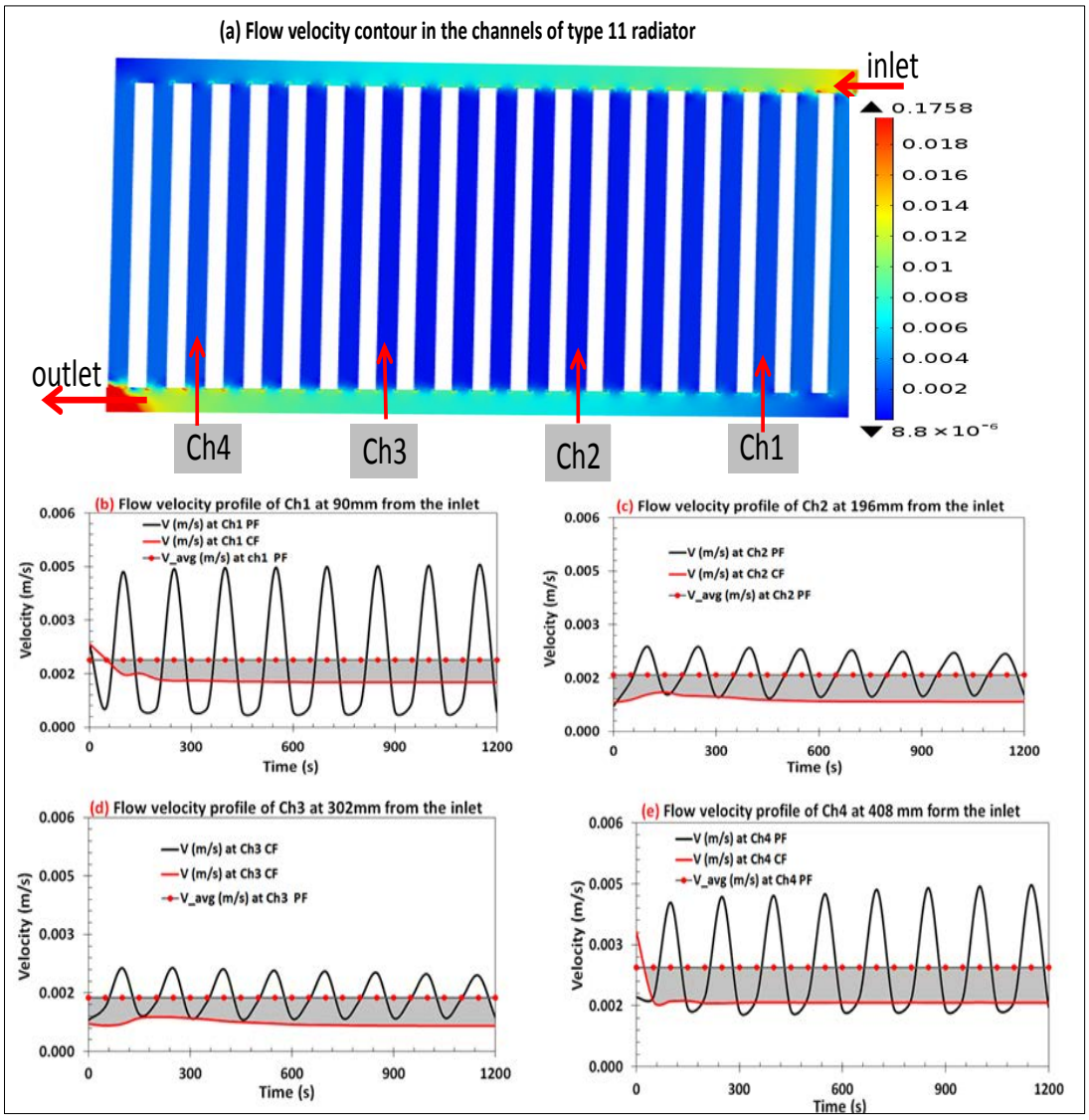

Figure 4.23 velocity distribution profiles and the velocity of the proposed pulsed flow compared to the constant along the channels

$$h = \frac{q_{conv}}{T_b - T_{sur}} \tag{4.22}$$

Where; h is the local convection heat transfer coefficient, q_{conv} is the convective heat flux magnitude, T_b is the average bulk hot water temperature and T_s is the average internal wall surface temperature of the radiator channels.

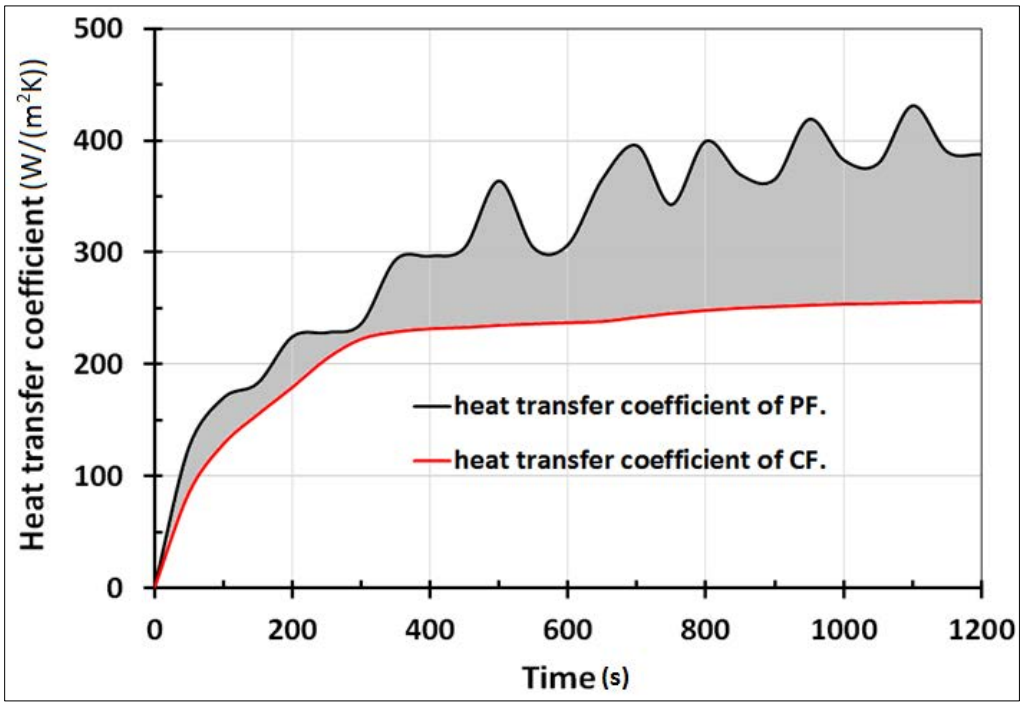

Figure 4.24 the enhanced convective heat transfer coefficient on the water side (internal) channel walls due to the pulsed flow compared to constant flow

Figure 4.24 clearly shows that the best pulsed flow produced higher heat transfer coefficient compared to the constant flow. The percentage of heat transfer coefficient enhancement is calculated using eq. (23) and shown in figure 4.25.

$$\mathrm{HTE}(\%) = \left(\frac{h_{PF}}{h_{CF}} - 1 \right) \times 100 \qquad (4.23)$$

Where; HTE(%) is percentage of heat transfer enhancement, h_{PF} is heat transfer coefficient of the pulsed flow and h_{CF} is heat transfer coefficient of the constant flow.

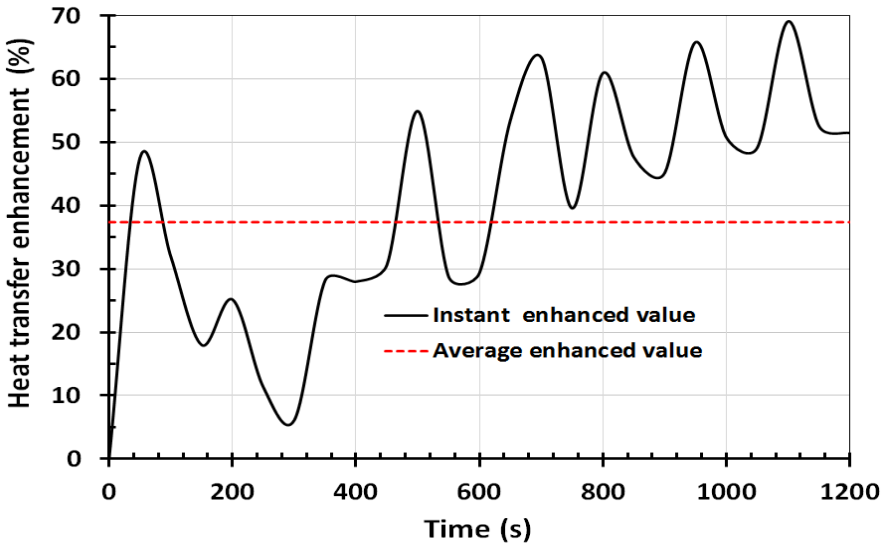

Figure 4. 25 the average and instant heat transfer coefficient enhancement of the hydronic radiator

Figure 4.25 shows that the percentage of heat transfer enhancement ranges from 5% to 70% and an average enhancement of 38% can be achieved compared to the constant flow. The heat transfer enhancement can be attributed to the higher mixing of the flow along the wall channel of the radiator thus improving the heat transfer rate of the radiator. These heat transfer enhancements due to pulsed flow enables the radiator to produce higher energy at low hot water supply flow rate leading to higher specific heat output and higher energy saving.

4.6 Summary

Finite element modelling of hydronic radiators was performed using conjugate heat transfer in COMSOL Multiphysics to investigate the effect of pulsating flow on their heat transfer performance. Based on the finite element modelling results the following summary can be drawn:

Flow pulsation technique was shown to enhance the heat transfer performance of hydronic panel radiators used in central heating systems. Both type10 and type11 radiators were investigated at various inlet flow conditions using constant and pulsed flow scenarios. The radiator at pulsed flow was simulated at various flow frequencies and various flow amplitudes. The CFD results were analysed based on the specific heat output, LMTD, mean temperature and water outlet temperature of the radiator.

Results showed that a reduction in the energy consumption of up to 18.9% (for type10 radiator) and 24.9% (for type11 radiator) can be achieved without affecting the radiator LMTD of 50^{o}C for constant inlet temperature of 75^{o}C. The pulsed flow also improved the thermal inertia of the radiator which is important for effective responses of the heating control system. The effect of pulsed flow at lower inlet temperature to the radiator was similar to that at high temperature. Example the specific heat output enhancement with inlet temperatures of 60^{o}C and 75^{o}C were 23.4% and 24.9% respectively.

The energy savings produced by the pulsed flow is due to the creation of higher local velocity in the flow channels of the radiators compared to the constant flow. The higher flow velocity due to pulsed flow resulted in enhancing the convective heat transfer coefficient of the hot water compared to the constant flow case by an average of 38%.

CHAPTER 5

CFD MODELLING OF HEATED ROOM

5.1 Introduction

In chapter 3 the indoor comfort was investigated using the MatLab/Simulink model however results of the Simulink model was based on the lumped heat transfer analysis; assuming uniform heat transfer in the entire heated space. The CFD modelling of hydronic radiators was described in chapter 4 and demonstrated the potential of energy saving due to pulsating the flow into central heating radiators. But the savings should be achieved without affecting the indoor comfort. Thus further CFD simulation of the heated space is required to predict the various local indoor comfort parameters distribution and to assess the effects of the pulsed flow on indoor comfort.

The importance of CFD for building design is growing rapidly. CFD has become a common design tool to investigate the indoor environmental conditions by building researchers and scientists. Numerical simulation of buildings was applied to predict energy usage, indoor comfort parameters including thermal comfort and indoor air quality [101, 104-105 and 162-163]. According to ASHRAE standards 55 maintaining indoor comfort is a key objective when attempting to reduce the energy consumption of buildings integrated with central heating systems [169-170]. Therefore this work will investigate the effect of pulsed flow method, studied in chapter 3 and 4 and shown to produce over 20% reduction in energy consumption of hydronic heating radiators on the comfort parameters of the heated space.

In this research work, the indoor parameters of the heated room were investigated using the temperature of the radiators operating at constant and pulsed flow conditions presented in chapter 4. The finite element modelling of the room was investigated at two conditions including room without occupants (empty room) and room with the presence of occupants.

Results were analysed on the basis of indoor temperature, velocity, Draught Risk (DR), Percentage of Dissatisfied (PD) and Percentage Experience Draught (PED) for the case of the heated room without occupants at both constant and pulsed flow conditions.

For the case of heated room with occupants the results also included the indoor thermal comfort (relative humidity, temperature) and indoor air qualities (CO_2 concentration) at constant and pulsed flow scenarios. The CFD approach for the proposed heated room was modelled in COMSOL Multi-Physics using the flow diagram shown figure 5.1. The definition of some of the abbreviated words shown in figure 5.1 are; constant flow (CF), pulsed flow (PF), indoor air quality (IAQ), indoor temperature (air temperature and radiant temperature), relative humidity (RH), air velocity (Vel), indoor CO_2 concentration (CO_2), Draught Risk (DR), Percentage of Dissatisfied (PD) and Percentage Experience Draught (PED).

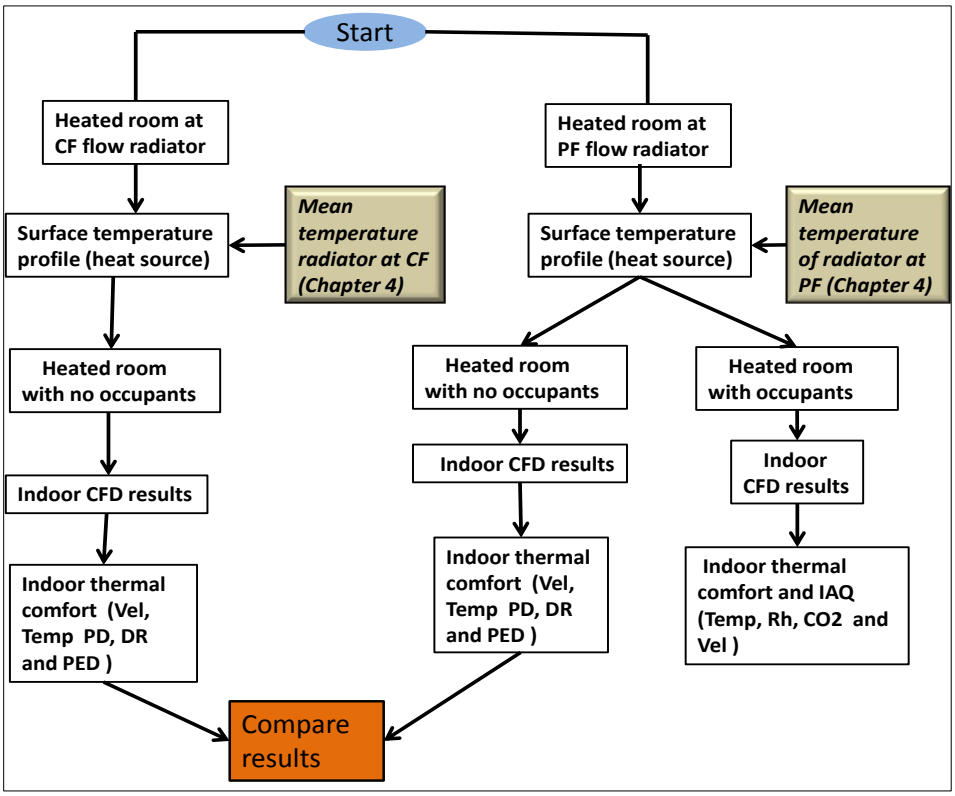

Figure 5.1 flow diagram of heated room CFD methodology

5.2 Governing equations

COMSOL Multi-physics software was used to model the heated room using the predicted hydronic radiator surface temperature presented in chapter 4. COMSOL is a user friendly software where the user defined function can be applied easily compared to other CFD packages such as ANSYS Fluent and CFX [160- 171]. The finite element modelling of the heated room was carried out using energy equations (conjugate heat transfer physics) and mass transport equation (transport of diluted species physics) as described in section 5.2.1 and 5.2.2 respectively.

5.2.1 Energy equations

The conjugate heat transfer physics is used to simulate heat transfer at interfaces between solids and fluids as it was defined in chapter 4. The turbulent model of Reynolds Average Navier Stokes (RANS) was used for predicting the pressure and velocity fields through the heated space [101]. Various literature sources showed that the k-ε turbulence model predicts the actual flow pattern better than any other models in CFD numerical simulations [156]. Therefore the governing equations of momentum, mass, energy conservation and k-Ɛ turbulent model as described in section 4.2 of chapter 4, equations (4.1) to (4.6) were used to model the heated room.

Heat is transferred from the radiator surface to air in the heated space by natural convection. Natural convection heat transfer is applied using buoyancy driven volume force due to the density difference of the indoor air expressed as eq. (4.12)

Surface to surface radiation was also applied for the heat transfer between internal surfaces of the walls and the radiator surface (hot surface) at constant emissivity value of 0.85 and 0.85 respectively as expressed using eq. (5.1) to eq. (5.3) [95, 101].

$$q_{radiative} = \varepsilon_s (G - \sigma_s T^4_{sur}) \tag{5.1}$$

Where:

$$G = G_n(J) + F_{ind}\sigma_s T^4_{ind} + G_{sur} \tag{5.2}$$

$$J = (1-\varepsilon_s).G + \varepsilon_s.\sigma_s.T^4_{sur} \tag{5.3}$$

Where:ε_s, σ_s, T_{sur}, T_{ind}, q, G_{sur}, J, G, F_{ind} and G_n are the emissivity constant, the Stefan Boltzmann constant (5.670373*10-8 J/(m^2.K^4), spatial temperature of the radiator surface, indoor air temperature, heat flux due to radiation (W/m^2), irradiation from surface (W/m^2), total local radiosity (sum of reflected irradiation and emitted irradiation) (W/m^2), sum of irradiation (W/m^2), view factor and mutual irradiation (W/m^2) [161].

Convection cooling was applied on the surface of all external walls and glazing windows at constant heat transfer coefficient of 10W/(m^2.K) and ambient temperature of 5^{o}C expressed as eq. (5.4).

$$q_{conv} = h(T_{amb} - T_{sur}) \tag{5.4}$$

Where: h local convection heat transfer coefficient, T_{amb} is external temperature, T_{sur} is temperature of the external wall surface and q_{conv} is convective heat flux.

5.2.2 Transport of Diluted Species equations

Transport of diluted species physics is user interface model available under Chemical Species Transport of the model wizard in COMSOL. It uses Fick's law of diffusion for modelling mass transport of diluted species in solutions and solids [161]. Transport of diluted species physics is applied in the proposed heated room model to investigate the CO_2 concentration and moisture content of the indoor air (relative humidity) for the heated room with occupants.

Eq. (5.5) to (5.6) shows the mass balance equation including the transport of diluted species.

$$\frac{\partial C}{\partial t} + Vel.\nabla C = \nabla.(D\nabla C) + RXN \tag{5.5}$$

$$N = -D\nabla C + Vel.C \tag{5.6}$$

Where: C is the concentration of the species in (mol/m^3), D denotes the diffusion coefficient in (m^2/s), RXN is a reaction rate expression for the species in (mol/(m^3·s)), Vel is the velocity vector in m/s and N is the inward mass flux in (mol/(m^2.s)).

5.3 CFD modelling of heated space

The CAD of the heated room integrated with radiator as a heat source and mechanical ventilation is produced in COMSOL software as shown in figure 5.2. The heating and ventilation components of the heated room are working in counteracting manner. Therefore appropriate positioning of the two components in central heating system can play a key role in reducing energy consumption as well as maintaining comfort of the occupants. The panel radiator was positioned beneath the window 50mm away from the wall behind, 150mm above the floor as recommended by radiator test standard of EN BS 442 [173-174]. The mechanical ventilation is positioned just above the window.

In this work, the CAD of the heated room was designed to simulate the heated room at two different conditions (room with no occupants and room with occupants). Firstly an empty room (with no occupant) was designed as shown in figure 5.2 to investigate the thermal parameters of the heated room including indoor comfort temperature (air temperature and radiant temperature) , indoor air velocity, Draught Risk (DR), Percentage of Dissatisfied (PD) and Percentage Experience Draught (PED). The dimension of the proposed heated room is 5.5m length, 3.5m width and 2.7m height. It consists of radiator as heat source, ventilation air inlet and outlet, window, door, walls and air volume in the room envelope.

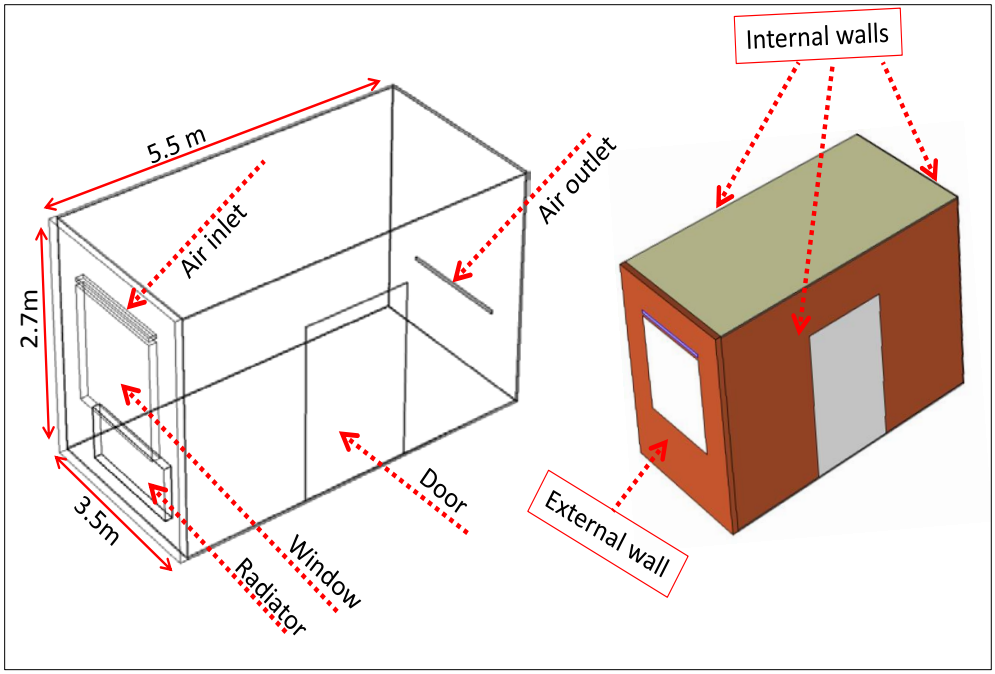

Figure 5.2 CAD design of the proposed heated room model with no occupants

Secondly the same size heated room was simulated with 5 occupants who act as a source of moisture, heat and CO_2 as shown in figure 5.3. The simulation of the heated room with occupants was conducted to investigate the indoor thermal comfort (indoor

comfort temperature, velocity and humidity) and the indoor air qualities (CO_2 concentration). The occupants are represented as a simple rectangular box for geometrical simplicity.

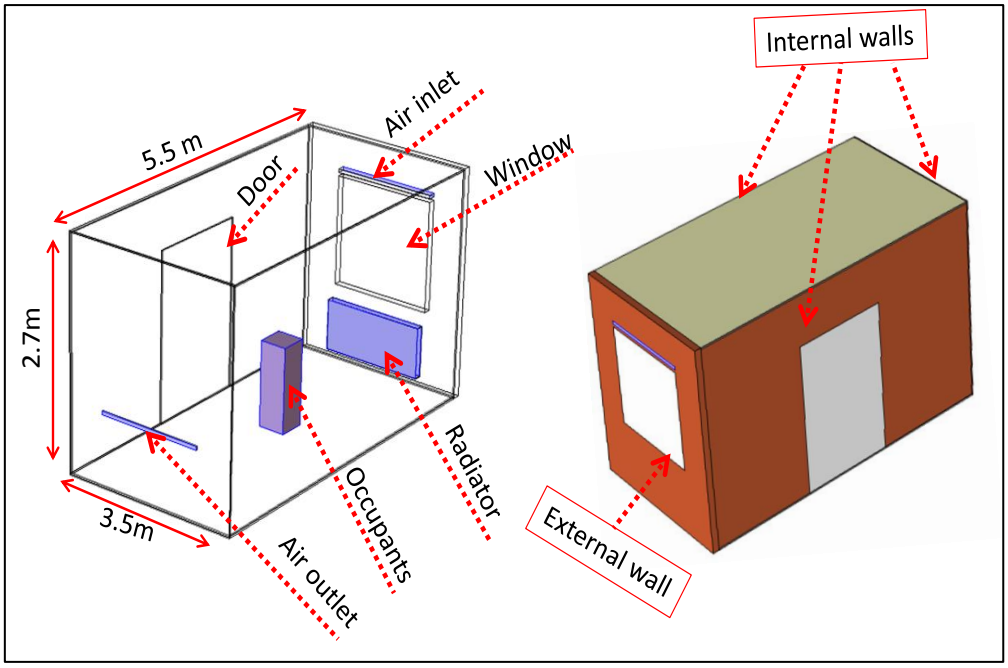

Figure 5.3 CAD design of the proposed heat room model with occupants

Table 5.1 shows the thermal properties of all materials used to construct the heated space including the thermal conductivity, density and specific heat capacity [175].

Table 5.1 thermal properties of room model materials

Components	Materials	k (W/(m.K))	C_p (J/(kg.K))	ρ (kg/m^3)
Internal wall	Bricks	0.84	600	1700
External wall	Bricks	0.62	800	1700
Window and door	Glass	0.96	600	2200
Floor and Ceiling	Wood	0.42	842	1200
Radiator	Steel	16.5	475	7850
Air volume	Air	0.025	1005	1.2
Door	wood	0.14	1200	650

5.3.1 Mesh sensitivity of the room finite element modelling

During the finite element modelling of the heated room, it is important to investigate the meshing effect on the CFD results. 3D cut point (see figure 5.4) was used to investigate the indoor temperature at various mesh distribution at both pulsed and constant flow conditions.

The indoor temperature was selected as it is the main thermal comfort criterion that can be easily affected by the heating radiator. Tetrahedral mesh was used in the modelling the heated space as it gives better element quality to any complicated geometry leading to more accurate simulation results [161]. Table 5.2 shows the number of mesh elements used in the mesh sensitivity study. Figures 5.5 and 5.6 show the indoor temperature variation with time at the centre position of the heated room for constant and pulsed flow to the heating radiator respectively.

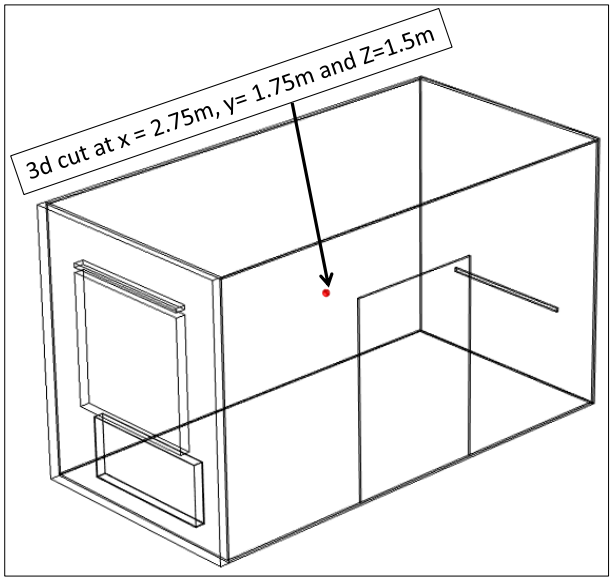

Figure 5.4 the selected point for meshing sensitivity investigation of the heated room

Table 5.2 the element number of meshing procedure of the heated room

Number of runs	Mesh element number
Run 1	2013918
Run 2	1528337
Run 3	1000191
Run4	100000

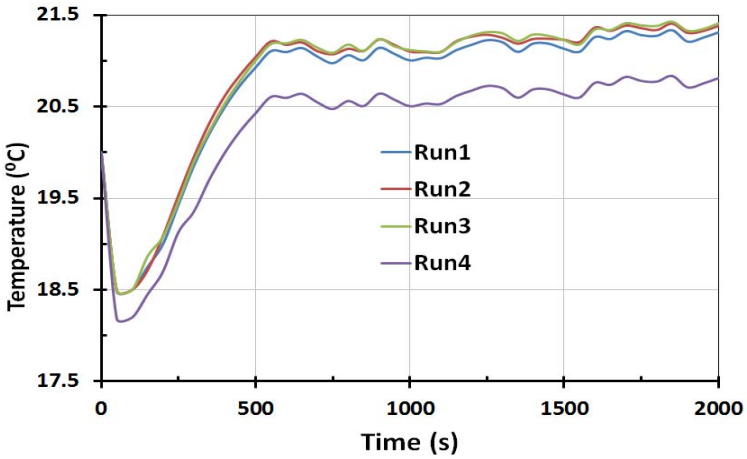

Figure 5.5 indoor temperatures using various meshing configuration at constant flow

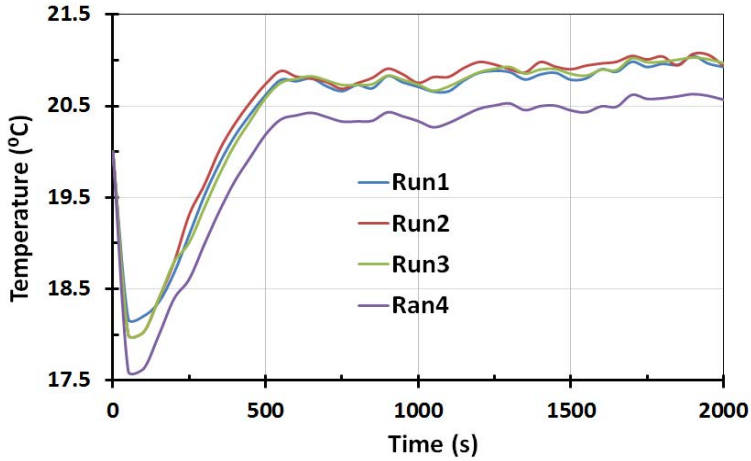

Figure 5.6 indoor temperatures using various meshing configuration at pulsed flow

Results show that the average deviations of the indoor temperature for the first three runs are 0.35% and 0.41% for the radiator operating at constant flow and pulsed flow respectively. However for the fourth run considerable temperature difference was obtained as it is clearly shown in figures 5.5 and 5.6. Thus based on the results of mesh sensitivity study, the element number shown in run3 (with element number of 1000191) was used to simulate the heated room.

5.4 CFD results of the heated room with no occupants

Before presenting the results of the numerical simulation, the assumptions used in the finite element modelling of the heated room with no occupants for cases of constant and pulsed flow to the radiator are summarised as:

- There was no water flow in the radiator; instead transient temperature profile obtained from simulating the hydronic radiator (chapter 4) was applied on the surface of the radiator inside the room.
- The room was initially set to indoor temperature of 20^{o}C.
- Winter average temperature of the UK was taken as 5^{o}C for the outside wall, window and ventilation air inlet.
- All internal walls were assumed as adiabatic boundary conditions
- The ventilation air flow rate was assumed to be 7.5 l/s per person as recommended by ASHRAE 62-1999.

- The room was assumed to be empty; all heat gains from the sun, light bulbs, other equipment were neglected and the only heat source was the panel radiator.
- Only energy equation was used as a governing equation for the room with no occupants

5.4.1 CFD results at constant flow

In this simulation the transient mean temperature of the radiator operating at constant water flow rate as predicted in chapter 4 was applied at the surface of the radiator as boundary condition for modelling the heated space. Figure 5.7 shows the predicted transient mean temperature of the radiator at constant hot water flow rate 0.011kg/s and inlet temperature of 75^{o}C. The predicted mean surface temperature of the radiator was fitted using a polynomial equation as expressed in equation eq. (5.7).

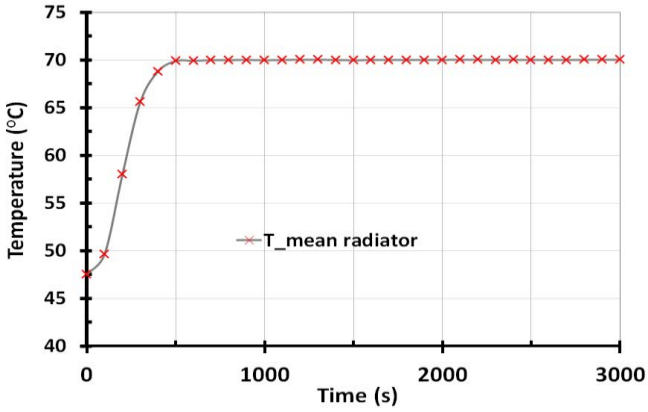

Figure 5.7 transient mean temperature of the radiator operating at constant flow hot water supply

Equation (5.7) was applied to the radiator surface inside the heated room to serve as a heat source; reducing computational time and memory constraints without affecting the results.

$$T_{mean} = (t <= 500) \times (9^{-7} \times t^3 - 0.001 \times t^2 + 0.3562 \times t + 320.65) + (t > 500) \times (343.11) \quad (5.7)$$

Figure 5.8 shows local temperature distribution along horizontal and vertical cut planes at the middle of the heated room with no occupants.

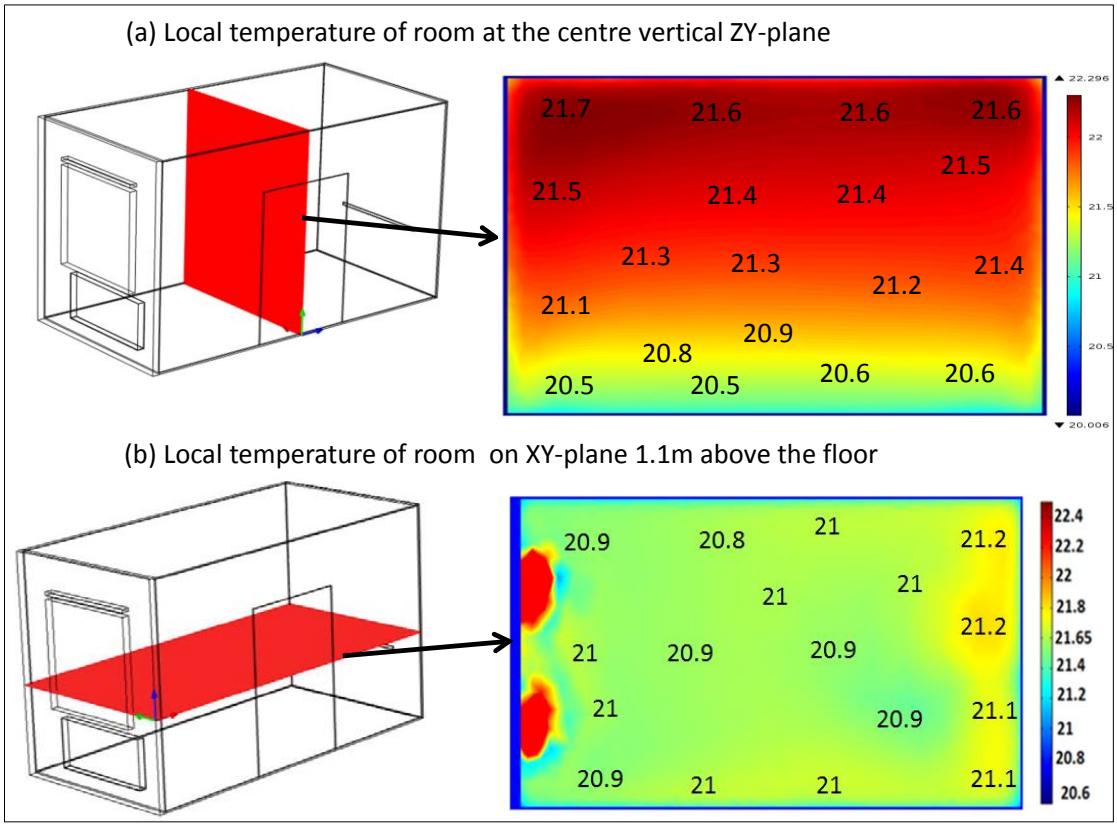

Figure 5.8 local temperature distribution contours of the indoor with no occupants along (a) vertical cut plane and (b) horizontal cut plane operating at constant flow radiator heat source at 2000s

Figure 5.8 (a) shows that the local temperature varies from 20.5°C at the bottom (close to the floor) of the room to 21.7°C at the top of the room (close to the ceiling or roof). The temperature increased from the bottom of the room to the ceilings due to

the buoyancy effect where light hot air rises up while the heavy cold air moves down to the floor. Figure 5.8(b) shows the local temperature distributions around 1.1m above the floor with maximum and minimum temperature of 21.2^{o}C and 20.8^{o}C respectively. The uniform temperature distribution along the horizontal plane at 1.1m above the floor of the room shows that the indoor temperature in the comfort zone (close to the head of sitting human) is well distributed.

Figure 5.9 shows the local indoor velocity of the heated room operating at constant hot water flow to the radiator. According to the international comfort standards of EN ISO 7730, the indoor air velocity is recommended to be less than 0.15 m/s unless special phenomena are required. It is clear from figure 5.9 that the local air velocity in the heated room is well distributed with maximum air velocity of 0.15m/s. The lower air velocity in the bottom of the heated room indicates that the draught risk that causes discomfort around the ankle level of the occupants is low. This shows that the panel radiator heat source is well positioned and able to counteract the fresh air flow by ventilation before it reaches the floor of the heated room.

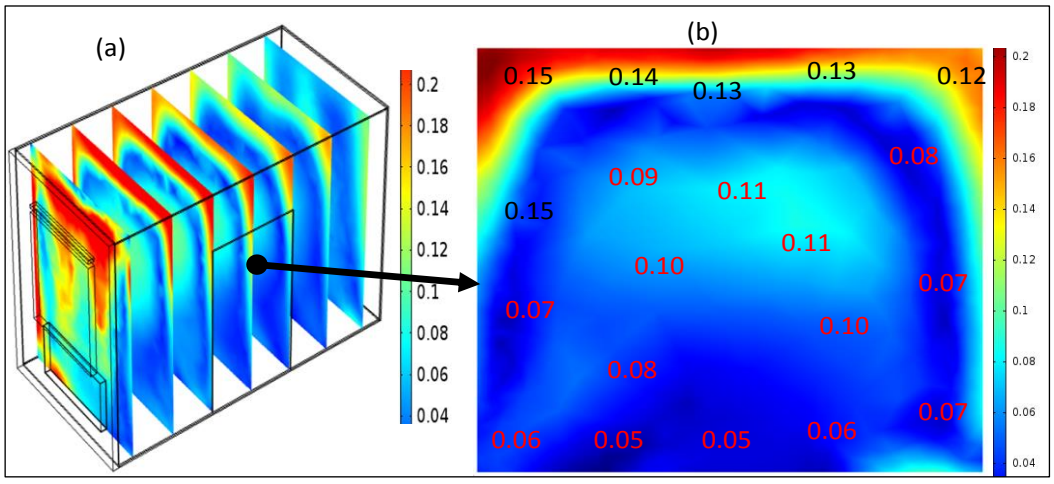

Figure 5.9 local indoor air velocity distributions in m/s (a) slice contour of the room volume and (b) vertical cut plane of air velocity contour operating at constant flow radiator spatial temperature at 2000s

5.4.2 CFD results at pulsed flow

In the simulation of the heated room at pulsed flow the transient mean temperature of the radiator operating at pulsed flow as investigated numerically in chapter 4 was applied. Figure 5.10 shows the predicted mean temperature of the radiator at pulsed hot water flow. The predicted transient mean surface temperature of the radiator was fitted using a polynomial equation as shown in eq. (5.8) which was used as a boundary condition at the panel radiator surface in the heated space model.

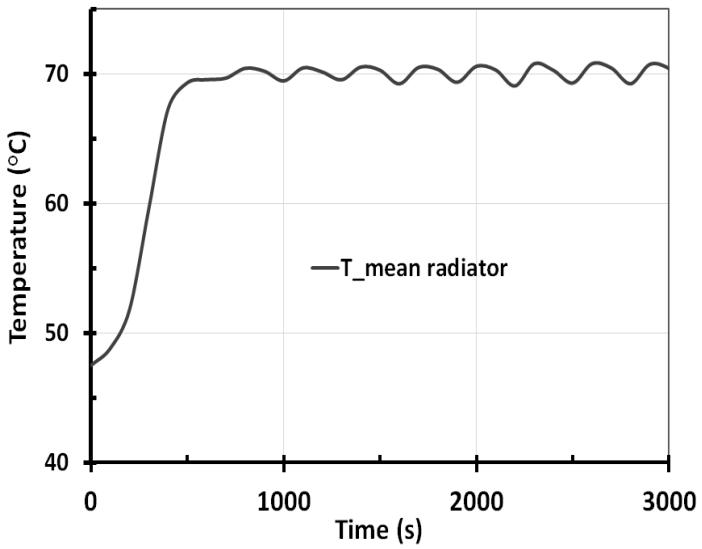

Figure 5.10 transient mean temperature of the radiator operating at pulsed flow scenario of the water hot water supply

$$T_{mean} = (t <= 500)*(9^{-7}*t^{3} - 0.001*t^{2} + 0.36*t + 320.15) + (t > 500)*(343.11 + wv) \quad (5.8)$$

$$\text{where: } wv = A.\sin(2\prod f\, t + \phi)$$

Where: T_{mean}, t, wv, f, A and ϕ are mean temperature of the radiator (^{o}C), time (s), sinewave function, frequencies in (Hz), amplitudes, and phase angle. The fluctuation of the panel radiator mean temperature operating at pulsed flow shown in figure 5.10 is estimated using sinusoidal wave function. Figure 5.11 shows the local temperature distribution along horizontal and vertical planes at the middle of the heated room with no occupants and panel radiator operating at pulsed flow. As shown in figure 5.11(a) the minimum indoor temperature of 20.5 ^{o}C occurred close to the floor of the heated space; while the maximum indoor temperature of 21.8^{o}C occurred close to the roof similar to those obtained in section 5.4.1 with constant hot water flow to the radiator.

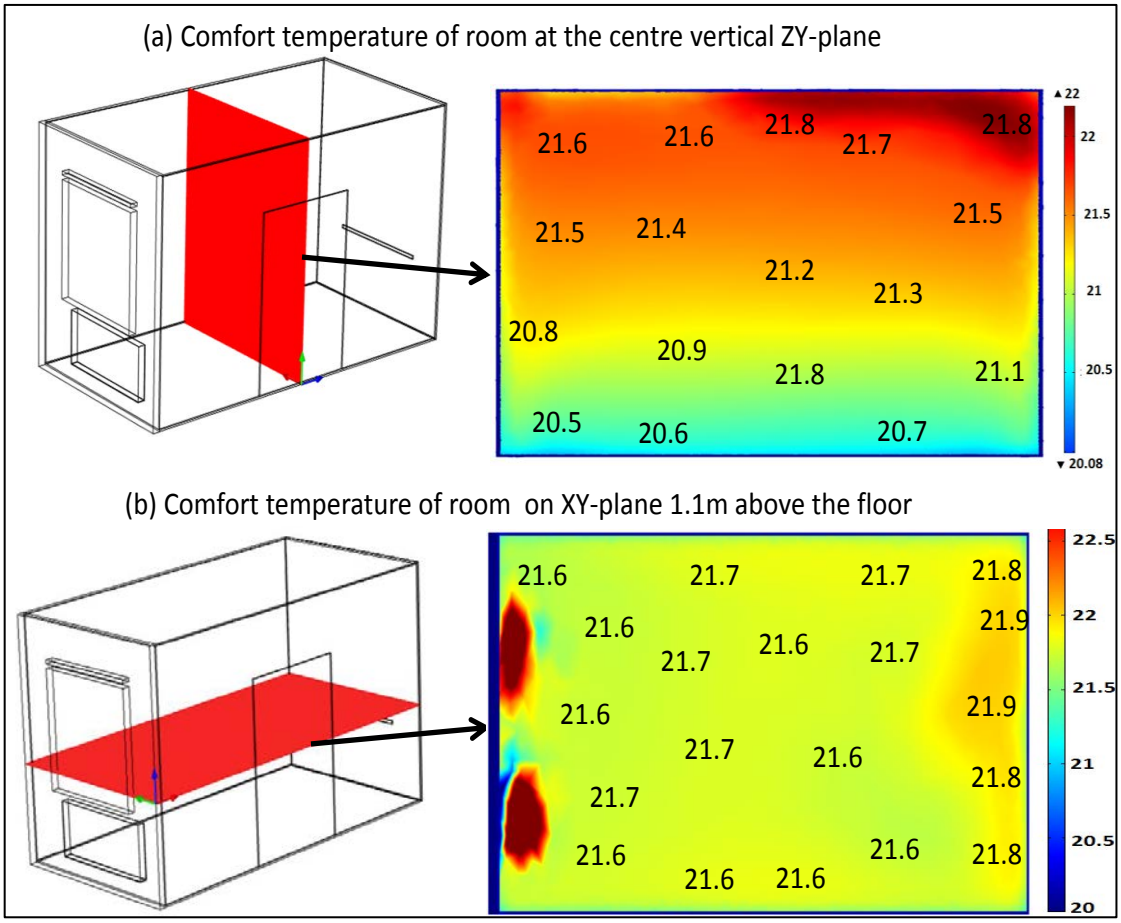

Figure 5.11 local temperature distribution contours of the indoor with no occupants along (a) vertical cut plane and (b) horizontal cut plane operating for the pulsed flow radiator heat source at 2000s

Figure 5.11(b) shows that for the plane located at 1.1m above the floor level of the maximum and minimum temperature of the heated room with radiator operating at pulsed flow are 21.9°C and 21.6°C respectively. The lower indoor air temperature difference of this horizontal plane indicates that the temperature is uniform around the room. Thus the indoor temperature distribution of the room operating at pulsed flow are in a good agreement with EN ISO 7730 comfort standards with recommended indoor temperature limit of 20± 2°C for the typical UK outdoor temperature of 5°C.

Figure 5.12 shows the local indoor velocity of the heated room with the radiator at pulsed flow. The indoor air velocity is less than 0.15 m/s as recommended by the international comfort standards documented in EN ISO 7730. This low velocity reduces the draught risk that cause discomfort around the ankle level of the occupants.

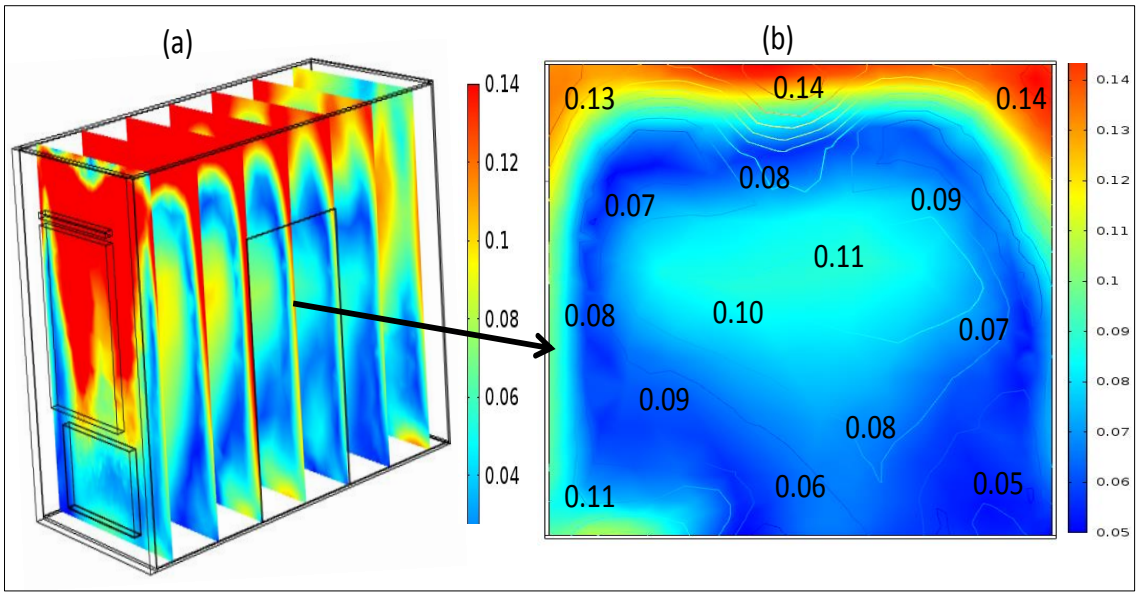

Figure 5.12 local indoor air velocity distributions in m/s: (a) slice contour of the room volume and (b) vertical cut plane of air velocity contour operating at pulsed flow radiator spatial temperature at 2000s

In conclusion the local temperature and local velocity distribution within the heated room with no occupants (empty) and with panel radiator operating at pulsed as well as constant flows are in agreement with the thermal indoor comfort standards. Further details of thermal comfort parameters for the heated room operating at constant and pulsed flows compared to published work [174] are discussed in the following sections.

5.4.3 Indoor comfort parameter comparison

According to ASHRAE 55 standards the recommended occupants indoor comfort margin is considered from 0.15m (ankle level) to 1.1m above the floor level for person sitting in an office and 0.15m to 1.7m for a standing person.

The indoor draught rating depends on the indoor air velocity and indoor temperatures of the heated room, therefore achieving the right comfort temperature and velocity leads to better draught rating of the indoor environment [174]. The indoor draught rating is recommended to be below 15% according to the indoor comfort standards. The finite element modelling of the heated room with no occupants and pulsed flow radiator was compared against constant flow and published work.

Figure 5.13 shows the predicted indoor air velocity and comfort temperature profile at specified vertical positions in the heated room under pulsed flow compared to constant flow and published work [174]. In figure 5.13 (a) and (b) the indoor air temperature and velocity are taken at the vertical centre line of the simulated room x,

y, Δz values of 2.75m, 1.75m, 2.66m respectively. In figure 5.13 (c) and (d) the indoor temperature and velocity are taken at 1m away from the surface of the wall surrounding the room x, y, Δz value of 4.5m, 1.75m, 2.66m respectively. It is clear from figure 5.13 that the temperature and velocity profile of the simulated heated room under pulsed flow are in good agreement with constant flow and published work [174]. The published work was carried using three hydronic skirting heating systems supplied by low-temperature hot water to investigate if thermal skirting boards were able to produce indoor comfort for the tested room and all works were carried out based on the international indoor comfort standards. Thus results of the heated room simulated in this work showed that the pulsed flow radiator is capable of fulfilling the comfort criterion of the indoor comfort temperature (air and radiant temperatures) and velocity distribution as recommended by international standards.

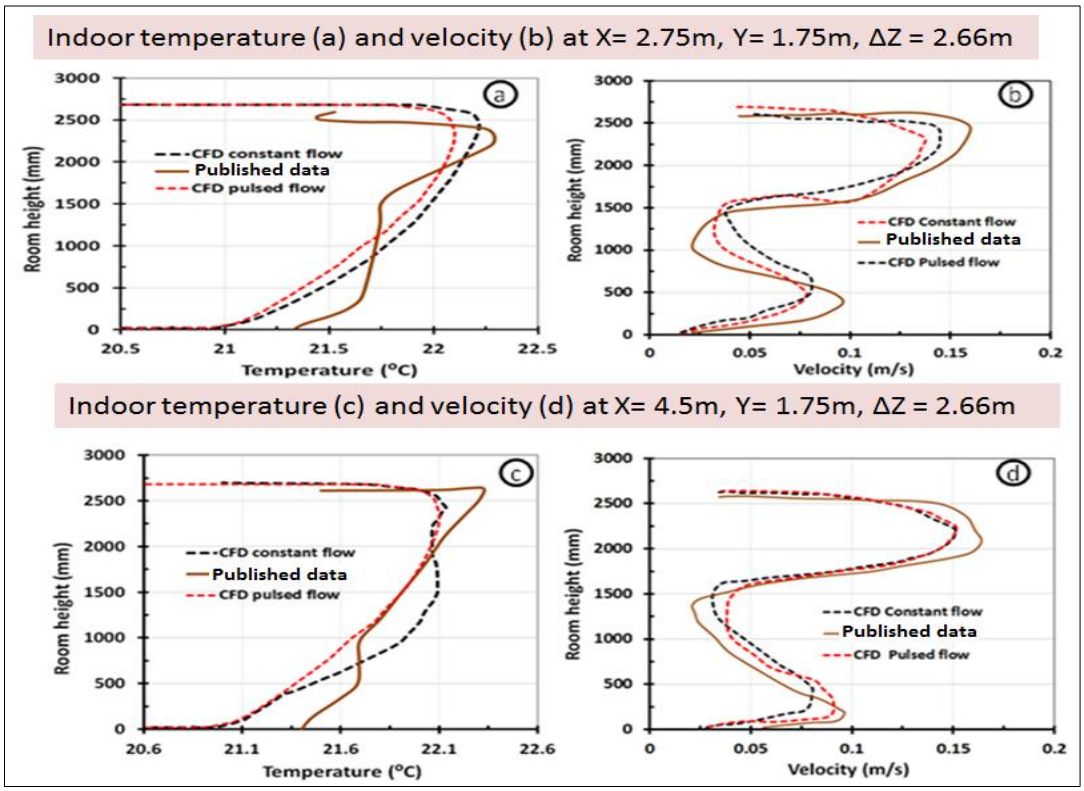

Figure 5.13 predicted indoor temperature and velocity profiles compared to the published work at 2000s

The discomfort due to draught in a ventilated room is estimated by Draught Risk (DR) parameters which depend on the local turbulence intensity (TI) of the room and it is expressed as eq. (5.11). The turbulence intensity (TI) is expressed using eq. (5.12) [174-177]. The Percentage of Dissatisfied (PD) due to draught as expressed by eq. (5.13) refers to people who are exposed to indoor air velocity with turbulence intensity ranging from 35 to 55% under sedentary conditions and dissatisfied. There is also other important mathematical equation that predicts the Percentage Experience Draught (PED) of sedentary occupants of the ventilated room expressed using eq. (5.14). The three draught prediction equations are included in both ASHRAE standard 55 and EN ISO 7730 indoor comfort zone standards. The indoor comfort temperature (T_{ind}) is the average of indoor air temperature and radiant temperature.

$$DR = \left[(3.143 + 0.3696 * Vel_{ind} . TI).(34 - T_{ind}) * (Vel_{ind} - 0.05)^{0.6223} \right] \tag{5.11}$$

Where:

$$TI = \frac{V'}{U} \tag{5.12}$$

$$PD = 13.8 * 10^{3} . \left[(\frac{Vel_{ind} - 0.04}{T_{ind} - 13.7} + 2.93 * 10^{-2})^{2} - 8.54 * 10^{-4} \right] \tag{5.13}$$

$$PED = 113 * (Vel_{ind} - 0.05) - 2.15 * T_{ind} + 46 \tag{5.14}$$

Where; Vel is indoor velocity, T is indoor temperature, V' is Root-Mean-Square (RMS) of the turbulent velocity fluctuations at a particular location over a specified period of time, U is the average of the velocity at the same location over the same time period.

Figure 5.14 shows the CFD predicted draught discomfort condition in the heated rooms under constant and pulsed flow conditions compared to published data [174].

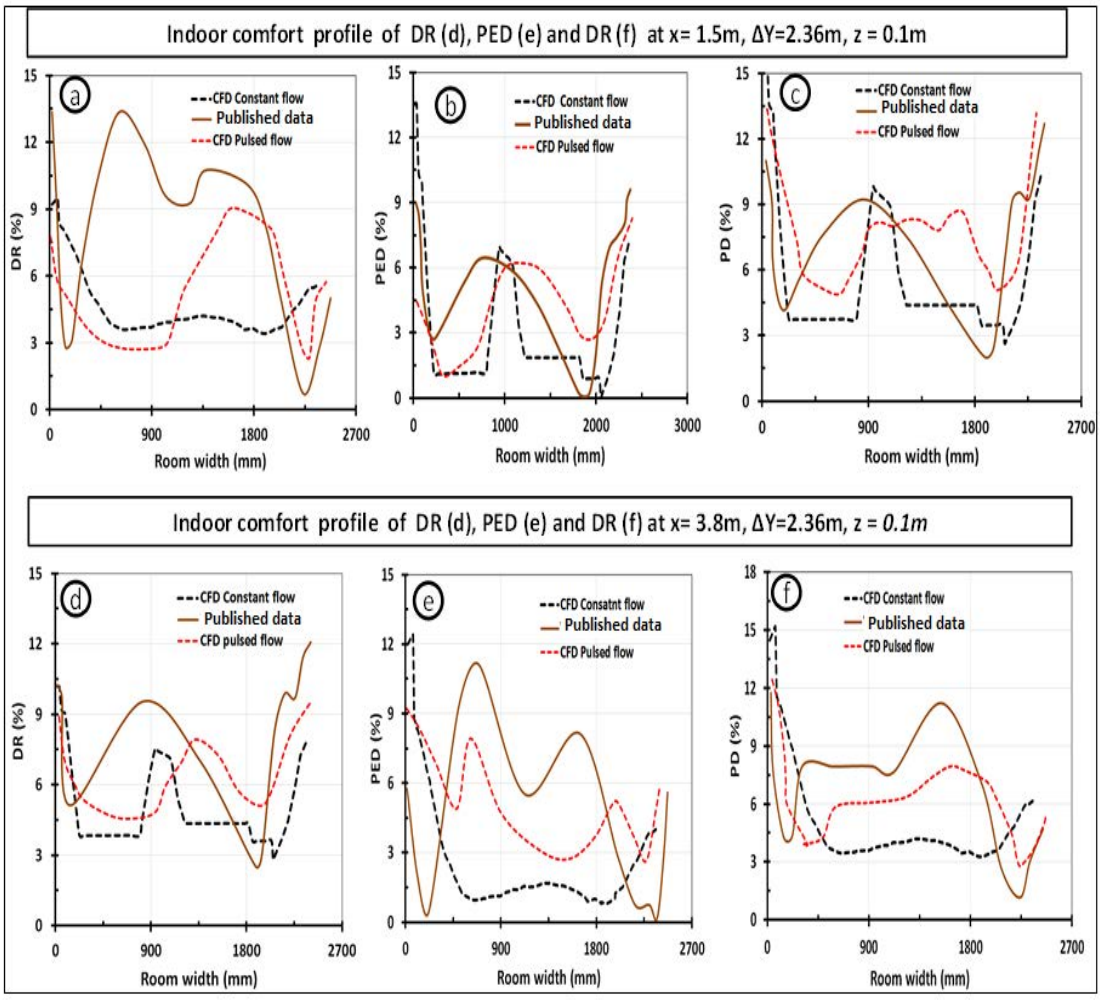

Figure 5.14 draught rating comfort parameters of the simulated heated room with no occupants for the pulsed and constant flow compared to validated data at 2000s

Figures 5.14 (a), (b) and (c) show the DR, PED and PD at ankle level of 0.1m horizontally along the width of the room (y-axis) and at coordinate values of x, Δ y, z of 1.5m, 2.36m, 0.1m respectively. Also figures 5.14 (d), (e), (f) depict the DR, PED and PD at ankle level of 0.1m horizontally along width of the room (y-axis) and values of x, Δ y , z of 3.8m, 2.36m, 0.1m respectively.

It can be seen from figure 5.14 that all the draught rating comfort parameters are less than 15% as recommended by international standards of ISO 7730-2005 and ASHRAE 55-1992. The results show that the downdraught air is well suppressed along the ankle level in the room for both pulsed and constant hot water flow conditions to the panel radiator. Particularly, the predicted draught parameters for pulsed flow show that it can be used in central heating system without affecting the comfort of the occupants.

5.5 CFD of heated room with occupants inside

In section 5.4 the thermal comfort in a heated room with no occupants was investigated at both pulsed and constant flow operating conditions. In this section the heated room with occupants will be modelled to investigate the effect of pulsed flow on the thermal comfort and indoor air qualities.

Figure 5.15 shows the input and output parameters considered in modelling the heated space with occupants. The main input parameters are the heat output from the radiator (Q_rad) as heat source, fresh air velocity (Va_inlet) generated by mechanical

ventilation, ambient temperature (T_amb) as outside temperature, the moisture generation from occupants Rh_ind), CO_2 concentration of outdoor air (CO_2_amb), indoor CO_2 generation by occupants and moisture content of outdoor air (Rh_amb). The difference between the ambient temperature and indoor temperature causes heat loss through windows (Qwin_loss) and walls (Qwal_loss). Also there is energy loss due to the exhaust air from the ventilation outlet (Va_outlet). The investigated output parameters are the thermal comfort including indoor comfort temperature (air and radiant temperature), indoor air velocity (Vel_ind), relative humidity (Rh_ind) and indoor air quality in terms of CO_2 concentration (CO_2_ind). The numerical simulation of the occupied room is investigated using radiator operating at pulsed flow with transient mean surface temperature shown in figure 5.10 and the geometrical configuration shown in figure 5.3.

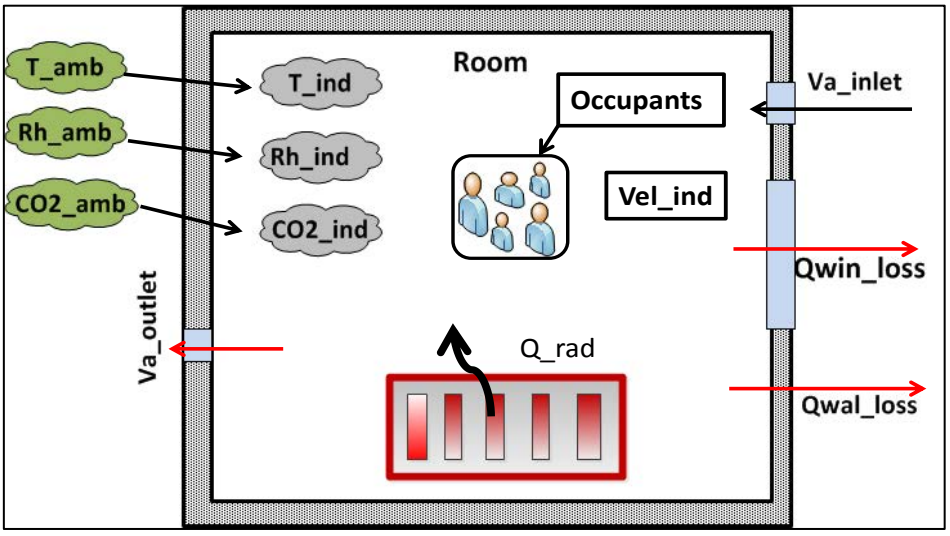

Figure 5.15 the schematic diagram of heated room model with occupants

To investigate the thermal comfort and indoor air qualities of heated room occupied with five people, the two physics used were the conjugate heat transfer physics and the transport of diluted species physics as described in section 5.2. In addition to all

assumptions considered for the heated room with no occupants as defined in section 5.4, the following assumptions and boundary conditions were applied for the modelling of the room with occupants.

- Diluted species physics for indoor air CO_2 concentration as well as relative humidity were used as governing equations.
- The heated room was occupied by five people and surface area of each adult was estimated to be $1.8m^2$. The occupants are assumed to occupy a box that has surface equal to the total area of the occupants.
- Moisture generation from the occupants is estimated based on the international ASHRAE standards to range from 1.8 kg/day to 2.7 kg/day per person and for this work an average value of $2.48*10^{-5}$ kg/s per person was applied as input mass flux in mole/(m^2.s) [152].
- The outdoor air was assumed as UK winter average temperature of 5^oC with relative humidity of 80% applied as boundary condition of input mass of water vapour per unit volume of air [152].
- The indoor air humidity was assumed to be 50% initially at 20^oC indoor temperature.
- The diffusion coefficient of air and CO_2 are; $2.21*10^{-5}$ m^2/s and $1.41*10^{-5}$ m^2/s respectively [161].
- The CO_2 generation from the occupants is 0.00416 l/s per person as recommended by ASHRAE, applied as inward mass flux boundary condition in (mole/($s.m^2$)) on the top surface of the box representing the occupants.
- The CO_2 concentration of typical ambient air is assumed to be 350PPM applied as inflow boundary condition in (mole/m^3) as recommended by ASHRAE.

- The indoor CO_2 concentration was initially assumed as 400PPM applied in mole/m^3.
- Ventilation flow rate of 7.5 l/s per person in the occupied zone was applied as air ventilation boundary condition based on five occupants in the heated room as recommended by ASHRAE 62-1999.

5.5.1 CFD results and discussion of heated room with occupants

The predicted indoor thermal comfort and indoor air qualities (IAQ) of the simulated occupied room were analysed on the basis of international standards including ISO 7730-2005, ASHRAE 55-1992 as well as ASHRAE 62-1999. The output parameters used to assess the thermal comfort and indoor air quality include temperature 20^{o}C±2^{o}C, indoor air velocity ≤ 0.15 m/s, indoor relative humidity 50%±10 % and indoor CO_2 concentration limited to ≤ 1000 PPM. Figure 5.16 shows the temperature, velocity, relative humidity and CO_2 concentration contours along the cut plane shown in figure 5.16 (a).

The maximum and minimum indoor temperatures along the cut plane are 21.5^{o}C and 19.9^{o}C which are within the recommended target temperature of 20±2^{o}C. The maximum and minimum indoor air velocity values are 0.15m/s and 0.05m/s respectively which agree with the recommended indoor velocity of less than 0.15m/s. Figure 5.16 shows that the highest air velocity occurs at the top left and bottom right corners of the plane which does not affect the comfort of the user as they are not accessible.

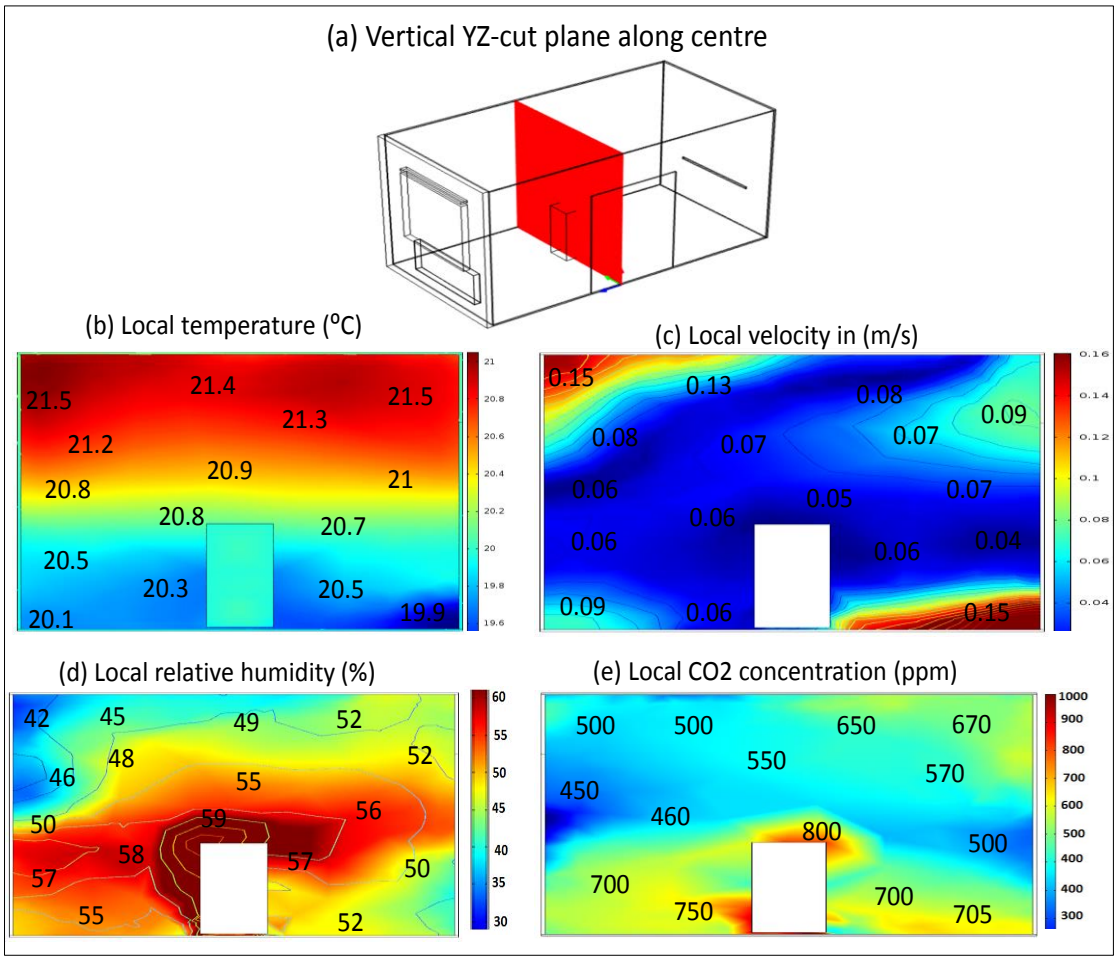

Figure 5.16 the local contour of indoor thermal comfort and indoor air quality corresponds to the cut plane shown in figure 5.16(a) at pulsed flow 2000s

The minimum and maximum local indoor relative humidity are 42% and 59% which are within the desired target of 50%±10%. Finally the indoor air quality represented by the indoor CO_2 concentration showed minimum and maximum values of 400PPM to 800PPM which are lower than the recommended value of 1000PPM. This lower indoor CO_2 concentration in the room indicates that there is no indoor air quality concern for the occupants of the heated room. Figure 5.17 shows temperature, velocity, relative humidity and CO_2 concentration at various planes within the heated room with occupants.

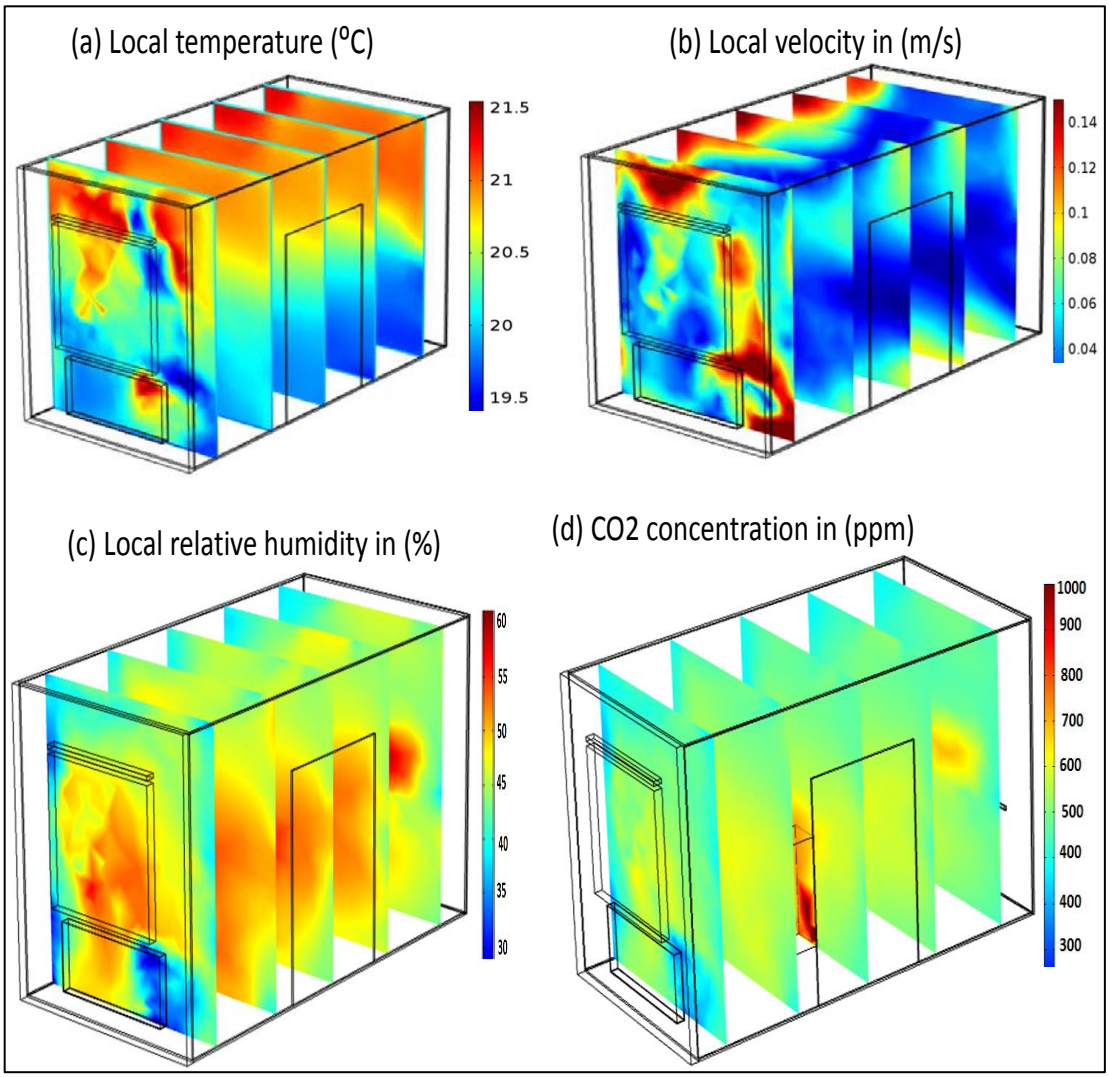

Figure 5.17 local slice planes of the indoor thermal comfort and indoor air qualities at pulsed flow at 2000s

Figure 5.17 shows that all the depicted local parameters including the indoor local temperature, velocity, relative humidity and CO_2 concentration are uniformly distributed in the heated space. Figure 5.18 shows the trends taken from centre plane of the room at specific points of 150mm and 1500mm above the floor with time.

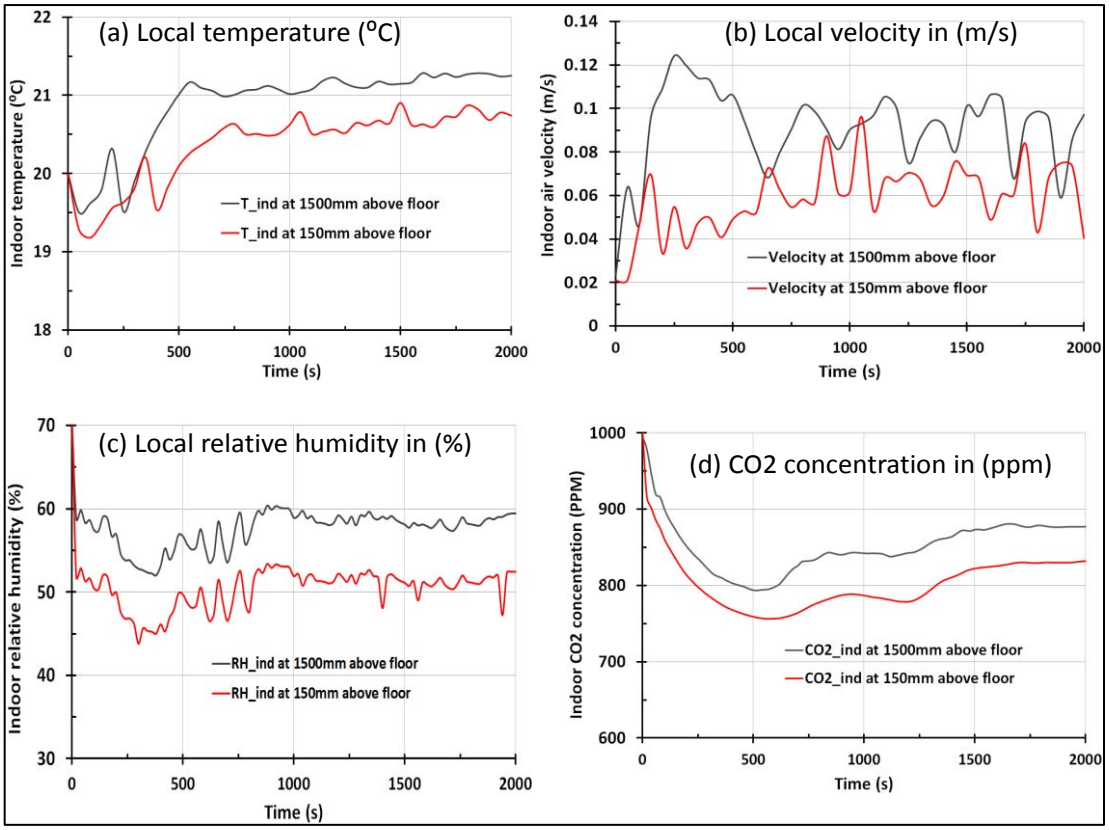

Figure 5.18 the indoor thermal comfort and indoor air qualities of the simulated room at specified points above the floor at the centre of the room with time at pulsed flow

In figure 5.18 the selected points represented the ankle level (150mm) and neck level (1500mm) of the indoor occupants which are the sensitive positions of the human occupants. Maintaining lower fluctuations of the thermal comfort parameters including temperature, velocity and humidity at the two selected points indicates achieving thermal comfort both at the top and bottom position in the room. Regarding the indoor air qualities maintaining the CO_2 concentration below 1000ppm regardless of fluctuation indicates that adequate amount of fresh air is supplied to the room though the ventilation system.

Using CFD simulation all the indoor thermal comfort and indoor air quality parameters were investigated and the results showed that the heated room operating at

pulsed flow satisfy the comfort criterion recommended by national and international building standards. Thus the energy saving predicted in chapter 4 due to the pulsed hot water flow to hydronic radiator can be achieved without affecting the indoor comfort of the occupants.

5.6 Summary

Firstly the heated room without occupants was simulated using constant and pulsed flow conditions in COMSOL Multiphysics. The heated room without occupants was simulated to investigate thermal comfort (indoor temperature) and draught rating (DR, PED, and PD). The indoor draught depends on the indoor air velocity, indoor temperature and indoor turbulent intensities. Results of the heated room without occupants were compared with published data showing good agreement with both the published data and the recommended international comfort criterion.

Secondly the room with occupants was simulated using the spatial temperature of the radiator operating at pulsed flow scenario to investigate indoor comfort including; indoor temperature, air velocity, relative humidity and CO_2 concentration. Results showed that indoor temperature of 20±1.6^{o}C, indoor velocity of less than 0.15m/s, relative humidity of 50±9% and CO_2 concentration of less than 800ppm were achieved and are in good agreement with international comfort standards of ASHRAE 55 and EN ISO 7730.

In chapters 3 and 4 the energy saving due to using pulsed flow was analysed based on the specific heat output showing that about 25% of energy saving can be achieved. In

this chapter the simulation results showed that the potential energy saving due to flow pulsation for panel radiators can be achieved while maintaining the indoor comfort standards of the occupants.

CHAPTER 6

EXPERIMENTAL FACILITIES

6.1 Introduction

In chapters 3 to 5 the effect of flow pulsation was investigated analytically and numerically showing the potential of reducing energy consumption without compromising indoor comfort. Therefore experimental work is required to measure the temperature distribution of the hydronic heating panel radiator and heated room. Figure 6.1 shows the flow diagram of the process of developing the test facility and experimental work required at various operating conditions.

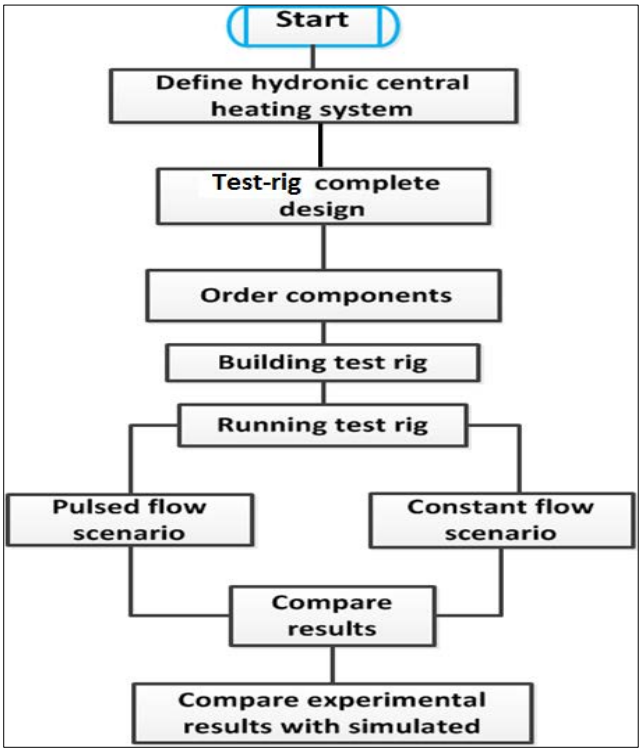

Figure 6.1 the flow diagram of the experimental work

Experimental evaluation of the heat output from the radiator and the comfort parameters for the room with constant and pulsed flow is required to verify the modelling and prove the effect of pulsation [88, 168]. In this chapter the experimental facilities used to investigate the thermal performance of the hyronic central heating system are described. The design, construction, instrumentation, and commissioning of the test facility are first described in sections 6.2 to 6.6. Section 6.7 describes the testing procedure used while section 6.8 evaluates the uncertainty in the measurement taken and section 6.9 gives the summery of the chapter. Figure 6.1 shows the flow diagram of the process of developing the test facility and experimental work required at various operating conditions.

The design of test rig is performed according to BS EN 442 radiator standards [178]. The inlet hot water flow of the hydronic radiator was constructed to perform various flow strategies including constant and pulsed flow strategies. All the measuring components such as thermocouples, LM 35 temperature controller sensor, and the flow meter are calibrated against standard measuring devices.

6.2 Design and construction of test facility

The test rig was developed to investigate the heat output and temperature distribution of the hydronic radiator at various hot water inlet flow conditions. The proposed heated room was setup to determine the temperature distribution in the envelope which represents single room with central heating system. Figure 6.2 shows a

schematic diagram and figure 6.3 shows a pictorial view of the proposed test rig for the hydronic heating system developed in this work.

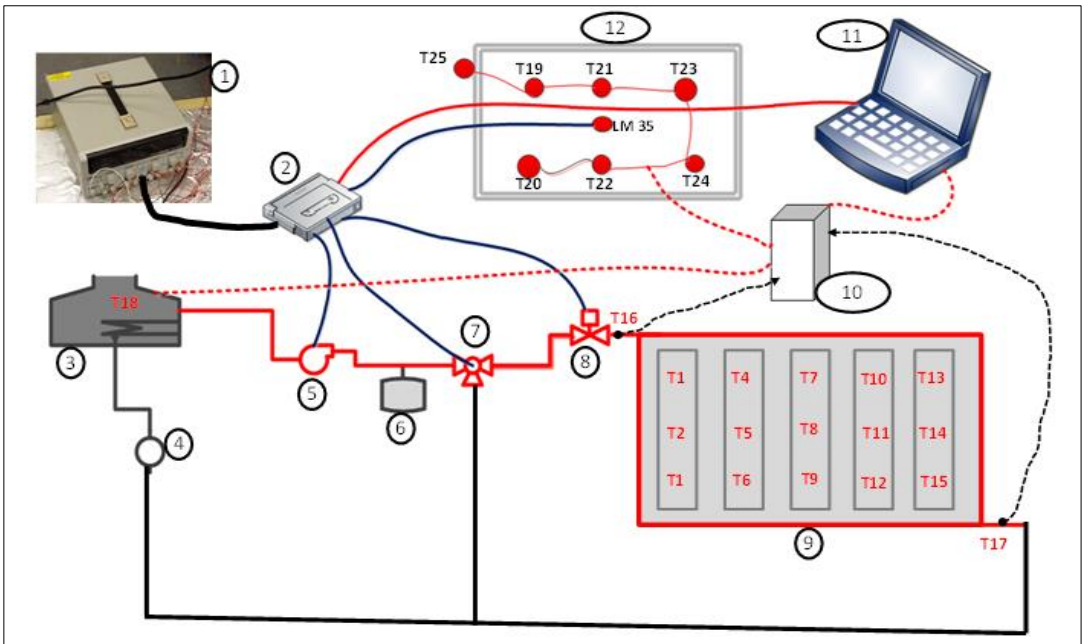

Indicator	Description	Indicator	Description
1	Power supply	9	Heating radiator
2	Control box	10	Data logger
3	heater	11	Computer
4	Flow meter	12	Heated room
5	Pump	T1 to T15	Radiator surface thermocouples
6	Exp. vessel	T16 to T18	In/out probe thermocouples
7	3 way valve	T19 to T25	Indoor/outdoor thermocouples
8	2 way valve	LM 35	Temperature controller

Figure 6.2 the schematic diagram of the proposed test rig

The main components of the test rig are the hydronic heating system assembly, instrumentation and the control system developed for this work. The main components of the test facilities are presented in the following sections.

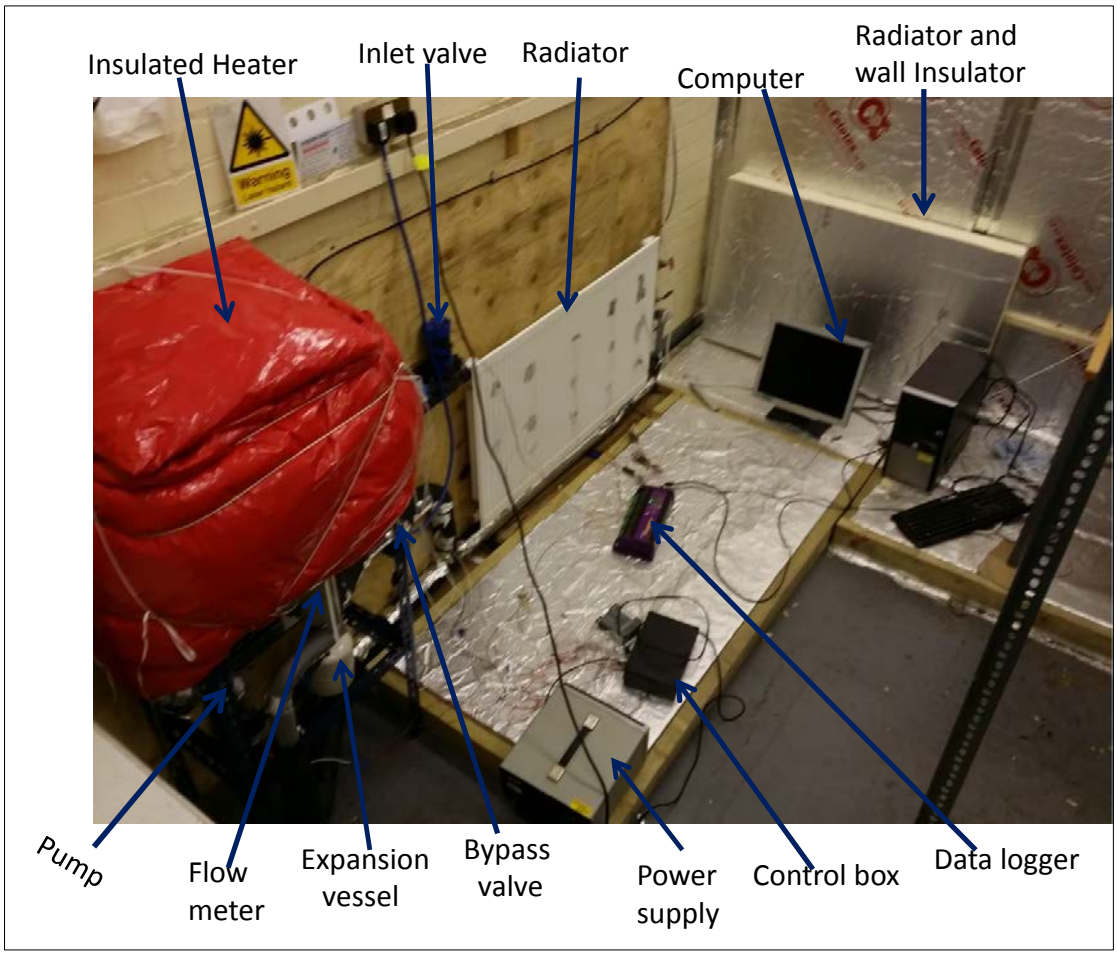

Figure 6.3 the pictorial view of the proposed test rig

6.3 Hydronic heating system

In this section the main components of the hydronic central heating system used in the test rig are described as follows.

- 3kW of thermostat heater installed in a thermally insulated water cylinder (3) that provides the 2.5kW/(24hr) heat loss as recommended by BS 5615 1985.
- Centrifugal circulation pump (5) driven by 12V or 24V DC power from TOTTON PUMPS with operating conditions of 1.4 bar pressure, 95^{o}C temperature, 5m head and flow rate of 35 l/min.

- 2 litres- Varem Extravare LC water expansion vessel (6) operating at pre-charge of 3.5bar, maximum pressure of 8bar and the maximum operating temperature of 99^{o}C.
- Electronic valves including three ways bypass valves (7) and two way valves (8). CWX mini motorised valve is normally used to close ball valves operating at 10bar pressure, 100^{o}C temperature, and maximum power requirement of 5W supplied from 24V DC/AC power source
- Type11 Hydronic panel radiator (9) (single finned radiator) from WICKS was used for this test with heat output capacities of 928W and size of 1m length and 0.6m height. The heat output of the radiator is estimated based on the BS EN 442 radiator standards operating at inlet and outlet temperature of 75^{o}C and 65^{o}C respectively. The radiator was insulated to minimise the convection heat transfer loss to the surrounding air when the surface temperature measurement was taking place. The insulator used for the radiator was Celotex insulation board of 0.1m thick with thermal conductivities of 0.022W/(m.K). The radiator was attached to the wall using screwed bracket on the fin side of the panel. The fin configuration of the panel radiator and the insulation arrangement is shown in figure 6.4.
- 15mm diameter copper flow pipes were used to connect the closed loop typical hydronic central heating system. All flow pipes were insulated using polyethylene material, with thermal conductivity of 0.0334W/(m.K) and 25mm thickness as shown in figure 6.4.
- The test room (12) has the dimensions of 4.2m lengths, 3.8m widths, 3.2m heights and represents a single heated room using hydronic central heating system. The external wall was insulated using Celotex insulation board of 0.1m thick, 1.2m width, 2.4m high and thermal conductivity of 0.022W/(m.K). The insulation

boards are joined to each other using timber and the gap between each parts are sealed using Celotex Foil Insulation tape as shown in figure 6.5.

- Standing timber poles are arranged at equal intervals with respect to each other on the floor of the room and are used for fitting temperature measuring thermocouples when testing the heated room as shown in figure 6.5.

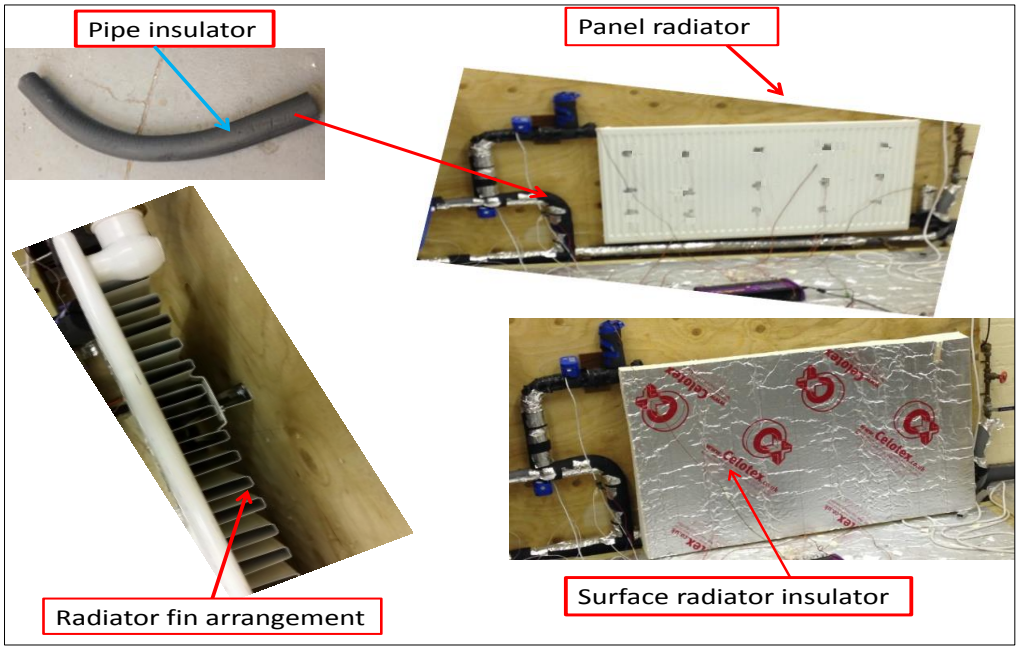

Figure 6.4 the panel radiator configuration view and the insulators used

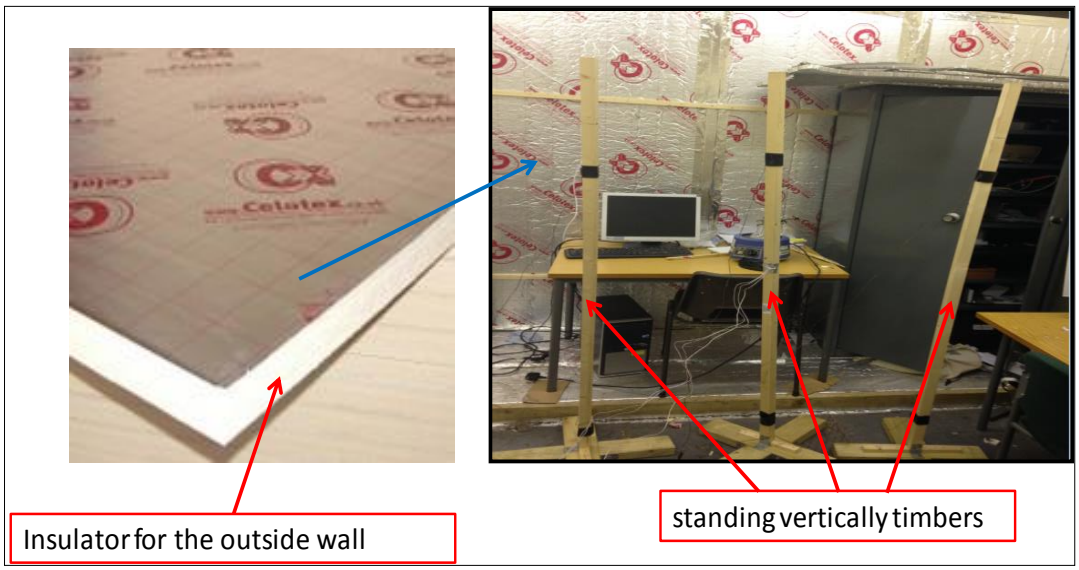

Figure 6.5 the indoor thermocouple layout outside wall insulator and standing timbers

6.4 Instrumentation

The developed test rig was operated by computerised measurements and computer codes for the microcontroller. The temperature was monitored and recorded using USB interface between the computer and the data logger. DataTaker model DT85-3 which has up to 32 channels isolated or 48 common referenced analog inputs was used for logging the various measurements taken in this work. Data is extracted from the dataTaker to the computer using USB interface at 1s sampling rate and the channels are easily connected to the data measuring sensors including: temperature, voltage, current of 4-20mA loops, bridge, resistance, strain gage and so on. This model of Data Taker can store up to 5 million of data points in user defined memory. The flow rate is measured and monitored manually using Platon NXG flow meter.

6.4.1 Temperature measurement

Two types of thermocouples were used to measure the temperature distribution around the surface of panel radiator, hot water and indoor/outdoor air temperatures. The hot water temperature at various points in the heating system were measured using T-type probe thermocouples from Omega (model number TJC100-CASS-M050G-150) with diameter of 1.5mm, 150mm probe length, 1000mm cable length. The inlet and outlet temperatures of the hot water are measured by inserting the probe in the flow channel as shown in figure 6.6. The probes are connected to the data logger and then data is transferred to the computer for evaluation.

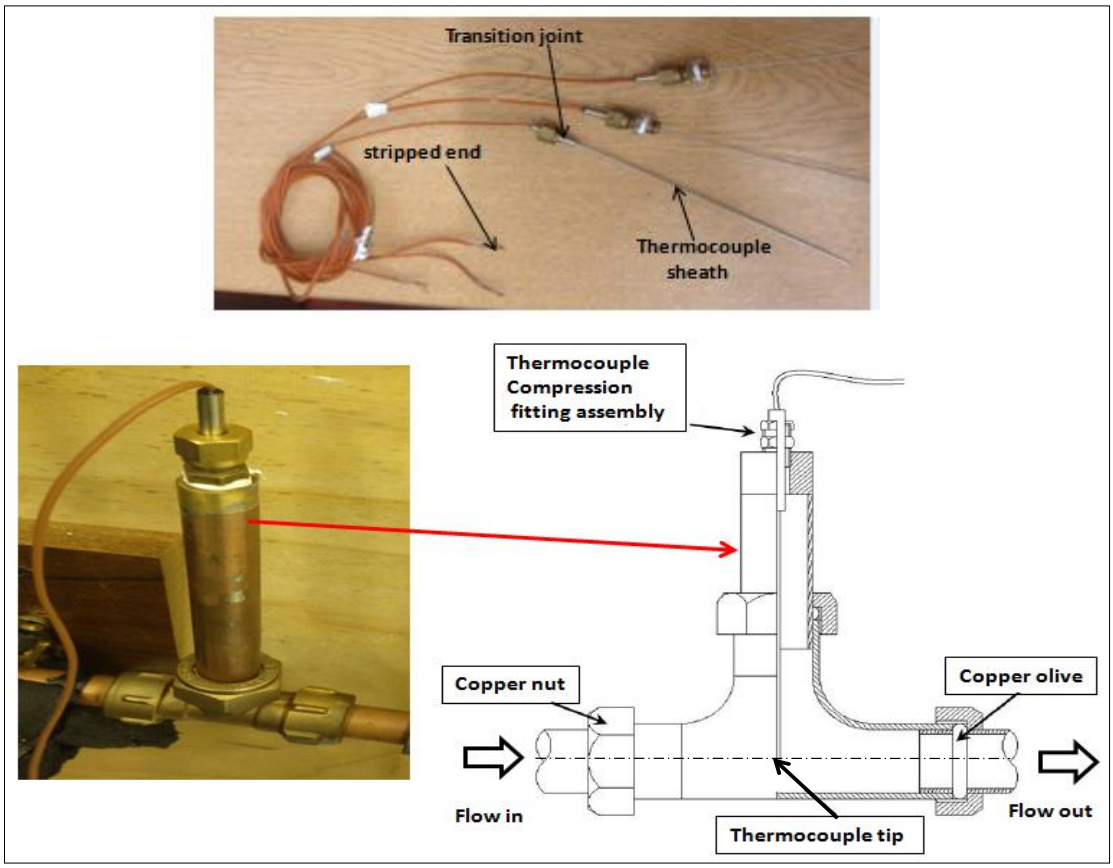

Figure 6.6 the probe thermocouple configuration along the flow channel of inlet and outlet radiator

The probe thermocouples used to measure the indoor/outdoor temperature is T-type thermocouples with 0.5mm probe diameter, 150mm probe length and 1000mm length from Omega (Model number TJC100-CASS-M050). To measure the room indoor temperatures at various positions, 6 thermocouple probes were fitted on the timber poles. On each pole two probes were fitted one at ankle level above the floor (150mm) and another at human neck level (1500mm). These positions correspond to the human comfort zone in a room as recommended by the international standard found in ASHRAE. Figure 6.7 shows the timber poles with thermocouple poles attached using aluminium foil tape. As shown in figure 6.7 the thermocouple sheath attached to the poles are fully exposed to the surrounding air in order to measure the indoor air temperature.

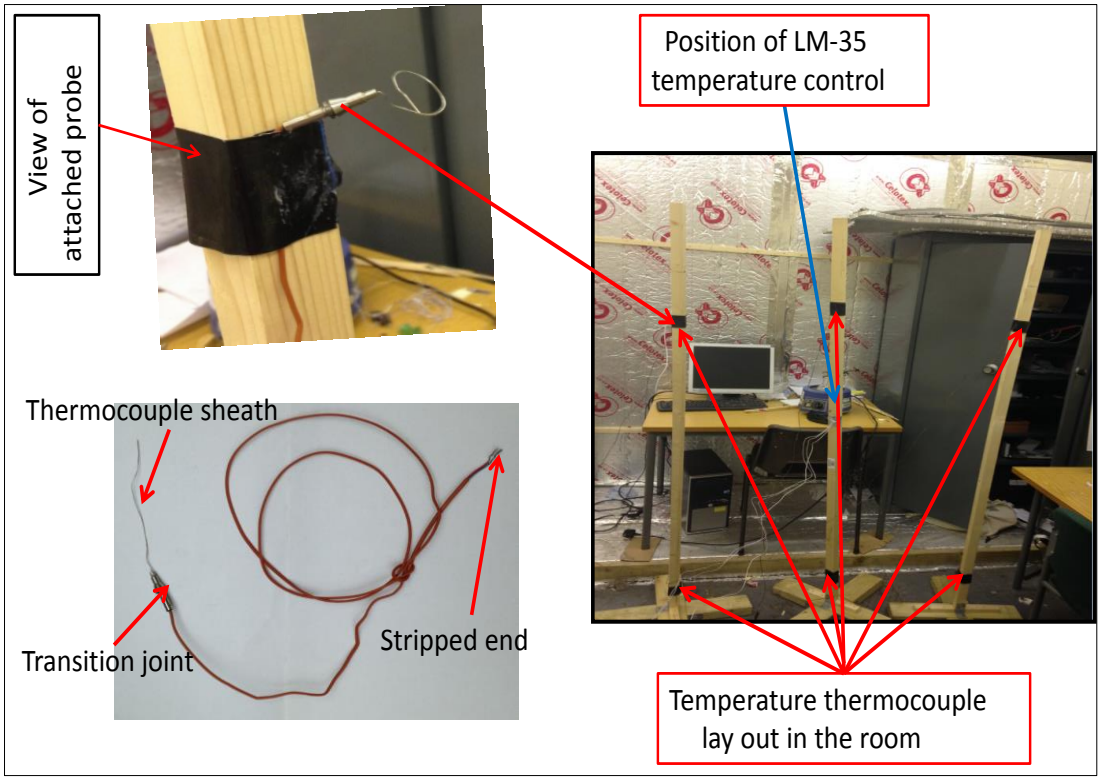

Figure 6.7 the thermocouple probe arrangement probe arrangement in the tested heated room

A T-type surface thermocouples of 0.13 mm diameter, 1000mm length from Omega (model number; 5TC-TT-TI-36-1M) were used to measure surface temperature distribution of the radiator at various positions. 15 surface thermocouples were arranged in 3 rows and 5 columns array as shown in figure 6.8. The surface thermocouples were attached to the surface of the radiator using Aluminium Foil Tape and the sheaths were fully covered from the surrounding air. The radiator was insulated on the surface where thermocouples were positioned using the Celotex insulation of 100mm thick to avoid the effect of the surrounding air. An extension wire was used to extend the thermocouple from the probe position to the data logger.

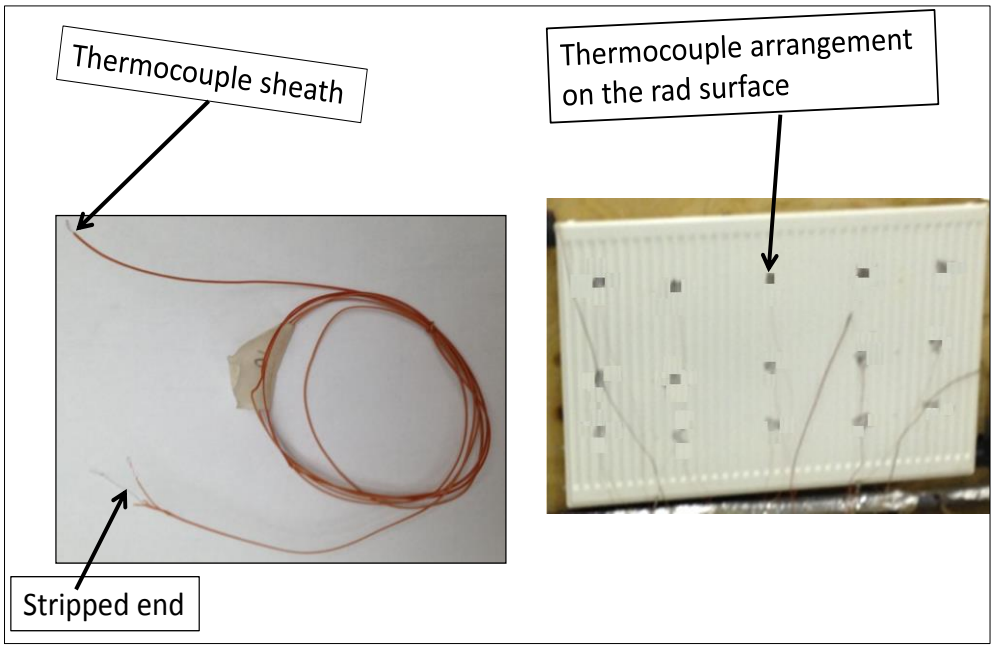

Figure 6.8 the thermocouple arrangement on the surface of the radiator

All the thermocouples used to measure the temperature were calibrated using Resistance Thermometer Detector Platinum100 (RTDPt100) in water path with manually adjustable temperature. Figure 6.9 shows the bath water pot used to calibrate the thermocouples. All the thermocouples were tied together along the RTDPt100 and inserted in the water path at the same level of the sheath end; all thermocouples signals were logged to the DataTaker DT85 channels for evaluation. Figure 6.10 shows the example of the relation between RTDPt100 and the thermocouple readings using linear fitting with R^2 of 0.9998 using eq. (6.1). Equation (6.1) is used to calculate the curve fit value ($\bar{x}$) required for determining the uncertainty of thermocouples. All the temperature measuring thermocouples have similar behaviour as shown in figure 6.10 and the figures of the 24 thermocouples used in this work are presented in appendix B.

$$T = 1.0091x - 0.3963 \quad (6.1)$$

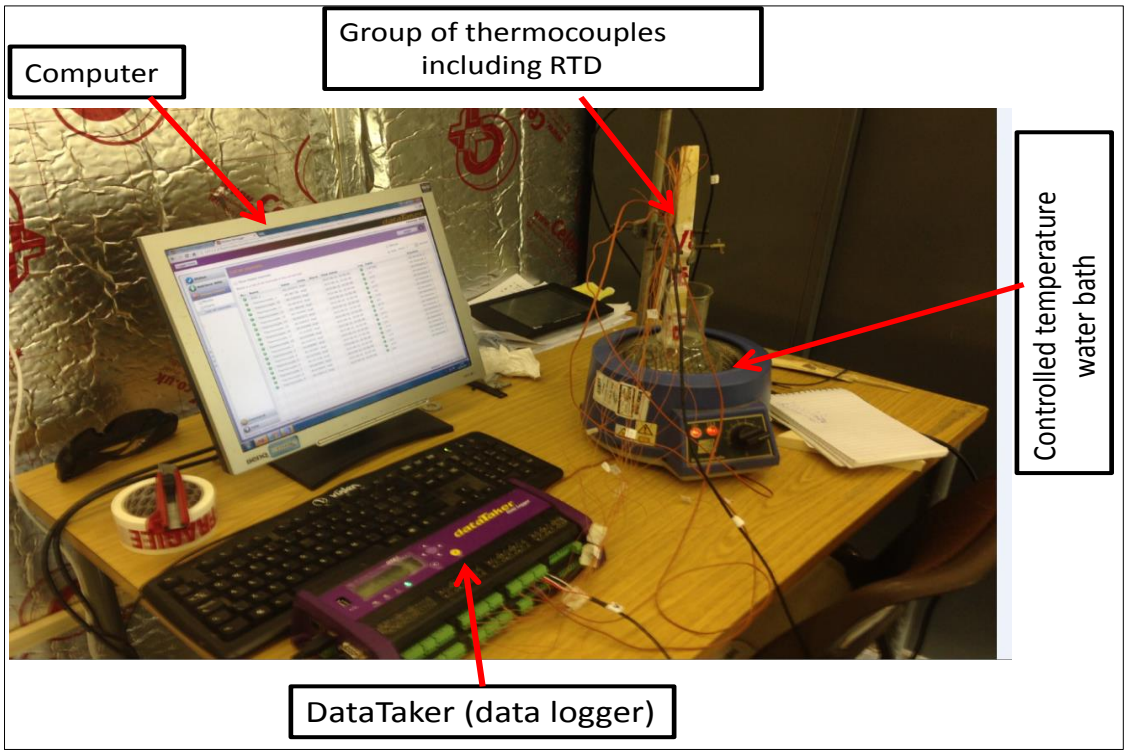

Figure 6.9 calibration set up of the thermocouples

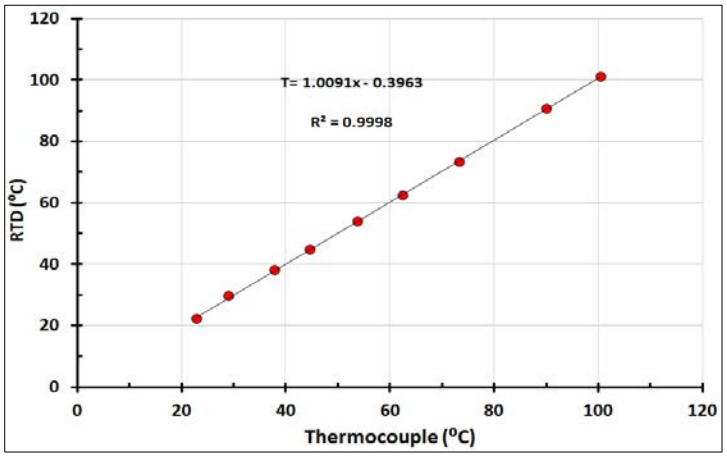

Figure 6.10 temperature relations between RTD and the thermocouples

6.4.2 Flow rate measurement

The hot water flow rate was measured using Platon NGX standard glass variable area (Rotameter) flow meter with accuracy of ±1.25% and flow rate ranging from 0.0027 kg/s to 0.05 kg/s (10 l/hr to 180 l/hr). The Platon flow meter operates safely up to

100°C temperature and up to 16bar pressure. The flow meter was fitted vertically to the flow line using M5 Nut sealed Viton on stainless steel units. The proposed flow rate for this experimental work ranged from 0.022 kg/s to 0.042 kg/s (80 l/hr to 150 l/hr) well within the range of the selected flow meter capacity. The flow meter was calibrated using labelled standard bucket and stop watch as shown in figure 6.11.

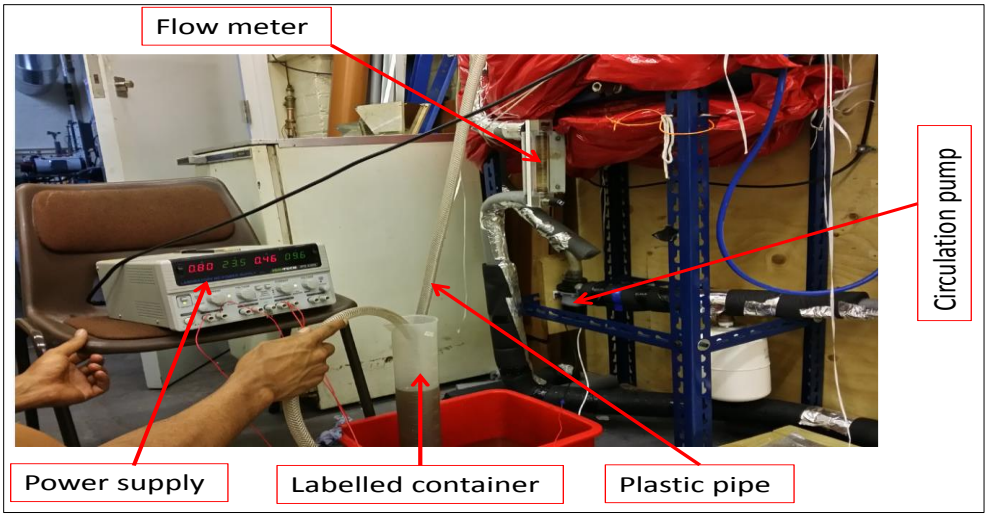

Figure 6.11 flow meter calibration set up

The flow meter was calibrated while maintaining constant power supply to the pump at 23.5V and 0.80A. The hot water flow was maintained at average operating temperature equal to the outlet temperature of the radiator of 65°C. The relation between the flow rate of the flow meter and the standard bucket filling is shown in figure 6.12. The R^2 value of the linear fitting 0.9993 expressed using eq. (6.2). Equation (6.2) is used for calculating the curve fit parameter ($\bar{x}$) in predicting the uncertainty parameters of the flow meter.

$$V_w = 0.9992\,x - 0.0048 \qquad (6.2)$$

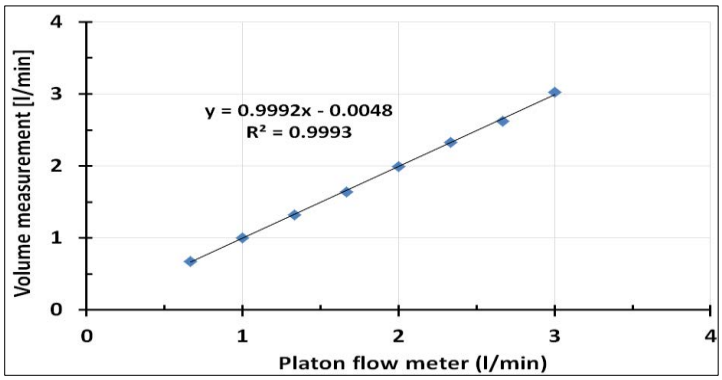

Figure 6.12 calibration of Platon flow meter using standard graduated bucket

6.5 Control system

To enable the pulsed flow operation a control system was developed using Arduino micro controller system consisting of Arduino mega 2560 micro controller, Arduino motor shield R3, mother board, LM35 temperature controller sensor and connecting wires as shown in figures 6.13 and 6.14. The Arduino control system is operated using a developed C++ code in Arduino software. The Arduino software is a user friendly open source free software and the Arduino hardware is available in the market at a reasonable price.

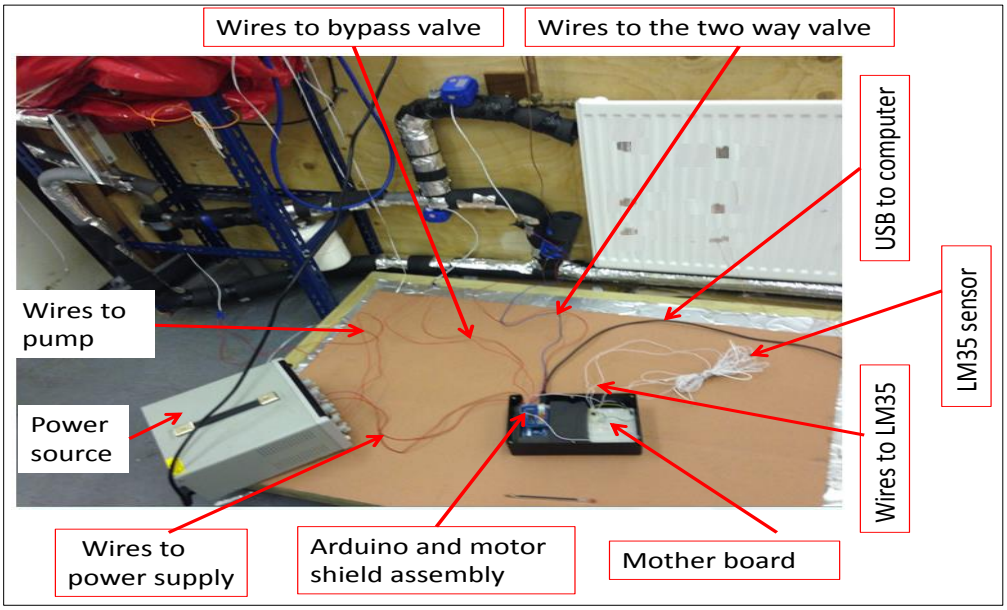

Figure 6.13 pictorial view of the proposed control system

The software is capable of producing codes for various operating control automation systems including, various flow and process control strategies. A code was produced in C++ format in the Arduino open source software and uploaded to the micro controller to command the valves operating at constant and pulsed flow conditions [179]. The code developed for operating at constant and pulsed flow scenario is shown in appendix B. The developed circuit for the control was enclosed in a water resistant plastic box to avoid any electrical shock. All the wires were connected to the appropriate components correctly before the power supply turned on for testing. Arduino mega 2560 can operate with input voltage of 7-12V and current limit of 50mA per pin therefore a power supply that gives the required current and voltage was selected.

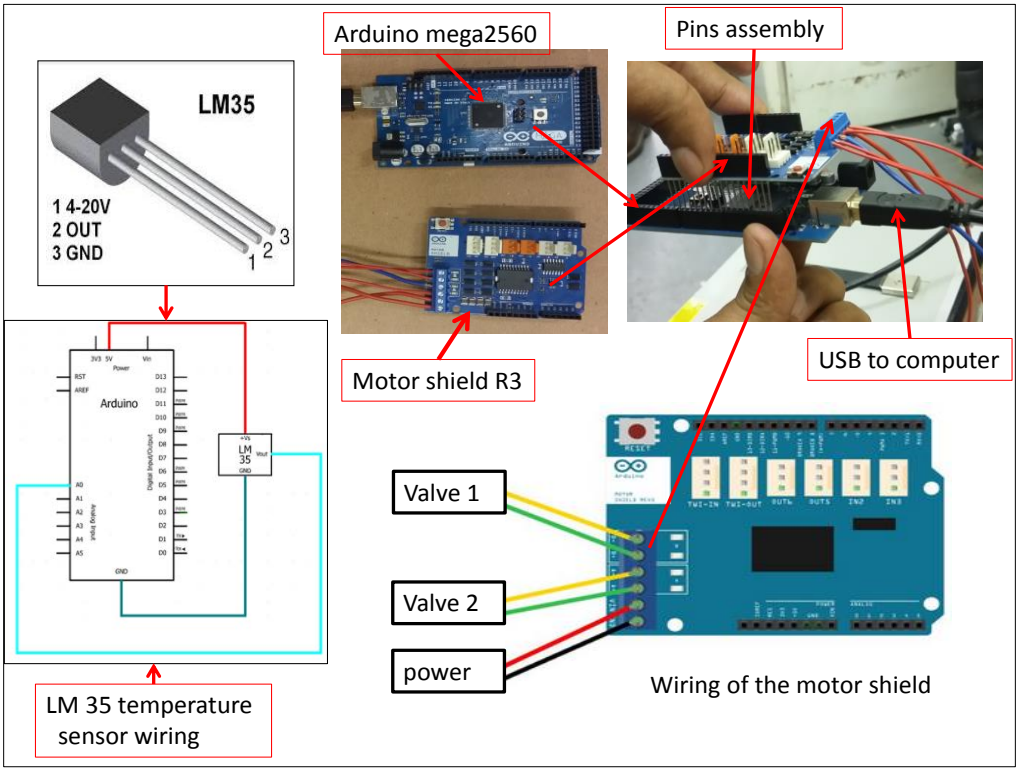

Figure 6.14 the schematic diagram of the controller components and proposed wiring system

The power supply used for this application was 24V DC power supply model SO-TECH IPS3303, 195W Bench Power Supply with RS Calibration, 3 Output 0 → 30V, 5V and 0 → 3A. The LM 35 temperature control sensor was calibrated against the Resistance Thermometer Detector Platinum100 (RTDPt100) at ambient temperature of the room. Figure 6.15 shows the RTDPt100 measured temperature compared to that of the LM35 temperature sensor with R^2 of 0.9927. Eq. (6.3) is obtained from figure 6.15 and used to calculate the curve fit parameters ($\bar{x}$) for determining uncertainty of the LM35 sensor.

$$T_{LM} = 0.3395x + 15.29 \tag{6.3}$$

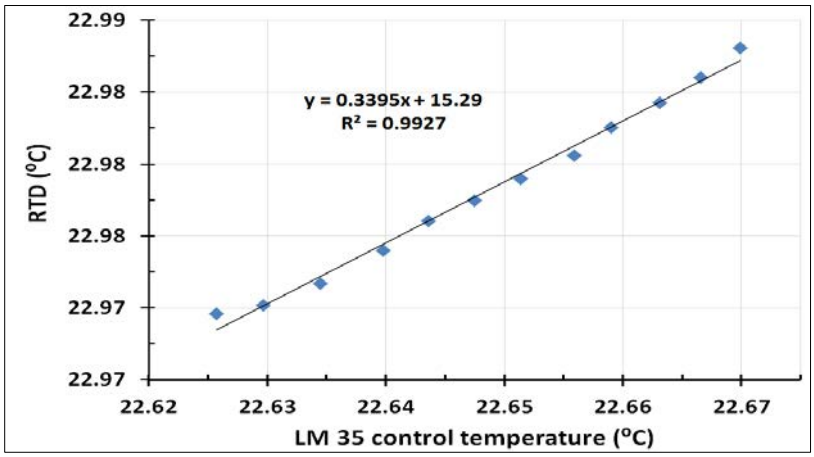

Figure 6.15 temperature relations between RTD and LM 35 temperature control sensor

6.6 Commissioning

After completing the installation of the hydronic panel radiator heating system including valves, circulation pump, heater, and the control system, a process of commissioning the system was initiated. Various tests were conducted to investigate

the range of operating conditions of the hydronic heating system. First the air inside the panel radiator was removed using the bleeding valve available on the panel radiator. Once the air was removed from the radiator; the pump was turned on to circulate the water through the entire system while the bleeding valve was left open until the water started to flow out; thus ensuring that the system is filled with water. The three way bypass valve and the two way inlet valve were inspected by operating at alternating opening and closing way; that is when the bypass valve is closed the two ways inlet valve was opened and vice versa. The inspection for the two types of valves was carried out by turning on the pump and checking if there is continuous return of water via the glass flow meter. While inspecting the valves and radiator plumbing system, the connecting pipes were checked to avoid any leakage in the complete system. Once the inspection was carried out the system was ready to conduct the test following the procedure described in the following section.

6.7 Experimental Procedure

Two sets of experiments were carried out, one set at constant hot water flow to the radiator and other set was at pulsed flow. Firstly the tests were conducted with the radiator insulated on one side using Celotex insulator defined in section 6.3 to investigate the temperature distribution on the surface of the panel radiator. For the insulated radiator 15 thermocouples were used to collect data and evaluate the uniformity of the temperature on the surface of the radiator in both constant and pulsed flow conditions. Secondly the radiator was tested without insulation at constant and pulsed flow cases (as recommended BS EN 442 radiator standards). Results for the radiator without insulation were analysed on the basis of outlet water temperature.

The testing procedure is summarised as follows:

1. The air from the panel heating radiator was fully removed using the procedure described in section 6.6 and filled with water.
2. The flow meter was set to the desired flow rate manually before starting the system and then adjusted after the system start to the required reading.
3. The power supplied to the pump was set to constant values of 23.5V and 0.80A to avoid fluctuation of the flow rate. Also the power supply to the Arduino micro controller was set to 9.8V and 0.40A to avoid damage to the micro controller.
4. The heater temperature was set to the desired temperature using the thermostat and the hot water temperature was monitored using probe thermocouple positioned at the outlet of the heating tank.
5. The doors in the room were closed to avoid high cold air flow into the room.
6. Using a computer, the DataTaker was set to log data at 10seconds interval and each of the thermocouples were identified in the computer by the number given on its label.
7. The C++ code produced in Arduino software was uploaded using USB interface to the Arduino mega 2560 micro-controller for the constant and pulsed flow operating scenarios. Using the LM35 temperature control sensor, the radiator was set to operate as follows:-

- ***Constant flow operating command:***

  $\#\text{for } T_{LM35} \subseteq 20^{o}C$

The inlet motorised valves opened continuously while the bypass valve is closed.

$\# \text{ for } T_{LM35} \supset 20^{o}C$

The inlet motorised valves is closed continuously while the bypass valve is open continuously until temperature decreases to 20°C.

- ***Pulsed flow operating command:***

$\# \text{ for } T_{LM35} \subseteq 20^{o}C$

In this case the flow is pulsed by operating the inlet motorised valve and the bypass valve as on and off in an alternating way that is when the inlet valve is on the bypass valve is off and vice versa to produce the flow pulse amplitude and frequencies as programed in the computer code.

$\# \text{ for } T_{LM35} \supset 20^{o}C$

The inlet motorised valves is closed while the bypass valve is open continuously until temperature goes down to 20°C.

8. Using the control system and developed code, set the flow rate to the desired value. For constant flow rate 0.022 kg/s and for pulsed flow rate amplitude ranging from 0.0326kg/s to 0.0412kg/s as well as frequency ranging from 0.0083Hz to 0.033Hz can be achieved using the developed test facility.

6.8 Uncertainty

The uncertainty of the measurements is estimated using standard equations described in [180-181]. In this work the uncertainty is divided into two main sections including uncertainty of thermocouple and uncertainty of flow meter. All the random errors including repeatability error are statistical and can be estimated using the mean standard deviation of 95 % confidence level.

6.8.1 Uncertainty of thermocouples and LM35 (temperature sensor)

All thermocouples used as well as the LM35 temperature control sensor were calibrated using Resistance Thermometer Detector (RTD) with high accuracy of ±0.025K and the uncertainty in their measurement are evaluated using eq. (6.4).

$$U'_{thermo} = \sqrt{(U'_{st})^2 + (U'_{curve-fit})^2} \quad (6.4)$$

Where U'_{st} uncertainty of the standard (RTD), $U'_{curve-fit}$ is the uncertainty of the curve fit and U'_{thermo} is the uncertainty of the thermocouple sensors.

$$U'_{curve-fit} = t_{n-1,95\%} S_{\bar{x}} \quad (6.5)$$

$$S_{\bar{x}} = \frac{\sigma}{\sqrt{n}} \quad (6.6)$$

$$\sigma = \sqrt{\frac{1}{n-1}\sum_{i=1}^{n}(x_i - \bar{x})^2} \quad (6.7)$$

Where; n is number of data point, n-1 is the degree of freedom, $t_{n-1,\ 95\%}$ is student contribution factor, $S_{\bar{x}}$ is standard deviation of the mean, and σ the standard deviation [180]. Table 6.1 shows the calculation of the uncertainty for one of the T-type thermocouples while Table 6.2 shows the calculation of the uncertainty for LM35 control sensor.

Table 6.1 the thermocouple measurement uncertainty calculations

Data point	RTDPt100 reading (x_i)	Measurement of thermocouple	Curve fit equation ($\bar{x}$) T = 1.0091x - 0.3963	Deviation $(x_i - \bar{x})^2$
1	22.12	22.97	22.78	0.4356
2	29.53	29.10	28.97	0.3136
3	38.01	37.89	37.84	0.0289
4	44.82	44.62	44.63	0.0361
5	53.95	53.86	53.95	0.0000
Summation of deviation points ($\sum_{i=1}^{n}(x_i - \bar{x})^2$) = 0.8142				
Degree of freedom (n-1) = 4				
Standard deviation (σ) =0.4511				
Standard deviation of mean ($S_{\bar{x}}$)=0.2018				
Uncertainty of the thermocouple ($U'_{urve-fit}$) = 0.56K				

Table 6.2 LM35 temperature control sensor measurement uncertainty calculations

Data point	RTDPt100 reading (x_i)	Measurement of LM35 temperature control sensor	Curve fit equation ($\bar{x}$) T = 0.3395x + 15.29	Deviation $(x_i - \bar{x})^2$
1	22.50	22.62	22.96	0.014
2	22.61	22.64	22.97	0.1296
3	22.75	22.66	22.98	0.0529
4	22.76	22.7	22.99	0.0529
5	22.80	22.75	23.02	0.0484
Summation of deviation points ($\sum_{i=1}^{n}(x_i - \bar{x})^2$) = 0.2978				
Degree of freedom (n-1) = 4				
Standard deviation (σ) =0.2728				
Standard deviation of mean ($S_{\bar{x}}$)=0.122				
Uncertainty of the LM35 ($U'_{urve-fit}$) = 0.34K				

The uncertainty of the thermocouple measurement is ±0.56K and the uncertainty of LM35 temperature control is as low as ±0.34K. Figure 6.16 shows the calibration of

the RTDPt100 against ice temperature of 0°C. As the uncertainty of the RTDPt100 sensor (U'_{st}) is small (±0.03K) compared to the uncertainty of measuring device ($U'_{urve-fit}$); the (U'_{st}) value was neglected. Thus uncertainty of the measuring device ($U'_{urve-fit}$), was used to calculate the overall thermocouples uncertainty as well as the uncertainty of the LM35 sensors.

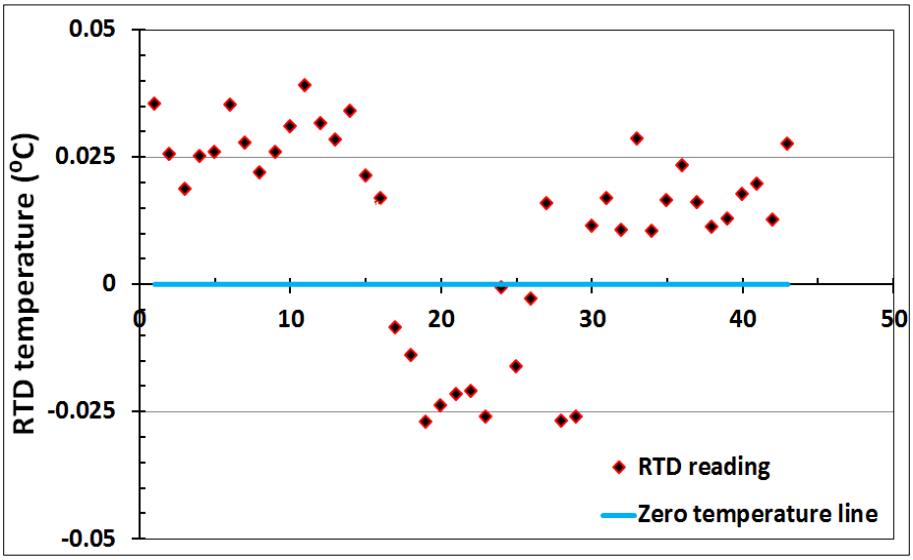

Figure 6.16 calibration of the RTD against ice temperature at 0°C

6.8.2 Uncertainty of the flow meter

In section 6.4.2, the Platon flow meter used in the test facility was calibrated using graduated cylinder and stop watch. The flow meter readings were then plotted versus the calculated flow rate (V_w) using eq. (6.8). The uncertainty of the Platon flow meter (U'_{fm}) is then calculated based on the uncertainty of the curve fitting ($U'_{cuve-fit}$) and uncertainty of the calibration method (V_{vc}) as shown in eq. (6.9).

$$V_w = \frac{\Delta V_f}{\Delta t} \tag{6.8}$$

$$U'_{fm} = \sqrt{(U'_{vc})^2 + (U'_{curve-fit})^2} \quad (6.9)$$

U'_{vc} the uncertainty of the cylinder graduated volume (calibrating method) given as eq. (6.10).

$$U'_{VC} = \sqrt{\left(\frac{\partial V_w}{\partial V_f}\Delta V\right)^2 + \left(\frac{\partial V_w}{\partial t}\Delta t\right)^2} \quad (6.10)$$

V_w is the flow rate of water calculated using eq. (6.8), in (ml/min), V_f is the total volume of the collecting cylinder in (ml), ΔV is the error in measuring the volume which is equal to the step in the graduating scale of the measuring cylinder, Δt is the minimum time that can be counted when cylinder is filling with water and t is time in seconds. The uncertainty of the calibration method is estimated using eq. (6.11).

$$U'_{VC} = \sqrt{\left(\frac{1}{t}\Delta V\right)^2 + \left(\frac{V_f}{t^2}\Delta t\right)^2} \quad (6.11)$$

Using ΔV of 10ml, Δt of 1/60, the calculated uncertainty U_{vc} is ±0.32ml/s. The tabulated calculation of the uncertainty for the flow rate measurement is shown in table 6.3. As shown in table 6.3 the uncertainty of the flow meter is ±0.77ml/s or ±3.6% of full scale.

Table 6.3 the flow rate measurement uncertainty calculations

Data point	Cylinder	Platon flow	Curve fit equation ($\bar{x}$)	Deviation

	volume (x_i)	meter	$V_w = 0.9992x - 0.0048$	$(x_i - \bar{x})^2$
1	3.00	3.03	3.02	0.0004
2	2.67	2.63	2.62	0.0025
3	2.33	2.33	2.32	0.0001
4	2.00	1.99	1.98	0.0001
5	1.67	1.64	1.63	0.0016
Summation of deviation points ($\sum_{i=1}^{n}(x_i - \bar{x})^2$) = 0.0047				
Degree of freedom (n-1) = 4				
Standard deviation (σ) =0343				
Standard deviation of mean ($S_{\bar{x}}$)=0.0153				
Uncertainty curve fit ($UN_{urve-fit}$) = 0.71				
Uncertainty of graduated cylinder tank (U_{vc}) = 0.32				
Uncertainty of the flow rate ($UN_{fm} = \sqrt{(UN_{vc})^2 + (UN_{urve-fit})^2}$) = 0.77ml/s				

6.9 Summary

In this chapter the experimental facility developed to investigate the effect of pulsating flow on the performance of hydronic heating panel radiator is fully described. The facility consists of hot water circulating system comprising of electrically heated water tank, circulating pump and control system. Arduino control system comprising of Arduino mega 2560 micro controller, Arduino motor shield R3, mother board, LM35 temperature control sensor, connecting wires was developed and a computer code was made to enable constant and pulsed flow operating conditions.

The constant flow rate at 0.022 kg/s and pulsed flow rate with amplitude ranging from 0.0326kg/s to 0.0412kg/s as well as frequency ranging from 0.0083Hz to 0.033Hz can be achieved using the developed test facility. The heating facility was

instrumented with thermocouples to measure hot water temperature at various points in the hot water circuit. Also the surface of the radiator and the heated space were fitted with thermocouples at various points to assess the radiator heating output and the room thermal comfort parameters. The heating facility was commissioned and the experimental testing procedure was described.

CHAPTER 7

EXPERIMMENTAL RESULTS AND VALIDATION

7.1 Introduction

In chapters 3 analytical model of the hydronic central heating system was developed using Matlab/Simulink. In chapters 4 and 5 the hydronic heating system was numerically simulated using finite element modelling in COMSOL Multi-physics software. In chapter 6 the experimental facility and the experimental methodology were described. This chapter describes the experimental results and the validation of the predicted numerical modelling results.

The experimental testing of the hydronic radiator was performed according to BS EN 442 radiator test standards [166, 178 and 182]. The heated room was configured to have similar physics and boundary conditions to the modelled room with natural ventilation via the door openings. The natural ventilation was modelled using the open boundary condition due to the pressure difference.

The experimental results of the hydronic radiator were analysed using local surface temperature distribution (non-insulated and insulated radiator) as well as the hot water inlet/outlet temperature (non-insulated radiator). Also experimental results of the heated room model were analysed using local indoor air temperature variation.

7.2 Experimental results of radiator

The hydronic panel radiator used for experimental testing is type 11 radiator of 1000mm length and 600mm height. Figure 7.1 shows the thermocouple layout of the radiator where the surface thermocouples labelled as T1 to T15 were used to measure the surface temperature of the radiator for CFD validation. The probe thermocouples labelled as T16 to T17 were used to measure the hot water inlet and outlet temperature of the radiator (in accordance to the BS EN 442 radiator standard tests).

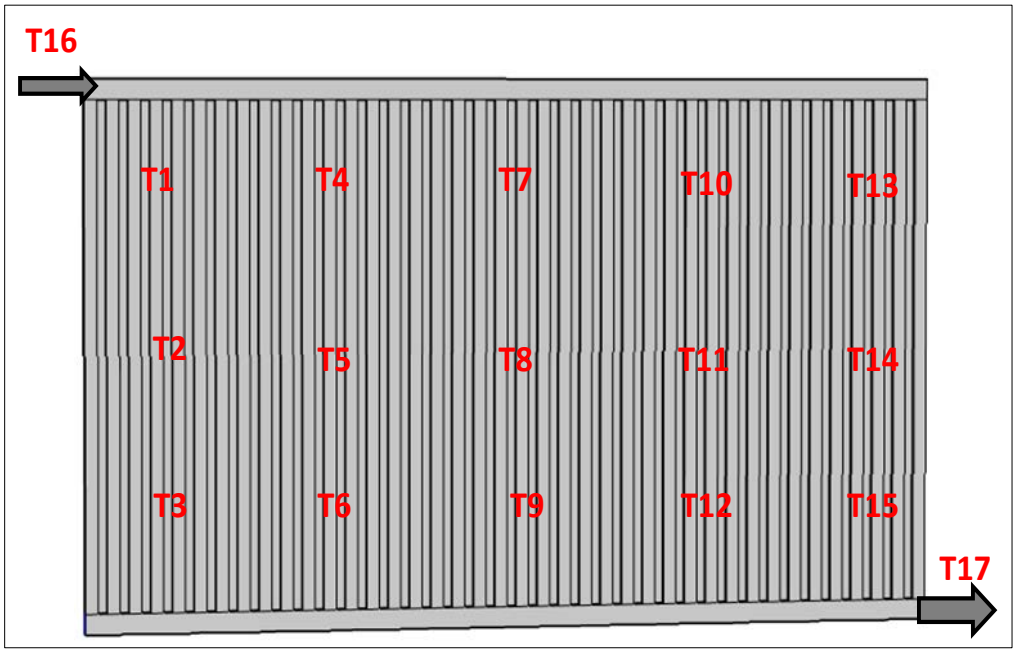

Figure 7. 1 radiator thermocouple layouts

As shown in figure 7.1 the T1 to T15 are surface thermocouples attached to the radiator surface using aluminium foil tape. T16 and T17 are probe thermocouples inserted inside the pipe and placed in the desired potion using the thermocouple compression fitting assembly as shown in figure 6.6, chapter 6.

7.3 Experimental results of non-insulated radiator at constant flow

The hydronic panel radiator operating at constant flow of 0.022kg/s and inlet temperature of 75^{o}C was tested experimentally according to the radiator standard testing. Figure 7.2 shows the experimental results of local surface temperature of the radiator at the points shown in figure 7.1 for non-insulated radiator.

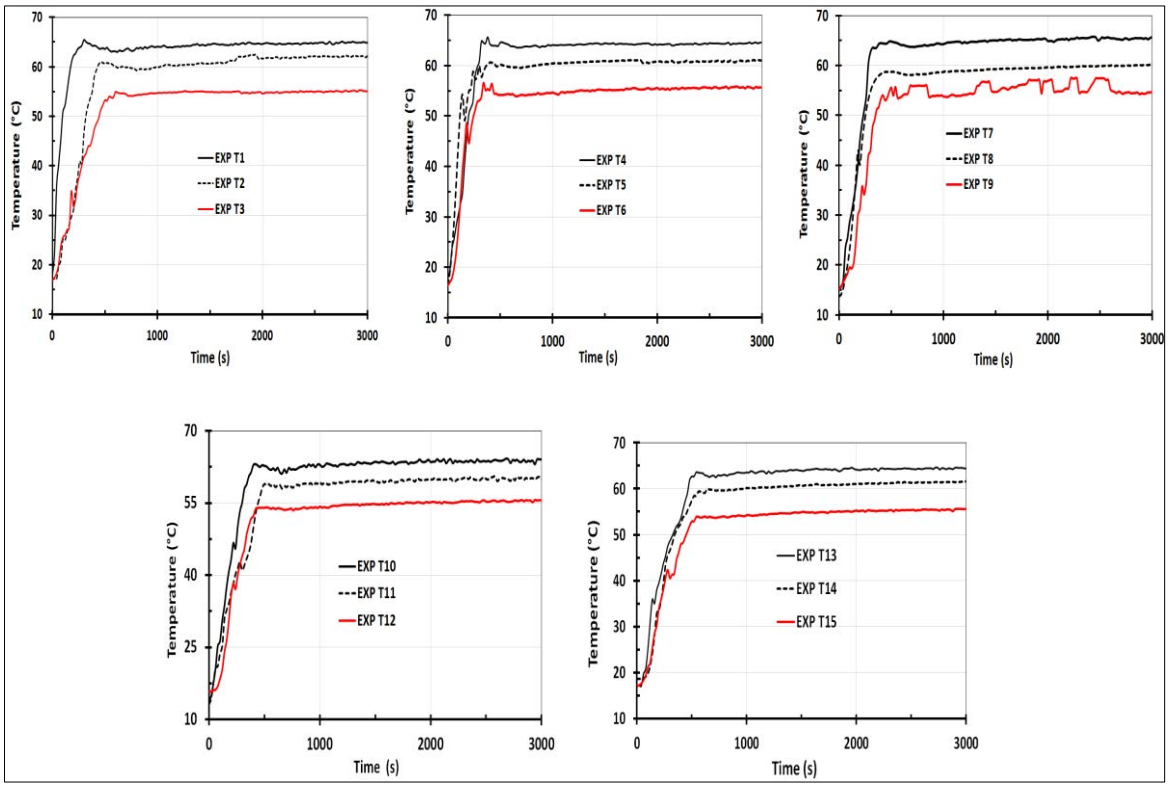

Figure 7.2 local surface temperature distribution of surface radiator measured experimentally (EXP) at constant flow

As shown in figure 7.2 the local temperature distributions of the radiator is higher at the top of the panel radiator and decreases towards the bottom. As the light hot water rise up due to buoyancy, the heavy colder water flow to the lower part of the radiator. Figure 7.3 shows the average local surface temperature of the experimental results

calculated using eq. (7.1). Also figure 7.3 shows the effect of thermocouple uncertainty measurement of ±0.56K described in chapter 6 using the error bars.

$$T_{average} = \frac{\sum_{1}^{n} T_n}{n} \tag{7.1}$$

Where; T is temperature, n is the number of thermocouples used (15 thermocouples).

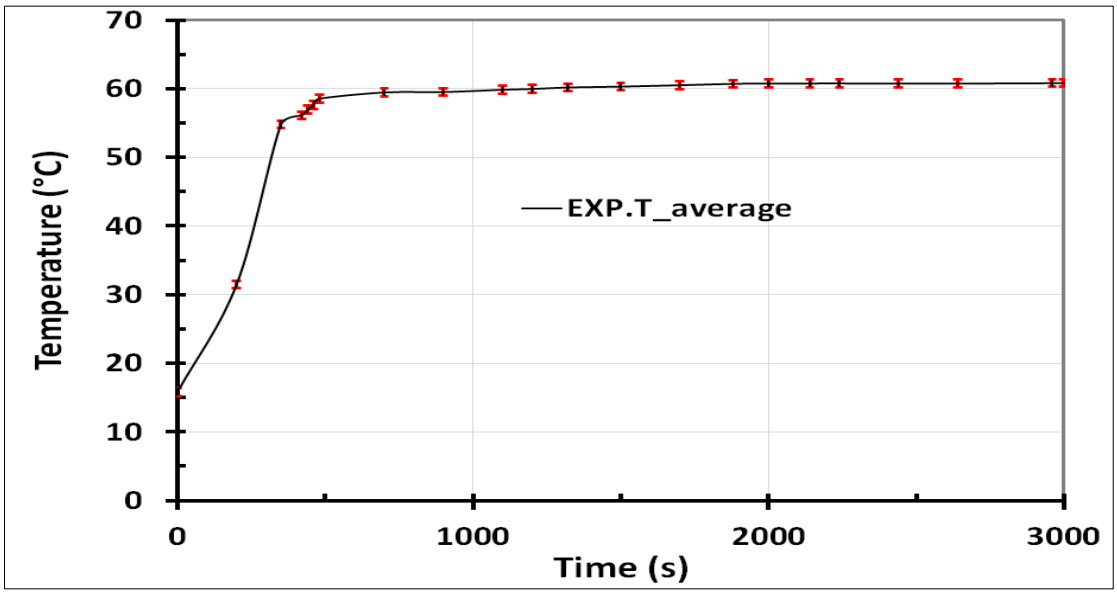

Figure 7.3 the average surface temperature of the radiator operating at constant flow measured experimental (EXP) and the error bars due to the measurement uncertainty

As shown in figure 7.3 the average surface temperature of the radiator operating at constant flow is about 60°C. It is also clear that in figure 7.3 the effect of the thermocouples measurement uncertainty is very small which does not have visible effect on the experimental results of the radiator surface temperature. This average

surface temperature was used to select the best flow required to operate the radiator at pulsed flow in the following sections.

Figure 7.4 shows the measured inlet and outlet temperatures of the radiator. Also figure 7.4 shows the effect of thermocouple uncertainty measurement of ±0.56K determined in chapter 6 on the hot water outlet temperature of the radiator.

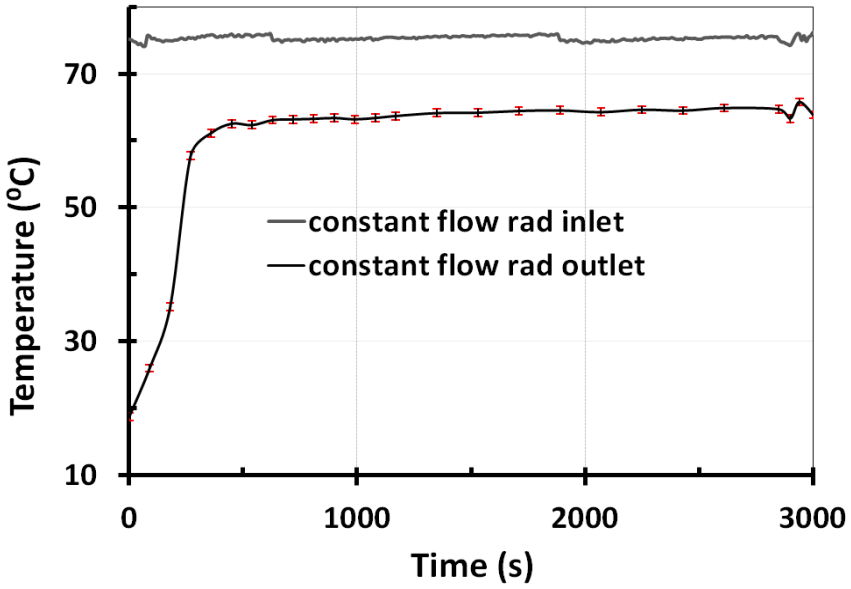

Figure 7.4 inlet and outlet temperature of the hot water measured experimentally at constant flow and the error bars due to the measurement uncertainty

As shown in figure 7.4, the measured inlet and outlet hot water temperatures are 75°C and 64.2°C respectively. In this case the hot water outlet temperature was found to be slightly lower than the recommended value of 65°C by EN BS 442 radiator test standards with deviation of 1.3%. It is also clear that the effect of the thermocouples uncertainty is very small highlighting the accuracy of the experimental results of the radiator hot water outlet temperature.

7.3.1 Experiential results of non-insulated radiator at constant flow rate using various inlet temperature

The panel radiator (type 11) with attached fins shown in figure 7.1 was tested experimentally at various inlet temperatures ranging from 60^{o}C to 75 ^{o}C at constant flow rate of 0.022kg/s. Figure 7.5 shows the average surface temperature of the panel radiator measured experimentally.

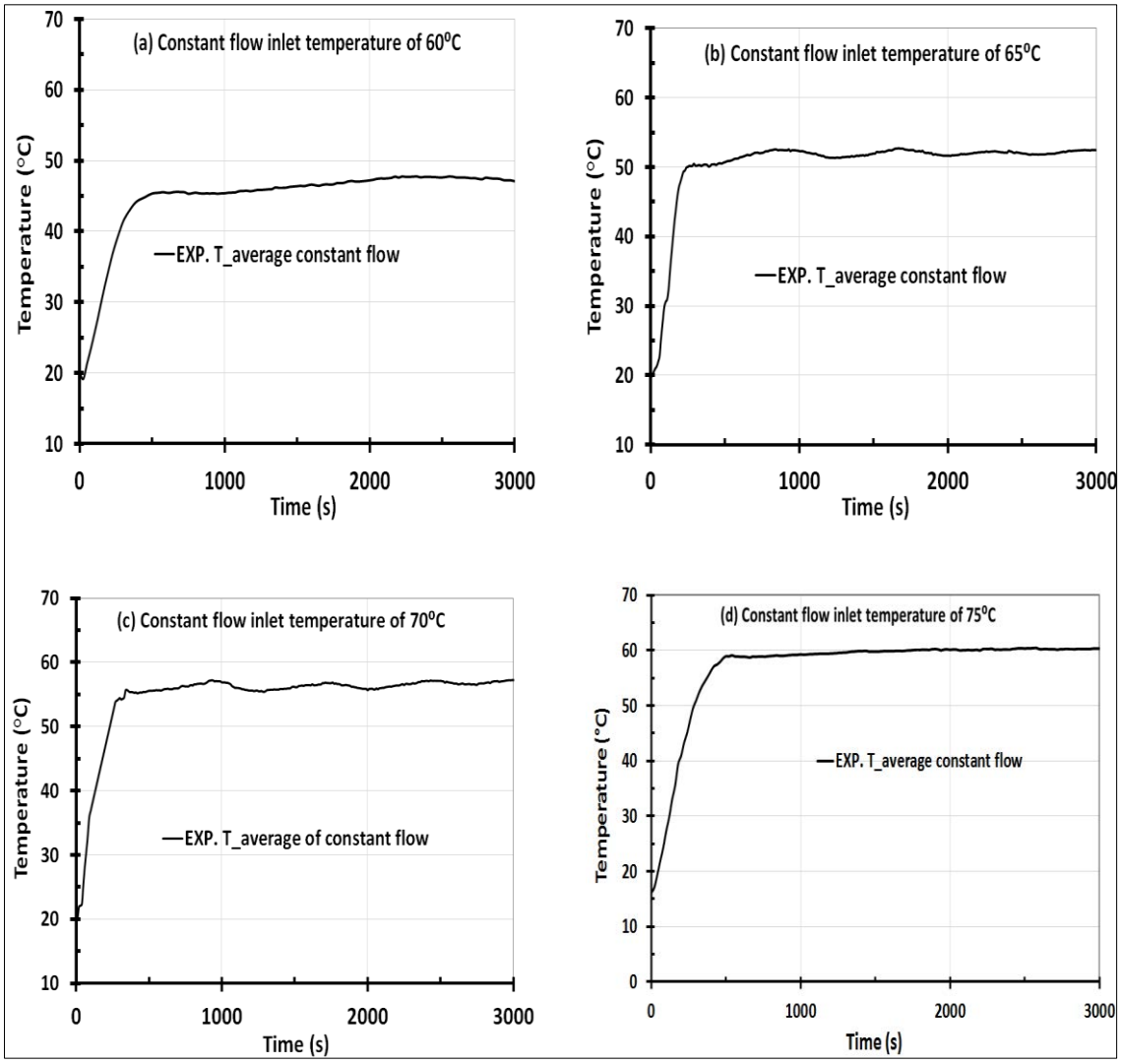

Figure 7.5 experimental results of average surface temperature for radiator at constant flow conditions

As shown in figure 7.5, the experimental results of average surface temperature for the panel radiator operating at various inlet temperatures decreases as the inlet temperature decreases. The results of the constant flow radiator at various inlet temperatures will be compared to the experimental results of radiator operating at pulsed flow using various inlet temperatures to investigate the variation of energy saving due to the pulsed flow at various hot water inlet temperatures.

7.4 Experimental results of non-insulated radiator at pulsed flow

In chapters 3 and 4 it was concluded that pulsating the hot water flow to the hydronic radiator results in significant reduction in energy consumption without compromising user comfort using analytical and numerical modelling respectively. In this section the experimental results of pulsating the flow to a type11 hydronic radiator will be described. Several experiments were carried out to investigate the effect of pulsating flow at various amplitudes, various frequency and various hot water inlet temperatures.

7.4.1 Experimental results of non-insulated radiator at various flow amplitudes

The effect of flow amplitude was investigated experimentally using input values shown in Table 7.1 and results were analysed using the average surface temperature of the panel radiator.

Figure 7.6 shows the measured average surface temperature of the panel radiator at various pulsed flow amplitudes corresponding to the input values shown in table 7.1.

Table 7.1 pulsed flow amplitudes at constant frequency of 0.209 rad/s

Amplitudes (kg/s)	Average mass (kg/s)	Reduction in mass flow rate of PF compared to CF (%)	Flow frequencies (Hz)	Inlet temp (^{o}C)
0.0412	0.0163	5	0.033	75
0.0384	0.0174	10	0.033	75
0.0368	0.0184	15	0.033	75
0.0348	0.0192	20	0.033	75
0.0326	0.0206	25	0.033	75

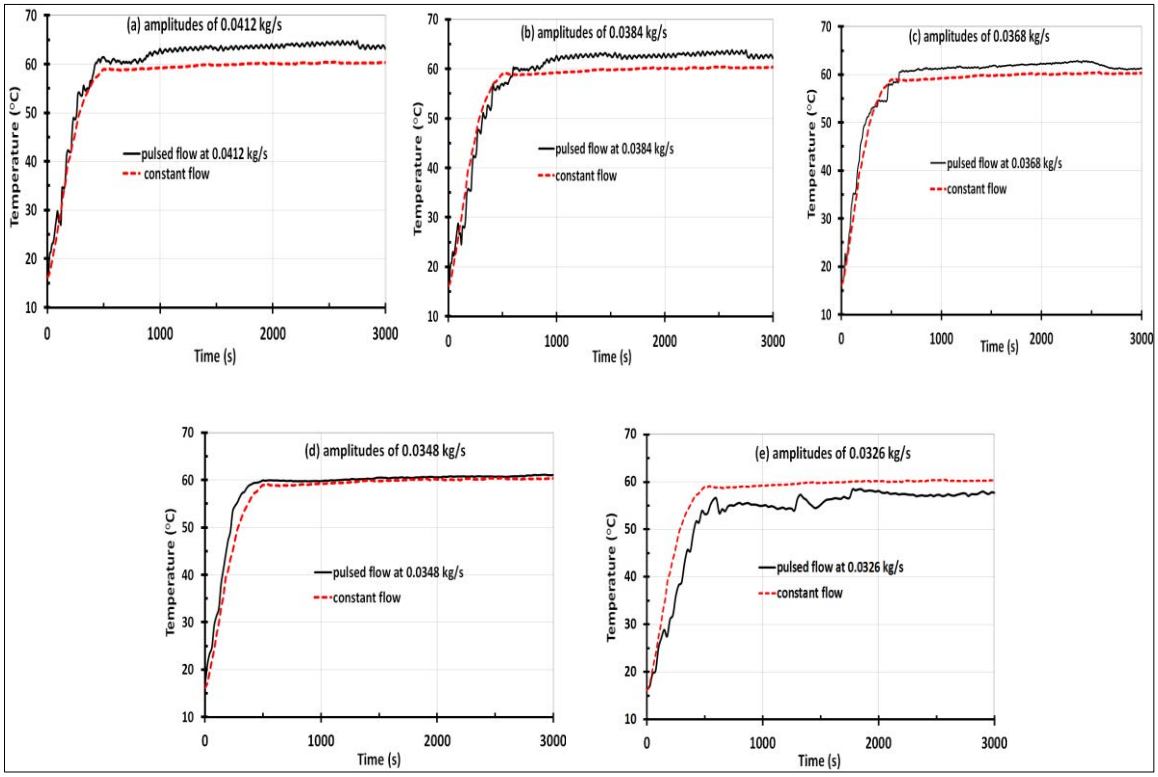

Figure 7.6 average surface temperature of radiator at various flow amplitudes of the pulsed flow compared to the constant flow

It can be seen that the average surface temperature of the radiator operating at various flow amplitudes of the pulsed flow decreases as the flow amplitude decreases. As

shown in figure 7.6 the average surface temperature of the radiator decreased from 63.5^{o}C to 58^{o}C as the flow amplitude decreased from 0.0412 kg/s to 0.0326 kg/s respectively. Based on the results of the pulsed flow at various flow amplitudes, the average surface temperature that matches with the surface temperature of radiator operating at constant flow will be selected as the best flow amplitudes for further testing at various flow frequencies. It is clear from figure 7.6 (d) the average surface temperature of the radiator tested at pulsed flow amplitude of 0.0348 kg/s matches well that of the radiator tested at constant flow. Thus the best pulsed flow amplitude of 0.0348 kg/s that matches with constant flow (conventional) is selected for further testing at various flow frequencies.

7.4.2 Experimental results of non-insulated radiator at various flow frequencies

The effect of flow frequencies is tested experimentally using values listed in Table 7.2 as input parameters. The flow frequency that gives better temperature distribution with lower fluctuation and matches with the results of constant flow radiator was selected as the best flow frequency of the pulsed flow. Figure 7.7 shows the measured average surface temperature of radiator operating at various pulsed flow frequencies.

It is clear from figure 7.7 that the average surface temperature of the radiator is 60^{o}C. However the temperature fluctuation increases as the frequency decreases which may affect the indoor comfort temperature of occupants, thus the radiator with low fluctuation was selected. The fluctuation of the average surface temperature of the radiator at pulsed flow varies from 60^{o}C±0.2^{o}C at 0.033Hz to 60^{o}C±2^{o}C at 0.0083Hz.

Therefore the best flow frequency performance that matched the average surface temperature of the radiator operating at constant flow scenario (figure 7.3) with low temperature fluctuation was 0.033Hz. Figures 7.6 and 7.7 of 0.0348kg/s and 0.033Hz respectively produce average radiator surface temperature similar to that of constant flow.

Table 7.2 pulsed flow frequency at constant amplitudes of 0.0348 m/s

Amplitudes (kg/s)	Average mass (kg/s)	Mass of pulsed flow compared to constant flow (%)	Flow frequencies (Hz)	Inlet temp (^{o}C)
0.0348	0.0174	20	0.033	75
0.0348	0.0174	20	0.016	75
0.0348	0.0174	20	0.011	75
0.0348	0.0174	20	0.0083	75

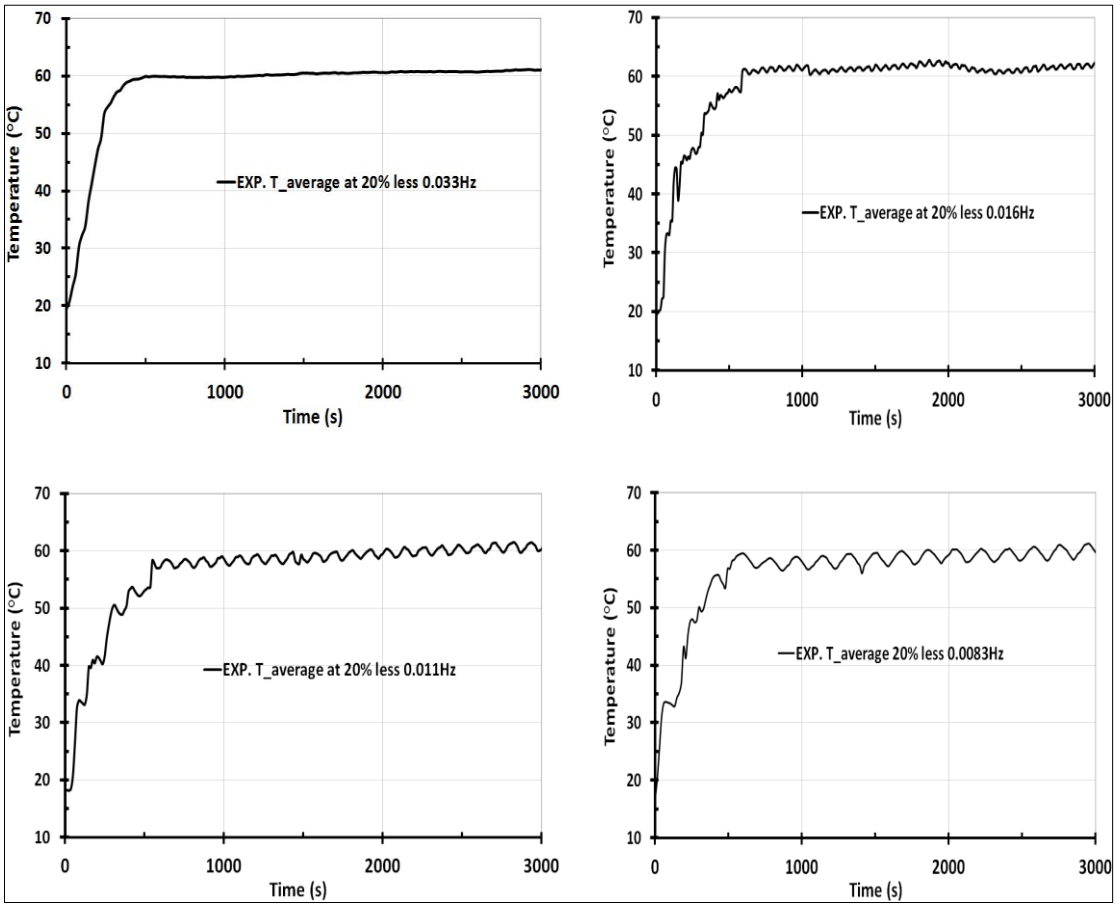

Figure 7.7 average surface temperature of radiator at various pulsed flow frequencies

Hence the radiator operating at the selected flow amplitude and frequency was analysed based on the radiator surface temperature distribution and hot water inlet and outlet temperatures in the following section.

7.4.3 Experimental results of non-insulated radiator at the best selected pulsed flow

The best flow amplitude and frequency of the pulsed flow was tested experimentally on the basis of the EN 442 radiator standard test targeting the temperature difference between inlet and outlet of 10^{o}K. The pulsed flow with frequency of 0.033Hz and amplitude of 0.0348kg/s was applied at inlet temperature of 75^{o}C. Figure 7.8 shows the local surface temperature of the radiator corresponding to the surface thermocouples labelled T1 to T15 as shown in figure 7.1.

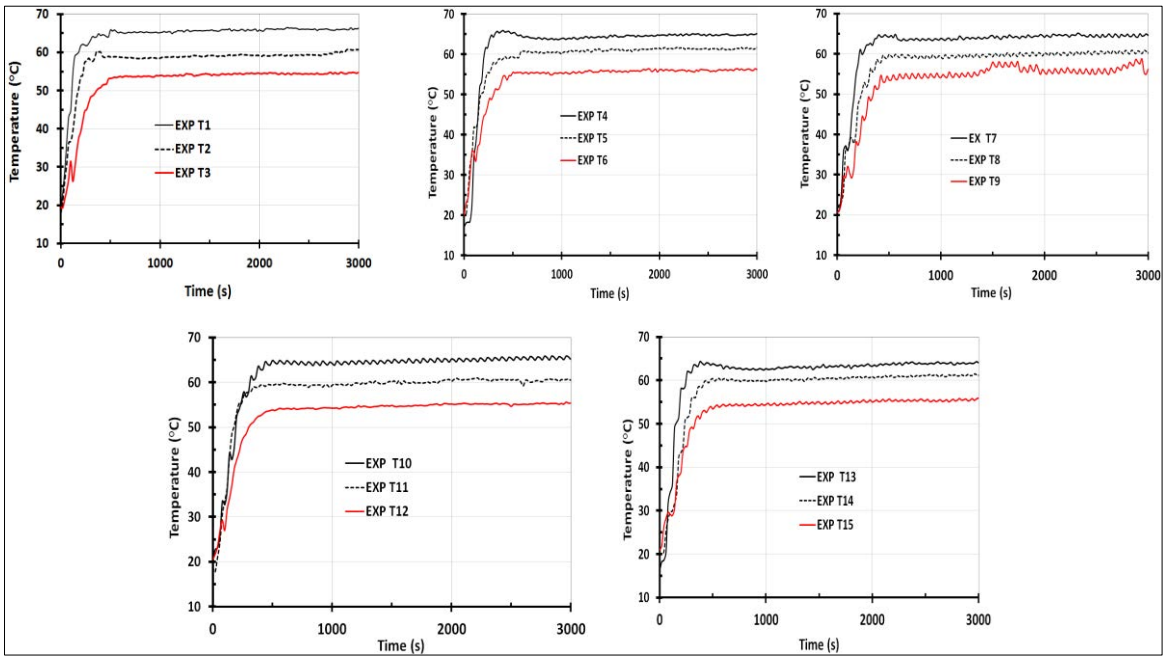

Figure 7.8 local surface temperature of non-insulated radiator measured experimentally (EXP) operating at the best selected pulsed flow

It is clear from figure 7.8 that the surface temperature of the radiator decreases towards the bottom of the vertical channels of the hydronic radiator in a similar manner as described in section 7.2 for the case of constant flow testing. Figure 7.9 shows the average radiator surface temperature of the selected pulsed flow compared to the average radiator surface temperature of the constant flow (figure 7.3). It is clearly shown in figure 7.9 that the average radiator surface temperature of the selected best pulsed flow with amplitude of .0348 kg/s and frequency 0.033Hz is about 60 ^{o}C; also it is in good agreement with the average radiator surface temperature at constant flow.

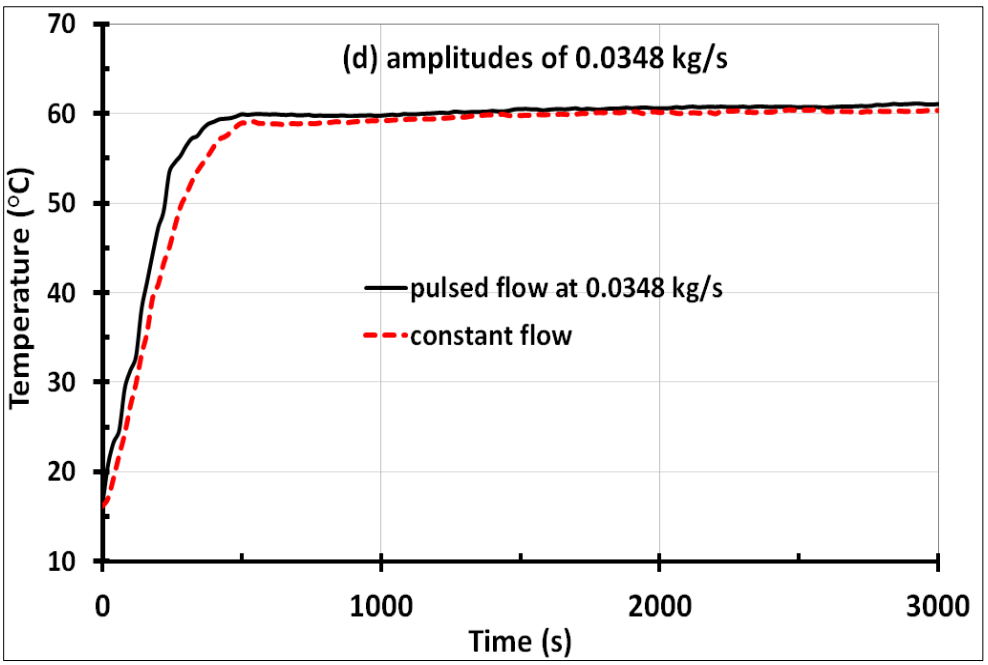

Figure 7.9 average surface temperature of the best selected pulsed flow radiator compared to constant flow

Figure 7.10 shows the inlet/outlet hot water temperature of the hydronic radiator operating at the best pulsed flow amplitude and frequency compared to the constant flow. The inlet/outlet hot water to the radiator is experimentally measured using the

probe thermocouples shown in figure 7.1 labelled by T16 (inlet) and T17 (outlet). It can be seen that with average inlet temperature of 75°C, the average outlet temperature is 65.7°C. This is in good agreement with the BS EN442 radiator test standards which recommend temperature difference 10°K between the hot water inlet and outlet of the radiator. Also the trends of pulsed flow inlet and outlet temperature matched well the trends of fitted with inlet and outlet temperature of the radiator operating at constant flow as it is clearly shown in figure 7.10. The selected pulsed flow radiator was tested experimentally with amplitude of 0.0348kg/s and frequency of 0.033Hz using various inlet temperatures in the next section.

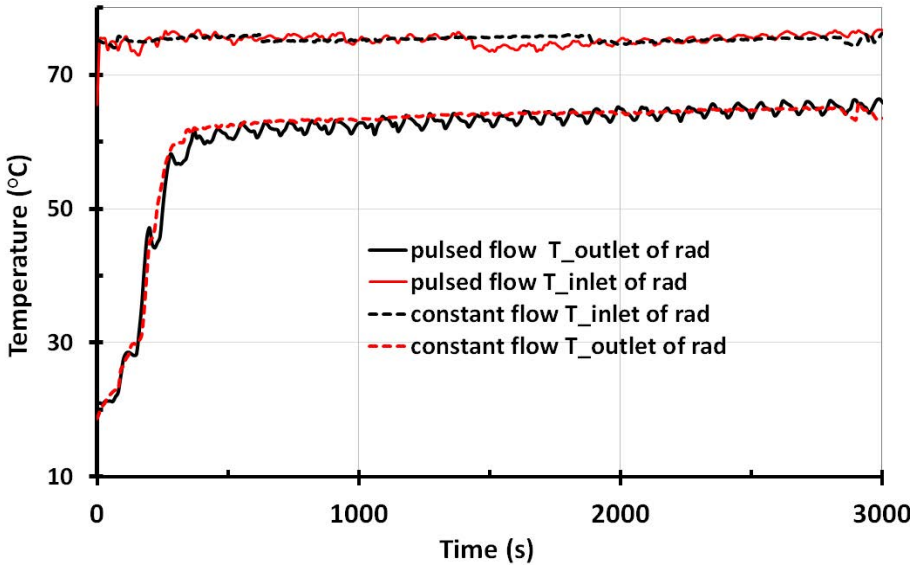

Figure 7.10 inlet and outlet temperature of the hot water for the best pulsed compared to constant flow

7.4.4 Experimental results of non-insulated radiator with pulsed flow at various inlet temperatures

The best pulsed flow was experimentally tested at various inlet temperatures. Table 7.3 shows the input parameters used when the radiator was tested using pulsed flow at

various inlet temperatures. Figure 7.11 shows the experimental results of average surface temperature for the pulsed flow operating radiator at various hot water inlet temperatures.

Table 7.3 various inlet temperatures at constant flow frequency and amplitudes

Inlet temp (^{o}C)	Amplitudes (kg/s)	Average mass flow rate (kg/s)	Mass of pulsed flow less compared to constant flow (%)	Flow frequencies (Hz)
60	0.0348	0.0174	20	0.033
65	0.0348	0.0174	20	0.033
70	0.0348	0.0174	20	0.033
75	0.0348	0.0174	20	0.033

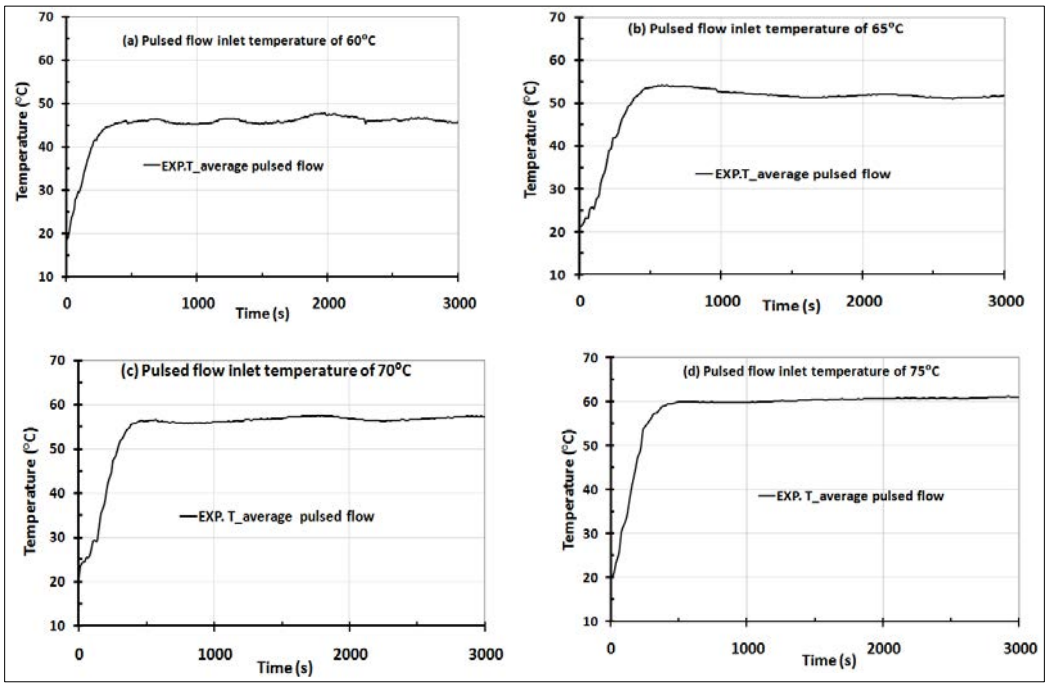

Figure 7.11 average surface temperature of the radiator at pulsed flow measured experimentally at the specified inlet temperature

The reason for testing the radiator at various inlet temperatures is to investigate the effect of flow pulsation at low inlet temperature on energy saving compared to constant flow radiator. If the potential heat transfer enhancement of flow pulsation for

radiator supplied with low inlet temperature is substantial, then flow pulsation can be used for hydronic heating system utilizing heat pumps that supply hot water at lower temperature than those obtained using boilers. It is clear from figure 7.11 that the average surface temperature of the radiator decreases as the inlet hot water temperature decreases.

7.5 Experimental results of energy saving due to the pulsed flow

In this section the energy savings due to the pulsed flow compared to the constant flow (conventional flow) is determined using specific heat output of the hydronic panel radiator central heating system. Figure 7.12 shows the measured specific heat output of the radiator at the best pulsed flow compared to that of constant flow using various hot water inlet temperatures ranging for 60^{o}C to 75^{o}C.

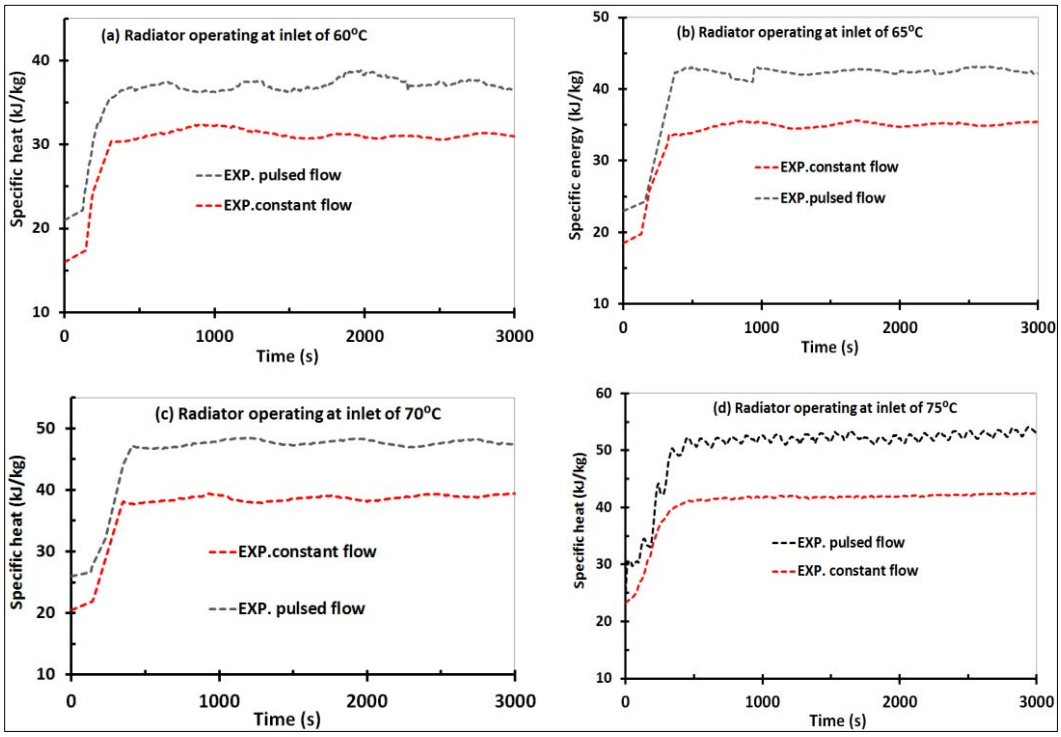

Figure 7.12 the experimental results of specific heat output at pulsed and constant flow type11 radiator

The experimental specific heat output of the radiator was calculated using eq. (3.45). The higher specific heat output achieved with the pulsed flow compared to the constant flow highlights the potential of energy saving that can be achieved. This energy saving is attributed to the heat transfer enhancement of the radiator due to the pulsed flow, thus lower average mass flow rate can be used leading to reduction in energy consumption. Table 7.4 shows the energy saving achieved by pulsed flow at various hot water inlet temperature calculated using eq. (4.10).

Table 7.4 the energy saved at pulsed flow when radiator operating at varying inlet temperature

Inlet temperature	Experimental % energy saving
60^{o}C	22.1
65^{o}C	22.9
70^{o}C	22.8
75^{o}C	23.2

It is clear from table 7.4 that significant energy saving (22.1% to 23.2%) can be achieved using the pulsed flow compared to the constant flow at all the inlet hot water temperatures used in the testing (60^{o}C to 75^{o}C). The results showed that pulsed flow can be used for a wide range of heating applications to significantly reduce energy consumption and CO_2 emission.

7.6 Experimental results of the heated room

The test room used in this research represents a single room heated using hydronic panel radiator central heating system. The room was ventilated naturally; the fresh air is flowing into the room via the openings around the external walls. The U-value of

the external wall, internal walls, ceiling, floor and door of the room are 0.28W/(m^2K), 0.186W/(m^2K), 0.1W/(m^2K), 0.1W/(m^2K) and 0.5W/(m^2K) respectively. The U value of each component is calculated from the materials properties of the tested room using equations (3.16) to (3.18) presented in chapter 3. Figure 7.13 shows the experimental tested room dimensions and components.

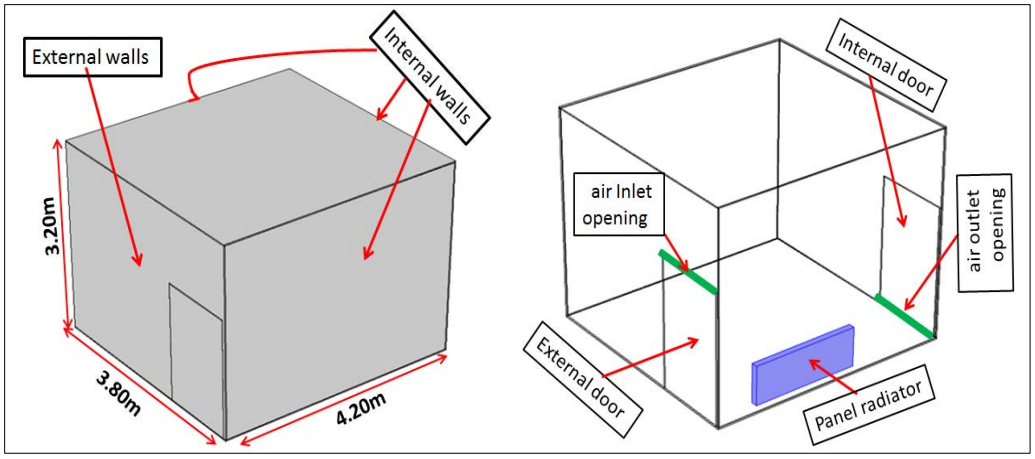

Figure 7.13 the tested room dimensions and parameters

The numerically predicted results of the heated room will be validated against experimental results on the basis of indoor comfort temperature. The indoor comfort temperature is estimated using adaptive indoor comfort temperature for naturally ventilated heated room expressed in eq. (7.2) according to ASHRAE standards 55 with 90% acceptability which depends on the outdoor temperature [183].

$$T_{comfort} = (0.31.T_{amb} + 17.8) \pm 2.5 \qquad (7.2)$$

Based on eq. (7.2) and using an average outdoor UK winter temperature of 5°C, the comfort temperature can be taken as 20°C. Thus $T_{comfort}$ is 20°C± 2.5°C was considered as target temperature for the tested room both in the numerical and

experimental investigations. In the experimental tests thermocouple probes are positioned at 150mm (ankle level) and 1500mm (neck level) high from the floor level in the heated room envelope. The proposed layout of the probes on the basis of vertical positions from the floor level was selected in consideration of occupants' sensitive parts of the body as described in ASHRAE standards. Figure 7.14 shows thermocouple probe layout along the indoor envelope of the tested room; the probes were positioned parallel (ZY-plane) and perpendicular (XZ-plane) to the heating panel radiator. The LM35 temperature control is positioned in the centre of the room 1.1m above the floor level and it was set at temperature of 20^{o}C as described in chapter 6. T1 to T6 in figure 7.14 represent the positions of the thermocouples in the heated room envelope.

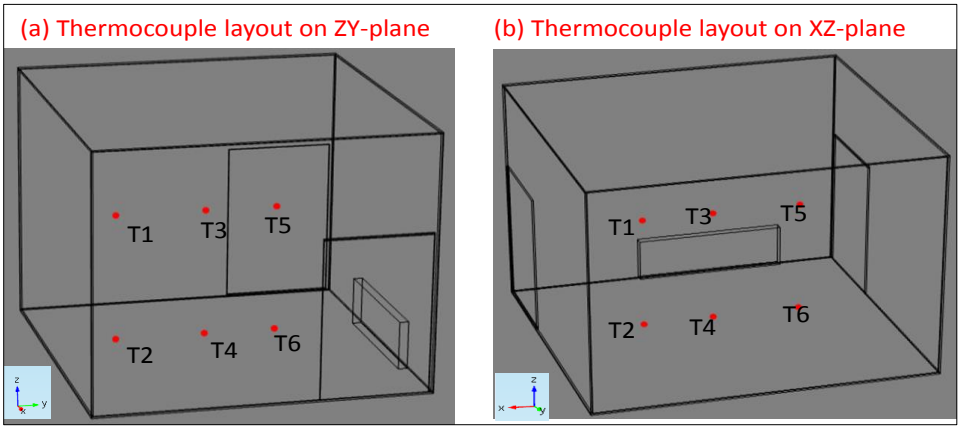

Figure 7.14 the probe thermocouple layout of tested room for both pulsed and constant flow cases

7.6.1 Indoor temperature at constant flow radiator

Figure 7.15(a) and Figure 7.15(b) show the measured indoor temperature of the thermocouple probes shown in figure 7.14 on the YZ-plane and XZ-plane at constant hot water flow of 0.022kg/s and 75^{o}C inlet temperature to the radiator.

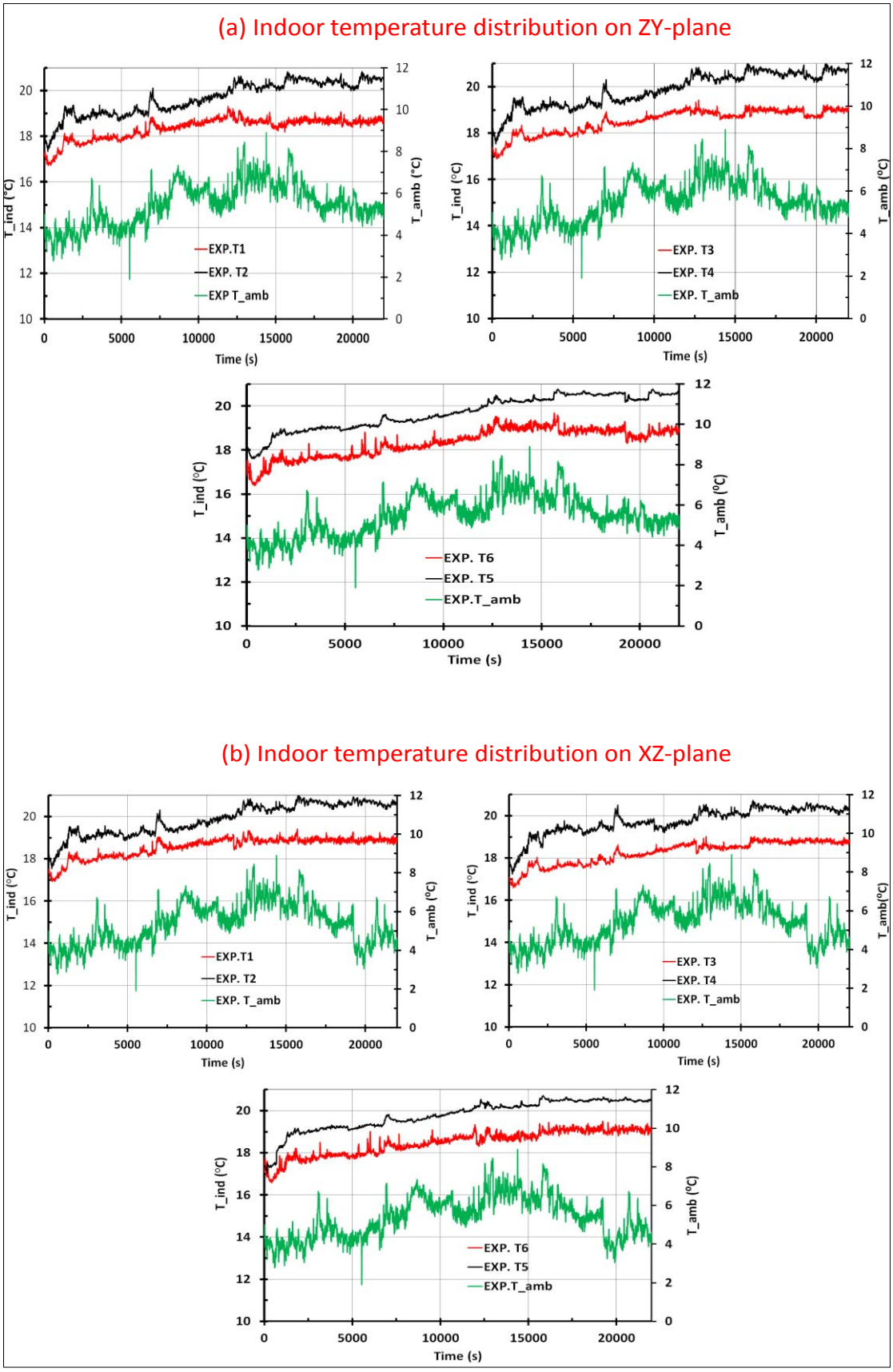

Figure 7.15 the measured indoor and outdoor temperature of the heated room at constant flow

As shown in figure 7.15 the indoor temperature distributions are within the recommended limit of the indoor comfort international legislation documented in ASHRAE standards 55 which can be estimated using eq. (7.2). The minimum and maximum temperatures of room in the YZ-plane are 18.3^{o}C and 20.9^{o}C respectively. The minimum and maximum temperature of the room in the XZ-plane is 18.2^{o}C and 20.7^{o}C respectively. It is also clear that from figure 7.15 that when the test was conducted, the average measured outdoor temperature was about 5^{o}C.

7.6.2 Indoor temperature at pulsed flow radiator

Figure 7.16(a) and Figure 7.16(b) show the measured indoor temperature using the thermocouple probes described in figure 7.14 for the radiator operating at the best pulsed flow condition with frequency and amplitude of 0.033Hz and 0.0348kg/s respectively and hot water inlet temperature of 75^{o}C.

As shown in figure 7.16(a) the minimum and maximum temperature of the heated room in the YZ-plane is 18.03^{o}C and 20.6^{o}C respectively. Also it is clearly shown from the trends of figure 7.16(b) that the minimum and maximum temperatures of the heated room in the XZ-plane are 18.1^{o}C and 20.5^{o}C respectively. The indoor temperature distribution of the room when the radiator is operating at pulsed flow agreed well with the international standards limit of 20± 2.5^{o}C as calculated using eq. (7.2). It is clear from figure 7.16 that the average measured temperature of the ambient was about 5^{o}C when the test was carried out.

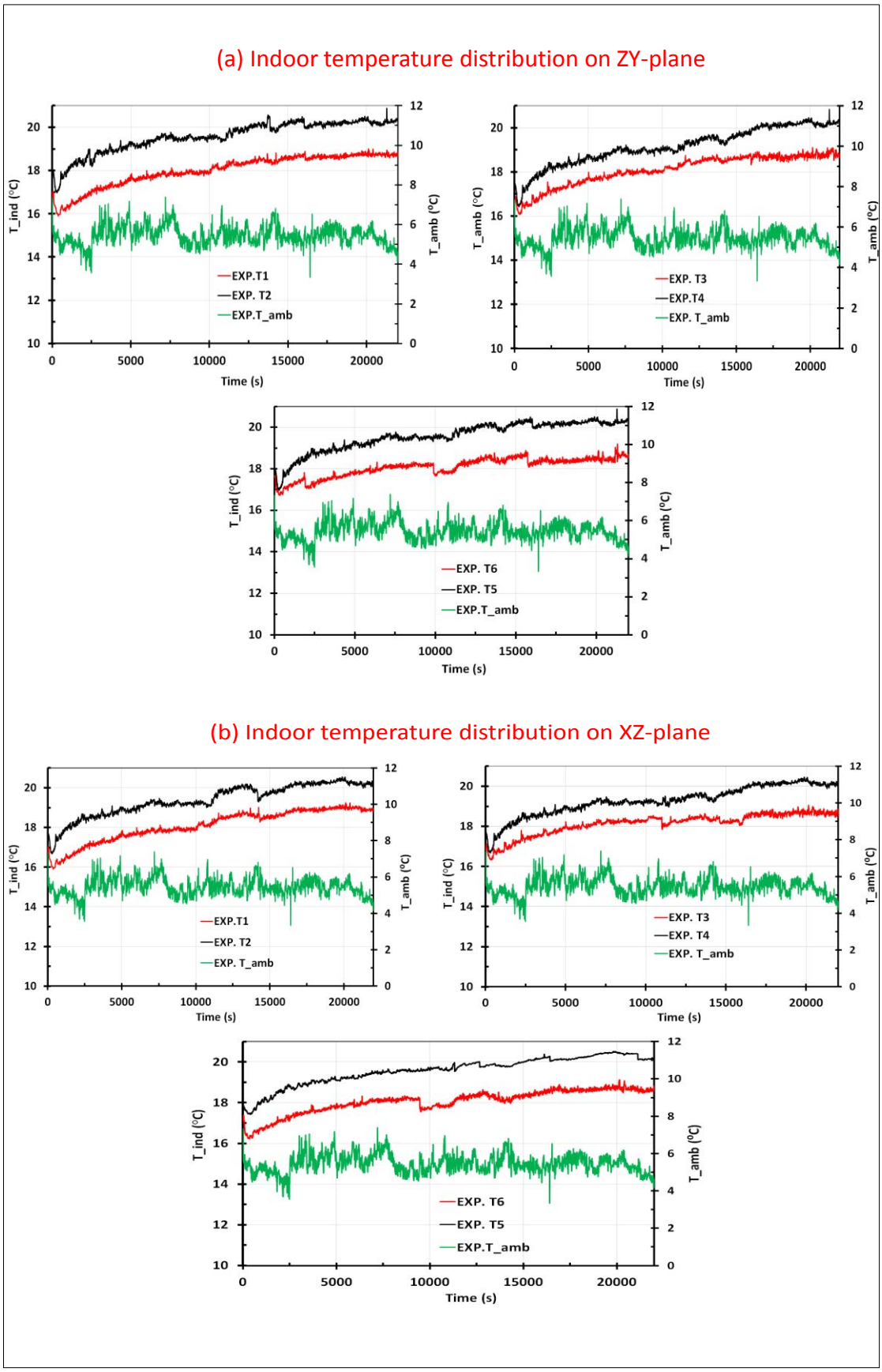

Figure 7.16 the measured indoor and outdoor temperature of the heated room at pulsed flow

From the results shown in figure 7.15 and figure 7.16, one can easily observe that the local temperature distribution of the heated room operating at pulsed flow (this work) is in good agreement with that of room heated by a radiator operating with constant flow to the radiator (conventional).

7.7 Validation of CFD results

In this section simulation results (CFD) of the radiator operating at constant flow, radiator operating at pulsed flow, indoor temperature when radiator operating at constant flow, indoor temperature when the radiator operates at pulsed flow and specific energy saving due to the pulsed flow compared to constant flow will be compared to the experimental results. The percentage deviation of the numerical results (CFD) compared to experimental (EXP) results are expressed using eq. (7.3) [94-95].

$$\text{Error (deviation)}\% = \left|\frac{\text{EXP} - \text{CFD}}{\text{EXP}}\right| \times 100 \tag{7.3}$$

7.7.1 Validation of CFD simulation for non-insulated radiator operating at constant flow

The simulation results of radiator operating at constant flow was validated using the measured radiator surface temperature and the hot water outlet temperature as described in section 7.2, figure 7.1. Figure 7.17 shows the measured local surface

temperature of the radiator compared to the predicted (CFD) results using thermocouples labelled T1 to T4 (figure 7.3) and results of the thermocouples labelled T5 to T15 are shown in appendix C.

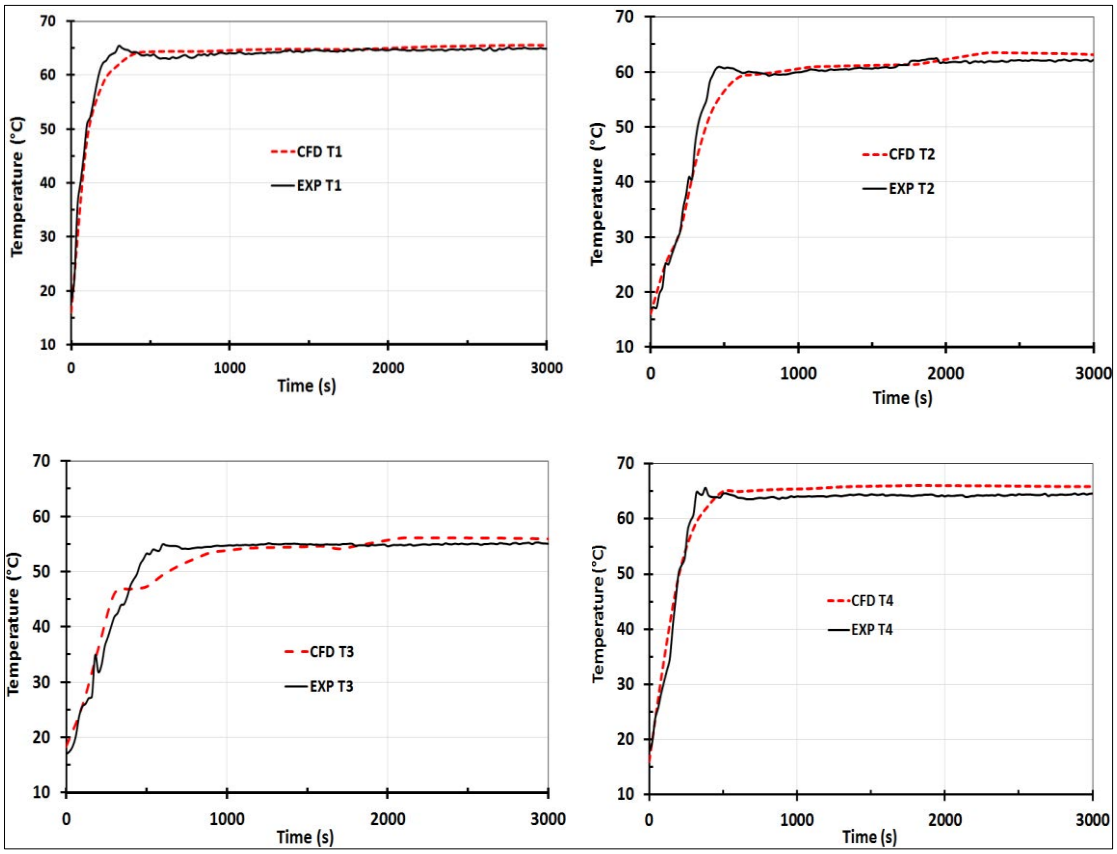

Figure 7.17 measured (EXP) radiator surface temperature T1 to T4 compared to numerically (CFD) predicted values

As shown in figure 7.17, the CFD predicted local surface temperatures of hydronic radiator at constant flow are in good agreement with the experimental results with maximum deviation of ±3.6%. Also figure 7.18 shows the CFD contour of the non-insulated radiator operating using constant flow compared to the experimental data labelled thermocouples T1 to T15 highlighting the good agreement between predicted and measured temperatures.

The inlet/outlet hot water temperature of the numerical (CFD) simulation compared to the experimental results showed good agreement with maximum deviation of ±1.86% as shown in figure 7.19.

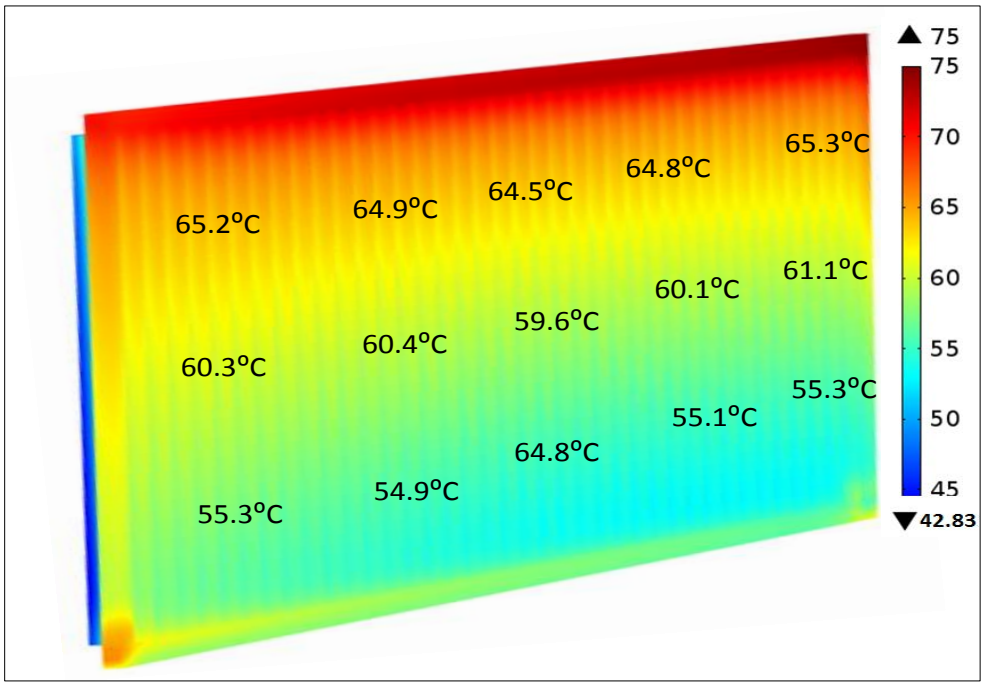

Figure 7. 18 CFD contour of constant flow non-insulated radiator compared to experimental data at 2000s

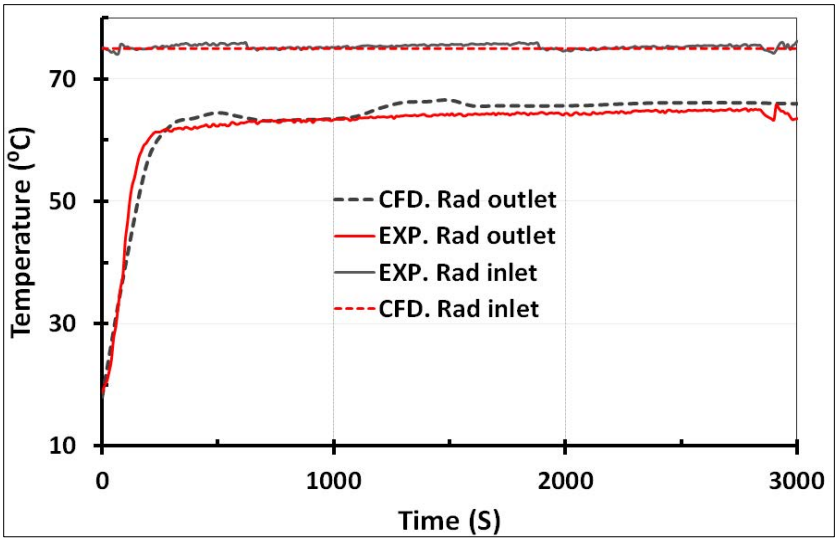

Figure 7.19 hot water inlet and outlet temperature of the radiator results CFD compared to experimental results at constant flow

Figure 7.20 shows the average surface temperature numerically (CFD) predicted against experimental (EXP) results. Results of the constant flow hydronic panel radiator at various inlet temperatures ranging from 60°C to 75°C and inlet flow rate of 0.022kg/s were validated on the basis of average surface temperature. For the radiator operating at constant flow (conventional) the numerical results of average radiator surface temperature compared to the experimental results (figure 7.20) showed maximum deviation of ±2.8%.

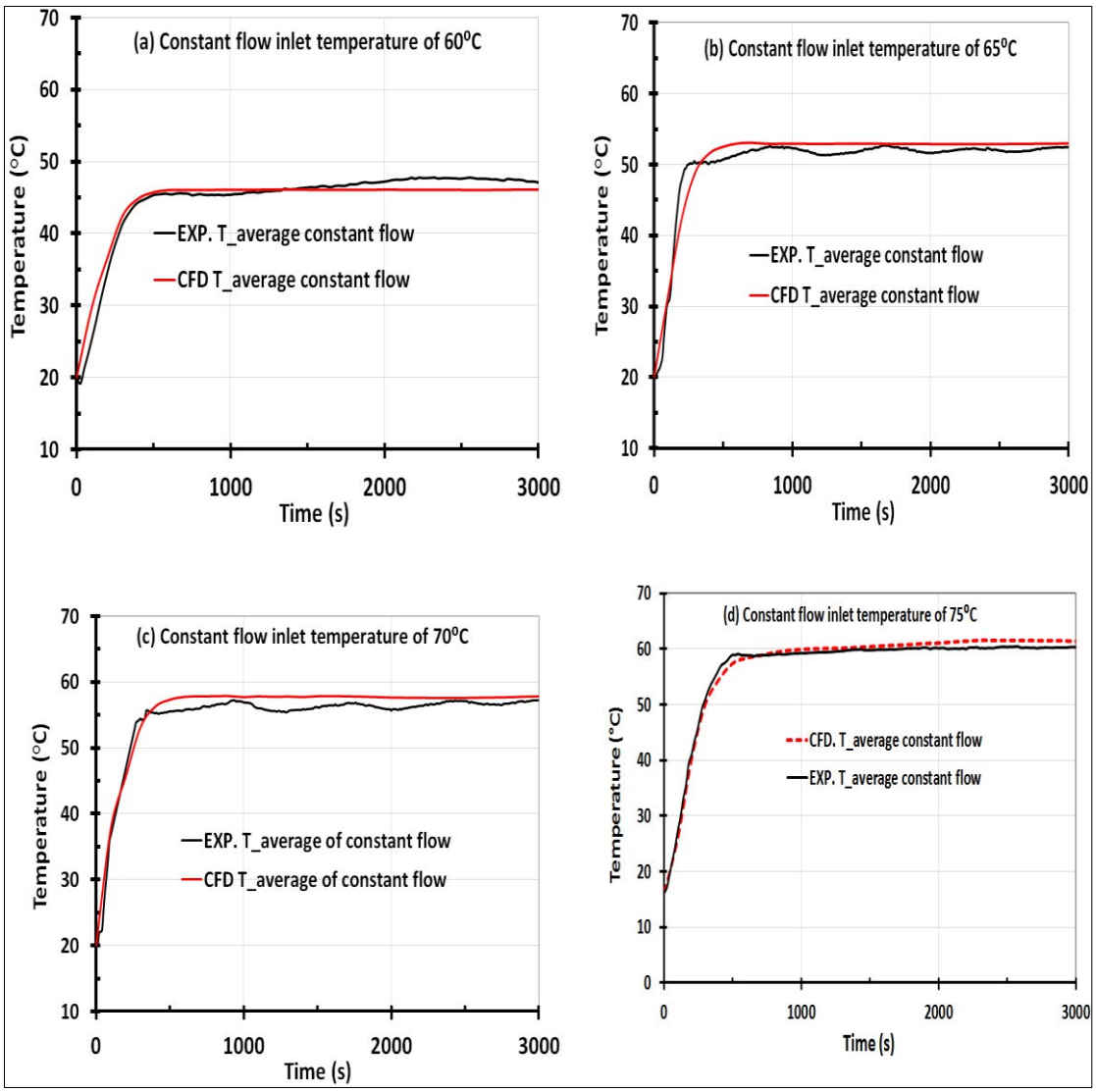

Figure 7.20 the average surface temperature of the radiator at constant flow predicted (CFD) results compared to the experimental (EXP) results

7.7.2 Validation of CFD simulation for non-insulated radiator operating at pulsed flow

The numerical (CFD) results of the best pulsed flow is validated against the best pulsed flow experimental (EXP) results on the basis of local surface temperature, hot water inlet/outlet temperature and the average surface temperature at various inlet hot water temperatures. Figure 7.21 shows the local surface temperature of selected thermocouple points on the surface of the hydronic panel radiator (T1 to T4). From the 15 surface thermocouples labelled T1 to T15 in figure 7.1 the first four thermocouples (T1 to T4) are shown in figure 7.21 while the remaining thermocouples labelled T5 to T15 are shown in appendix C. As shown in figure 7.21 the CFD results of the local surface temperature of the radiator operating at pulsed flow are in good agreement with the experimental results with maximum deviation of ±4.1%.

As shown in figure 7.21 the maximum deviation of the CFD results compared to the experimental results for the local surface temperature of the pulsed flow radiator is achieved at ±4.1%.

Figure 7.22 compares the CFD predicted and experimentally measured results of the inlet/outlet hot water temperature of the hydronic radiator operating at the best pulsed flow amplitude and frequency. As shown in figure 7.22 the radiator outlet hot water temperature of 65±0.7^{o}C was achieved. The maximum deviation of the numerical (CFD) results compared to the experimentally (EXP) measured hot water outlet temperature is ±2.1%.

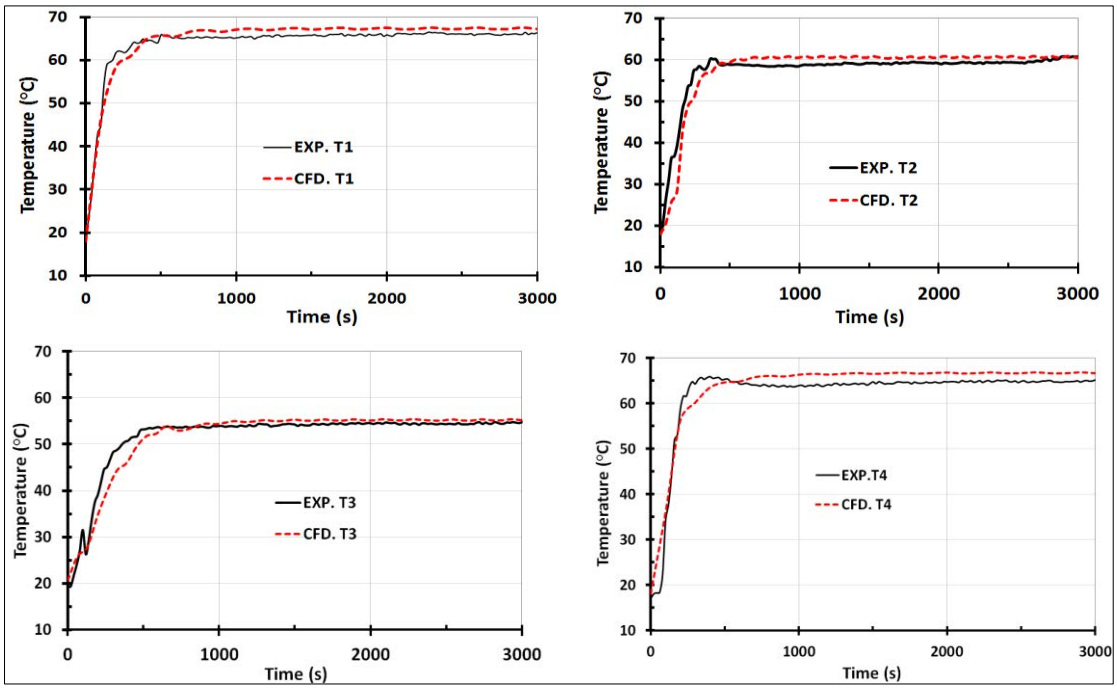

Figure 7. 21 local surface temperatures of the best selected pulsed flow radiator numerical (CFD) results compared to experimental (EXP) results

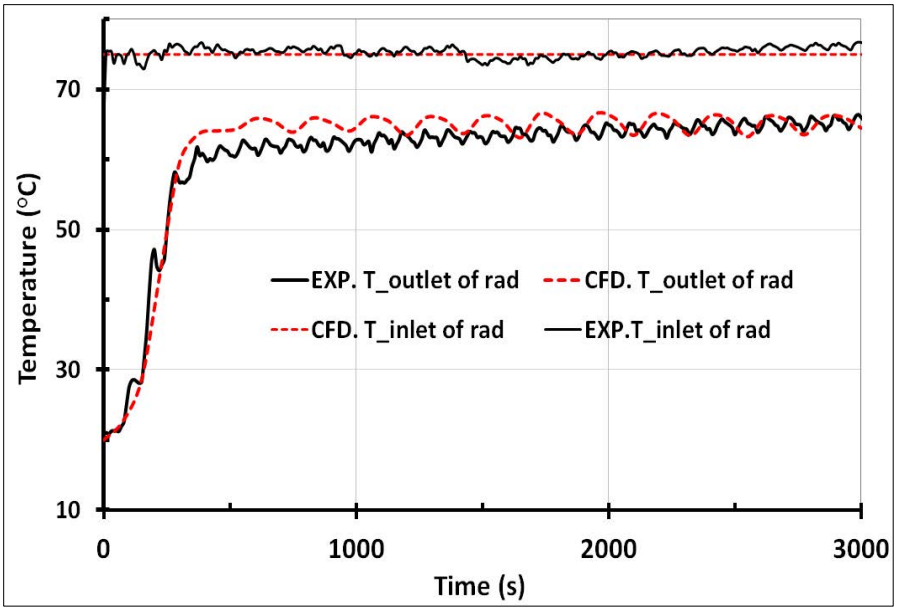

Figure 7.22 the hot water inlet and outlet temperature for numerically predicted (CFD) compared to experimental (EXP) of the best operating pulsed flow radiator

The numerical (CFD) results of the hydronic radiator at various hot water inlet temperatures of the best pulsed flow are compared to the experimental (EXP) results using the average surface temperature of the radiator as shown figure 7.23. The

maximum deviation of the numerical results compared to the experimental results of the radiator operating at pulsed flow and inlet temperature of 75°C is about ±2.5%.

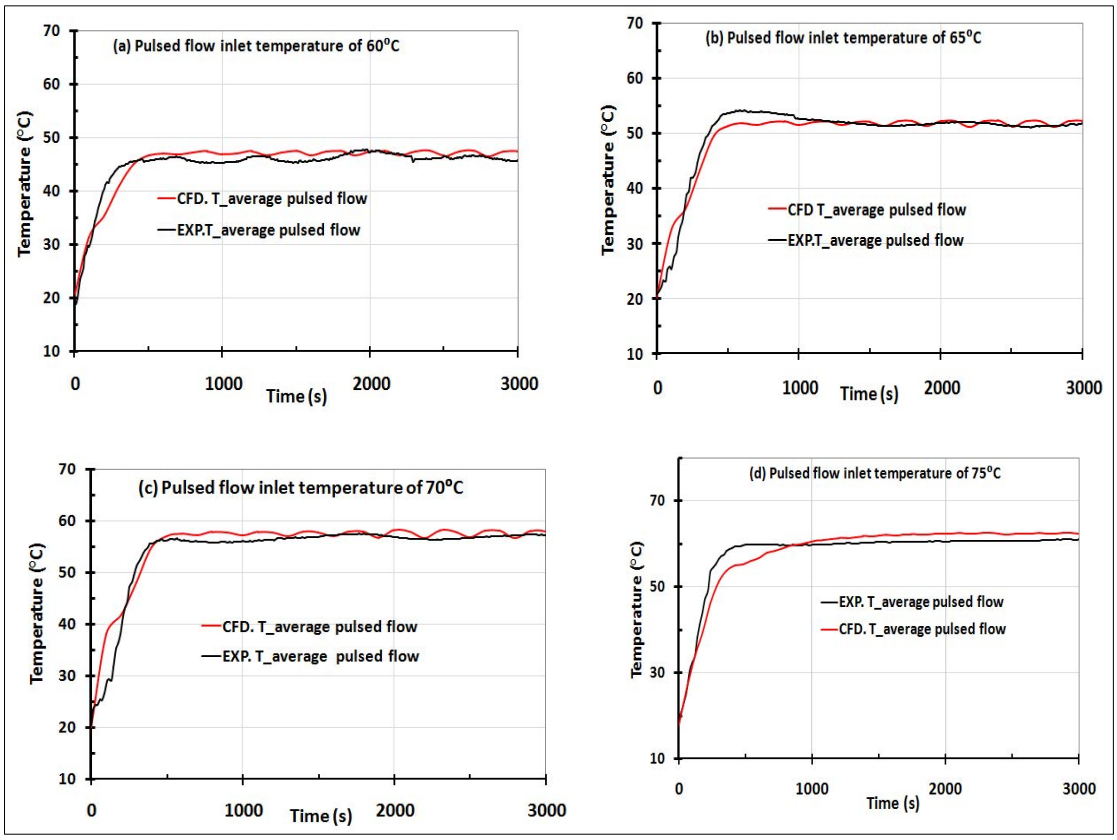

Figure 7.23 the average surface temperature of the radiator operating at pulsed flow of predicted results compared to the experimental results at the various hot water inlet temperature

7.7.3 Validation of the energy saving due the pulsed flow

The energy saving due to the pulsed flow predicted by the simulation work was validated on the basis of specific heat output. The specific heat outputs of the radiator obtained numerically and experimentally are calculated using eq. (3.45). Figure 7.24 shows the specific heat output of the pulsed flow compared to the constant flow for both numerically and experimentally tested hydronic panel radiator at various inlet temperatures.

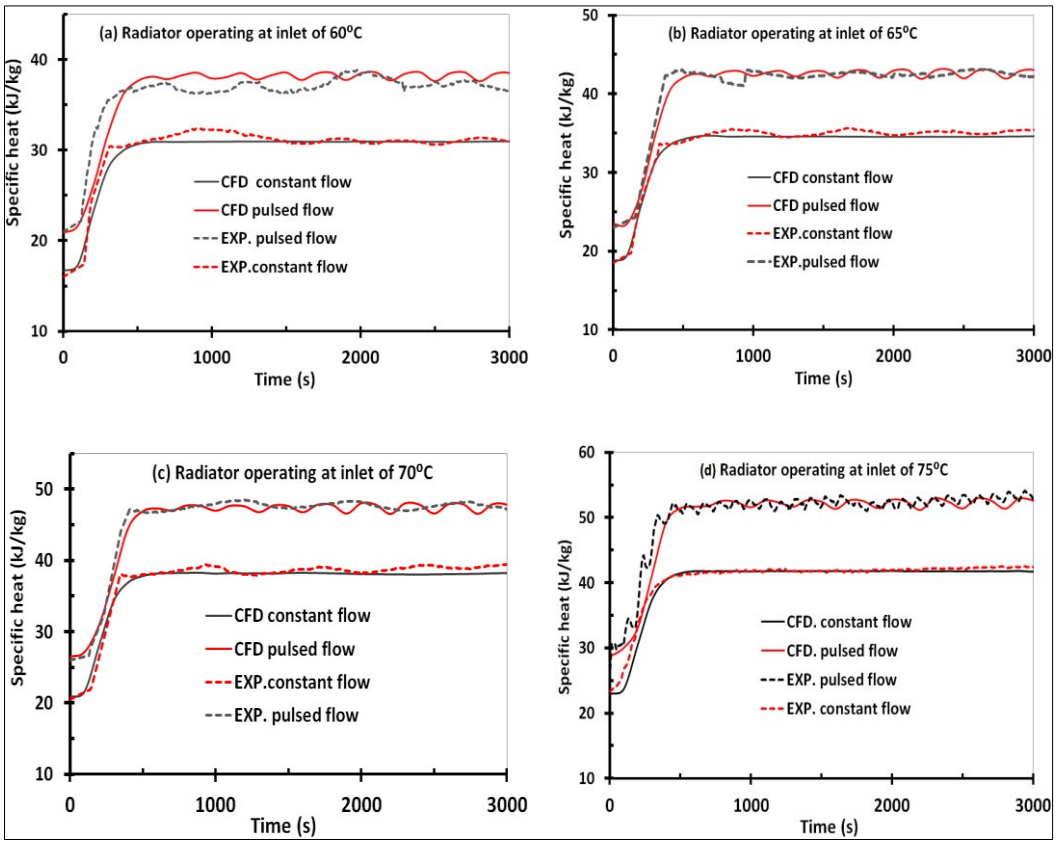

Figure 7.24 the specific heat output of hydronic panel radiator numerical results compared to experimental results at constant and pulsed flow conditions

The percentage of energy saving from the radiator due to the pulsed flow compared to the constant flow is calculated using eq. (4.21). Firstly the percentage of energy saving due to the pulsed flow compared to the constant flow for the numerically predicted values were calculated. Then the percentage of savings due to pulsed flow compared to constant flow for the experimentally tested hydronic radiator was calculated. Then the difference in percentage of energy savings between the numerical and experimental results is calculated using eq. (7.1) giving the percentage deviation of the results presented in this research work. Table 7.5 shows the estimated energy saving of the tested hydronic radiator due to the pulsed flow compared to constant flow using the numerical results and the experimental results as well as the calculated deviation between both results.

Table 7.5 the energy saved at pulsed flow when radiator operating at varying inlet temperature using numerical and experimental results

Inlet temperature	Numerical (%) savings	Experimental (%) savings	Deviation (%)
60^{o}C	23.40	22.1	1.3%
65^{o}C	23.36	22.9	0.46
70^{o}C	24.1	22.8	1.3%
75^{o}C	24.90	23.2	1.7%

The energy saving due to the pulsed flow as predicted by the numerical results are in good agreement with those achieved by the experimental results with maximum deviation of ±1.7% as shown in table 7.5. Based on the above results it can be concluded that the pulsed flow can be used for wide range of heating applications for saving significant amount of energy.

7.8 Validation of CFD simulation of indoor temperature

The numerically predicted (CFD) results were validated against experimental (EXP) results on the basis of the local indoor air temperature using the thermocouple layout described in figure 7.14 where the probes are positioned parallel (ZY-plane) and perpendicular (XZ-plane) to the heating panel radiator. The CFD predicted indoor temperature of the room was validated for radiator operating at constant flow described in section 7.3 and radiator operating at pulsed flow described in section 7.4.3.

7.8.1 Validation of CFD simulation heated room at constant flow

The CFD predicted indoor temperature of the room with the radiator operating at constant flow (conventional flow) is validated on the basis of temperature measured

using thermocouples installed at points shown in figure 7.14. The probes are positioned as recommended by the international comfort standards as described in section 7.6. Figure 7.25(a) and Figure 7.25(b) show the CFD predicted indoor temperature compared to the experimental (EXP) results.

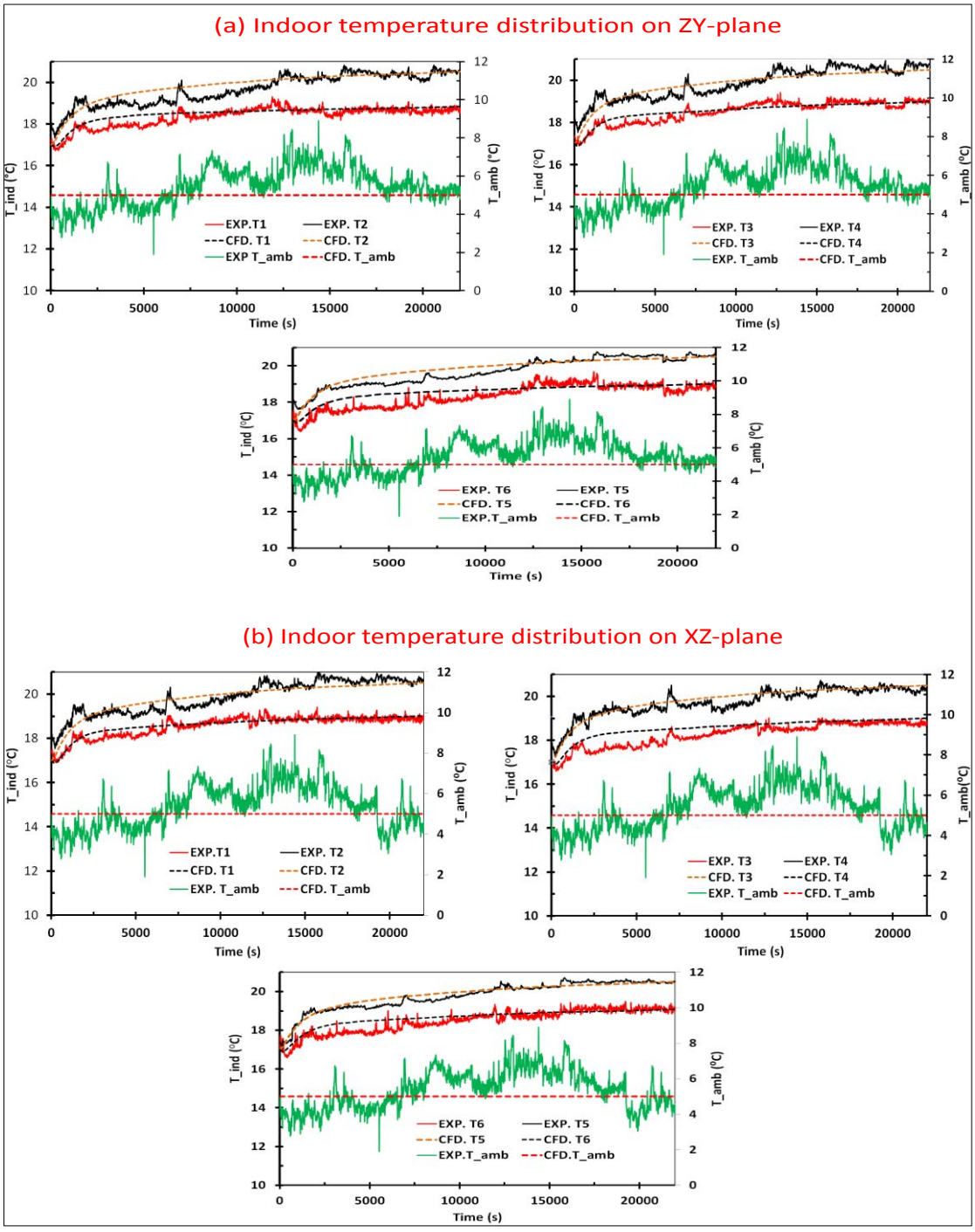

Figure 7. 25 indoor and outdoor temperatures of the heated room numerical (CFD) results compared to experimental (EXP) results for radiator operating at constant flow

The measured minimum and maximum indoor temperatures in the YZ-plane are 18.3^{o}C and 20.9^{o}C respectively. The measured minimum and maximum indoor temperatures in the XZ-plane are 18.2^{o}C and 20.7^{o}C respectively. The numerically (CFD) predicted values of the local indoor temperature are in good agreement with the experimentally (EXP) measured values with maximum deviation of ±2.83% when the system reached steady state temperature It is clear from figure 7.25 that the average measured temperature of the outdoor was about 5^{o}C during the test period.

7.8.2 Validation of CFD simulation of heated room at pulsed flow

The numerical results of the heated room at pulsed flow are validated against the experimental results on the basis of the indoor temperature distribution using the thermocouples shown in figure 7.14. Figure 7.26(a) and Figure 7.26(b) show the predicted indoor temperature compared to experimental (EXP) results on the basis of the probes layout on YZ-plane and XZ-plane respectively for the heated room with radiator operating at pulsed flow.

The numerical results of the indoor temperature are in good agreement with the experimental results with maximum deviation of ±2.15 % when the temperature reached steady state. From the numerical and experimental results of the heated room using pulsed flow radiator, the comfort temperature was achieved as recommended by the ASHRAE standards of indoor thermal comfort criterion.

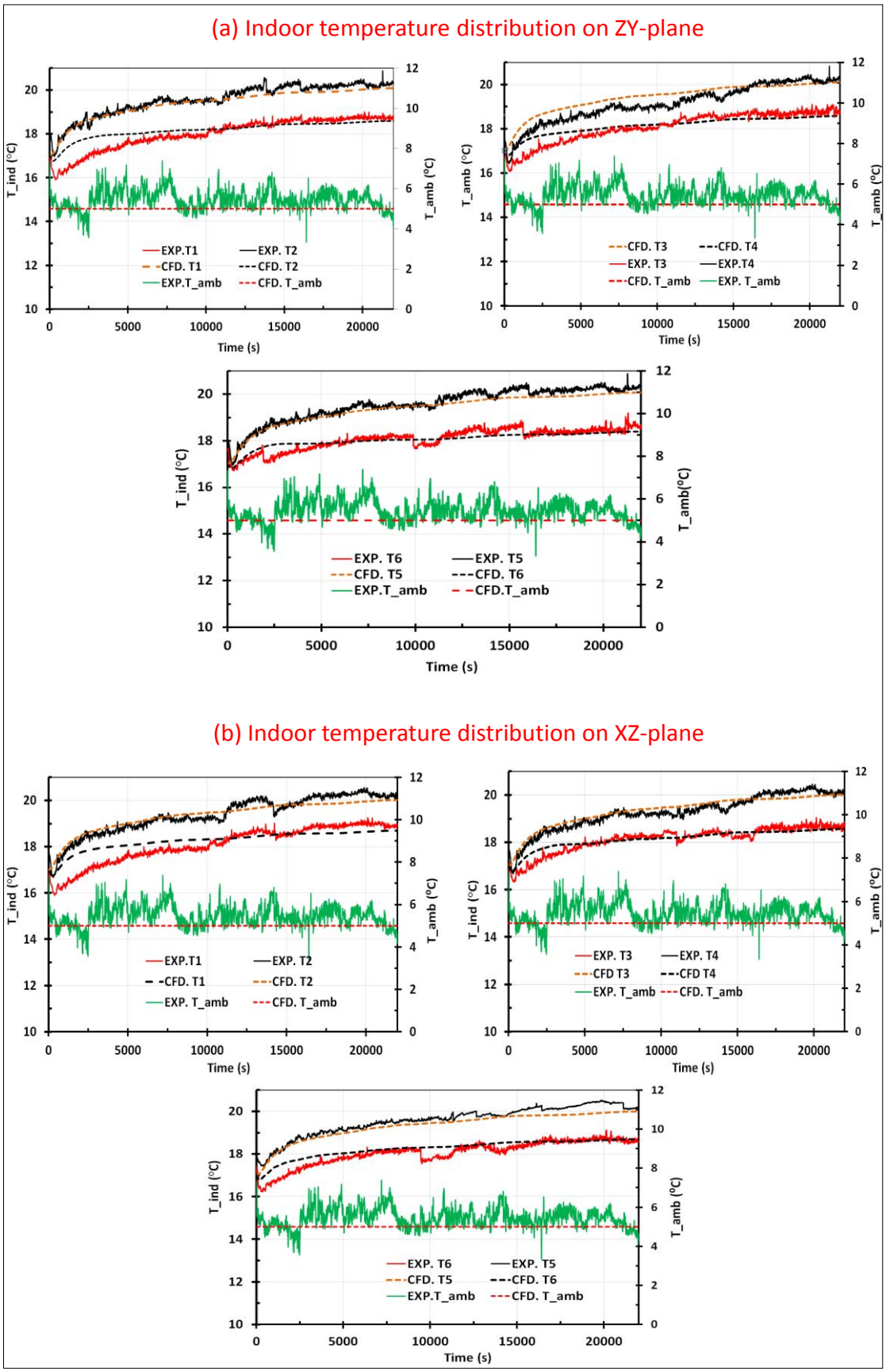

Figure 7.26 indoor and outdoor temperatures of the heated room numerical (CFD) results compared to experimental (EXP) results for radiator operating at pulsed flow

7.9 Experimental results and validation of insulated radiator

In this section the radiator was insulated to minimise the convection heat transfer loss to the surrounding air when the surface temperature measurement was taken. The insulator used for the radiator was Celotex insulation board of 0.1m thick with thermal conductivities of 0.022W/(m.K). The one side insulated radiator (radiator side opposite to the attached fins side) was tested to validate the CFD results of radiator surface temperature distribution. The local surface temperature of the insulated radiator was validated at both constant and pulsed flow scenario.

7.9.1 Experimental results of insulated radiator at constant flow

Figure 7.27 shows the experimental results of local surface temperature of the radiator at the points shown in figure 7.1 when the radiator was insulated.

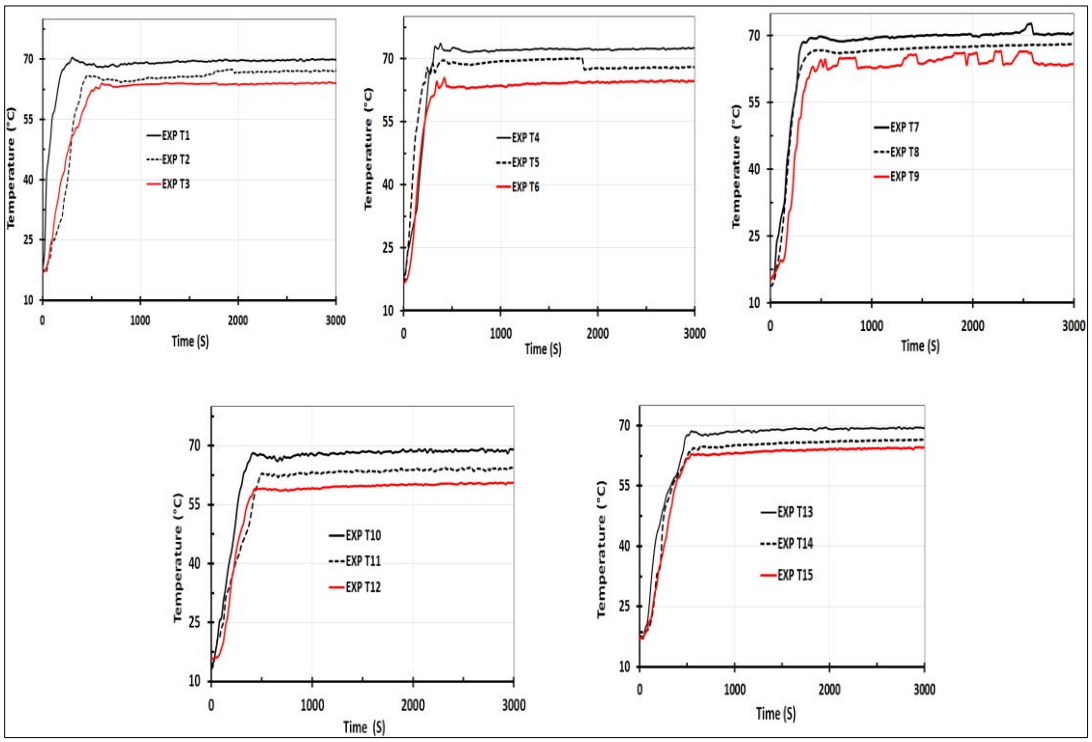

Figure 7. 27 local surface temperature distribution of surface radiator measured experimentally (EXP) at constant flow (when radiator was insulated)

As shown in figure 7.27 the local temperature distributions of the radiator is high at the top of the panel radiator and decreases towards the bottom. As the light hot water rises up due to buoyancy force, the heavy colder water flows to the lower part of the radiator. Figure 7.28 shows the average local surface temperature of the experimental results calculated using eq. (7.1).

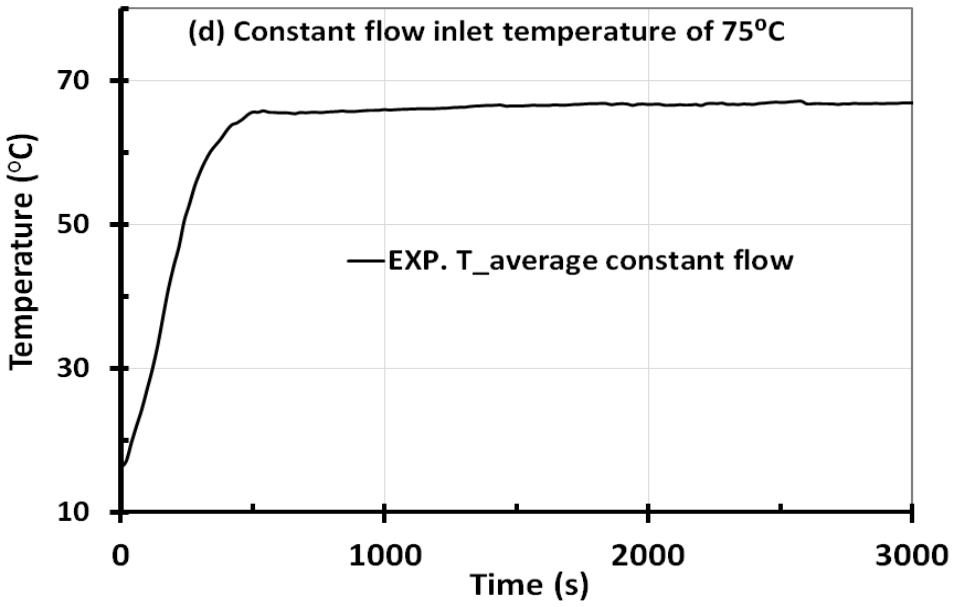

Figure 7.28 the experimentally measured average surface temperature of the radiator operating at constant flow (when radiator was insulated)

As shown in figure 7.28 the average surface temperature of the radiator operating at constant flow is about 67°C.

7.9.2 Validation of CFD simulation for the insulated radiator at constant flow

The simulation results of radiator operating at constant flow were validated using the measured local radiator surface temperature. Figure 7.29 shows the measured local

surface temperature of the radiator compared to the predicted (CFD) results using thermocouples labelled T1 to T4 and results of the thermocouples labelled T5 to T15 are shown in appendix C.

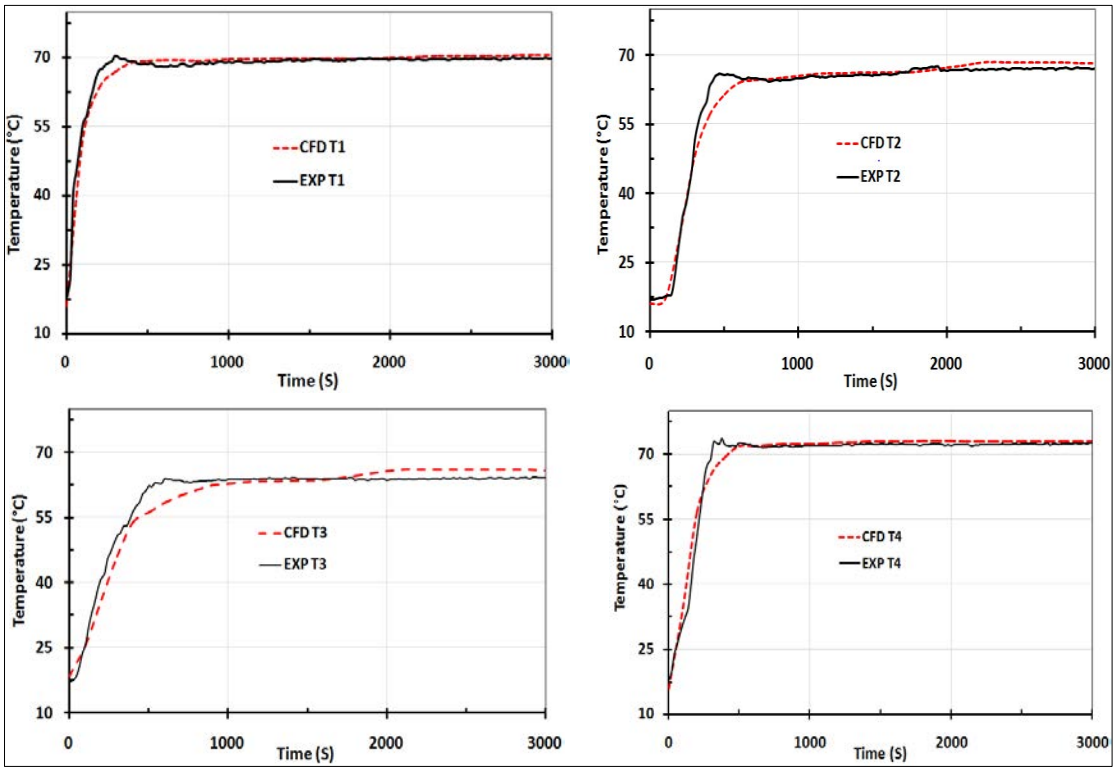

Figure 7.29 comparison of numerically (CFD) and experimentally measured (EXP) local temperature T1 to T4 of surface radiator for operating at constant flow (when radiator was insulated)

As shown in figure 7.29, the CFD predicted local surface temperatures of insulated radiator at constant flow are in good agreement with the experimental results with maximum deviation of ±3.34%.

7.9.3 Experimental results insulated radiator at pulsed flow

The best pulsed flow with frequency of 0.033Hz and flow amplitude of 0.0348kg/s was applied at inlet temperature of 75^{o}C. Figure 7.30 shows the local surface

temperature of the radiator corresponding to the labelled surface thermocouples of T1 to T15 as shown in figure 7.1 when the radiator was insulated.

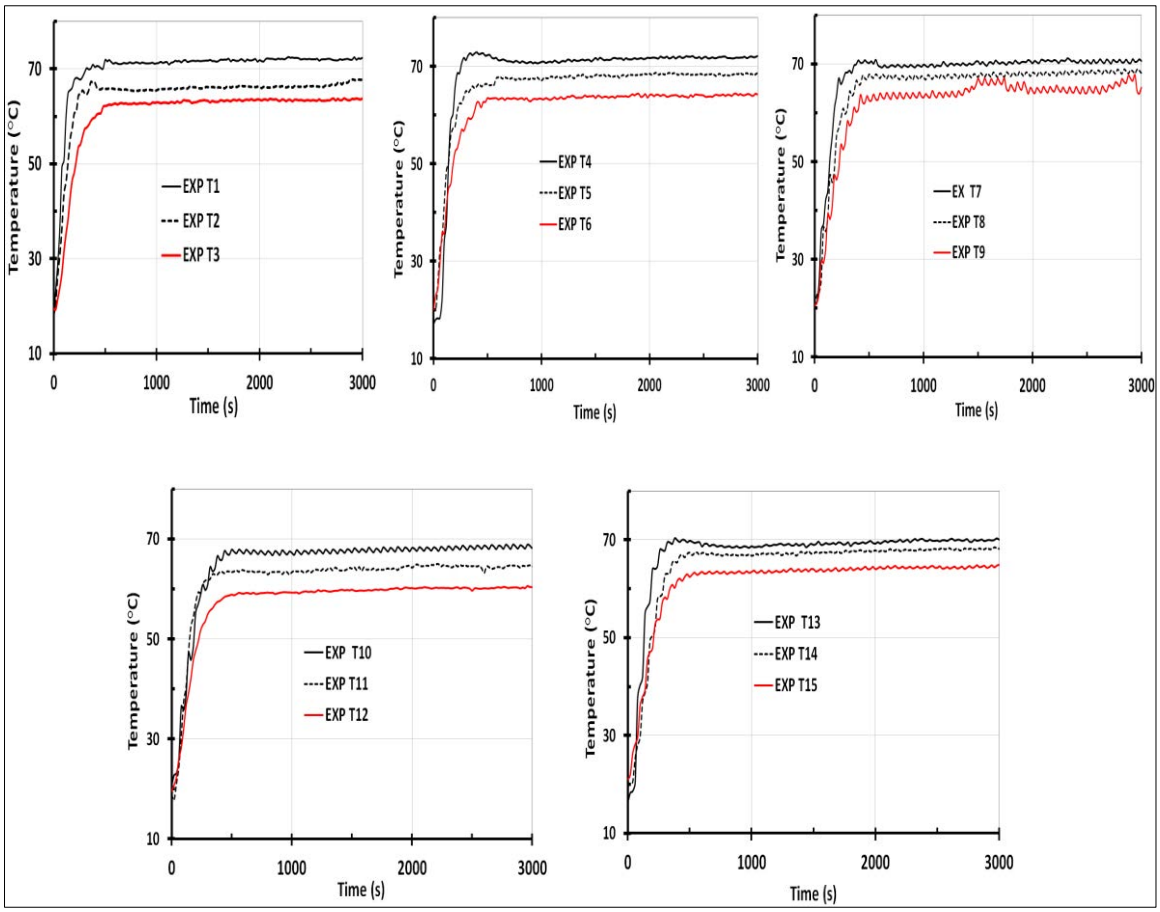

Figure 7. 30 experimentally measured (EXP) local surface temperature of the radiator operating at the best selected pulsed flow (when radiator was insulated)

It is clear from figure 7.30 that the surface temperature of the radiator decreases towards the bottom of the vertical channels of the hydronic radiator in a similar manner as described in section 7.9.1 for the case of constant flow testing for insulated radiator. Figure 7.31 shows the average radiator surface temperature of the selected pulsed flow compared to the average radiator surface temperature of constant flow. It is clearly shown in figure 7.31 that the average radiator surface temperature of the selected best pulsed flow with amplitude of 0.0348 kg/s and frequency of 0.033Hz is

about 67.2°C which matches well with the average insulated radiator surface temperature at constant flow of 67°C.

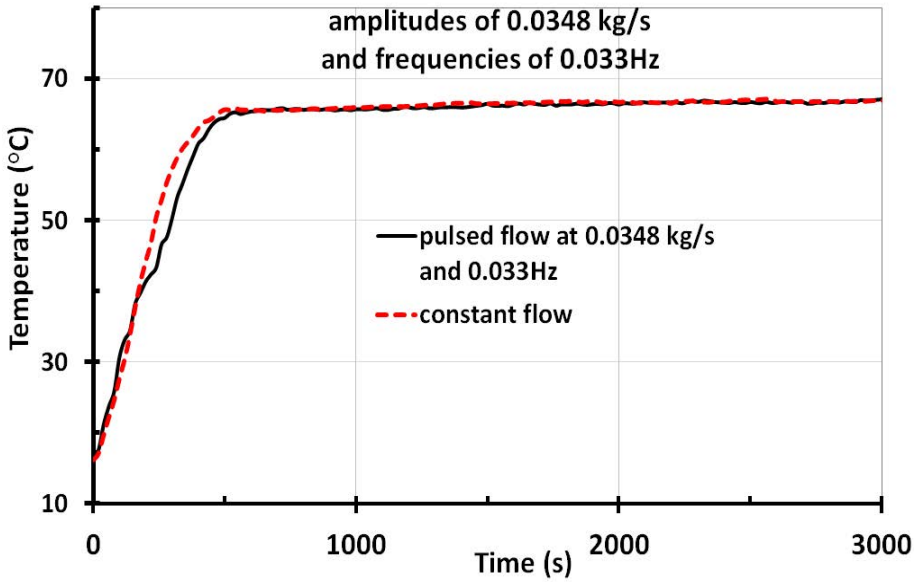

Figure 7.31 average surface temperature of the best selected pulsed flow radiator compared to constant flow (when the radiator was insulated)

7.9.4 Validation of CFD simulation for the insulated radiator operating at pulsed flow

The numerical (CFD) results of the best pulsed flow is validated against the best pulsed flow experimental (EXP) results on the basis of local radiator surface temperature (when insulated). Figure 7.32 shows the local surface temperature of selected thermocouple points on the surface of the hydronic panel radiator (T1 to T4) as illustrated in figure 7.1. From the 15 surface thermocouples labelled T1 to T15, the first four thermocouples (T1 to T4) are shown in figure 7.32 while the remaining thermocouples labelled T5 to T15 are shown in appendix C. As shown in figure 7.32 the CFD results of the local surface temperature of the insulated radiator operating at

pulsed flow are in good agreement with the experimental results with maximum deviation of ±3.83%.

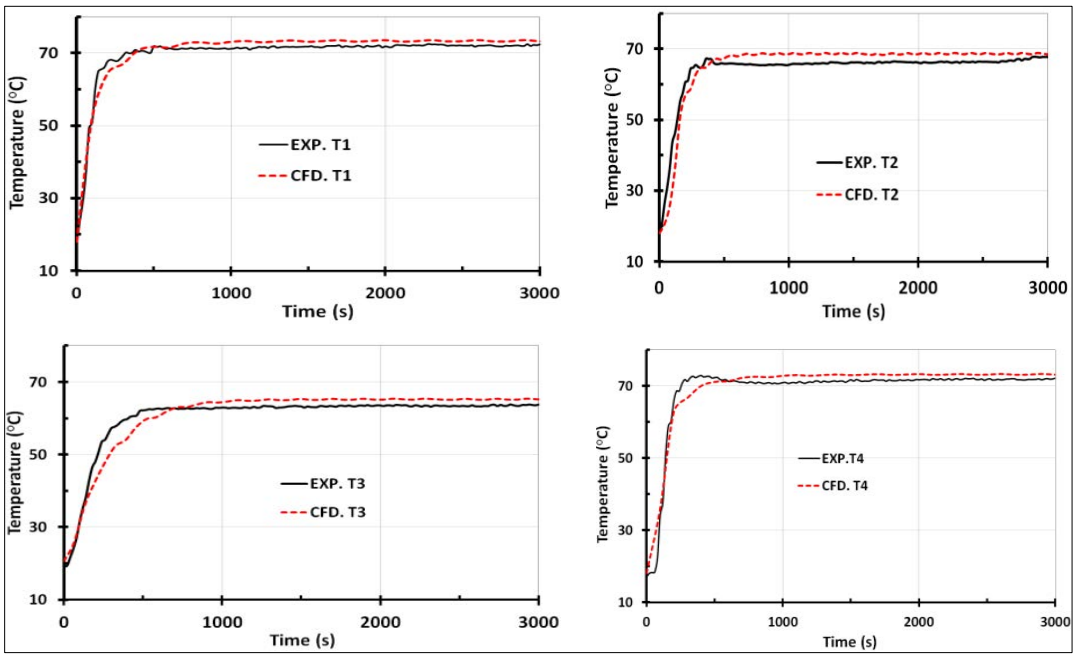

Figure 7.32 local surface temperatures of the best selected pulsed flow radiator numerical (CFD) results compared to experimental (EXP) results (when radiator was insulated)

7.10 Summary

In this chapter the experimental results are analysed and the numerical results obtained in chapters 4 and 5 are validated against experimental results. The experimental tests were performed in consideration of the international standards applied in hydronic heating radiators and indoor comfort temperature.

The central heating system of hydronic radiator was analysed experimentally on the basis of average surface temperature, hot water inlet and outlet temperature, specific heat output, and indoor temperature of the tested room.

The numerical results were validated against experimental results with good agreement for both constant flow and pulsed flow radiators with maximum deviation of ±3.34% and ±4.1% respectively on the basis of local radiator surface temperature. Furthermore the hydronic radiator was tested at various hot water inlet temperatures for both constant and pulsed flow and maximum deviation between numerical and experimental results are ±2.8% and ±2.5% respectively on the basis of the mean radiator surface temperature.

Energy saving due to the pulsed flow was estimated using specific heat output of the radiator. The radiator operating at pulsed flow using various inlet temperatures were compared to the corresponding radiator operating at constant flow using numerical and experimental results. The maximum percentage of the energy saving was 24.9% numerically, 23.2% experimentally at inlet temperature of 75^{o}C for the pulsed flow compared to constant flow radiators. The maximum deviation of the potential energy savings based on numerical results compared to experimental result is ±1.7%.

The indoor temperature was experimentally measured and the numerical results were validated against experimental results. The maximum deviation of the predicted indoor temperature was ±2.83% at constant flow and ±2.15% at pulsed flow. All indoor temperatures were achieved as recommended by ASHRAE standard 55 with 90% acceptability (described in section 7.6).

Generally all the numerical results were in good agreement with experimental results in all of the tested models. Thus the proposed flow pulsation is a potentially viable

method for saving energy in hydronic heating system using panel radiator without compromising indoor comfort parameters.

CHAPTER 8

CONCLUSIONS AND FUTURE WORK

8.1 Introduction

Improving the heat output of the hydronic central heating system in buildings can play a major role in energy saving thus reducing fossil fuel consumption and CO_2 emission. Current panel radiators of hydronic central heating systems are operating at constant flow strategy with thermostat control device. This constant flow operating mode is not efficient in terms of energy consumption; therefore an alternative operating scenario is required to enhance the heat output of the panel radiator. The main aim of this research is to investigate the effect of pulsed flow on the energy consumption of panel radiators in hydronic central heating systems. The proposed pulsed flow was investigated in terms of enhancing the heat output of the radiator without compromising the user thermal comfort defined by ASHRAE standard 55 and EN ISO 7730.

Comprehensive literature review of hydronic central heating system including means of enhancing the heat output of radiators, applications of various heat sources, criterion for assessing the human comfort and techniques used to simulate their performance like analytical and computational fluid dynamic methods. Based on the comprehensive literature review, it was concluded that no published work was found regarding the use pulsed flow for enhancing hydronic radiator of central heating system. Therefore this research project is set to assess the thermal performance of the

hydronic panel radiator and the indoor comfort using pulsed flow. The work was performed using dynamic control modelling, numerical modelling (CFD) and experimental testing.

8.2 Conclusion

Based on the work carried out to investigate the effect of pulsed flow on hydronic central heating system in terms of thermal energy output of the radiator and the thermal comfort in the heated space, the following conclusions can be drawn.

Dynamic control model of a single heated room integrated with hydronic radiator central heating system was developed in MatLab/Simulink to investigate energy consumption and indoor comfort conditions using pulsed and constant flow scenarios. Initially the heated room was modelled without occupants (empty room) and results showed that 20-22% energy can be saved by altering the constant flow to pulsed flow when radiator was operating at On/Off control manner. Also about 27% of energy can be saved by changing the On/Off control to the PID control system when pulsed flow was compared to constant flow.

The embedded control system was developed for the room with 5 occupants to investigate indoor thermal comfort and indoor air quality (IAQ). Results showed that indoor CO_2 concentration, of 1000PPM±50PPM, indoor relative humidity of 50±5% and indoor temperature of 20±1.6^{o}C also results are in good agreement with international standards for indoor environment. The modelling results showed that about 20% and 34.5% energy can be saved using flow pulsation compared to constant

flow from heating radiators and fan ventilation system respectively. Also using the pulsed flow applied in this work the pump power can be reduced by about 12% compared to the pump operating at constant flow.

CFD models were developed using finite element modelling in COMSOL Multi-physics software. The radiator was numerically simulated using constant and pulsed flow including type11 and type10 radiators. Both constant and pulsed flow to the radiator were modelled at various input conditions; particularly the pulsed flow radiator was modelled at various flow amplitudes ranging from 0.0326kg/s to 0.0412kg/s and various flow frequencies ranging from 0.0083Hz to 0.033Hz. CFD of the heated room was also developed in COMSOL and investigated at constant and pulsed flow scenarios.

Results showed that about 18.9% (for type10 radiator) and 24.9% (for type11 radiator) of energy can be saved using pulsed flow compared to constant flow. The radiator was also modelled at various inlet temperature ranges from 60^{o}C to 75^{o}C at interval of 5^{o}C and energy saving of 23.4% at 60^{o}C to 24.9% at 75^{o}C was achieved.

The experimental facility was developed that consists of hot water circulating system comprising of electrically heated water tank, circulating pump and control system. Arduino control system comprising of Arduino mega 2560 micro controller, Arduino motor shield R3, mother board, LM35 temperature control sensor, connecting wires was constructed and a computer code was developed to enable constant and pulsed flow operating conditions.

Thus the numerical results of type11 hydronic radiators were validated experimentally using both constant and pulsed flow conditions with maximum deviation of ±3.34% and ±3.83% respectively. Also the maximum percentage of energy saving was 24.9% predicted numerically (CFD) and 23.2% measured experimentally (EXP) with maximum deviation of ±1.7%.

Results of the finite element modelling of the indoor comfort in the heated room without occupants and with occupants showed that indoor temperature of $20^{o}C \pm 1.6^{o}C$, indoor draught parameters of below 15%, indoor velocity of below 0.15m/s, relative humidity of 50%±9% and CO_2 concertation of below 1000ppm±50ppm are achieved. This shows that the energy saving produced by using pulsed flow was achieved without compromising international standards. The maximum deviations of numerical results compare to experimental results for indoor temperature are ±2.83% for constant flow and ±2.15% for the pulsed flow.

Generally the numerical results were in good agreement with the experimental result in all the developed models. The saved energy due to the pulsed flow is attributed to the heat transfer enhancement of the radiator which led to higher heat output at lower average mass flow rate of the hot water. The heat transfer enhancement is attributed to the increase of instant flow velocity inside the radiator due to the pulsation effect of the hot water flow rate in the radiator channels.

8.3 Future work

Results of this work showed that flow pulsation offers the potential to produce energy saving in hot water based central heating and air ventilation systems. Based on the conclusion made in this thesis, further work is required to establish flow pulsation more as a robust and desirable flow strategy for other cooling and heating applications. The following future investigations are suggested:

- Other types of hydronic heating system such as skirt board, floor heating need to be tested, to investigate the potential of energy saving using pulsed flow strategy.

- Based on UK 2020 vision the use of heat pumps for domestic heating application are set to increase from 28000 in 2010 to 1.2m in 2020. These heat pumps deliver lower supply temperature to the hydronic heating system, thus large surface area of heat emitter will be needed to heat the same space. To overcome the challenge of larger area of heat emitter using low temperature; flow pulsation needs to be tested to investigate radiator performance at hot water temperature as low as 40^{o}C such as those supplied by ground source heat pumps. Thus verifying the effect of flow pulsation on radiator heating performance at low hot water temperatures will enable establishing low grade waste heat sources for heating or cooling purposes.

- Further study is required to investigate the effect of flow pulsation on natural gas supply to the central heating boiler.

- Effect of flow pulsation on ventilation system of fan showed encouraging percentage of enhancement when dynamically modelled using the embedded

MatLab/Simulink. Thus experimental study is required to validate the potential of energy saving using pulsation operation of ventilation fan.

- Optimization of geometrical design combined with the flow pulsation for hydronic heating radiator needs to be investigated. This can be helpful to get the best geometry design in combination with flow pulsation that leads to optimum heat output from the hydronic radiator.

REFERENCES

[1] S. Mandley, R. Harmsen, E. Worrell. Identifying the potential for resources and embodied energy savings with in the UK buildings sector. Energy and Buildings 2015; 86: 841–851.

[2] A.Beizaee, D.Allinson, K. J. Lomas, E.Foda, D. L. Loveday. Measuring the potential of zonal space heating controls to reduce energy use in UK homes: The case of un-furbished 1930s dwellings. Energy and Buildings 2015; 92:29–44.

[3] D. Dineen, B.P. Ó Gallachóir. Modelling the impacts of building regulations and a property bubble on residential space and water heating. Energy Buildings 2011; 43: 166-178.

[4] J. A. Myhren, S. Holmberg. Design considerations with ventilation-radiators: Comparisons to traditional two-panel radiators. Energy and Buildings 2009; 41:92–100.

[5] I. Korolija, L. Marjanovic-Halburd, Y. Zhang, V. I. Hanby. UK office buildings archetypal model as methodological approach in development of regression models for predicting building energy consumption from heating and cooling demands. Energy and Buildings 2013; 60: 152–162.

[6] J. Phil. Energy efficiency in buildings CIBSE Guide F. 2 ed. 2004, Great Britain, Page Bros. (Norwich) Ltd., Norwich, Norfolk, NR6 6SA. : CIBSE Publications Department.

[7] J. A. Myhren, S. Holmberg. Improving the thermal performance of ventilation radiators the role of internal convection fins. International Journal of Thermal Sciences 2011; 50: 115-123.

[8] M. Razmara, M. Maasoumy, M. Shahbakhti, R.D. Robinett. Optimal exergy control of building HVAC system. Applied Energy 2015; 156:555–565.

[9] S. Mandley, R. Harmsen, E. Worrell. Identifying the potential for resource and embodied energy savings within the UK building sector. Energy and Buildings 2015; 86: 841–851.

[10] E. Wilkes. Energy Consumption in the UK (2015) Overall energy consumption in the UK since 1970 [online]

[11] http://www.idhee.org.uk/HHTF.pdf (Heating and Hot Water Pathways to 2020) [accessed 20/08/2015]

[12] M. Shahrestani, R. Yao, G. K. Cook. Characterising the energy performance of centralised HVAC&R systems in the UK. Energy and Buildings 2013; 62: 239–247.

[13] D. Rogers, M. Foster, C. Bingham. Experimental investigation of a Recursive Modelling MPC system for space heating within an occupied domestic dwelling Building and Environment 2014; 72:356-367.

[14] The Carbon Plan Delivering our low carbon future. Department of Energy & Climate Change. December 2011:(online)

[15] N. Eyre, P. Baruah. Uncertainties in future energy demand in UK residential heating Energy Policy 2014.

[16] H.W. L. Danny, L. Yang, C. L. Joseph. Impact of climate change on energy use in the built environment in different climate zones- A review. Energy 2012; 42:103-112.

[17] M. R. Hall, S. P. Casey, D. L. Loveday, M. Gillott. Analysis of UK domestic building retrofit scenarios based on the E.ON Retrofit Research House using energetic hygrothermics simulation Energy efficiency, indoor air quality, occupant comfort, and mould growth potential. Building and Environment 2013; 70:48-59.

[18] A. Parkinson, P. Guthrie. Evaluating the energy performance of buildings within a value at risk framework with demonstration on UK offices. Applied Energy 2014; 133:40–55.

[19] S. Obyn, G. van Moeseke. Comparison and discussion of heating systems for single-family homes in the framework of a renovation. Energy Conversion and Management 2014; 88: 153–167.

[20] D. Anastaselos, I. Theodoridou, A. M. Papadopoulos, M. Hegger. Integrated evaluation of radiative heating systems for residential buildings. Energy 2011; 36:4207-4215.

[21] M. Mikk, J. Kurnitski. Low temperature radiator heating distribution and emission efficiency in residential buildings. Energy and Buildings 2014; 69:224–236.

[22] K. B.Wittchen, S. Aggerholm. Calculation of building heating demand in EPIQR. Energy and Buildings 2000; 31:137–141.

[23] N. Soaresa, J.J. Costab, A.R. Gasparb, P. Santos. Review of passive PCM latent heat thermal energy storage systems towards buildings' energy efficiency Energy and Buildings 2013; 59:82–103.

[24] A. Foucquier, S. Robert, F.de ricSuard, L. Ste´ phan, A. Jay. State of the art in building modelling and energy performances prediction- A review. Renewable and Sustainable Energy Reviews 2013; 23:272–288.

[25] I.Korolija, Y.Zhang, L.Marjanovic-Halburd, V. I. Hanby. Regression models for predicting UK office building energy consumption from heating and cooling demands. Energy and Buildings 2013; 59:214–227.

[26] A. M. Rodrigues, M. G. Gomes. Natural ventilation of a room with an atmospheric-vent water heater in both on- and off-states. Energy and Buildings 2014; 74:53–60.

[27] A. Ploskić. Technical solutions for low-temperature heat emission in buildings, in Department of Civil and Architectural Engineering. KTH Royal Institute of Technology 2013.

[28] D. Pineau, P. Rivière, P. Stabat, P. Hoang, V. Archambault. Performance analysis of heating systems for low energy houses. Energy and Buildings 2013; 65:45–54.

[29] G. Margarethe H. Justine C. Keith Jones. University Domestic energy consumption—what role do comfort, habit and knowledge about the heating system play? Energy and Buildings 2013; 66:626–636.

[30] X. Wang, C. Huang, W. Cao, X. Gao, W. Liu. Experimental Study on Indoor Thermal Stratification in Large Space by under Floor Air Distribution System (UFAD). Engineering 2011; 3:384-388.

[31] T. Kane, S.K. Firth, K.J. Lomas. How are UK homes heated? A city-wide, socio-technical survey and implications for energy modelling. Energy and Buildings 2015; 86:817–832.

[32] O. Ibrahim, F. Fardoun, R. Younes, H. Louahlia-Gualous. Review of water-heating systems: General selection approach based on energy and environmental aspects. Building and Environment 2014; 72:259-286.

[33] M. Maivel, J. Kurnitski. Heating system return temperature effect on heat pump performance. Energy and Buildings 2015; 94:71–79.

[34] B. Kilkis. Exergy metrication of radiant panel heating and cooling with heat pumps. Energy Conversion and Management 2012; 63:218–224.

[35] A. Ucar, M. Inalli. Thermal and economic comparisons of solar heating systems with seasonal storage used in building heating. Renewable Energy 2008; 33:2532-2539.

[36] N. J. Kelly, P. G. Tuohy, A. D. Hawkes. Performance assessment of tariff-based air source heat pump load shifting in a UK detached dwelling featuring phase change-enhanced buffering. Applied Thermal Engineering 2014; 71: 809-820.

[37] R. Gupta, R. Irving. Development and application of a domestic heat pump model for estimating CO_2 emissions reductions from domestic space heating, hot water and potential cooling demand in the future. Energy and Buildings 2013; 60:60–74.

[38] T. Nuytten, B. Claessens, K. Paredis, J. Van Bael, D. Six. Flexibility of a combined heat and power system with thermal energy storage for district heating. Applied Energy 2013; 104:583–591.

[39] P. Lauenburg, J. Wollerstrand. Adaptive control of radiator systems for a lowest possible district heating returns temperature. Energy and Buildings 2014; 72:132–140.

[40] G. Cao, H. Awbi, R. Yao, Y. Fan, K. Sirén, R. Kosonen, J. Zhang. A review of the performance of different ventilation and airflow distribution systems in buildings. Building and Environment 2014; 73:171-186.

[41] J.N. T. William, B. A.Hazim. Experimental investigation into the thermal performance of a residential hybrid ventilation system. Applied Thermal Engineering 2015; 77:142-152.

[42] K. Chmutina, C. Goodier. Alternative future energy pathways Assessment of the potential of innovative decentralised energy systems in the UK. Energy Policy 2014; 66:62–72.

[43] A. Alamgholilou, E. Esmaeilzadeh. Experimental investigation on hydrodynamics and heat transfer of fluid flow into channel for cooling of rectangular ribs by passive and EHD active enhancement methods. Experimental Thermal and Fluid Science 2012; 38 61–73.

[44] L. Léal, M. Miscevic, P. Lavieille, M. Amokrane, F. Pigache, F. Topin, B. Nogarède, L. Tadrist. An overview of heat transfer enhancement methods and new perspectives: Focus on active methods using electroactive materials. International Journal of Heat and Mass Transfer 2013; 61:505–524.

[45] F. V. Castellões, J. N.N. Quaresma, R. M. Cotta. Convective heat transfer enhancement in low Reynolds number flows with wavy walls. International Journal of Heat and Mass Transfer 2010; 53:2022–2034.

[46] Z. S. Kareem, S. Abdullah, T. M. Lazim, M.N. M. Jaafar, A. F. A. Wahid. Heat transfer enhancement in three-start spirally corrugated tube: Experimental and numerical study. Chemical Engineering Science 2015; 134:746–757.

[47] J. Liu, G. Xie, T. W. Simon. Turbulent flow and heat transfer enhancement in rectangular channels with novel cylindrical grooves. International Journal of Heat and Mass Transfer 2015 81:563–577.

[48] D. L. Gutierrez, A. Hernandez-Guerrero, J. L. Luviano-Ortiz, J. C. Leon-Conejo. Numerical and experimental analysis of heat transfer enhancement in a grooved channel with curved flow deflectors. Applied Thermal Engineering 2015; 75:800-808.

[49] U. V. Awasarmol, A.T. Pise. An experimental investigation of natural convection heat transfer enhancement from perforated rectangular fins array at different inclinations. Experimental Thermal and Fluid Science 2015; 68: 145–154.

[50] A. Korichi, L. Oufer. Heat transfer enhancement in oscillatory flow in channel with periodically upper and lower walls mounted obstacles. International Journal of Heat and Fluid Flow 2007; 28:1003–1012.

[51] S. Gunes, V. Ozceyhan, O. Buyukalaca. Heat transfer enhancement in a tube with equilateral triangle cross sectioned coiled wire inserts. Experimental Thermal and Fluid Science 2010; 34:684–691.

[52] H. M. Sahin, E. Baysal, A. R. Dal, N.S. ahin. Investigation of heat transfer enhancement in a new type heat exchanger using solar parabolic trough systems. International journal of hydrogen energy 2015; 1-13.

[53] Z. J. Zheng, M. J. Li, Y.L. He. Optimization of porous insert configurations for heat transfer enhancement in tubes based on genetic algorithm and CFD. International Journal of Heat and Mass Transfer 2015; 87:376–379.

[54] A. K.Soti, R. Bhardwaj, J. Sheridan. Flow-induced deformation of a flexible thin structure as manifestation of heat transfer enhancement. International Journal of Heat and Mass Transfer 2015; 84:1070–1081.

[55] A. Abdollahi, M. Shams. Optimization of shape and angle of attack of winglet vortex generator in a rectangular channel for heat transfer enhancement. Applied Thermal Engineering 2015; 81:376-387.

[56] Z. Zhang, H. Yan, W. Yang, Y. Zhou, Y. Ding, C. Guan. Heat transfer enhancement in the tube fitted with Left Right helical blade rotors. Applied Thermal Engineering 2013; 55 95-101.

[57] P. Promvonge, S. Eiamsa-ard. Heat transfer enhancement in a tube with combined conical-nozzle inserts and swirl generator. Energy Conversion and Management 2006; 47:2867–2882.

[58] R. Bhadouriy, A. Agrawal, S.V. Prabhu. Experimental and numerical study of fluid flow and heat transfer in an annulus of inner twisted square duct and outer circular pipe. International Journal of Thermal Sciences 2015; 94: 96-109.

[59] T. Yousefi, B. Jaberi, A.Y. Noohdani, B. Farahbakhsh, M.ZiadSaghir. Heat transfer enhancement in T-Tube convertor concept using nanofluids. International Journal of Thermal Sciences 2015; 91:125-132.

[60] A.A. Mohamad. Myth about nano-fluid heat transfer enhancement. International Journal of Heat and Mass Transfer 2015; 86:397–403.

[61] Y. M. Chung, P. G. Tucker. Numerical studies of heat transfer enhancements in laminar separated flows. International Journal of Heat and Fluid Flow 2004; 25:22–31.

[62] R. B. Lakeh, M. Molki, Enhancement of convective heat transfer by electrically-induced swirling effect in laminar and fully-developed internal flows. Journal of Electrostatics 2013; 71:1086-1099.

[63] M. Kaneda, A. Tsuji, H. Ooka, K. Suga. Heat transfer enhancement by external magnetic field for paramagnetic laminar pipe flow. International Journal of Heat and Mass Transfer 2015; 90:388–395.

[64] M. Peng, T. Wang, X. Wang. Effect of longitudinal electrode arrangement on EHD-induced heat transfer enhancement in a rectangular channel. International Journal of Heat and Mass Transfer 2016; 9:3 1072–1081.

[65] B. Tajik, A. Abbassi, M. Saffar-Avval, A. Abdullah, H. Mohammad-Abadi. Heat transfer enhancement by acoustic streaming in a closed cylindrical enclosure filled with water. International Journal of Heat and Mass Transfer 2013; 60:230–235.

[66] S. Orandrou, J. Roy, Y.Bailly, E.Poncet, La. Girardot, D.Ramel. Determination of the heat transfer coefficients for the combined natural and streaming convection on an ultrasonic transducer. International Journal of Heat and Mass Transfer 2013; 62:402–410.

[67] B. Li, X. Han, Z. Wan a, X. Wang, Y. Tang. Influence of ultrasound on heat transfer of copper tubes with different surface characteristics in sub-cooled boiling. Applied Thermal Engineering 2016; 92:93–103.

[68] D. J. Sailor, D. J. Rohli, Q. Fu. Effect of variable duty cycle pulsations on heat transfer enhancement for an impinging air jet. International Journal of Heat and Fluid Flow 1999; 20:574-580.

[69] J. Mohammadpour, M. Rajabi-Zargarabadi, A. S. Mujumdar, H. Ahmadi. Effect of intermittent and sinusoidal pulsed flows on impingement heat transfer from a concave surface. International Journal of Thermal Sciences 2014; 76:118-127.

[70] Y. Wang, Y. L. He, W. W. Yang, Z. D. Cheng. Numerical analysis of flow resistance and heat transfer in a channel with delta winglets under laminar pulsating flow. International Journal of Heat and Mass Transfer2015; 82:51–65.

[71] H. Saitoh. Flow and heat transfer around the flat plate installed in a rectangular duct with flow pulsation. 16th International Symposium on Transport Phenomena, Prague 2015.

[72] J. E. DEC, J. O. Keller. Pulse Combustor Tail-Pipe Heat-Transfer Dependence on Frequency, Amplitude, and Mean Flow Rate COMBUSTION AND FLAME 1989; 77:359-374.

[73] A.E. Zohir. The Influence of Pulsation on Heat Transfer in a Heat Exchanger for Parallel and Counter Water Flows. New York Science Journal 2011.

[74] M. A. Habib, S. A. M. Said, A. A. Al-Farayedhi, S. A. Al-Dini, A. Asghar, S. A. Gbadebo. Heat transfer characteristics of pulsated turbulent pipe flow. Heat and Mass Transfer 1999; 34: 413-421.

[75] M. Jafari, M. Farhadi, K. Sedighi. Pulsating flow effects on convection heat transfer in a corrugated channel A LBM approach. International Communications in Heat and Mass Transfer 2013; 45:146–154.

[76] B. Olayiwola, P. Walzel. Cross-flow transport and heat transfer enhancement in laminar pulsed flow. Chemical Engineering and Processing 2008; 47:929–937.

[77] L. I. Guoneng, Z. Youqu, H.U. Guilin, Z. Zhiguo. Convective Heat Transfer Enhancement of a Rectangular Flat Plate by an Impinging Jet in Cross Flow. Chinese Journal of Chemical Engineering 2014; 22:489-495.

[78] M. Pourgholam, E. Izadpanah, R. Motamedi, S. E. Habibi. Convective heat transfer enhancement in a parallel plate channel by means of rotating or oscillating blade in the angular direction. Applied Thermal Engineering 2015; 78: 248-257.

[79] J. Shi, J. Hu, S. R. Schafer, C.L. Chen. Numerical study of heat transfer enhancement of channel via vortex-induced vibration. Applied Thermal Engineering 2014; 70 838-845.

[80] F. Baffigi, C. Bartoli. Heat transfer enhancement in natural convection between vertical and downward inclined wall and air by pulsating jets. Experimental Thermal and Fluid Science 2010; 34: 943–953.

[81] H. Gomaa, A.M. Al Taweel. Effect of oscillatory motion on heat transfer at vertical flat surfaces. International Journal of Heat and Mass Transfer 2005; 48:1494–1504.

[82] P. S. Mahapatra, N.K. Manna, K. Ghosh, A. Mukhopadhyay. Heat transfer assessment of an alternately active bi-heater undergoing transient natural convection. International Journal of Heat and Mass Transfer 2015; 83:450–464.

[83] D. Klein, G. Hetsroni. Enhancement of heat transfer coefficients by actuation against an impinging jet. International Journal of Heat and Mass Transfer 2012; 55: 4183-4183.

[84] A. Ploski, S. Holmberg. Low-temperature baseboard heaters with integrated air supply e An analytical and numerical investigation. Building and Environment 2011; 46: 176-186.

[85] J. A. Myhren, S. Holmberg. Performance evaluation of ventilation radiators. Applied Thermal Engineering 2013; 51:315-324.

[86] G.C. E. Tsioliaridou, N.F. Tsagas. Experimental investigation of a low energy consumption air conditioning system based on conventional central heating installation. Energy and Buildings 2006; 38:45–52.

[87] A. Ploski, S. Holmberg. Performance evaluation of radiant baseboards (skirtings) for room heating- An analytical and experimental approach. Applied Thermal Engineering 2014; 62:382-389.

[88] A.K.A. Shati, S.G. Blakey, S.B.M. Beck. The effect of surface roughness and emissivity on radiator output. Energy and Buildings 2011; 43:400–406.

[89] S.M.B. Beck, S.C. Grinsted, S.G. Blakey, K. Worden. A novel design for panel radiators. Applied Thermal Engineering 2004; 24:1291–1300.

[90] K. Kerrigan, H. Jouhara, G.E. O'Donnell, A.J. Robinson. A naturally aspirated convector for domestic heating application with low water temperature sources. Energy and Buildings 2013; 67: 187–194.

[91] K. Kerrigan, H. Jouhara, G.E.O.Donnell, A.J. Robinson. Heat pipe-based radiator for low grade geothermal energy conversion in domestic space heating; Simulation Modelling Practice and Theory 2011; 19: 1154–1163.

[92] B. Kilkis. Exergy metrication of radiant panel heating and cooling with heat pumps. Energy Conversion and Management 2012; 63:218–224.

[93] A. M. Diaz, C. O. Galan, J. B. B. Rodriguez, J. J. F. Calleja. Thermal analysis of a stoneware panel covering radiators. Applied Energy 2014; 131: 248–256.

[94] S. K. Roy, B. L. Avanic. Optimization of a space radiator with energy storage. International Communications in Heat and Mass Transfer 2006; 33: 544–551.

[95] E. Aydar, I. Ekmekçi. Thermal efficiency estimation of the panel type radiators with CFD analysis. Journal of Thermal Science and Technology 2012; 32:63-71.

[96] M. Embaye, R.K. AL-Dadah, S. Mahmoud. Thermal performance of hydronic radiator with flow pulsation-Numerical investigation Applied Thermal Engineering 2015; 80:109-117.

[97] L. D. Pereira, D. Raimondo, S. P. Corgnati, M. G. da Silva. Assessment of indoor air quality and thermal comfort in Portuguese secondary classrooms: Methodology and results. Building and Environment 2014; 81: 69-80.

[98] G. M. Huebner, J. Cooper, K. Jones. Domestic energy consumption—what role do comfort, habit, and knowledge about the heating system play. Energy and Buildings 2013; 66:626–636.

[99] C. Zhu, N. Li, D. Re, J. Guan. Uncertainty in indoor air quality and grey system method. Building and Environment 2007; 42: 1711–1717.

[100] I. Sarbu, C. Sebarchievici. Aspects of indoor environmental quality assessment in buildings. Energy and Buildings 2013; 60:410–419.

[101] J. A. Myhren, S. Holmberg. Flow patterns and thermal comfort in a room with panel floor and wall heating. Energy and Buildings 2008; 40: 524–536.

[102] Z. Sun, S. Wang. A CFD-based test method for control of indoor environment and space ventilation. Building and Environment 2010; 45:1441–1447.

[103] L. Wang, N. H. Wong. Coupled simulations for naturally ventilated rooms between building simulation (BS) and computational fluid dynamics (CFD) for better prediction of indoor thermal environment. Building and Environment 2009; 44:95–112.

[104] K. Horikiri, Y. Yao, J. Yao. Modelling conjugate flow and heat transfer in a ventilated room for indoor thermal comfort assessment. Building and Environment 2014; 77: 135-147.

[105] O. Arslan, R. Kose. Thermo economic optimization of insulation thickness considering condensed vapour in buildings. Energy and Buildings 2006; 38:1400–1408.

[106] H. Ge, P. Fazio. Experimental investigation of cold draft induced by two different types of glazing panels in metal curtain walls. Building and Environment 2004; 39; 115 – 125.

[107] G. Sevilgen, M. Kilic. Numerical analysis of air flow, heat transfer, moisture transport and thermal comfort in a room heated by two-panel radiators. Energy and Buildings 2011; 43: 137–146.

[108] L. Tian, Z. Lin, Q. Wang. Experimental investigation of thermal and ventilation performances of stratum ventilation. Building and Environment 2011; 46:1309-1320.

[109] T. Liua , Z. Liua, G. Lia , Z. Zuoa. Comparative Study of Numerical Simulation of Indoor Thermal Environment in the Pattern of Personalized Ventilation and Stratum Ventilation. Procedia Engineering 2015; 121:785 – 791.

[110] H. J. Moriske, M. Drews, G. Ebert, G. Menk, C. Scheller, M. Schandube, L. Konieczny. Indoor air pollution by different heating systems: coal burning, open fireplace and central heating. Toxicology Letters 1996; 88:349-354.

[111] G. McGill, L. O. Oyedele, K. McAllister. Case study investigation of indoor air quality in mechanically ventilated and naturally ventilated UK social housing. International Journal of Sustainable Built Environment 2015.

[112] M. Ncube, S. Riffat. Developing an indoor environment quality tool for assessment of mechanically ventilated office buildings in the UK - A preliminary study. Building and Environment 2012; 53:26-33.

[113] J. Seoa, R. Ooka, J. T. Kim, Y. Nam. Optimization of the HVAC system design to minimize primary energy demand. Energy and Buildings 2014; 76:102–108.

[114] L. Yang, H. Yan, J. C. Lam. Thermal comfort and building energy consumption implications-A review. Applied Energy 2014; 115: 164–173.

[115] A. Buli_nska, Z. Popio, Z. Buli_nski. Experimentally validated CFD analysis on sampling region determination of average indoor carbon dioxide concentration in occupied space. Building and Environment 2014; 72:319-331.

[116] B. F. Warren, N. C. Harper Demand controlled ventilation by room C02 concentration: a comparison of simulated energy savings in an auditorium space Energy and Buildings 1991; 17: 87-96.

[117] P. L. Chan, P. H. F. Yu, Y. W. Cheng, C. Y. Chan, P. K. Wong. Comprehensive characterization of indoor airborne bacterial profile. Journal of Environmental Sciences 2009; 21:1148–1152.

[118] P. Wolkoff. Indoor air pollutants in office environments: Assessment of comfort, health and performance. International Journal of Hygiene and Environmental Health 2013; 216: 371– 394.

[119] J. W. Wan, K. Yang, W. J. Zhang, J. L. Zhang. A new method of determination of indoor temperature and relative humidity with consideration of human thermal comfort. Building and Environment 2009; 44:411– 417.

[120] A. Makhoul, K. Ghali, N. Ghaddar.Thermal comfort and energy performance of a low-mixing ceiling-mounted personalized ventilator system. Building and Environment 2013; 60:126-136.

[121] C. Chengmin, Z. Yufeng, M. Lijun. Assessment for central heating systems with different heat sources: A case study. Energy and Buildings 2012; 48:168–174.

[122] Z. Liaoa, A.L. Dexterb. A simplified physical model for estimating the average air temperature in multi-zone heating systems. Building and Environment 2004; 39:1013-1022.

[123] L. Peeters, J. V. Veken, H. Hens, L. Helsen , W. D. haeseleer. Control of heating systems in residential buildings: Current practice. Energy and Buildings 2008; 40:1446-1455.

[124] F. Tahersima, J. Stoustrup, H. Rasmussen. Eliminating Oscillations in TRV-Controlled Hydronic Radiators 50th IEEE Conference on Decision and Control and European Control Conference (CDC-ECC) Orlando, FL, USA, 2011.

[125] M. Embaye, R.K. AL-Dadah, S. Mahmoud. Effect of flow pulsation on energy consumption of a radiator in a centrally heated building. International Journal of Low-Carbon Technologies 2014; 0: 1-11.

[126] M. Gamberi, R. Manzini, A. Regattieri. Simulink_ simulator for building hydronic heating systems using the Newton–Raphson algorithm. Energy and Buildings 2009; 41:848–855.

[127] M. R. Kulkarni, F. Hong. Energy optimal control of a residential space-conditioning system based on sensible heat transfer modelling. Building and Environment 2004; 39:31-38.

[128] Q. Qi, S. Deng. Multivariable control of indoor air temperature and humidity in a direct expansion (DX) air conditioning (A/C) system. Building and Environment 2009; 44:1659–1667.

[129] R. Z. Homod, K. S. M. Sahari, H.A.F. Almurib. Energy saving by integrated control of natural ventilation and HVAC systems using model guide for comparison. Renewable Energy 2014; 71:639-650.

[130] N. Nassif. A robust CO_2-based demand-controlled ventilation control strategy for multi-zone HVAC systems. Energy and Buildings 2012; 45: 72–81.

[131] S. R. West, J. K. Ward, J. Wall. Trial results from a model predictive control and optimisation system for commercial building HVAC. Energy and Buildings 2014; 72:271–279.

[132] J. W. Moon, JH. Lee, S. Kim. Application of control logic for optimum indoor thermal environment in buildings with double skin envelope systems. Energy and Buildings 2014; 85:59–71.

[133] G.C. Bakos, A. Sismanis. Modelling of small scale central heating installation using artificial neural networks aiming at low electric energy consumption. Energy and Buildings 2013; 62:126–132.

[134] J. Gustafsson, J. Delsing, J. Deventer. Improved district heating substation efficiency with a new control strategy. Applied Energy 2010; 87: 1996–2004.

[135] L. Liu, L. Fu, Y Jiang. A new wireless on-off control technique for adjusting and metering household heat in district heating system. Applied Thermal Engineering 2012; 36:202-209.

[136] B. Lehmann, D. Gyalistras, M. Gwerder, K. Wirth, S. Carl. Intermediate complexity model for Model Predictive Control of Integrated Room Automation. Energy and Buildings 2013; 58:250–262.

[137] M.Schmelas , T. Feldmann, E. Bollin. Adaptive predictive control of thermo-active building systems (TABS) based on a multiple regression algorithm. Energy and Buildings 2015; 103:14–28.

[138] Z. Liao, A.L. Dexter. The potential for energy saving in heating systems through improving boiler controls. Energy and Buildings 2004; 36:261–271.

[139] C. Verhelst, F. Logist, J. V. Impe, L. Helsen. Study of the optimal control problem formulation for modulating air-to-water heat pumps connected to a residential floor heating system. Energy and Buildings 2012; 45:43–53.

[140] A. Koca, Z. Gemici, Y. Topacoglu, G. Cetin, R. C. Acet, B. B. Kanbur. Experimental investigation of heat transfer coefficients between hydronic radiant heated wall and room. Energy and Buildings 2014; 82:211–221.

[141] A. Persily. Challenges in developing ventilation and indoor air quality standards: The story of ASHRAE Standard 62. Building and Environment 2015; 1-9.

[142] S. Wei, R. Jones, P. Wilde. Driving factors for occupant-controlled space heating in residential buildings. Energy and Buildings 2014; 70: 36–44.

[143] J. Srebric, Q. Chen. An example of verification, validation, and reporting of indoor environment CFD analyses. ASHRAE Transactions 2002; 108:185-194.

[144] M. Adolph, N. Kopmann, B. Lupulescu, D. Müller. Adaptive control strategies for single room heating. Energy and Buildings 2014; 68: 771–778.

[145] A. S. White. Simulation of Domestic Boiler Control. International journal of simulation system science and technology 2010; 11:22-32.

[146] T. Fatemeh, S. Jakob, R. Henrik. An analytical solution for stability-performance dilemma of hydronic radiators. Energy and Buildings 2013; 64: 439–446.

[147] I. Ballarini, V.Corrado. Analysis of the building energy balance to investigate the effect of thermal insulation in summer conditions. Energy and Buildings 52 2012) 168–180.

[148] A. Beghi, L. Cecchinato, M. Rampazzo, F. Simmini. Energy efficient control of HVAC systems with ice cold thermal energy storage. Journal of Process Control 2014; 24:773–781.

[149] B. Anna, P. Zbigniew, B Zbigniew. Experimentally validated CFD analysis on sampling region determination of average indoor carbon dioxide concentration in occupied space. Building and Environment 2014; 72:319-331.

[150] M. K. Mohamad. Control system of building using modelling and simulation. PhD thesis 2014.

[151] S.L.C. Hugo, K.U. L. Hens. Heat, Air and Moisture Transfer in Highly Insulated Building Envelopes (Hamtie). International Energy Agency, 2002.

[152] D.S.Sougan, L. Damiano. CO_2-based demand control ventilation (DCV). ASHRAE Journal 2004; 47-53.

[153] https://www.plumbnation.co.uk/site/boilers/?manufacturer=worcester&page=1 [[accessed 25/10/2014].

[154] engineeringtoolbox.com [accessed on 12/10/2014].

[155] T. Glatzel, C.Litterst, C. Cupelli, T. Lindemann, C.Moosmann,R.Niekrawietz, W.Streule, R.Zengerle, P.Koltay. Computational fluid dynamics (CFD) software tools for microfluidic applications – A case study. Computers & Fluids 2008; 37:218–235.

[156] A. Ploskic; S. Holmberg. Performance evaluation of radiant baseboards (skirtings) for room heating-Analitical and experimental approach. Applied Thermal Engineering 2014; 62: 382-389.

[157] J. Are Myhren, S. Holmberg. Performance evaluation of ventilation radiator. Thermal Science and Technology 2012; 32:2, 63-71.

[158] A. Berkan. Simulation of the heater test room defined by EN442 standard and virtual testing of different type of heaters (PhD thesis). 2011

[159] T. ÜÇOK ERKEK, A. GÜNGÖR. EXPERIMENTAL PERFORMANCE EVALUATION OF PCM THERMAL STORAGE IN A PANEL RADIATOR Mediterranean Congress of Climatization, Istanbul, 3-4 October, 2013.

[160] X. Shuai, S. Cheng, G. Antonini. Pulsation effects on convective heat transfer in the laminar flow of a viscous fluid. The Canadian Journal of Chemical Engineering, 1994; 72: 468 – 475.

[161] COMSOL Multiphysics version 4.3.

[162] I. Gherasim, N. Galanis, C. T.Nguyen .Heat transfer and fluid flow in a plate heat exchanger. Part II: Assessment of laminar and two-equation turbulent models. International Journal of Thermal Sciences 2011, 50:1499-1511.

[163] M. A. John, S. Halberg. Design Consideration with ventilation-radiators comparisons to traditional two-panel radiators. Energy and buildings 2009; 41: 92-100.

[164] H. Kana, Y. Yufeng, Y. Jun. Modelling conjugate flow and heat transfer in a ventilated room for indoor thermal comfort assessment. Building and Environment 2014; 77:135-147.

[165] P. T. Bhaskoro, I. Syed, M. S. Aris. Numerical analysis of air flow, heat transfer, moisture transport and thermal comfort in a room heated by two-panel radiators. Energy and Buildings 2011; 43:137–146.

[166] F. Ascione, N. Bianco, C. D. Stasio, G. M. Mauro, G. P. Vanoli. Dynamic insulation of the building envelope: Numerical modelling under transient conditions and coupling with nocturnal free cooling. Applied Thermal Engineering 2015; 84:1-14.

[167] Z. Fanga, N. Li a, B. Li, G. Luo, Y. Huanga. The effect of building envelope insulation on cooling energy consumption in summer. Energy and Buildings 2014; 77:197–205.

[168] R. J. Deara, G. S. Brager. Thermal comfort in naturally ventilated buildings: revisions to ASHRAE Standard. Energy and Buildings 2002; 34:549–561.

[169] F. Cappelletti, A. Prada, P. Romagnoni, A. Gasparella. Passive performance of glazed components in heating and cooling of an open-space office under controlled indoor thermal comfort. Building and Environment 2014; 72:131-144.

[170] Q. Minglua, X. Liang, S. Deng, J. Yiqiang. Improved indoor thermal comfort during defrost with a novel reverse-cycle defrosting method for air source heat pumps. Building and Environment 2010; 45:2354-2361.

[171] G. Heidarinejad, M. H. Fathollahzadeh, H. Pasdarshahri. Effects of return air vent height on energy consumption, thermal comfort conditions and indoor air quality in an under floor air distribution system. Energy and Buildings 2015; 97:155–161.

[172] J. Langmans, A. Nicolai, R. Klein, S. Roels. A quasi-steady state implementation of air convection in a transient heat and moisture building component model. Building and Environment 2012; 58:208-218.

[173] K. Bangert, Radiator heat transfer augmentation by changes to wall surface roughness and emissivity. University of Sheffield, 2010.

[174] A. Ploskic, S. Holmberg. Heat emission from skirting boards. Building and Environment 2010; 45:1123-1133.

[175] The Harmonisation of Thermal Properties of Building Materials:http://www.esru.strath.ac.uk/Documents/89/thermop_rep.pdf [accessed 30/09/2014].

[176] J. R. D. Dear, G.S. Brager. Thermal comfort in naturally ventilated buildings: revisions to ASHRAE Standard 55. Energy and Buildings 2002; 34:549-561.

[177] Z. Vlahostergios, D.Missirlis, M.Flouros, C. Albanakis, K.Ykinthos. Effect of turbulence intensity on the pressure drop and heat transfer in a staggered tube bundle heat exchanger. Experimental Thermal and Fluid Science 2014; 60: 75-82.

[178] A. Berkan. Simulation of the heater test room defined by EN442 standard and virtual testing of different type of heaters (PhD thesis). 2011.

[179] https://www.arduino.cc/en/main/software**[accessed 03/08/2015].** [accessed 15/07/2015].

[180] http://www.danielsoper.com/statcalc3/calc.aspx?id=10 [accessed 15/07/2015].

[181] A. M. Elsayed. Heat Transfer in Helically Coiled Small Diameter Tubes for Miniature Cooling Systems. PhD thesis (online). 2011.

[182] T. ÜÇOK ERKEK, A. GÜNGÖR. EXPERIMENTAL PERFORMANCE EVALUATION OF PCM THERMAL STORAGE IN A PANEL RADIATOR Mediterranean Congress of Climatization, Istanbul, 3-4 October, 2013.

[183] https://www.korado.com/common/downloads/radik-steel-panel-radiators.pdf [accessed 15/08/2015].

Appendix A

(A.1) Heated room embedded MatLab code

```
function

[dT_room_dt,Q_window,Q_Trans,Q_int,Q_vent_s,dW_ind_dt,Rh_ind,dC_ind_d
t] = fcn(T_ind,Q_rad,V_pp,W_ind,T_amb,Rh_amb,Madd_rev,G,CO2_ind)

%, dW_ind_dt,dC_ind_dt
% calcualting the window thermal loss and gaind of the intersted room


I = 0;             %w/m^2;
SC = 0.87;
U_window = 3;        %W/(m^2K)
A_window = 1.82;     %m^2;
h_amb =22.5;           %W/m^2K
alpha= 0.2;
T_so = T_amb+alpha*I/h_amb;

Q_window = -(U_window*A_window*(T_so-T_ind) +I*SC*A_window);

%Q_loss due walls, floors,and ceilings,

U_wall = 0.86;
U_floor=0.35;
U_ceiling=0.3;
A_wall=13.5;
A_floor=20;
A_ceiling=20;
V_rm = 54;

n = 5; % number of people;
Q_pp = 100*n; %w
Q_comp = 150; %W
Q_ele  = 50;  % W

Q_int = Q_pp+Q_comp+Q_ele;

% Q_loss due ventilation  (sensible)

% N= 3/3600;       %ACH       %m^3
rho = 1.2;      %kg/m^3
Cp_a= 1200;      %J/Kg/K
V_flr = 0.6*A_floor;

Q_vent_s = ((V_pp+V_flr)/1000)*rho*Cp_a*(T_ind-T_amb);

Q_Trans = U_wall*A_wall*(T_ind-T_amb)+U_floor*A_floor*(T_ind-
T_amb)+U_ceiling*A_ceiling*(T_ind-T_amb);

dT_room_dt = (Q_rad+Q_int-Q_vent_s-Q_Trans-Q_window)/(V_rm*Cp_a*rho)
```

```
%function [dW_ind_dt,Rh_ind,W_amb,Q_vent_l] =
fcn(V_pp,W_ind,T_amb,T_ind,Rh_amb,Madd_rev)

P_amb = 101325; %pa
P_ind = 101325; %Pa
% Ps_amb =256*T_amb-3373; %pa
% Ps_ind = 256*T_ind-3373; %Pa;
T_amb1 = T_amb+273;
T_ind1= T_ind+273;

Ps_amb = (exp(77.345+0.0057*T_amb1-7235/T_amb1))/T_amb1^8.2;

Ps_ind = (exp(77.345+0.0057*T_ind1-7235/T_ind1))/T_ind1^8.2;

W_amb = (0.622*Rh_amb*Ps_ind)/(P_amb-Rh_amb*Ps_amb);

%  W_ind = (0.622*Rh_ind*Ps_ind)/(P_ind-Rh_ind*Ps_ind);

Rh_ind= (W_ind*P_ind)/(Ps_ind-(W_ind+0.622));

rho_m= 1.1;
h_fg = 2260*10^3;
A_floor=20;

V_rm = 54;
M_rm = 1.2*V_rm;   % kg
% M_pp = 0.00001857;
M_pp = 0.00001;
V_flr = 0.6*A_floor;

Q_vent_l= rho_m*h_fg*((V_pp+V_flr)/1000)*(W_ind-W_amb);

dW_ind_dt= ((((V_pp+V_flr)/1000)*rho_m)*(W_amb-
W_ind)+M_pp+Madd_rev)/M_rm

%function dC_ind_dt = fcn(V_pp,G,CO2_ind)


% G= 5*10^-6 % m^3/s about 990 ppm
CO2_amb = 0.0004 % m^3/s about 300 ppm
V_rm = 54     %m^2

dC_ind_dt = (G*4+(V_pp/1000)*CO2_amb-(V_pp/1000)*CO2_ind)/(V_rm)
```

(A.2) Embedded code for the radiator model

```
function [dTdt,Q_rad,LMTD] = fcn(m_w,T_in_rad,T_rad_out,T_ind)

C_p_w=4180 %J/kg/K
C_p_rad=800 %J/kg/K
```

```
M_rad=5; %kg
A=2.2%m^2
h=8.5; %W/m^2/K
M_w =3; %kg;
LMTD=((T_in_rad+T_rad_out)/2)-T_ind;
term1=C_p_w*m_w*(T_in_rad-T_rad_out)/(C_p_rad*M_rad+C_p_w*M_w);
term2 = h*A*LMTD/(C_p_rad*M_rad+C_p_w*M_w);
dTdt=2*(term1-term2);

% dTdt =2*(term1)

Q_rad=h*A*LMTD;
```

(A.3) Embedded code for the boiler model

```
functiondT_bdt = fcn(Tb_in,Tb_out,Q_b, m_dot)

C_p_w1=4180; %J/kg/K
C_p_hex1=420; %J/kg/K
M_w1=12; %kg
M_hex1=7;%kg
eff_b=0.9;

Term1 = (eff_b*Q_b-(m_dot*C_p_w1*(Tb_out-Tb_in)));
Term2 =(C_p_w1*M_w1+C_p_hex1*M_hex1);

dT_bdt= 2*(Term1/Term2);
```

Appendix B

The following figures show the temperature relations between RTD and the thermocouples. This is part of the thermocouple calibration work presented in chapter 6 section 6.2.2.1 and the thermocouples in figures B1.1 and B1.2 are for the surface thermocouples; while figure B1.3 is for probe thermocouples.

(B.1) Calibration surface thermocouples

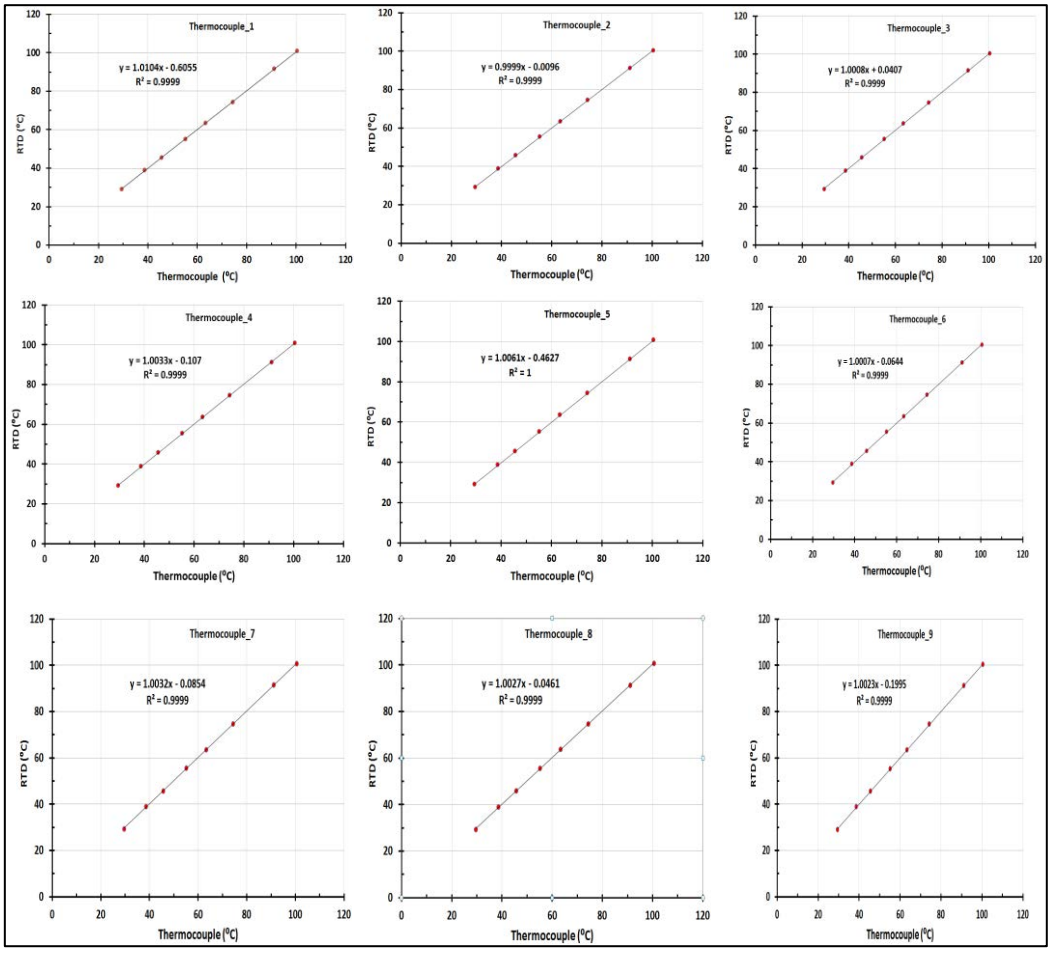

Figure B1.1 temperature relations between RTD and surface thermocouples 1 to 9

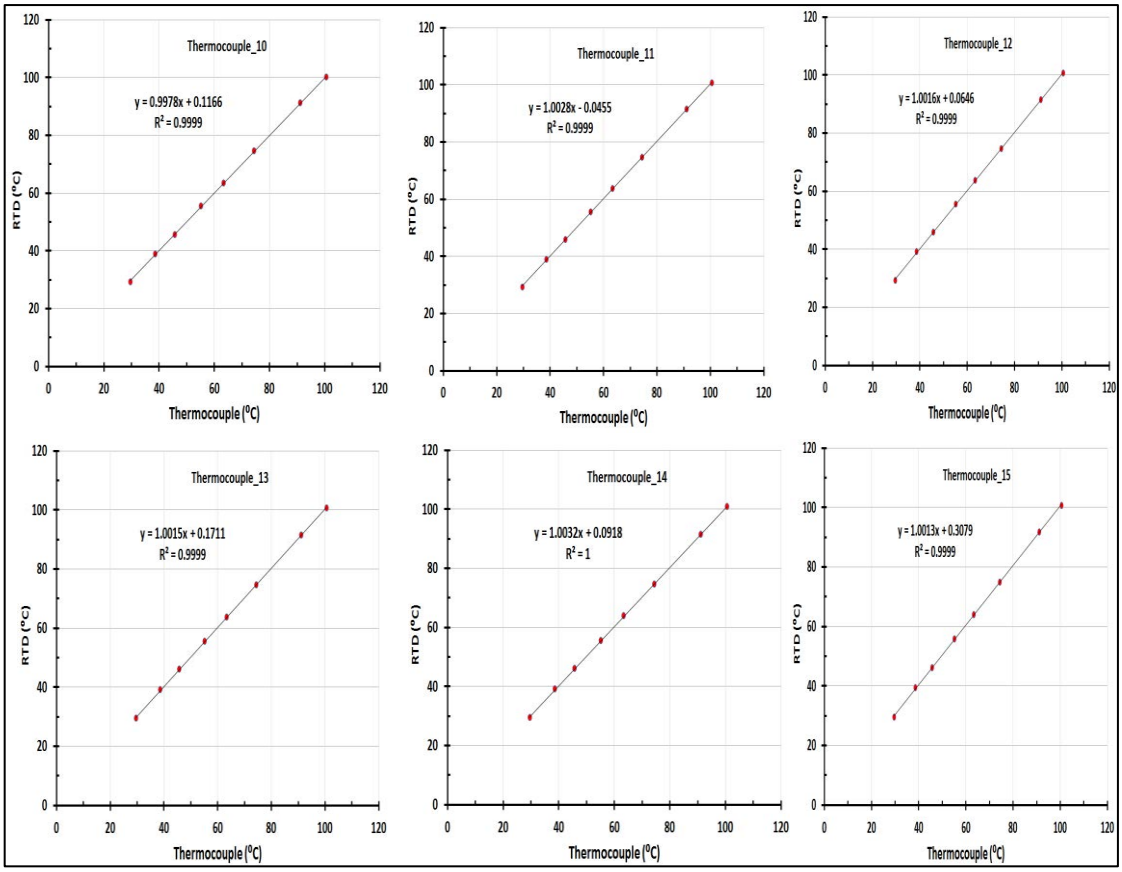

Figure B.1.2 temperature relations between RTD and surface thermocouples 10 to 15.

(B.2) Calibration of probe thermocouples

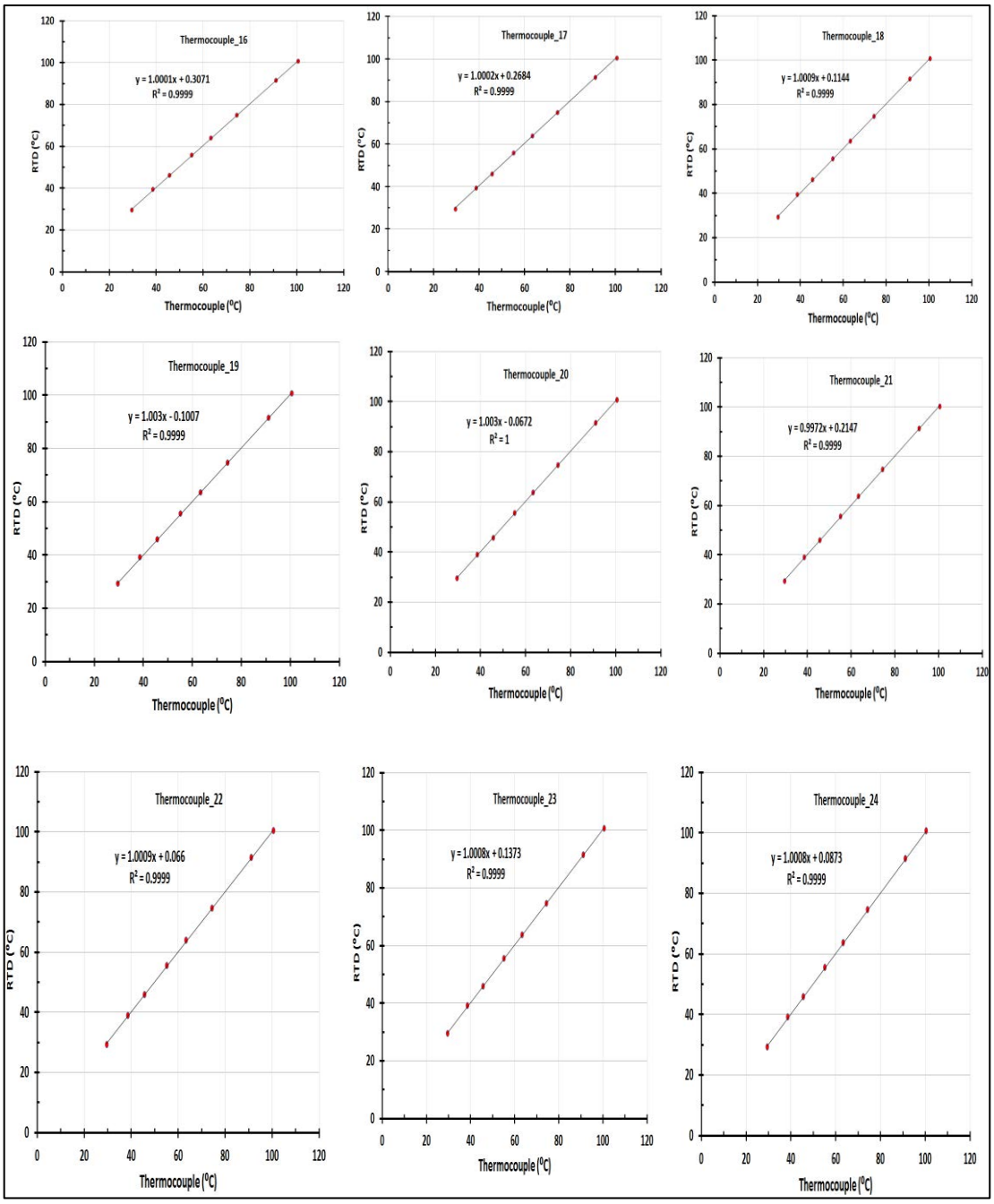

Figure B1.3 temperature relations between RTD and probe thermocouples include thermocouple 16 to 21 for the heated room, thermocouple 22 to 23 for the inlet/outlet of hot water radiator and thermocouple 24 is the for the outdoor air.

The following code was developed in Arduino open source software aiming to control the operating condition of the hydronic radiator at constant and pulsed flow strategies as described in chapter 6 section 6.2.3.

(B.3) Arduino code for operating radiator

(B.3.1) constant flow

```
floattempC;
inttempPin=0; //Temp sensor plugged analog pin 0
intmotorPin=4;
void setup()
{
Serial.begin(9600); // opens the serial port communicate with the temp sensors
  //Setup Channel A
pinMode(12, OUTPUT); //Initiates Motor Channel A pin
pinMode(9, OUTPUT); //Initiates Brake Channel A pin
  //Setup Channel B
pinMode(13, OUTPUT); //Initiates Motor Channel A pin
pinMode(8, OUTPUT);  //Initiates Brake Channel A pin
pinMode(motorPin,OUTPUT); // motor ouside of the shield
}
void loop()
{
tempC = analogRead(tempPin);
tempC = (5.0*tempC*100.0)/1024.0;
Serial.print("T=");
```

```
Serial.print (tempC);
Serial.print ("degC");
Serial.println();
delay (15000);

if (tempC>20)
{
digitalWrite(9, HIGH);  //Engage the Brake for Channel A  (forward valve)
digitalWrite(8, LOW);  //Disengage the Brake for Channel B (by pass valve)
digitalWrite(4, HIGH); //turn on the signals
}
else
{
digitalWrite(12, HIGH); //Establishes forward direction of Channel A
digitalWrite(9, LOW);   //Disengage the Brake for Channel A (forward valve)
analogWrite(3, 255);   //Spins the motor on Channel A at full speed

digitalWrite(13,HIGH); //Establishes forward direction of Channel B
digitalWrite(8, HIGH);   //Engage the Brake for Channel B (bypass valve)
analogWrite(11, 255);   //Spins the motor on Channel B at full speed
}
}
```

(B.3.2) Pulsed flow scenario

```
floattempC;
inttempPin=0; //Temp sensor plugged analog pin 0
intmotorPin=4;
void setup()
{
Serial.begin(9600); // opens the serial port communicate with the temp sensors
  //Setup Channel A
pinMode(12, OUTPUT); //Initiates Motor Channel A pin
pinMode(9, OUTPUT); //Initiates Brake Channel A pin

  //Setup Channel B
pinMode(13, OUTPUT); //Initiates Motor Channel A pin
pinMode(8, OUTPUT);  //Initiates Brake Channel A pin

pinMode(motorPin,OUTPUT); // motor ouside of the shield
}
void loop()
{
tempC = analogRead(tempPin);
tempC = (5.0*tempC*100.0)/1024.0;
Serial.print("T=");
Serial.print (tempC);
Serial.print ("degC");
```

```
Serial.println();
//delay (15000);

if (tempC>20)
{
  digitalWrite(9, HIGH);  //Engage the Brake for Channel A  (forward valve)
digitalWrite(8, LOW);  //Disengage the Brake for Channel B (by pass valve)
digitalWrite(4, HIGH); //turn on the signals
}
else
{
  //Motor A forward @ full speed
digitalWrite(12, HIGH); //Establishes forward direction of Channel A
digitalWrite(9, LOW);   //Disengage the Brake for Channel A (forward valve)
analogWrite(3, 255);   //Spins the motor on Channel A at full speed

digitalWrite(13,HIGH); //Establishes forward direction of Channel B
digitalWrite(8, HIGH);   //Engage the Brake for Channel B (bypass valve)
analogWrite(11, 255);   //Spins the motor on Channel B at full speed

digitalWrite(4, LOW); //turn off the signals

delay(15000);

digitalWrite(12, HIGH); //Establishes forward direction of Channel A
```

```
digitalWrite(9, HIGH);   //Engage the Brake for Channel A (forward valve)
analogWrite(3, 255);   //Spins the motor on Channel A at full speed

digitalWrite(13, HIGH); //Establishes forward direction of Channel B
digitalWrite(8, LOW);   //Disengage the Brake for Channel B (bypass valve)
analogWrite(11, 255);   //Spins the motor on Channel B at full speed

digitalWrite(4, HIGH); //turn on the signals

delay(15000);
}
}
```

Appendix C

Validation of the local temperature distribution of the radiator operating at pulsed and constant flow scenario tested numerically as well as experimentally.

(C.1) Validation surface temperature for non-insulated radiator

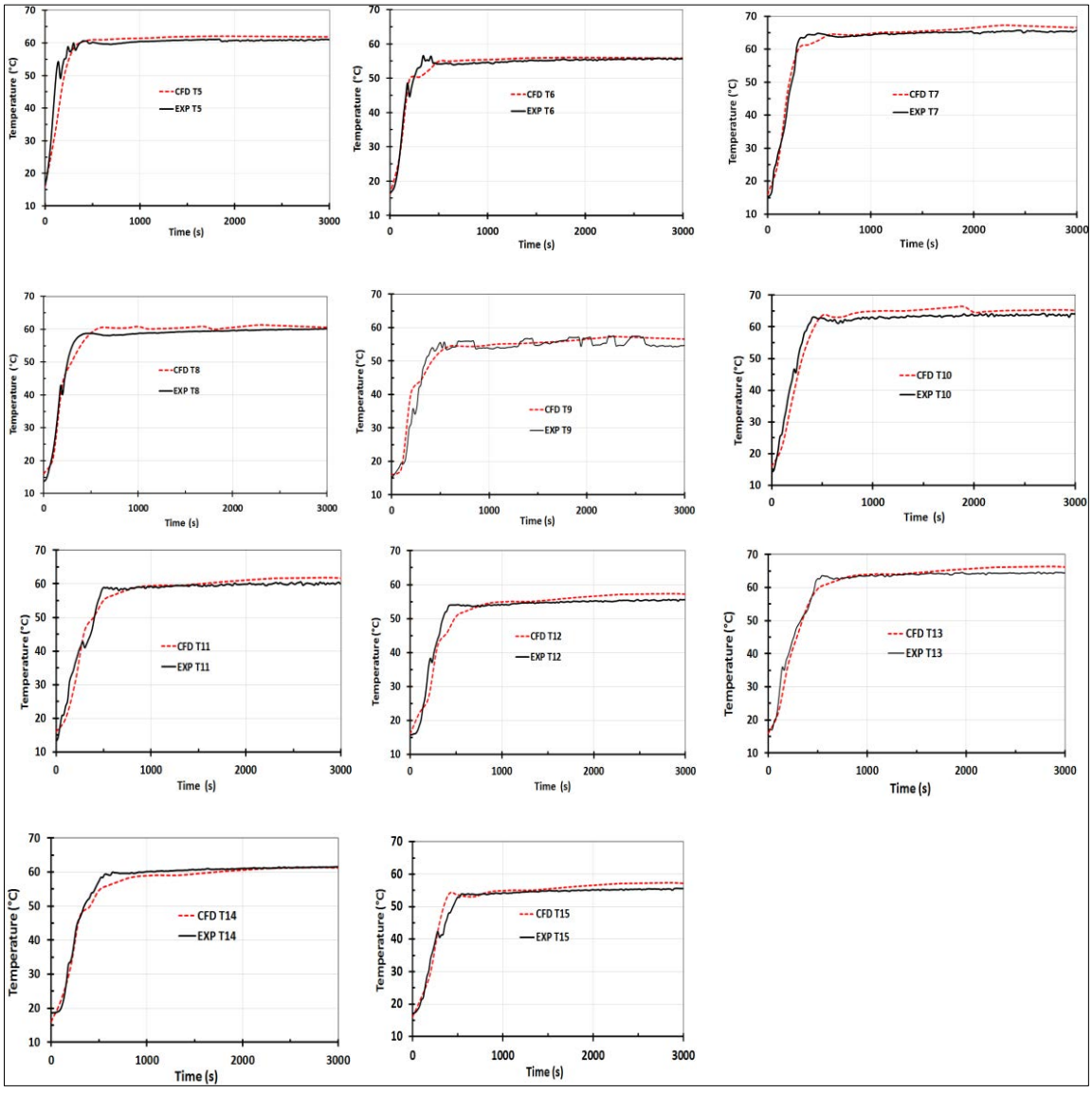

Figure C.1.1 local surface temperature distribution on non-insulated radiator for numerically (CFD) and experimentally (EXP) using T5 to T15 operating at constant flow

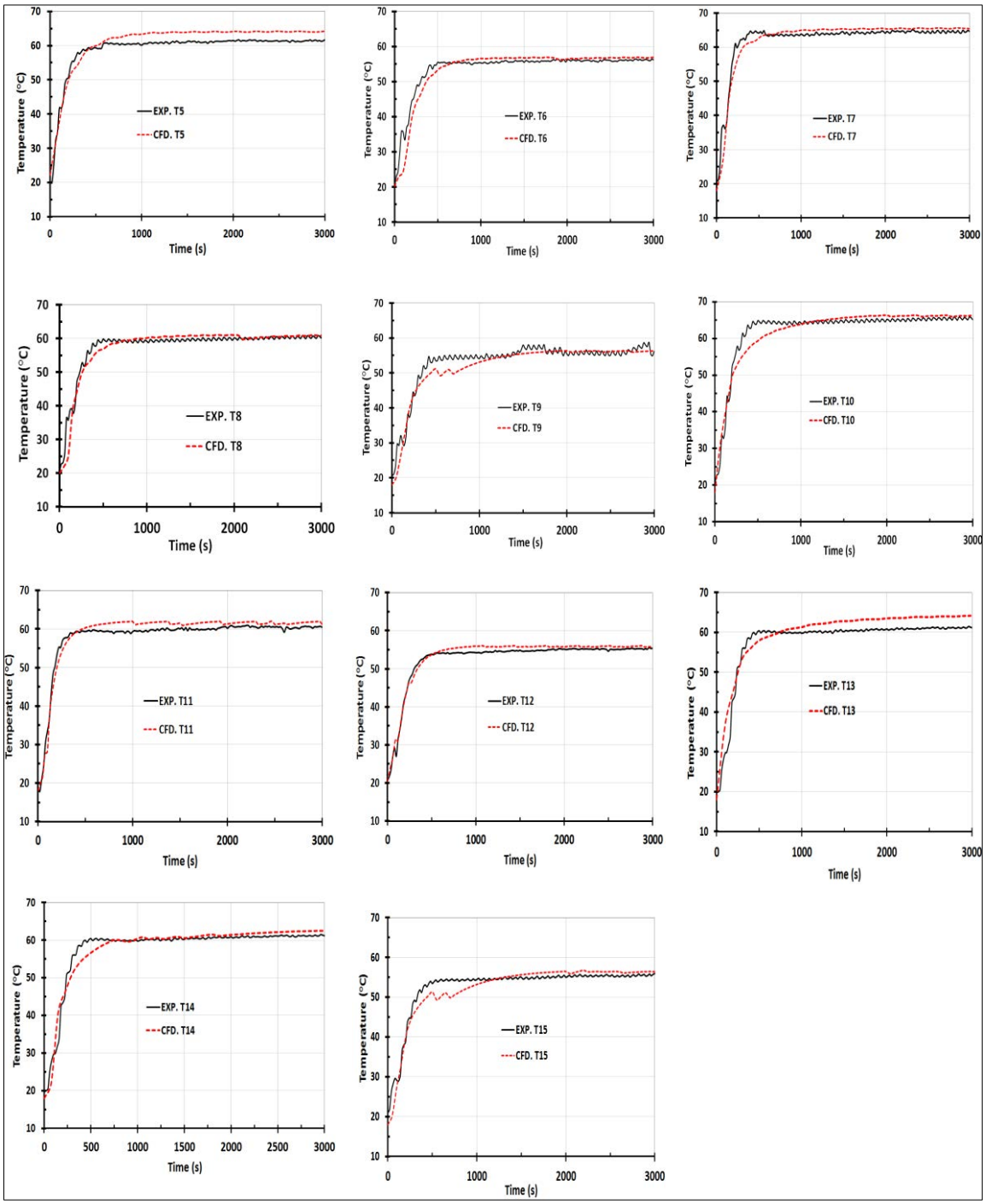

Figure C.1.2 local surface temperature distribution on non-insulated radiator at experimentally (EXP) and numerically (CFD) for T5 to T15 radiator operating at the best selected pulsed flow

(C.2) Validation surface temperature for insulated radiator

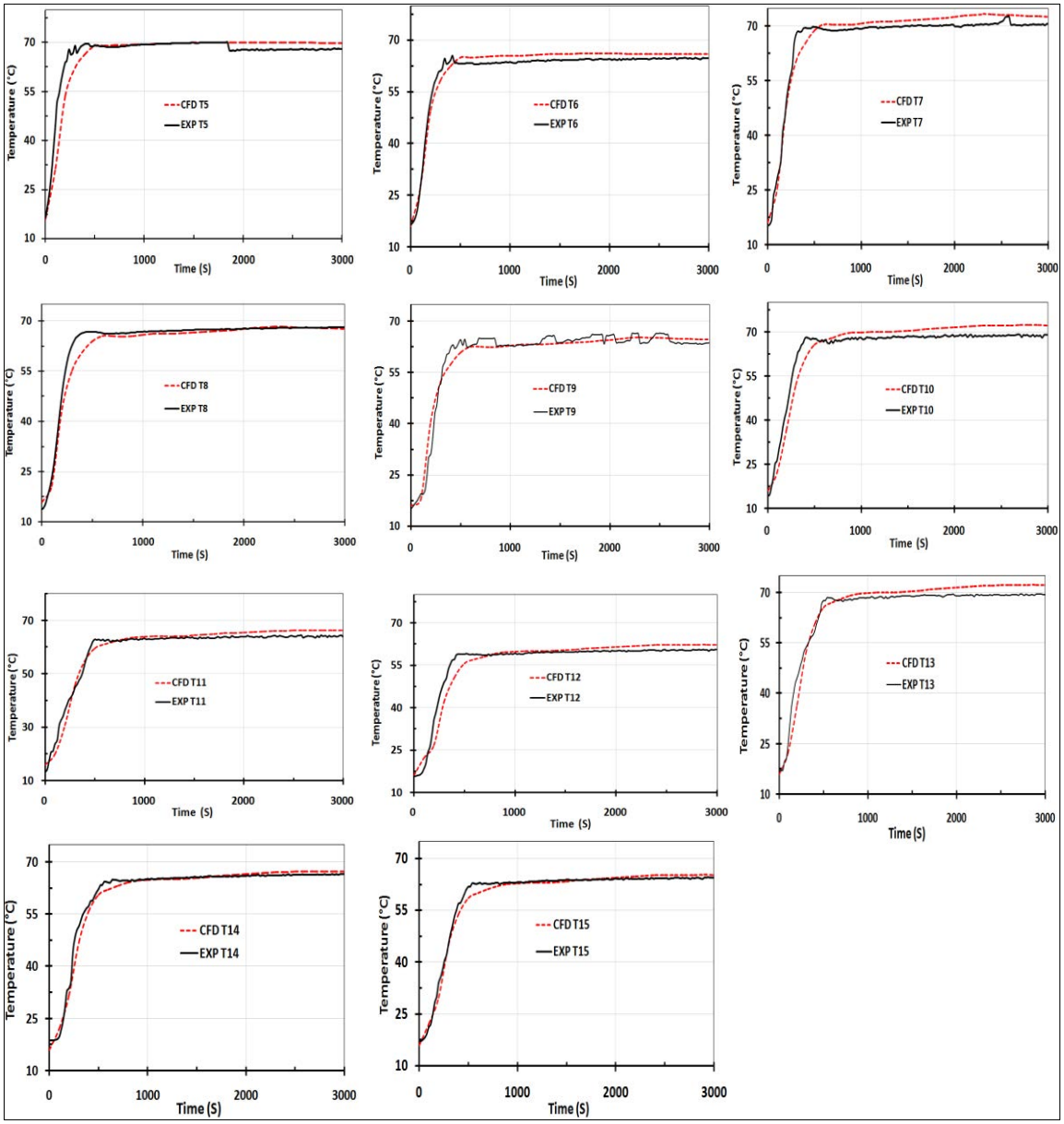

Figure C.2.1 local surface temperature distribution of insulated radiator for numerically (CFD) and experimentally (EXP) T5 to T15 operating at constant flow

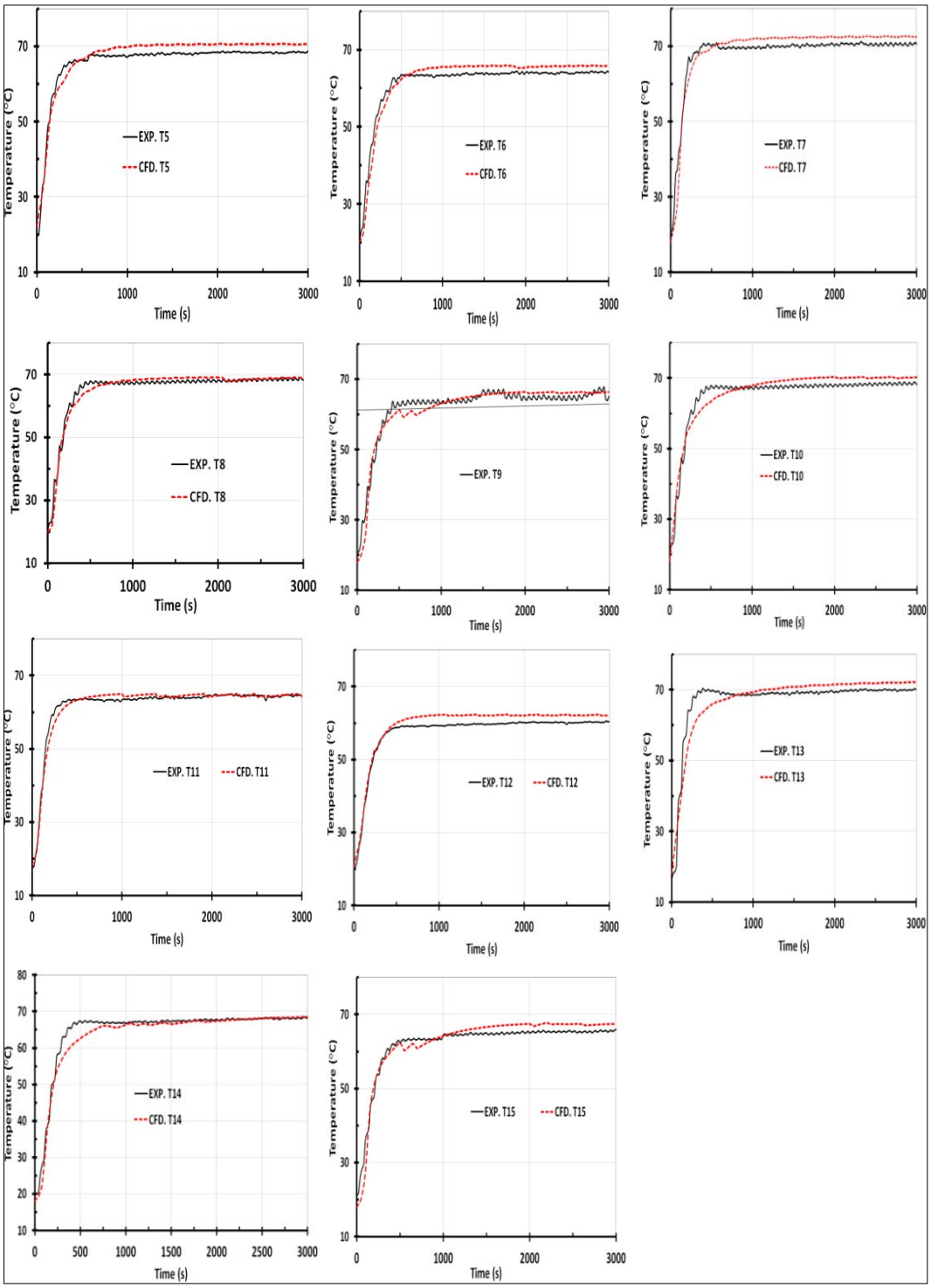

Figure C.2.2 local surface temperature distribution of insulated radiator at experimentally (EXP) and numerically (CFD) on T5 to T15 radiator operating at the best selected pulsed flow